



HAL
open science

Impact of surface properties of cation-exchange membranes on the formation of Ca^{2+} and Mg^{2+} containing scales during electro dialysis of their aqueous solutions

Marina Andreeva

► **To cite this version:**

Marina Andreeva. Impact of surface properties of cation-exchange membranes on the formation of Ca^{2+} and Mg^{2+} containing scales during electro dialysis of their aqueous solutions. Chemical and Process Engineering. Université Paris-Est; Kuban State agrarian university, 2017. English. NNT : 2017PESC1018 . tel-01759303

HAL Id: tel-01759303

<https://theses.hal.science/tel-01759303>

Submitted on 5 Apr 2018

HAL is a multi-disciplinary open access archive for the deposit and dissemination of scientific research documents, whether they are published or not. The documents may come from teaching and research institutions in France or abroad, or from public or private research centers.

L'archive ouverte pluridisciplinaire **HAL**, est destinée au dépôt et à la diffusion de documents scientifiques de niveau recherche, publiés ou non, émanant des établissements d'enseignement et de recherche français ou étrangers, des laboratoires publics ou privés.



Thèse en cotutelle internationale

présentée pour obtenir le titre de DOCTEUR
de l'Université Paris-Est et l' Université d'État du Kouban

Spécialité: Chimie et Sciences des Matériaux

Etude du colmatage des membranes échangeuses d'ions lors de l'électrodialyse de solutions de sels de Ca^{2+} et Mg^{2+} : influence des propriétés de surface

Marina ANDREEVA

Soutenue publiquement le 26/10/2017 devant un jury composé de :

<i>Rapporteurs</i>	Gérald POURCELLY, Professeur	Université de Montpellier
	Kateryna FATYEYEVA, Maître de Conférences	Université de Rouen
<i>Président du jury</i>	Patrick FIEVET, Professeur	Université de Franche-Comté
<i>Examineurs</i>	Victor NIKONENKO, Professeur	Université d'État du Kouban
	Florence LUTIN, Ingénieur	Eurodia Industrie S.A.
	Natalia PISMENSKAYA, Professeur	Université d'État du Kouban
<i>Directeurs de thèse</i>	Lasâad DAMMAK, Professeur	Université Paris-Est Créteil
	Natalia KONONENKO, Professeur	Université d'État du Kouban
<i>Invité</i>	Christian LARCHET, Professeur	Université Paris-Est Créteil



Ph.D. Thesis under an international cotutelle agreement

to obtain the degree of DOCTOR
of the Paris-Est University and the Kuban State University

Speciality: Chemistry and Materials Science

Impact of surface properties of cation-exchange membranes on the formation of Ca^{2+} and Mg^{2+} containing scales during electro dialysis of their aqueous solutions

Marina ANDREEVA

PhD defence day 26/10/2017 in front of a committee composed of :

<i>Reviewers</i>	Gérald POURCELLY, Professor	Montpellier University
	Kateryna FATYEYEVA, Assistant Professor	University of Rouen
<i>Jury president</i>	Patrick FIEVET, Professor	University of Franche-Comté
<i>Examiners</i>	Victor NIKONENKO, Professor	Kuban State University
	Florence LUTIN, Engineer	Eurodia Industrie S.A.
	Natalia PISMENSKAYA, Professor	Kuban State University
<i>Thesis supervisors</i>	Lasâad DAMMAK, Professor	Paris-Est Créteil University
	Natalia KONONENKO, Professor	Kuban State University
<i>Invited</i>	Christian LARCHET, Professor	Paris-Est Créteil University



Thèse réalisée au Institut de Chimie et des Matériaux Paris-Est

Equipe Systèmes Polymères Complexes

2-8 rue Henri Dunant

94320 Thiais

Tél : +33 (0)1 49 78 11 81

Fax : +33 (0)1 49 78 11 66

Web : <http://www.icmpe.cnrs.fr/>

Université d'État de Kouban

Equipe de chimie physique

149 rue Stavropolskaya

350040 Krasnodar

Tél : +7 (861) 219-95-01

Web : <https://kubsu.ru/>

Sous la direction de

Professeur Lasâad Dammak

dammak@u-pec.fr

Co-direction

Professeur Natalia Kononenko

kononenk@chem.kubsu.ru

*What you get by achieving your goals is not as important
as what you become by achieving your goals*

Zig Ziglar

Avant Propos

Excepté le chapitre bibliographique, cette thèse a été rédigée sous la forme d'un recueil de cinq publications parues ou soumises dans des revues à comité de lecture. L'indulgence du lecteur est donc sollicitée pour les répétitions inhérentes à ce choix de forme de rédaction.

Acknowledgements

So, the three-year scientific journey has passed. This work was realized in the frame of the French-Russian International Associated Laboratory "Ion-exchange membranes and related processes". I would like to thank the French Government and the Embassy of France in Russia for my French Postgraduate Award scholarship ("Metchnikov" program) in France, as well as the Russian Government for my Research Scholarship in Russia.

This thesis was done in the Laboratory of Complex Polymer Systems, Institute of Chemistry and Materials Paris-Est and the Laboratory of Physical Chemistry, Kuban State University. I would like to thank Valérie Langlois and Viktor Zabolotsky for having welcomed me in both laboratories.

My supervisors, Prof. Natalia Kononenko and Prof. Lassâad Dammak, you are the wonderful mentors. Thank you for encouraging my research independence as well as supporting my teaching goals. No doubt your advice over these years will make me a better academic.

I thank all the members of the jury, Prof. Gérald Pourcelly, Assoc. Prof. Dr. Kateryna Fatyeyeva, Dr. Florence Lutin, Prof. Victor Nikonenko, Prof. Patrick Fievet, Prof. Natalia Pismenskaya, Prof. Christian Larchet, who agreed to evaluate this work. I also want to thank you for letting my defense be an enjoyable moment, and for your brilliant comments and suggestions, thanks to you.

Special thanks I want to say to Prof. Victor Nikonenko for the patient guidance, encouragement and advice he has provided throughout my scientific journey. His guidance helped me in all the time of research and writing of this thesis. Prof. Natalia Pismenskaya, thank you for your constant support. Sometimes it seemed to me that only you understand how long it takes to make an experiment in reality.

I remember my first day in Paris, when the plane landed. I worried about everything: my language, adaptation, studies etc. And I met you in the airport my dear Prof. Christian Larchet and felt myself like I was at home. You are unbelievable person, you make experiments in the lab with luminous eyes and it gives me energy not to give up when I break one more capillary. And of course, thank you for the cultural life outside the lab.

The team at ICMPE, this has been a great place to study. There was always someone willing to help, and there was always someone to have a coffee with when I needed a break. You made my experimental work much comfortable by sharing your experience, helping with necessary equipment and reagents, and always being ready to support me. Rémi Perez and Ivan Cotrebil, thank you a lot for time, which we spent together, while you were working with

my samples. All my team in KubSU, they admire your images of membrane surfaces each time.

Of course, I would like to thank my girls, Natalia, Irina, Svetlana, from the lab in Russia for support and help in overcoming numerous obstacles I have been facing through my research.

My Russian friends from another lab in Russia, Violetta and Michail, you are treasures.

My family: Mum, Dad, Sveta and Lena. Thank you for all your support. The skype calls, the sleepless nights, the unconditional love. It all helped so much. Thank you in particular, Mum and Dad, for supporting my choice of education pathway and not letting me off the road.

Your support means the world to me.

Table of contents

List of figures	v
List of tables	xi
List of abbreviations.....	xii
Introduction	1
Chapter 1. Literature review	7
1.1 Ion-exchange membranes	8
1.1.1 The structure of ion-exchange membranes.....	9
1.1.2 Characterization of ion-exchange membranes.....	9
1.1.3 Methods of ion-exchange membrane modification	11
<i>1.1.3.1 Chemical modification</i>	<i>12</i>
<i>1.1.3.2 Mechanical modification</i>	<i>14</i>
<i>1.1.3.3 Electrochemical deposition</i>	<i>17</i>
1.2 Application of ion-exchange membranes	18
1.2.1 Conventional electrodialysis.....	18
1.2.2 Reverse electrodialysis	19
1.2.3 Electrodialysis metathesis.....	20
1.2.4 Bipolar membrane electrodialysis	21
1.2.5 Fuel cells.....	22
1.3 Concentration polarization and coupled effects of concentration polarization in electromembrane system	23
1.3.1 Concentration polarization in electromembrane system.....	23
1.3.2 Coupled effect of concentration polarization in electromembrane system.....	25
<i>1.3.2.1 Water splitting</i>	<i>25</i>
<i>1.3.2.2 Gravitational convection</i>	<i>27</i>
<i>1.3.2.3 Electroconvection</i>	<i>28</i>
1.3.3 Methods for studying the concentration polarization in an electromembrane system.....	31
<i>1.3.3.1 Voltammetry.....</i>	<i>32</i>
<i>1.3.3.2 Chronopotentiometry.....</i>	<i>34</i>
<i>1.3.3.3 Experimental cells for voltammetry and chronopotentiometry</i>	<i>37</i>
1.4 Fouling.....	41
1.4.1 Scale forming mechanisms	41

1.4.2 Methods for studying scaling on ion-exchange membranes	43
1.4.2.1 <i>Visualization of ion-exchange membranes scaling</i>	43
1.4.2.2 <i>Membrane characteristics depending on scaling in electro dialysis</i>	44
1.4.2.2.a <i>Membrane thickness, scaling content, membrane electrical conductivity</i>	44
1.4.2.2.b <i>Voltammetry and chronopotentiometry</i>	45
1.4.2.2.c <i>Contact angles</i>	46
1.4.2.3 <i>X-ray diffraction analysis</i>	47
1.4.3 Methods for prevention and control of ion-exchange membrane scaling	48
1.4.3.1 <i>Ion-exchange membrane modification</i>	48
1.4.3.2 <i>Cleaning agents</i>	49
1.4.3.3 <i>Pretreatment: Pressure-driven membrane processes</i>	49
1.4.3.4 <i>Mechanical action</i>	50
1.4.3.5 <i>Changing regimes of electro dialysis treatment</i>	50
1.4.3.5.a <i>Control of hydrodynamic conditions</i>	50
1.4.3.5.b <i>Electro dialysis reversal</i>	51
1.4.3.5.c <i>Pulsed electric field</i>	51
1.4.3.5.d <i>Overlimiting current regime</i>	52
1.5 Conclusions	54
References	57

Chapter 2. Effect of electrolyte nature and membrane surface properties on the development of electroconvection	70
Presentation of the article	71
Abstract	74
2.1 Introduction	75
2.2 Experimental	77
2.2.1 Protocol	77
2.2.2 Ion-exchange membranes	77
2.2.3 Materials	78
2.3. Results and discussion	79
2.3.1 Chronopotentiometry	79
2.3.2 Current–Voltage Characteristics	85
2.4 Conclusions	89
2.5 Acknowledgments	90

References	91
Chapter 3. Effect of homogenization and hydrophobization of a cation-exchange membrane surface on its scaling in the presence of calcium and magnesium chlorides during electrodialysis	94
Presentation of the article.....	95
Abstract.....	98
3.1 Introduction	99
3.2 Experimental.....	101
3.2.1 Ion-exchange membranes	101
3.2.2 Protocol	103
3.3. Results and discussion.....	104
3.3.1 Theoretical value of the limiting current density	104
3.3.2 Chronopotentiometry	105
3.3.3 pH changes.....	108
3.3.4 Scaling formation	110
3.3.5 Voltammetry	111
3.4 Conclusions	113
3.5 Acknowledgments.....	114
3.6 Appendix	115
References	116
Chapter 4. Effect of electroconvection, pH adjustment and pulsed electric field on membrane scaling in electrodialysis	121
Presentation of the article.....	122
Abstract.....	125
4.1 Introduction	126
4.2 Experimental.....	128
4.2.1. Membranes	128
4.2.2. Electrodialysis cell and experimental setup.....	130
4.2.3. Chronopotentiometric and voltammetry measurements	132
4.2.4. Analysis methods.....	132
4.3. Results and discussion.....	133
4.3.1 I-V curves.....	133
4.3.2 Chronopotentiograms	136
4.3.3 Scaling formation in constant current mode	140

4.3.4 Water splitting and effect of pH	141
4.3.5 Scale formation in PEF modes	144
4.4 Conclusions	148
4.5 Acknowledgments.....	149
References	150
Chapter 5. Effect of surface modification of cation-exchange membrane with polyaniline on polarization characteristics and scale formation	157
Presentation of the article 1.....	159
Abstract.....	161
5.1 Introduction.....	162
5.2 Experimental.....	163
5.2.1 Preparation of anisotropic MF-4SK/Polyaniline composites under the conditions of an external electric field.....	163
5.2.2 Polarization behavior of anisotropic MF-4SK/PANI composites.....	166
5.3 Conclusions	173
5.4 Acknowledgments.....	173
References	174
Presentation of the article 2.....	176
5.5 Experimental.....	178
5.5.1 Membranes	178
5.5.2 Analyses.....	178
<i>5.5.2.1 Membrane thickness</i>	<i>178</i>
<i>5.5.2.2. Membrane electrical conductivity</i>	<i>178</i>
<i>5.5.2.3. Contact angle measurements</i>	<i>179</i>
5.5.3 Electrodialysis cell and experimental setup.....	179
5.5.4 Protocol	180
5.6 Results and discussion.....	180
5.6.1. Physico-chemical characteristics of ion-exchange membranes.....	180
5.6.2 Voltammetry.....	180
5.6.3 Chronopotentiometry	182
5.7 Conclusions	187
References	189
General conclusions and perspectives	191

List of figures




Fig.1-1. Schematic representation of a membrane as a fragment of an electromembrane system: R^- - fixed ions; K, A – counter-ions and co-ions in the membrane and electrolyte solution;  - polymer matrix chains;  - bridges of polymer agent, cross-linking the main polymer matrix chains; - incorporations of an inert polymer imparting thermal stability, or mechanical strength, or elasticity to the membrane(adapted from [4])

Fig.1-2. Chemical structure of sulfo cation-exchange materials: a) polystyrene sulfonate, and b) perfluorinated membrane (Nafion[®]).

Fig. 1-3. Microphotographs of cross sections and AFM images of (a, c) the pristine and (b, d) composite sample turned (b) to polymerizing solutions, respectively (adapted from [22]).

Fig.1-4. Microphotographs of the membrane MA-40: a) initial; b) profiled (adapted from [4]).

Fig.1-5. SEM image of the surface of MK-40 (a) and MK-40*/Nf₂₀ (b) membranes and the cross section of a MK-40 (c) and MK-40*/Nf₂₀ (d) membranes (adapted from [34]).

Fig. 1-6. Total current density and partial current density of ions H^+ [$i(H^+)$] through MK-40 and its modifications (adapted from [34]).

Fig. 1-7. Schematic diagram illustrating the principle of electro dialysis (adapted from [40]).

Fig. 1-8. Schematic drawing illustrating the construction of a sheet flow stack design (adopted from [40]).

Fig. 1-9. Schematic drawing illustrating the RED system (adopted from [7]).

Fig. 1-10. Schematic diagram of the EDM process (adopted from [44]).

Fig. 1-11. Schematic drawing illustrating the principle of electro dialytic production of acids and bases from the corresponding salts with bipolar membranes (adopted from [40]).

Fig. 1-12. Scheme diagram illustrating the structure of PEMFC and the principle of operation(adapted from [49]).

Fig. 1-13. Concentration profile in an EMS. C_0 is the electrolyte concentration in the bulk solution; C_1 and C_2 are the electrolyte concentrations at the boundaries between the diluate and concentrate diffusion layers and the membrane, respectively; the bar over the letter designates that the quantity relates to the membrane phase; δ and d are thickness of diffusion layer and membrane, respectively.

Fig. 1-14. Scheme of gravitational convection (adapted from [66]).

Fig. 1-15. Mechanisms of electroconvection.

Fig. 1-16. Profiles of ion concentration: the distribution of electrolyte concentration near membrane surface at lower (curves 1, 1') and higher (curves 2, 2', 3) voltage; δ is the overall

diffusion layer thickness; δ_1 , δ_2 and δ_3 are the thicknesses of the electrically neutral region, extended SCR and quasi-equilibrium SCR, respectively; C_0 is the bulk electrolyte concentration. The difference between counter-ions (curve 2) and co-ions (curve 3) concentrations near the leftmembrane side corresponds to the appearance of the SCR (adapted from [81]).

Fig. 1-17. Principal scheme of the four-electrode cell.

Fig. 1-18. Typical I-V curve.

Fig. 1-19. Characteristic points of the chronopotentiogram.

Fig. 1-20. Schematic distribution of current lines at the homogeneous (a) and heterogeneous (b) membrane surfaces (adapted from [110]).

Fig. 1-21. Chronopotentiograms for heterogeneous (MA-41) and homogeneous (AMX) anion-exchange membranes in a 0.1 M solution NaCl. The membrane is in a vertical position, the current density is 17.2 mA cm^{-2} (adapted from [111]).

Fig.1-22. Scheme of the RMD cell. 1 – anion-exchange membrane under investigation, 2 – top half-cell with a NaCl solution (anode chamber), 3 – bottom half-cell with a NaCl solution (cathode chamber), 4 – inlet solution capillary, 5 – outlet solution capillary, 6 – Pt polarizing electrodes, 7 – Luggina-Haber capillaries, 8 – galvanostat, 9 – millivoltmeter, 10 – Ag/AgCl reference electrodes, 11 – pulley (adapted from [112]).

Fig. 1-23. The diagram of the experimental cell: membranes (1); plastic gaskets (2); elastic gaskets (3,4); square aperture (5); cathode (6); anode (7); plastic capillaries (8); Ag/AgCl chloride electrode or Luggin capillary (9); connecting pipe (10); stream spreader of a comb shape (11); the membrane studied (A^*); a cation-exchange membrane (C); an anion-exchange membrane (A) (adapted from [110]).

Fig. 1-24. Schematic illustration of scale formation schemes (adapted from [119]).

Fig. 1-25. Visualization of membrane fouling by photo imaging (A,B), optical microscopy (C), SEM (D), CLSM (E), AFM (F) (adapted from [116]).

Fig. 1-26. Schematic representation of the system for measuring membrane conductance (adapted from [129]).

Fig. 1-27. Chronopotentiograms obtained with 0.02M $\text{Fe}_2(\text{SO}_4)_3$ solutions and in the overlimiting range of currents for (a) Nafion 117 and (b) HDX 100 (adapted from [98]).

Fig. 1-28. Examples of contact angles measurement methods a) in air and b) in liquid (adapted from [134, 136]).

Fig.1-29. Dead-end filtration and cross-flow filtration (adapted from [150]).

Fig.1-30. Scheme of EDR and presence of foulants (adapted from [116]).

Fig. 2-1. Image of the surface of swollen MK-40 (a) and MK-40_{MOD} (b) membranes as obtained with a Zeiss AxioCam MRc5 light microscope.

Fig. 2-2. Chronopotentiogram of the MK-40_{MOD} membrane in 0.02 M CaCl₂ solution at a current density of $i = 4.8 \text{ mA cm}^{-2}$: $\Delta\varphi_{Ohm}$ is the ohmic potential drop immediately after turning on the power, $\Delta\varphi_{St}$ is the potential drop at the time the membrane system reaches the steady state, $\Delta\varphi'$ is the reduced potential difference defined by Eq. (2.1), and τ_{exp} is the transition time determined from the inflection point on the chronopotentiometric curve.

Fig. 2-3. Chronopotentiograms of the MK-40_{MOD} membrane, as measured for different electrolytes at $i / i_{lim}^{theor} = 0.8$. The data were obtained at current densities of $i = 1.5 \text{ mA.cm}^{-2}$ (NaCl), $i = 2.8 \text{ mA cm}^{-2}$ (CaCl₂), and $i = 2.5 \text{ mA cm}^{-2}$ (MgCl₂); the values of i_{lim}^{theor} are given in Table 2-2.

Fig. 2-4. Chronopotentiograms of the MK-40_{MOD} membrane, as measured for different electrolytes at $i / i_{lim}^{theor} = 2.2$. The data were obtained at current densities of $i = 4.5 \text{ mA cm}^{-2}$ (NaCl), $i = 7.7 \text{ mA cm}^{-2}$ (CaCl₂), and $i = 7.0 \text{ mA cm}^{-2}$ (MgCl₂).

Fig. 2-5. Initial portions of chronopotentiograms of the MK-40_{MOD} membrane in 0.02 M solutions of (a) NaCl and (b) MgCl₂ and the same curves shown in the differential form. The data were obtained at $i / i_{lim}^{theor} = 1.7$: $i = 3.5 \text{ mA cm}^{-2}$ (NaCl) and $i = 5.3 \text{ mA cm}^{-2}$ (MgCl₂).

Fig. 2-6. Plot of values for the first local maximum of reduced CP potential difference (open symbols) and the time taken to reach the maximum (closed symbols) versus the current density normalized to the limiting current density calculated by Eq. (2.5).

Fig. 3-1. SEM images of MK-40 membrane surface in dry (a) and swollen (b) states, the surface (c) and cross section (d) of MK-40_{MOD} membrane in the dry state.

Fig. 3-2. Principal scheme of the experimental setup. ED cell (1) consists of one concentration (2), one desalination (3) and two electrode chambers (4), two platinum polarizing electrodes (5) and two Ag/AgCl electrodes inserted in Luggin capillaries (6). A flow pass cell with a pH electrode (7) and a pH meter pHM120 MeterLab (8) are used for pH measurements. The current was set and the potential difference was measured using a potentiostat-galvanostat PARSTAT 2273 (9); the data were registered using a PC (10).

Fig. 3-3. Chronopotentiogram of an MK-40 membrane: $\Delta\varphi$ vs. t , in a 0,04M CaCl₂ solution at current density 11.5 mA.sm^{-2} . $\Delta\varphi_{Ohm}$ is the ohmic potential drop just after the current is switched on; $\Delta\varphi_{St}$ is the potential drop at the steady-state; $\Delta\varphi' = \Delta\varphi - \Delta\varphi_{Ohm}$ is the reduced potential drop; τ_{SAND} is the transition time. Stages I, II, and III are described in the text.

Fig. 3-4. Chronopotentiograms of MK-40 (dark blue (darker) lines) and MK-40_{MOD} (grey (lighter) lines) membranes measured in 0.04 M MgCl₂ (a) and 0.04 M CaCl₂ (b) solutions at $i/i_{\text{lim}}^{\text{th}} = 0.6, 1.4$ and 2.5.

Fig. 3-5. Time dependence of pH difference between the outlet and inlet solution passing through the desalination chamber in cases of MK-40//AMX-SB (solid lines) and MK-40_{MOD}//AMX-SB (dashed lines) measured in 0.04 M MgCl₂ (a) and 0.04 M CaCl₂ (b) solutions.

Fig. 3-6. SEM images of the surface of dry MK-40 membrane before (a) and after 5h electro dialysis of 0.04M MgCl₂ (b) solution and 0.04M CaCl₂ (c) at $i=1.4 i_{\text{lim}}^{\text{th}}$.

Fig. 3-7. Current-voltage curves for MK-40 and MK-40_{MOD} membranes in MgCl₂ (a) and CaCl₂ (b) solutions of different concentrations.

Fig. 4-1. SEM images of the membrane surfaces in a dry state: MK-40 (a), MK-40_{MOD} (b), MA-41 (d) and the cross section of MK-40_{MOD} membrane (c).

Fig. 4-2. Principal scheme of the experimental setup. ED cell (1) consists of one desalination (2), one auxiliary (3) and two electrode compartments (4), two platinum polarizing electrodes (5) and two Ag/AgCl electrodes inserted in Luggin capillaries (6). A mixed salt solution (7) composed of Na₂CO₃, KCl, CaCl₂ and MgCl₂ feeds the desalination compartment; NaCl solution (8) circulates through the auxiliary and two electrode compartments. A flow cell with a pH electrode (9) and a pH meter pHM120 MeterLab (10) are used for pH measurements. The current is supplied by KEITHLEY 220 current source (11), the potential difference is measured using HEWLETT PACKARD 34401A multimeter (12); the data are registered using a PC (13).

Fig. 4-3. I-V curves of the MK-40 (dark blue line) and MK-40_{MOD} (grey line) membranes in the model solution. $\Delta\phi_p$ is the "plateau" length; $1/R$ is the "plateau" slope; $i_{\text{lim}}^{\text{exp}}$ is the limiting current density determined (for the MK-40 membrane) by the intersection point of tangents.

Fig. 4-4. Schematic distribution of electric current lines near the surface of MK-40 (a) and MK-40_{MOD} (b) membranes. Due to low fraction of conductive area and narrow "gates" for ion passage, the funnel effect [29] results in high concentration polarization of MK-40 while electroconvection is low. The increased "gates" and more hydrophobic surface of MK-40_{MOD} membranes lead to lower concentration polarization and higher electroconvection. Adapted from [38].

Fig. 4-5. Chronopotentiogram of the MK-40_{MOD} membrane in the model solution, $\Delta\phi$ vs. t , and its derivative, $d(\Delta\phi)/dt$ vs t , in the model solution at $i=17.5 \text{ mA cm}^{-2}$. $\Delta\phi_{\text{ohm}}$ is the ohmic

potential drop just after the current is switched on; $\Delta\varphi_{st}$ is the potential drop at the steady-state; $\Delta\varphi' = \Delta\varphi - \Delta\varphi_{Ohm}$ is the reduced potential drop; τ is the transition time.

Fig. 4-6. Chronopotentiograms of the MK-40 and MK-40_{MOD} membrane measured in the model solution at $i=5.3 \text{ mA cm}^{-2}$ ($i < i_{lim}^{exp}$) (a) and $i=12.5 \text{ mA cm}^{-2}$ ($i > i_{lim}^{exp}$) (b) and in a 0.1 M NaCl solution at $i=5.3 \text{ mA cm}^{-2}$ and $i=12.8 \text{ mA cm}^{-2}$ (c)

Fig. 4-7. I-V curves (a) and the current density dependences of the size d of convection instability zone near the MK-40 and MK-40_{MOD} membranes in a membrane channel (the length is 4.2 cm, the intermembrane distance is 5 mm); a 0.02 M NaCl is fed with a velocity 0.2 mm s^{-1} . The data are obtained using an interferometric setup of the Mach-Zehnder type. The value of d is defined as the distance from the membrane surface on which the concentration profile has an unstable, oscillatory character. The curves are performed using experimental data from Ref. [57].

Fig. 4-8. SEM images of the surface of dry MK-40 (a- e), MK-40_{MOD} (g-h) and MA-41 (f, i) membrane after 5 h continuous electro dialysis of model solution at $i=10.5 \text{ mA cm}^{-2}$. (f) and (i) show the cases where the MA-41 membrane is used together with the MK-40 (f) or MK-40_{MOD} (i) membrane.

Fig. 4-9. Time dependence of the pH of diluate for the MK-40//MA-41 (dark blue line) and MK-40_{MOD}//MA-41 (grey line) membrane pairs at $i = 4 \text{ mA cm}^{-2}$, 9 mA cm^{-2} , 17.5 mA cm^{-2} .

Fig. 4-10. Concentration profiles obtained using the mathematical model based on the Nernst-Planck-Poisson equations developed by Urtenov et al. [69] (EC does not taken into account); the solid lines show the equivalent fractions of ions (C_i), the dashed line shows the product $(C_{Mg}(C_{OH})^2 \times 50)$ near a cation-exchange membrane (CEM). Arrows show the direction of H^+ and OH^- ion fluxes generated at the depleted CEM surface. Adapted from [40].

Fig. 5-1. Diagram of the formation of a polyaniline layer on the surface of the MF-4SK membrane under the conditions of an external electric field.

Fig. 5-2. Electronic absorption spectra of MF-4SK–PANI composites obtained under the conditions of an external electric field using (1)–(3) ammonium persulfate and (4) potassium dichromate as an oxidant of aniline: (1) MF-4SK/PANI-100-2, (2) MF-4SK/PANI-200-2, (3) MF-4SK/PANI-300-2, and (4) MF-4SK/PANI-100-1.

Fig. 5-3. Diagram of a unit for measuring the CVCs of the membrane system: (1) measurement cell, (2) near-electrode chambers, (3) platinum polarizing electrodes, (4) near-membrane chambers, (5) membrane under study, (6) Luggin–Haber capillaries, (7) auxiliary membranes, (8) silver/silver chloride electrodes, (9) Autolab pgstat302n

potentiostat/galvanostat, (10) PC, (11) Heidolph pumpdrive 5101 peristaltic pump, and (12) vessels for solutions.

Fig. 5-4. CVCs of the MF-4SK/PANI-1 composite in 0.05 M HCl measured in sequence; measurement no. (1) 1, (2) 5, (3) 10, (4) 12, and (5) 13.

Fig. 5-5. Chronopotentiograms of the MF-4SK/PANI-1 anisotropic composite measured in 0.05 M HCl at different polarizing currents i , A dm⁻²: (1) 11.3, (2) 7.0, (3) 6.5, (4) 2.8, and (5) 1.3.

Fig. 5-6. CVCs of the MF-4SK/PANI-1 anisotropic composite measured in 0.05 M HCl at (a) high ((1) 1.5×10^{-5} A s⁻¹ and (2) 4.6×10^{-5} A s⁻¹) and (b) low ((1) 0.4×10^{-5} A s⁻¹ and (2) 0.8×10^{-5} A s⁻¹) scan rates of the polarizing current.

Fig. 5-7. (a), (c) Integrated and (b), (d) differential CVCs of the MF-4SK/PANI composites in 0.05 M HCl obtained at different current densities using (a), (b) potassium dichromate and (c), (d) ammonium persulfate as an oxidant of aniline. Current densities during the synthesis of the composites, A dm⁻²: (1) 100, (2) 200, and (3) 300.

Fig. 5-8. Diagram of H⁺ and OH⁻ ion flows that appear in the EMS with the membrane orientated by its modified layer toward the (a) anode and (b) cathode (the modified layer is hatched).

Fig. 5-9. Image of the surface of swollen (a) MK-40 and (b) MK-40/PANI membranes as obtained with a Zeiss AxioCam MRc5 light and Altami microscope, respectively.

Fig. 5-10. I-V curves for MK-40 and MK-40/PANI membranes in the model solution and corresponding dependence of the pH of diluate solution.

Fig. 5-11. Chronopotentiogram of the MK-40 membrane in the model solution, $\Delta\phi$ vs. t , and its derivative, $d(\Delta\phi)/dt$ vs t , in the model solution at $i = 1.5i_{lim}^{exp}$. $\Delta\phi_{Ohm}$ is the ohmic potential drop just after the current is switched on; $\Delta\phi_{St}$ is the potential drop at the steady-state; τ is the transition time.

Fig. 5-12. Chronopotentiograms of MK-40 and MK-40/PANI membranes in the model solution and corresponding time dependence of the pH of diluate solution.

Fig. 5-13. The precipitate in the form of a gel on the MK-40/PANI membrane surface at $i=10.5$ mA cm⁻².

Fig. 5-14. SEM images of the surface of (a) Mg(OH)₂, (b) CaCO₃ and Ca(OH)₂ crystals on the MK-40 membrane surface facing the diluate after 5h of electro dialysis of model solution.

Fig. 5-15. The micelle structure.

List of tables

Table 1-1. The main characteristics of ion-exchange membranes.

Table 2-1. Some characteristics of ions and electrolyte solutions containing the ions (at 20°C).

Table 2-2. Parameters of current-voltage curves for the test membrane systems.

Table 3-1. Theoretical value of limiting current density of CEM, $i_{lim}^{th,CEM}$, and AEM, $i_{lim}^{th,AEM}$, in different electrolytes at 20°C.

Table 4-1. Some parameters of I-V curves of MK-40, MK-40_{MOD} and MA-41 membranes in the mixed model solution at 20°C.

Table 5-1. Conditions for the preparation of MF-4SK/PANI composites.

Table 5-2. Conditions for the preparation of MF-4SK/PANI composites.

Table 5-3. The main properties of the MK-40 and MK-40/PANI membranes.

Table 5-4. The values of limiting current densities for MK-40 and MK-40/PANI membranes in the mixed model solution at 20°C.

Table 5-5. The possible foulants and fouling modes.

List of abbreviations

AEM – Anion-exchange membrane
AFM – Atomic force microscopy
BM – Bipolar membrane
CEM – Cation-exchange membrane
CP – Concentration polarization
DBL – Diffusion boundary layer
EC – Electroconvection
ED – Electrodialysis
EDBM – Electrodialysis with bipolar membranes
EDL – Electric double layer
EDR – Electrodialysis reversal
EMS – Electromembrane system
IEM – Ion-exchange membrane
LCD – Limiting current density
PANI – Polyaniline
PD – Potential drop
PEF – Pulsed electric field
PEM – Polymer electrolyte membrane
PEMFC – Proton exchange membrane fuel cells
Ppy – Polypyrrole
RED – Reverse electrodialysis
RO – Reverse osmosis
SCR – Space charge region
SEM – Scanning electron microscopy
WS – Water splitting

Introduction

Ce travail est consacré à l'étude de l'effet des propriétés de surface des membranes d'échange d'ions sur la formation de précipités de composés de Ca^{2+} et de Mg^{2+} sur la surface de la membrane lors de l'électrodialyse de solutions aqueuses.

L'électrodialyse est l'une des technologies les plus développées utilisées pour le dessalement et la concentration des solutions d'électrolytes et pour la séparation des ions. Cette technique est basée sur la migration sélective des ions à travers les membranes échangeuses d'ions sous l'action d'un champ électrique appliqué comme force motrice.

La faible consommation d'énergie et l'efficacité élevée du courant sont les principaux avantages du procédé d'électrodialyse. Cependant, la polarisation de concentration et la formation de précipités introduisent des limites dans diverses applications. La polarisation de concentration, c'est-à-dire l'apparition de gradients de concentration sous l'action du courant électrique, est un phénomène inhérent à l'électrodialyse, qui permet le dessalement et la concentration. Il résulte de la différence entre les nombres de transport ionique dans la solution et dans la phase membranaire. La diminution de la concentration d'électrolyte à la surface de la membrane permet le dessalement de la solution, mais entraîne également une augmentation de la résistance électrique. Lorsque la concentration à l'interface approche de zéro, la densité de courant approche une certaine valeur de courant appelée densité de courant limite. Le transport d'ions par électrodifusion atteint une vitesse maximale et il apparaît de nouveaux phénomènes et mécanismes de transport, appelés effets couplés de polarisation de concentration. La dissociation de l'eau entraîne la génération d'ions H^+ et OH^- , qui participent au transfert du courant électrique mais aussi une diminution de l'efficacité du transfert d'ions des sels. De plus, la consommation d'énergie augmente et il apparaît des variations de pH des solutions dessalées et concentrées. Ces dernières peuvent entraîner la création de conditions favorables à la précipitation de sels peu solubles (scaling) à la surface ou à l'intérieur des voies conductrices d'ions (pores) de la membrane qui réduisent le transfert d'ions et créent une résistance supplémentaire au flux de solution et au transfert de masse. L'électroconvection, qui est une convection induite par le courant électrique au-dessus du courant limite, résultant de l'action du champ électrique sur les charges d'espace existant à l'interface membranaire, améliore au contraire le transfert de masse et limite le processus de dissociation de l'eau.

Les principaux procédés utilisés pour diminuer la polarisation de concentration et le scaling sont le prétraitement de la solution (en utilisant un traitement chimique et/ou une filtration à l'aide de membranes d'ultrafiltration ou d'microfiltration) et/ou ou une inversion périodique des polarités. Dans la méthode d'inversion de l'électrodialyse, la polarité des électrodes et la direction de l'écoulement sont modifiées en même temps. Les chambres de dessalement

deviennent des chambres de concentration, et réciproquement. La perte d'efficacité, de capacité et de produit final pendant le fonctionnement du changement de polarité de l'électrode sont les inconvénients de cette méthode. Cependant, lors de l'application d'un prétraitement de la solution et/ou d'une inversion de polarité, une certaine quantité d'ions faiblement solubles reste dans les solutions à traiter et la formation de précipité peut quand même se produire. L'idée principale de ce travail est d'utiliser d'autres possibilités «intrinsèques» pour réduire la formation du précipité. Nous allons essayer de modifier la surface de la membrane de manière à obtenir une membrane plus résistante à la formation de précipité que la membrane vierge. Plusieurs effets vont être appliqués. Ce sont l'homogénéisation, l'uniformisation et l'hydrophobisation de la surface, ce qui doit faciliter l'électroconvection et réduire la polarisation de concentration et la dissociation de l'eau. Une surface de membrane plus lisse réduit le risque de nucléation des cristaux sur la surface de la membrane. Une membrane hétérogène à faible coût (une membrane échangeuse de cations MK-40 fabriquée en Russie) est prise comme substrat. La modification est faite en pulvérisant sur la surface une couche très mince de Nafion[®], ce qui ne modifie pas sensiblement le coût de la membrane. Ainsi, en combinant la modification de surface et l'utilisation de régimes électriques spéciaux, nous espérons contribuer au développement de méthodes de prévention ou d'atténuation du scaling de la membrane.

Dans ce contexte, l'objectif principal de la présente étude est d'étudier l'effet des propriétés superficielles des membranes échangeuses de cations sur le développement des phénomènes couplés de polarisation de concentration et de formation de précipités dans les solutions contenant des cations Ca^{2+} et Mg^{2+} dans les procédés classiques d'électrodialyse.

La thèse de doctorat comprend 5 chapitres. Le premier chapitre est consacré à la revue de la littérature concernant les membranes d'échange d'ions, ainsi que des méthodes de modification et d'application des membranes échangeuses d'ions, la polarisation de la concentration et l'effet couplé de la polarisation de la concentration dans les procédés électromembranaires, la formation de précipités et leurs méthodes d'étude et les moyens permettant de les limiter. Dans le deuxième chapitre, nous avons étudié l'effet de la nature des électrolytes et de la surface de la membrane sur le développement de l'électroconvection. Le troisième chapitre est consacré à l'homogénéisation et à l'hydrophobisation d'une membrane échangeuse de cations sur le scaling en présence d'ions divalents. Le quatrième chapitre vise à étudier l'influence de l'électroconvection, du pH et de l'application d'un champ électrique pulsé sur l'atténuation du scaling. Dans la cinquième partie, nous proposons une autre méthode pour la préparation d'une membrane composite anisotrope par formation d'une couche de polyaniline sur une membrane échangeuse de cations. Nous étudions le

comportement électrochimique de la membrane composite et le processus de formation de précipité en présence d'ions divalents.

Dans chaque chapitre, l'état de l'art de chaque sujet est présenté et les méthodes expérimentales qui nous ont permis d'atteindre nos objectifs sont décrites.

This work is devoted to the study of the effect of ion-exchange membranes surface properties on the formation of scale of Ca^{2+} and Mg^{2+} compounds on the membrane surface during electro dialysis of aqueous solutions.

Electrodialysis is one of the highly developed technologies used for desalination and concentration of electrolyte solutions and for ion separation. It is based on ion selective migration through ion-exchange membranes under the action of applied electric field as the driving force.

Low energy consumption and high current efficiency are the advantages of electro dialysis process. However, concentration polarization and membrane scaling are the limitations in various applications of electro dialysis. Concentration polarization, i.e. appearance of concentration gradients under the action of electric current, is an inherent phenomenon in electro dialysis, which allows desalination and concentration and which arises as a result of the difference in the ion transport numbers in the solution and membrane phase. The decrease of electrolyte concentration at membrane surface allows solution desalination, but also leads to increasing potential drop. When the concentration at the interface approaches zero, the current density approaches a certain current value (the limiting current density). The ion transport by electrodiffusion becomes saturated and new phenomena and additional transport mechanisms develop, which are named coupled effects of concentration polarization. Water splitting results in generation of H^+ and OH^- ions, which participate in the transfer of the electric current. However, this leads to a decrease in the current efficiency towards the transfer of salt ions. Besides, the energy consumption increases and variations in the pH of desalted and concentrated solutions are produced. The latter may results in creation of the conditions where precipitation of sparingly soluble salts (scaling) occurs. The scale formation on the surface or inside the ion-conductive pathways (pores) of the membrane reduces the working area of the membrane and causes additional resistance to the flow of solution and mass transfer. Electroconvection, which is the current-induced convection resulting at overlimiting currents by the action of electric force upon the electric space charge, on the contrary, enhances the mass transfer and hinders the process of water splitting.

The main known methods for decreasing concentration polarization and membrane scaling are solution pretreatment (using chemical treatment and/or filtration using microfiltration and ultrafiltration membranes) and electro dialysis reversal. In the electro dialysis reversal, the electrode polarity and the flow direction are changed at the same time. The desalination chambers become concentration chambers, and vice versa. The loss in the current efficiency, capacity and final product during the operation of electrode polarity changing are the disadvantages of this method. However, when applying solution pretreatment and/or

electrodialysis reversal, a certain amount of sparingly soluble ions remains in solutions to be treated and the scale formation may occur. The main idea of this work is the use of other “intrinsic” possibilities to reduce scale formation. We try to modify the membrane surface in a way to obtain a membrane more resistant to scale formation than the pristine membrane. Several effects, which mitigate scaling, are applied. They are homogenization, smoothness and hydrophobization of the surface, which facilitate electroconvection and reduce concentration polarization and water splitting. A smoother membrane surface reduces the risk of nucleation of scale crystals on the membrane surface. A low cost heterogeneous membrane (a MK-40 cation-exchange membrane made in Russia) is taken as the substrate. The modification is made by casting on the MK-40 surface a very thin layer of Nafion[®] material, which does not noticeably increase the membrane cost. Thus, in this way, combining surface modification and the use of special electric regimes, we hope to make a contribution to the development of methods for prevention or mitigation of membrane scaling.

In this context, the main goal of the present study is investigation of the effect of surface properties of cation-exchange membranes on the development of coupled phenomena of concentration polarization and scale formation in the solutions containing Ca^{2+} and Mg^{2+} cations during conventional electrodialysis processes.

The doctoral thesis includes five chapters. The first chapter is devoted to the literature review concerning ion-exchange membranes, and methods of modifications and applications of ion-exchange membranes, concentration polarization and coupled effect of concentration polarization in electromembrane systems, scaling of ion-exchange membranes and methods for studying and mitigating the scale formation. In the second chapter, we study the effect of electrolyte nature and membrane surface properties on the development of electroconvection. The third chapter is devoted to the effect of homogenization and hydrophobization of a cation exchange membrane on its scaling in the presence of divalent ions during electrodialysis. The fourth chapter aims to study the influence of electroconvection, pH adjustment and pulsed electric field application on membrane scaling mitigation in electrodialysis. In the fifth part, a method for the preparation of an anisotropic composite membrane by the formation of polyaniline layer within a cation-exchange membrane is proposed. The electrochemical behavior of the composite membrane and the process of scale formation in the presence of divalent ions are studied.

In each chapter, the state of the art of each subject is presented, and the experimental methods that have enabled us to achieve our objectives are described.

Chapter 1

Literature review

1.1 Ion-exchange membranes

Ion-exchange membranes (IEMs) are polymers (usually in the form of a film), which contain positive or negative charged groups fixed to the polymer matrix (Fig. 1-1). The high density of these charged groups inside the macromolecule creates a space charge, which is compensated by an equivalent number of mobile charges of the opposite sign – counter-ions. The latter in the vicinity of the fixed charges groups create an ionic atmosphere and ensure the electroneutrality of the polymer. The membrane also contains a small number of mobile ions that have the same charge sign as fixed ions, which are called co-ions [1-3].

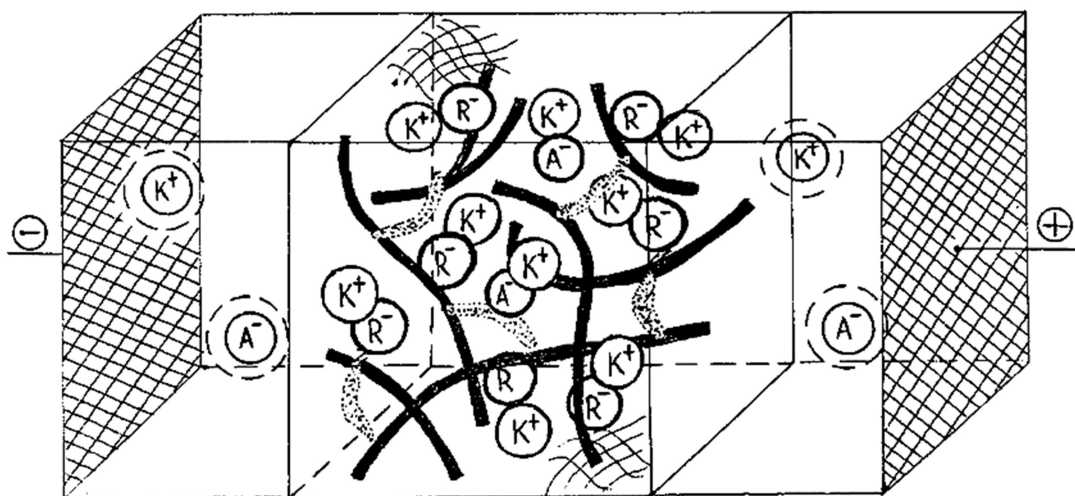


Fig. 1-1. Schematic representation of a membrane as a fragment of an electromembrane system: R^- - fixed ions; K^+ , A^- – counter-ions and co-ions in the membrane and electrolyte solution; — polymer matrix chains; — bridges of polymer agent, cross-linking the main polymer matrix chains; — incorporations of an inert polymer imparting thermal stability, or mechanical strength, or elasticity to the membrane(adapted from [4]).

When a membrane contacts a dilute electrolyte solution, the co-ions are almost completely excluded from the membrane phase and make only a slight contribution to the current transfer. This effect is called "Donnan exclusion" [1]. Application of an electric field to the membrane causes the movement of counter-ions, or electromigration. Therefore, an ideal membrane swollen by water or electrolyte solution is a polyelectrolyte with unipolar conductivity.

1.1.1 The structure of ion-exchange membranes

IEMs are based on polymeric materials such as aliphatic, cyclic, aromatic, etc. The chains of the polymer matrix are most often hydrocarbon or perfluorinated chains (Fig. 1-2). The perfluorinated chains are more chemically and thermally stable [5]. The following groups are used as fixed ions for cation-exchange membranes (CEMs): $-\text{SO}_3^-$, $-\text{COO}^-$, $-\text{PO}_3^-$ [6, 7]. The charge of these groups is compensated by positively charged counter-ions. In anion-exchange membranes (AEMs), positive charges are fixed to the matrix: $-\text{NH}_3^+$, $-\text{RNH}_2^+$, $-\text{R}_3\text{N}^+$ [7]. The charge of these groups is compensated by negatively charged counter-ions.

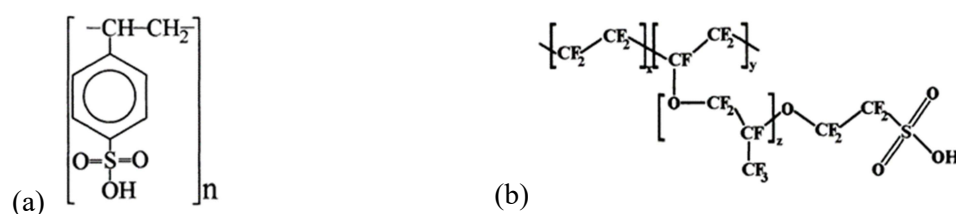


Fig. 1-2. Chemical structure of sulfo cation-exchange materials: a) polystyrene sulfonate, and b) perfluorinated membrane (Nafion[®]).

Electrodialysis membranes are often based on ion-exchange resins made of polystyrene cross-linked with divinylbenzene. These materials represent heterogeneous polymer compositions consisting of grinded resin (60-65 % by weight) and inert polymers (polyethylene, polyvinyl chloride and a number of other additives) and often reinforced by fibers to give the membrane the mechanical strength. The desire to achieve a more even distribution of charges and better electrochemical and separation properties of membranes led to the creation of homogeneous membranes. Fixed functional groups are introduced directly into the polymer film of these membranes [6].

Bipolar membrane (BM) is a special type of electromembrane material, which makes it possible to realize an important process of electrochemical production of acids and bases from the corresponding salts. These membranes are a bilayer system consisting of cation- and anion-exchange layers. The membrane generates oppositely directed flows of H^+ and OH^- ions by applying an electric field due to the water splitting reaction at the bipolar boundary inside the membrane [8].

1.1.2 Characterization of ion-exchange membranes

The properties of the membrane are divided into two categories: equilibrium or static properties, which are studied without an electric current ($i = 0$), and transport or dynamic

properties, which are studied by passing an electric current ($i \neq 0$) or in conditions of diffusion transport [3, 9]. The main characteristics of IEMs including equilibrium, electro transport and polarization properties are presented in Table 1-1.

Physico-chemical static properties of membranes	Transport properties		Polarization properties: I-V curve
	$i = 0$	$i = 0, \Delta c \neq 0$	$i \neq 0$
exchange capacity: Q , meq g ⁻¹	membrane potential: ΔE , V	conductivity: κ_m , S m ⁻¹	limiting current density: i_{lim} , A m ⁻²
water content: W , %	diffusion permeability: integral permeability coefficient P_m , m ² s ⁻¹	selectivity: transport number of ion, t_i	“plateau” length: Δ , V
specific moisture capacity: n_m , mol of H ₂ O per mol of functional groups		electro-osmotic permeability: t_w , mol of H ₂ O per F	effective resistance at low currents: R , Ω
contact angle: θ , °			resistance ratio of the region III to I: R_3/R_1
density: ρ , g cm ⁻³			
membrane thickness			

Table 1-1. The main characteristics of ion-exchange membranes.

The physico-chemical and mechanical properties of membranes [8] depending on the synthesis and the accompanying technological operations (pressing, fiber reinforcement, etc.) are evaluated by measuring the density, geometric dimensions in the dry and swollen state, and tensile strength. These properties involve also the exchange capacity which characterizes the number of charged groups fixed to the polymer matrix per unit membrane volume or mass. The amount of water absorbed by the membrane depends on the exchange capacity and determines its chemical behavior under process conditions. The moisture capacity of the membranes is an informative quantitative characteristic of their hydrophilic properties.

Measurement of the membrane potential served as a starting point for the creation of membrane electrochemistry, since the thermodynamic bases for this method and the experimental procedure were developed much earlier than the appearance of synthetic membranes and were used for the study of collodion and biological membranes. The diffusion permeability [8] of the charged membranes is a property that reduces the selectivity of ion transport across the membrane during electrodialysis and reverse osmosis. The quantitative characteristic of diffusion permeability is the integral permeability coefficient P_m .

The conductivity is one of the most important characteristics that determine the practical usefulness of IEMs. The value of conductivity provides rich information about the membrane

properties, since it depends on the structure, the nature and concentration of equilibrium solutions, the synthesis conditions and the polymer composition of the membrane material. The method can be used both for testing membranes in different states (for example, after synthesis or after treatment to assess the degradation degree), and for systematic studies.

The membrane permselectivity characterizes the ability of selective counter-ion transport through the membrane. This property is the most important, as it determines the application of membranes in technology. Quantitatively, the permselectivity is associated with the transport number of ion in the membrane. The transport number of counter-ions, the measure of permselectivity of IEMs, is the basic parameter determining the efficiency of electromembrane separation processes. This is related to the ratio of the concentration of ion-exchange groups in the membrane (fixed ion concentration) to the concentration of the outer solution [8]. Ionic transport number is a quotient of the current carried by an ionic component and the total current. The counter-ion transport number in modern commercial membrane in relatively dilute solutions (up to 1 M) is very close to 1 (>0.97 according to [10]) for homogeneous as well for heterogeneous membranes.

The electro-osmotic permeability of membranes is a property associated with the transfer through the membrane of a certain amount of water under the electric current [1, 11, 12]. The strength of the electric field causes electromigration of charged ions. These hydrated ions move under the action of the electric field together with the water of hydration. The water is transported by both cations and anions. Therefore, the measured volume of the transferred fluid represents the difference between the flow of water moving toward the cathode and the anode.

Voltammetry is the method to study electrochemical behavior of IEMs. The I-V curve provides information about limiting current density (LCD) values and coupled effects of concentration polarization such as water splitting phenomenon and current-induced convection (gravitational convection and electroconvection). All this extensive information can be obtained in the electromembrane system (EMS).

The measured quantities strongly depend on the used methods and experimental conditions (electrolyte nature, its concentration, temperature, stirring).

1.1.3 Methods of ion-exchange membrane modification

Modification of IEMs is a method of changing membrane structure in their bulk and/or on their surface in order to give the material new functional properties. The basic methods of membrane modification are as follows:

- chemical modification;
- mechanical modification;
- electrochemical deposition.

1.1.3.1 Chemical modification

Chemical modification of IEM refers to the chemical changes of a polymer matrix by treating it with various substances. For example, introduction of fixed charged groups in the membrane matrix changes essentially membrane properties. Recently, films from polysulfone and polyether ether ketone are used as the basis for new perspective IEMs, by treating them with chlorosulfonic and sulfuric acid, respectively [13, 14]. It is possible to obtain a set of ion-exchange, heat resistant and sufficiently strong membranes with good electrical conductivity and selectivity changing the degree of sulfonation.

Sata et al. [15] developed methods for the introducing the controlled amounts of surface-active polyelectrolytes in a charged polymer matrix. The result of these studies was the creation of electro dialysis membranes having the charge-selective properties and resistant to the fouling by surfactants. The charge-selective properties allow one to successful use of electro dialysis (ED) for the treatment of multicomponent solutions. Enhancement of electrical conductivity properties of IEMs may be achieved by introducing polypyrrole [16], viologene [17] and polyaniline (PANI) [18] into the sulfo-cationite film.

Chemical modification of industrial membranes such as Nafion[®] consisting in the change of hydrophilic properties of membranes is achieved in two ways:

- 1) the regulation of cluster formation near the fixed charged centers in the side chain is carried out at the stage of alkaline hydrolysis of sulfonyl fluoride groups by varying the concentrations and nature of the strong base (necessary for saponification) [19]. Depending on the hydration of the cation during the transition from LiOH to KOH or CsOH it is possible to obtain more or less water-saturated ion-dipole associates $[-SO_3 \dots H_2O \dots Me^+]$ and vary the swelling of the cluster zones;
- 2) carboxyl groups are introduced into the sulpho-cationite film from the receiving side of the membrane facing the anode [20] or the membrane surface is treated by amination [21] (to weaken the electro-osmotic transfer of water to the desalination chamber).

Berezina et. al [22] suggested an express method of synthesis of surface-modified membrane composites based on MF-4SK membrane (which is a Russian analogue of Nafion[®]). Composite MK-4SK/PANI membrane was obtained using the chemical synthesis of PANI through the successive diffusion of the monomer and polymerization initiator (ammonium persulfate) into water (Figs. 1-3a,b). The membrane modification by PANI results in a 2-3

fold decrease in the membrane surface roughness (Figs. 1-3c,d). This is probably due to lining of the modified size by polyaniline chains, which leads to surface smoothing.

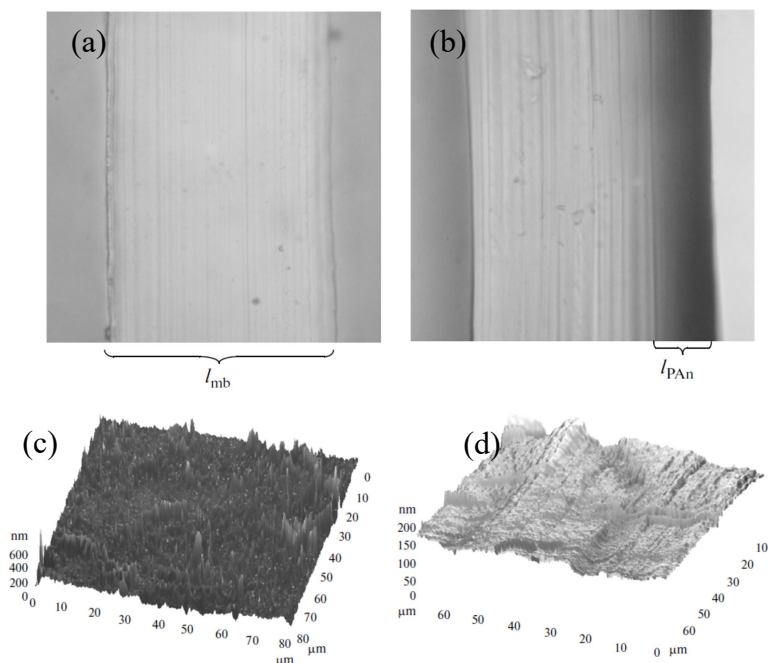


Fig. 1-3. Microphotographs of cross sections and AFM images of (a, c) the pristine and (b, d) composite sample turned (b) to polymerizing solutions, respectively (adapted from [22]).

Thermogravimetric analysis showed a higher thermal stability (590°C) of the MF-4SK/PANI membrane as compared to the pristine membrane ($405 - 550^{\circ}\text{C}$). Water transport electro-osmotically driven by the Na^+ ions is 3 times higher than that by the H^+ ions due to the difference in the transport mechanism of these ions in the electric field. The sodium ion is transported via the migration mechanism with its hydrate shell and entrains additional water molecules in dilute solutions, while the hydrogen ion moves through the membrane mainly via the Grotthuss mechanism [23]. The transport number of water in the MF-4SK membrane is 2-3 times higher in comparison with the MF-4SK/PANI composite. PANI acts as a barrier layer for water molecules. The modification by PANI causes a decrease by 50 – 70 % in the membrane diffusion permeability. Also asymmetry of diffusion permeability (about 10 %) was found for modified membrane. The diffusion permeability proved to be lower in the case of the composite orientation with its modified side turned towards the flow of electrolyte. Nevertheless, the decrease in the membrane conductivity by 85 % as compared to the pristine membrane occurs as a result of modification by PANI.

Ivanov et al. [24] explained this fact by the granular PANI morphology and existence of the so-called redox heterogeneity of PANI with the intermediate oxidation degrees. This means

the presence of well conducting regions separated by less conducting oxidized fragments in the whole polyaniline layer due to the block structure of this polymer.

In addition, polymerization of PANI on the surface of CEMs leads to a higher membrane selectivity for monovalent cations in comparison with bivalent cations [25]. Such monovalent selectivity can be useful in electrodialysis metathesis and selectrodialysis [26, 27] for concentration of divalent ions in product stream.

1.1.3.2 Mechanical modification

The methods of mechanical modification include, first of all, the production of BMs, when two oppositely charged membranes are pressed together [8, 28]. This leads to the production of a bilayer membrane, which exhibits special properties in the electric field depending on the orientation of the layers to the cathode or anode.

Mixed types of IEMs are mechanically obtained when heterogeneous membranes are formed from a mixture of cation- and anion-exchange resins and polyethylene [8]. As a result, a mosaic ion-exchange membrane is formed, containing inclusions of negatively and positively fixed ions randomly distributed in a neutral polymer matrix. Such membranes have ampholytic properties, and the electrical interactions of the heteropolar groups lead to the formation of additional pores, the proportion of which is determined by the ratio of the resins in the composition. Investigation of the properties of these membranes showed that they are capable of passing large organic ions, which is important, for example, in the ED of demineralization of sugar solutions containing impurities of coloring substances. The use of mixed type of IEMs in ED instead of AEM helps to reduce the effect of membrane fouling and increase the life of the ED apparatus.

Profiled membranes (Fig. 1-4) are obtained by hot pressing in a certain mode for the development of the membrane surface [29, 30]. The scientists of KubSU (Russia) developed new technology which involves pressing the IEMs preliminarily transformed into their swelled state [31]. The approach suggested by the authors allows one to increase the electrical conductivity of membranes and the fraction of active surface due to the destruction of the polyethylene film on the surface, which is formed in the course of hot pressing [32]. The use of profiled membranes in electro dialyzers provides higher transport numbers of counter-ions of the salt [31]; the rate of mass transfer, compared with usual smooth membranes, increases by a factor of four [33] due to the solution turbulence on the protrusions of the membrane surface and the growth of electroconvection (EC) in the over-limiting current mode.

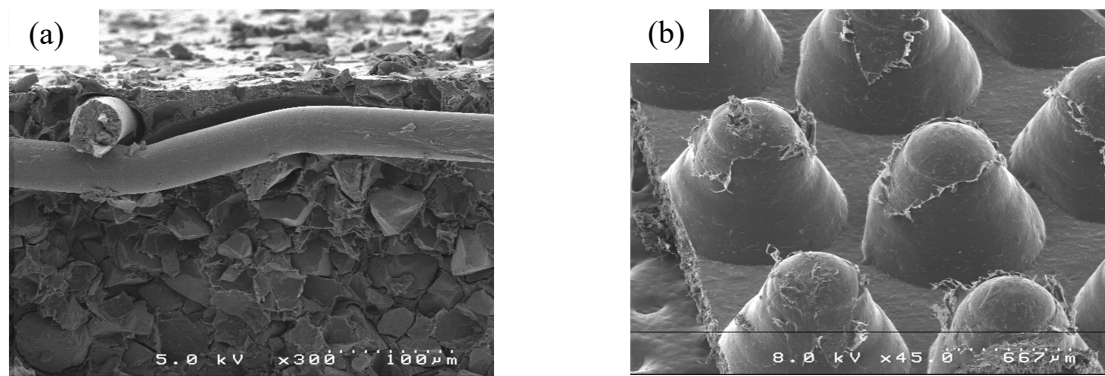


Fig. 1-4. Microphotographs of the membrane MA-40: a) initial; b) profiled (adapted from [4]).

Mechanical homogenization of heterogeneous CEMs was proposed in Refs. [34-36]. Fig. 1-5 shows SEM images of the surface and cross section of the pristine heterogeneous MK-40 membrane and its modifications.

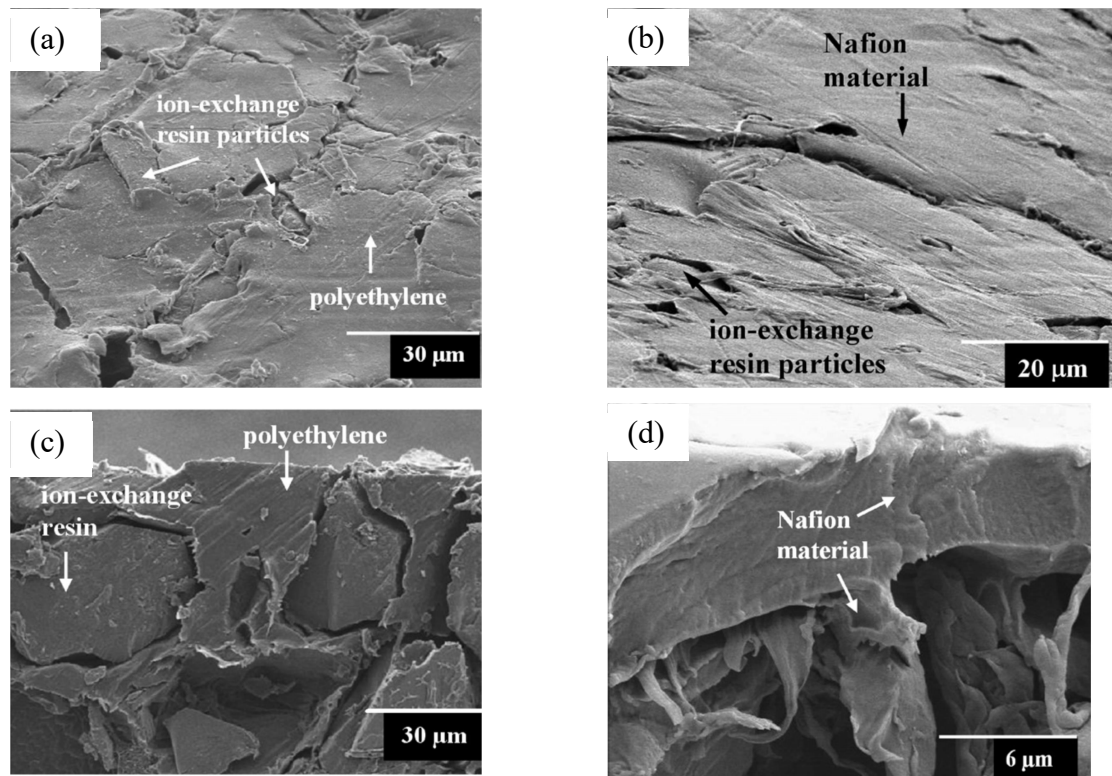


Fig. 1-5. SEM image of the surface of MK-40 (a) and MK-40*/Nf₂₀ (b) membranes and the cross section of a MK-40 (c) and MK-40*/Nf₂₀ (d) membranes (adapted from [34]).

The surface of MK-40 was modified in three ways:

- the special membrane roughing consisting of removal of a surface layer using an abrasive (MK-40*);

- the coating of roughed MK-40 membrane with a thin cation conductive layer of perfluorinated resin solution of Nafion[®] (MK-40*/Nf₂₀) (Figs. 1-5b,d);
- the coating of roughed MK-40 membrane with a thin layer of Nafion[®] dopted with a carbon material (MK-40*/Nf₂₀+CM).

An essential growth of LCD for MK-40*/Nf₂₀ membrane in comparison with other membranes (Fig. 1-6) was found [34]. There is a strong correlation between the rate of overlimiting transfer and the degree of surface hydrophobicity of studied membranes: the more hydrophobic the surface, the more intensive the overlimiting transfer. The main cause of the strong increase in the overlimiting current is the enhancement of the Na⁺ ion transport from the solution bulk to the membrane surface by EC [34].

Besides, the partial current of H⁺ ion produced in water splitting reaction was significantly lower in the case of modified membrane in comparison with the pristine one (Fig. 1-6).

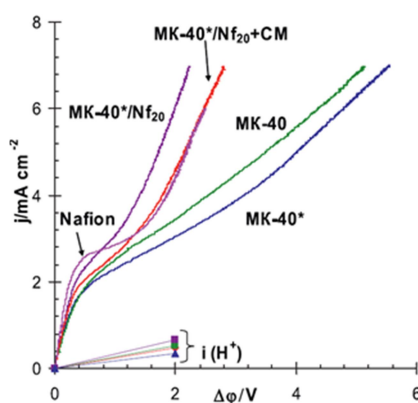


Fig. 1-6. Total current density and partial current density of ions H⁺ [$i(H^+)$] through MK-40 and its modifications (adapted from [34]).

The effects were explained by the influence of hydrophobicity on EC: the repulsion between water molecules and a hydrophobic surface cause slip of fluid over the surface. This increased electro-osmotic slip, which resulted in larger electroconvective vortices enhancing delivery of fresh solution from the bulk to the membrane surface. Moreover, the measurements of mass transfer coefficient, k , had shown the lowest k for the membrane after roughing (the MK-40* membrane) and the highest k for the MK-40*/Nf₂₀ membrane. The latter was due to the more intensive EC in the case of MK-40*/Nf₂₀ membrane. The effective transport numbers of H⁺ and OH⁻ ions in the MK-40*/Nf₂₀ are reduced by about two times and the salt-ion transfer intensified by EC increases up to 3.5 times [36].

1.1.3.3 Electrochemical deposition

Electrochemical methods include techniques for modifying the membrane surface under external electric field. In this case, a modifying additive is introduced into the solution that surrounds the membrane from the receiving side (which includes the main stream of the electrolyte ions). It was found that the introduction of an anion of dodecyl sulfate in a dilute solution of sodium sulfate in a system with an AEM leads to the electrosorption of this anion at the interface between the membrane and the solution immediately after the current is turned on [37]. As the electric current passes, the ions accumulate in the surface layer of the membrane and create a front of electrodiffusion through the entire volume of the membrane. After that, the modifying anions pass through the membrane. During this process, it is easy to observe the different state of the membrane and its properties during the transition from the modified state (a thin layer of oriented surface-active anions on the surface) to the completely saturated membrane with modifying ions. The change in transport properties indicates a weakening of the salt and ion transport due to additional obstacles. The membranes acquire new functional properties: asymmetry, charge selectivity or reduction of water transport under electric field.

Sivaraman et al. [38] used acrylic acid grafted fluorinated ethylene propylene copolymer membrane after sulfonation for electrochemical deposition of PANI on to the membrane. The deposition of PANI started from the surface of the membrane and grew up inside the membrane. The amount of PANI deposited depended upon the polymerization time. The electro dialysis experiments showed improved permselectivity for divalent cations.

Vázquez-Rodríguez et al. [39] studied the effect of synthesis conditions on the transport properties of commercial CMX membranes modified electrochemically by polypyrrole (Ppy). The quantity of Ppy in CEM, compactness of Ppy, and the charges on Ppy (negative or positive) were controlled effectively by changing the electrosynthesis conditions. The presence of Ppy in the membranes decreased the transport number of Na^+ and Mg^{2+} , and the reduction in transport number was more significant for Mg^{2+} .

These examples show that the membrane modification creates a sufficiently thin surface layer corresponding to small degrees of membrane saturation with a modifying component. In this case the surface has barrier functions, and in the membrane phase arises a new interface.

1.2 Application of ion-exchange membranes

ED and processes such as electrodialysis with bipolar membranes (EDBM), fuel cells are all based on IEMs and an electrochemical potential as driving force. But the process design and their applications can be rather different.

1.2.1 Conventional electrodialysis

Schematic diagram illustrating the principle of conventional ED is shown in Fig. 1-7. A series of AEMs and CEMs arrange in an alternating pattern between two electrodes. The AEMs and CEMs are separated by a spacer gasket and form individual chambers. If an electrolyte solution is pumped through these chambers and an electrical potential between the electrodes is applied the cations and anions migrate towards the cathode and anode respectively. Cations pass through the CEM membrane but they are retained by the AEM. Also the anions pass through the AEM but are retained by the CEM. The overall result is that an electrolyte is concentrated in alternate chambers while the other solutions are depleted of ionic components.

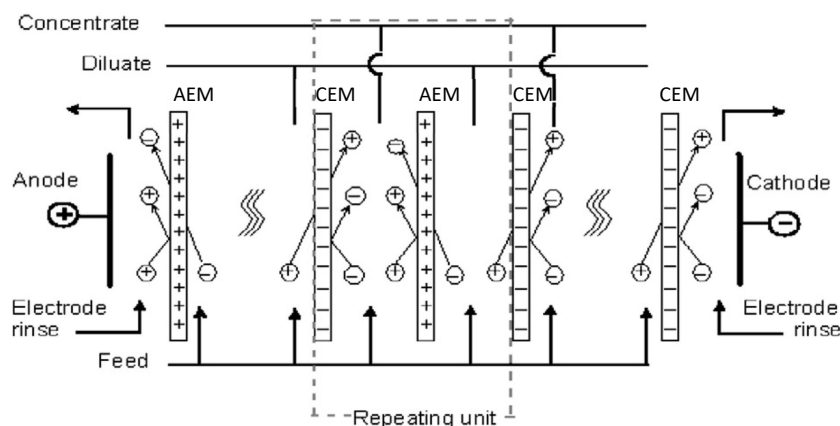


Fig. 1-7. Schematic diagram illustrating the principle of electrodialysis (adapted from [40]).

A cell pair consists of a CEM, an AEM, a concentration and desalination chambers. 100 to 200 cell pairs are arranged between the electrodes in an industrial size electrodialysis stack. Various spacer and stack constructions such as the so-called sheet flow or tortuous path flow stack design are used in practical applications [41]. The concept of a sheet flow stack is illustrated in Fig. 1-8. In a tortuous path stack design the membranes and spacers are arranged horizontally in a stack.

The spacers not only separate the membranes, they also contain the manifold for the distribution of the two different flow streams in the stack and provide the proper mixing of the solutions in the chambers.

The main difference between the sheet flow and the tortuous path flow spacer is that in the sheet flow spacer the chambers are vertically arranged and the process path is relatively short. The flow velocity of the feed is between 2 and 4 cm s⁻¹ and the pressure loss in the stack is correspondingly low, i.e. between 0.2 and 0.4 bar. In the tortuous path flow stack, the membrane spacers are horizontally arranged and have a long serpentine cut-out which defines a long narrow channel for the fluid path. The feed flow velocity in the stack is relatively high, i.e. between 6 to 12 cm s⁻¹ which provides a better control of concentration polarization and higher limiting current densities, but the pressure loss in the feed flow channels is quite high, i.e. between 1 and 2 bar.

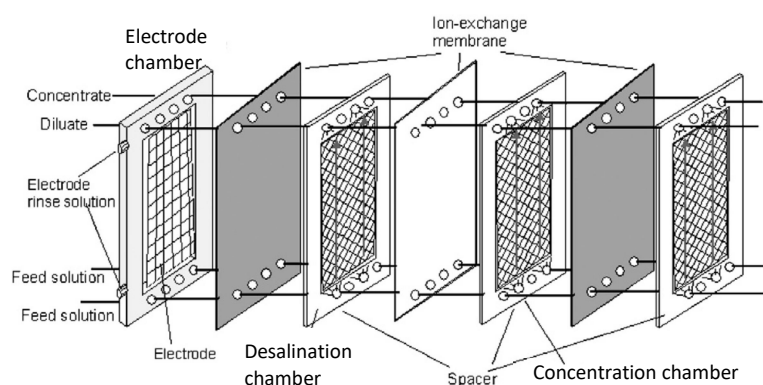


Fig. 1-8. Schematic drawing illustrating the construction of a sheet flow stack design (adapted from [40]).

Besides the presented stack designs, which are used in industry, there is a number of lab-cells used for studying membrane properties (see section 1.3.3.3).

1.2.2 Reverse electrodialysis

The production of energy by mixing fresh and sea water through IEMs is a process referred to as reverse electrodialysis (RED). RED system includes salt and fresh water chambers, IEMs, electrodes and electrode chambers with a suitable redox couple [7]. In RED process the fresh water chamber is placed between the salt water chambers (Fig. 1-9).

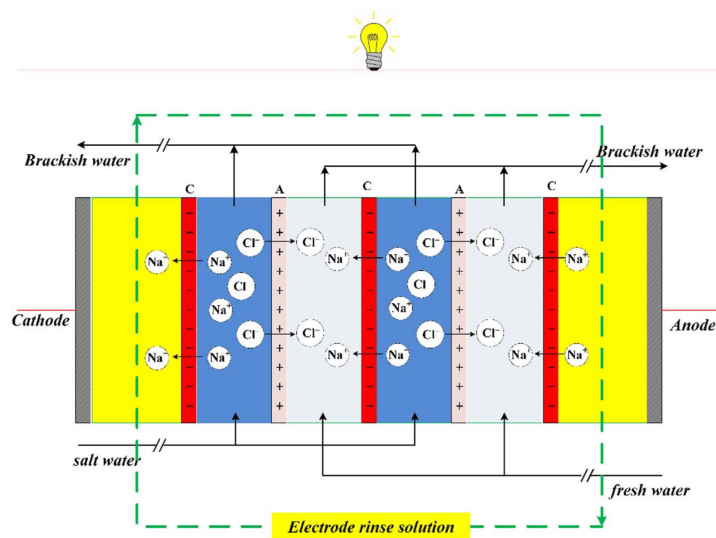


Fig. 1-9. Schematic drawing illustrating the RED system (adopted from [7]).

The chambers are separated by a CEM on the one side and an AEM on the other side. Due to the difference in concentration in salt and fresh water chambers, the cations and anions diffuse into the fresh water chambers [7]. The ionic diffusion flux generates an electrochemical potential. Electrodes receive the ions and convert them into an electrical current through an oxidation or reduction reaction. The electrical current generated is captured directly by an external load. The membrane can generate potential difference of around 30 mV with high internal resistance in mimicking sea water and river water [42].

The practical application of RED process is limited by the presence of multivalent ions in the seawater and river water sources. Therefore, IEMs with high selectivity for monovalent/multivalent ions are very beneficial for RED applications.

1.2.3 Electrodialysis metathesis

Electrodialysis metathesis (EDM) is used to maximize water recovery and produce concentrated salts from brines obtained as reject or secondary product in other membrane processes, e.g. reverse osmosis [43]. EDM is modified from the conventional ED. In the EDM system, four alternating IEMs form a repeating quad of four chambers and a substitution solution is added to provide the exchangeable ions for the metathesis reaction (Fig. 1-10) [44]. In the reaction, the feed solution, represented by MX , exchange cations and anions with the substitution solution, $M'X'$, to form new product salts, $M'X$ and MX' . For this purpose, two of the chambers contain the feed and a substitution solution, and are called dilute 1 (D1) and dilute 2 (D2) chambers, respectively. The other two chambers contain each the newly formed non-precipitating product salts, and are called concentrate 1 (C1) and concentrate 2 (C2)

chambers (Fig. 1-10). Depending on the intended product solution in the two concentrate chambers, an appropriate substitution salt solution is fed to the D2 chamber to initiate the double decomposition reaction with the feed solution from the D1 chamber. Salts formed in the C1 chamber are predominantly rich in anions and poor in cations from the D1 chamber. Salts formed in the C2 chamber are predominantly rich in cations and poor in anions from the D1 chamber. When sodium chloride is added as the substitution solution, the C1 chamber contains mixed sodium salts, and the C2 chamber contains mixed chloride salts [44].

The membrane selective to the transfer of singly charged ions can be used for mitigation of the scaling and fouling in the concentrate chamber when applying electro dialysis metathesis. The design of electro dialysis stack is organized in a way that there are two concentrate chambers. There are singly charged cations (such as Na^+) and multicharged anions (SO_4^{2-}) in one chamber, multicharged cations (such as Ca^{2+}) and singly charged anions (Cl^-) in the other one.

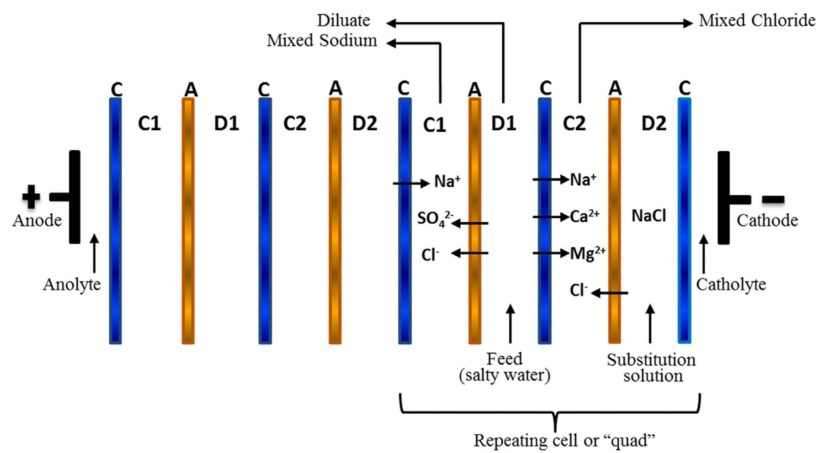


Fig. 1-10. Schematic diagram of the EDM process (adopted from [44]).

1.2.4 Bipolar membrane electro dialysis

The conventional ED can be combined with BMs and utilized to produce acids and bases from the corresponding salts [45]. In this process CEMs and AEMs are installed together with BMs in alternating series in an electro dialysis stack (Fig. 1-11). A typical repeating unit of an electro dialysis stack with BMs is composed of three chambers, two monopolar membranes and a BP. The chamber between the monopolar membranes contains a salt solution and the two chambers between the monopolar and the BMs contain, respectively, a base and an acid solution.

When an electrical potential gradient is applied across a repeating unit, protons and hydroxide ions generated in the membrane bipolar junction produce an acid and a base, respectively. The

process design is closely related to that of the conventional ED using the sheet flow stack concept. However, because of the significantly higher voltage drop across a BM, only 50 to 100 repeating cell units are placed between two electrodes in a stack.

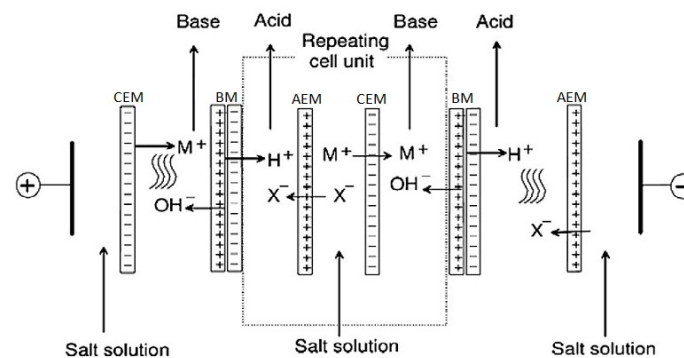


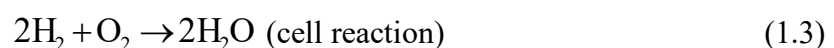
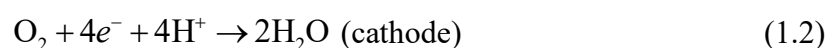
Fig. 1-11. Schematic drawing illustrating the principle of electrodiolytic production of acids and bases from the corresponding salts with bipolar membranes (adopted from [40]).

The utilization of EDBM to produce acids and bases from the corresponding salts is economically very attractive and has a multitude of interesting potential applications in the chemical industry as well as in biotechnology and water treatment processes.

1.2.5 Fuel cells

Fuel cells are electrochemical devices with high energy conversion efficiency, minimized pollutant emission and other advanced features. Proton exchange membrane fuel cells (PEMFC) are considered as a key issue against oil rarefaction and green house gas emissions [46]. High temperature PEMFCs have been proposed to solve problems of catalyst poisoning by CO and fuel cell electrode flooding, as well as to improve fuel cell efficiency, reduce the amounts of noble metal catalyst and avoid reactant humidification [47].

The power generating system in PEMFCs is an electrochemical reaction involving gases such as hydrogen, methanol, and ethanol. The reactions occurring in the fuel cell could be elucidated as follows:



The working principle of the fuel cell is schematically illustrated in Fig. 1-12. The hydrogen ions at the anode move to the cathode through the electrolyte membrane, which produces the electrical current with water as a by-product [48].

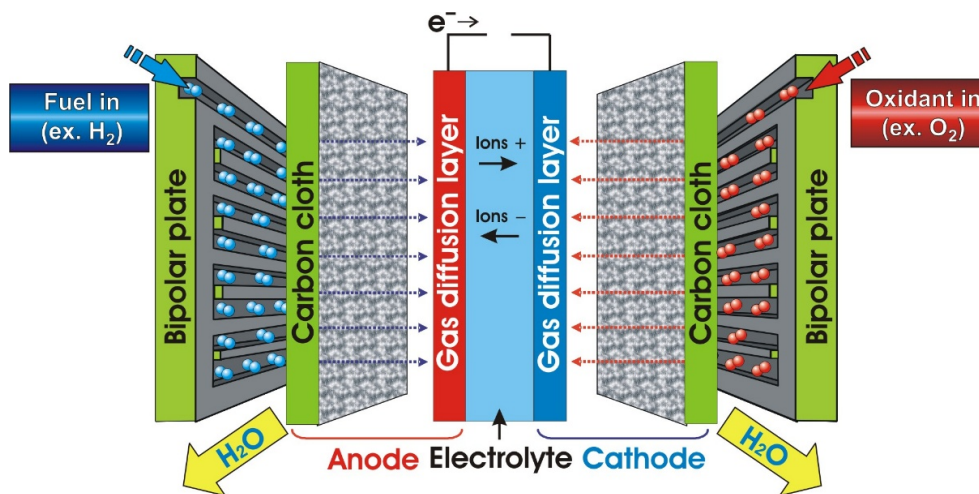


Fig. 1-12. Scheme diagram illustrating the structure of PEMFC and the principle of operation (adopted from [49]).

The key component of the PEMFCs is the polymer electrolyte membrane (PEM), which functions as an electrolyte to transfer the protons from the anode to the cathode, and provides a barrier to the passage of the electrons and fuel. Therefore, several researchers have focused on the development of reliable, high performance PEMs with high proton conductivity, low fuel permeability, high oxidative stability, good mechanical stability and low cost of fabrication of membrane electrolyte and assembly.

1.3 Concentration polarization and coupled effects of concentration polarization in electromembrane system

1.3.1 Concentration polarization in electromembrane system

Let us consider a concentration profile of an electrolyte in an IEM and the adjoining diffusion layers of an EMS (Fig. 1-13). Within the membrane, we consider the virtual electrolyte solution, which is in local equilibrium with a thin layer of membrane [50]. As there is equilibrium at the membrane boundaries, the real concentration in the solution and the virtual concentration in the membrane there are identical and the concentration profile is continuous (Fig. 1-13). When a direct current passes normal to the IEM, the counter-ions from the solution pass through the IEM by migration and diffusion. Due to the fact that the counter-ion

transport numbers in the membrane, \bar{t}_i , are almost twice as large as in the solution, t_i , the electrolyte concentration decreases near the membrane in one (desalination) chamber, C_1 , and increases in the neighboring (concentration) chamber, C_2 (Fig. 1-13). The phenomenon of concentration variation under the effect of electric current is called concentration polarization (CP).

The ion transport in solution or membrane is described by the extended Nernst–Planck equation with a convective term:

$$\vec{j}_i = -D_i \left(\nabla C_i + z_i C_i \frac{F}{RT} \nabla \varphi \right) + C_i \vec{V} \quad (1.4)$$

Here \vec{j}_i , D_i , C_i and z_i are the flux density, diffusion coefficient, concentration and charge number of ionic species i respectively; φ is the electric potential; F is the Faraday constant; R is the gas constant; T is the temperature; \vec{V} is the fluid velocity vector. The first term in the right-hand side of Eq. (1.4) represents diffusion, the second, migration, and the third, convection.

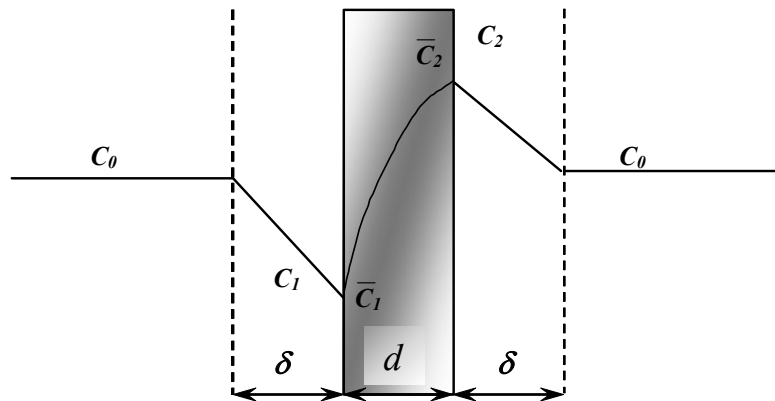


Fig. 1-13. Concentration profile in an EMS. C_0 is the electrolyte concentration in the bulk solution; C_1 and C_2 are the electrolyte concentrations at the boundaries between the diluate and concentrate diffusion layers and the membrane, respectively; the bar over the letter designates that the quantity relates to the membrane phase; δ and d are thickness of diffusion layer and membrane, respectively.

The current density, \vec{i} , is the sum of flux densities of all ionic species taking into account their charges:

$$\vec{i} = F \sum_i z_i \vec{j}_i \quad (1.5)$$

With a gradual increase in the electric current under these conditions the salt concentration near the membrane surface in desalination chamber, C_1 , is decreasing and tends to zero. The current density is determined by the bulk solution concentration, C_0 , and takes a critical value, called the limiting current density, i_{lim} , when $C_1 \ll C_0$:

$$i_{\text{lim}} = \frac{FDC_0}{(\bar{t}_i - t_i)\delta} \quad (1.6)$$

Here D is the electrolyte diffusion coefficient. Eq. (1.6) was first obtained by Peers in 1956 [51]. It can be seen that i_{lim} also depends on the difference in the ion transfer numbers in the phase of the membrane and the solution and on the thickness of the diffusion layer. Consequently, the polymer selectivity, the nature of the counter-ions and the convection of the solution will be reflected in the value of the limiting current.

Thus, following the classical electrochemical interpretation presented above, the formation of concentration gradients results in saturation of the current density caused by the vanishing interface concentration. When the current density tends to its limiting value, i_{lim} , the potential drop over a membrane surrounded by two diffusion boundary layers tends to infinity. However, in real EMS the limiting current density can be exceeded in several times at the expense of the emergence, near the membrane surface, of a complex of effects that are caused by concerted action of the flowing current and concentration variations in the system. These effects may be united by the term “coupled effects of concentration polarization”.

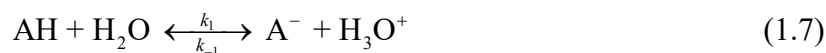
1.3.2 Coupled effect of concentration polarization in electromembrane system

1.3.2.1 Water splitting

Two effects explaining the overlimiting mass transfer are connected with the water splitting reaction at the membrane/solution interface. The emergence of additional charge carriers H^+ and OH^- ions that are generated during the water splitting in membrane systems [52], for a long time was considered as the principal and, frequently enough, sole, reason for the overlimiting mass transfer [53].

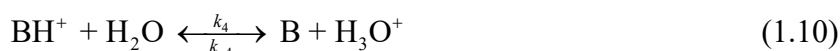
The water splitting reaction cannot occur in solution, it takes place rather within a thin layer in membrane. Indeed, there are several peculiar effects explaining the high rate of water splitting within the membrane interface. Simons [54] has proposed that the H^+ and OH^- ions

are generated in the course of protonation and deprotonation reactions involving the fixed charged groups as catalytic centers and water. These reactions for CEMs can be written as:



Here AH is a neutral acid; k is the chemical reaction rate constant.

For AEMs, similar reactions occur:



Here B is a neutral base, such as tertiary amine.

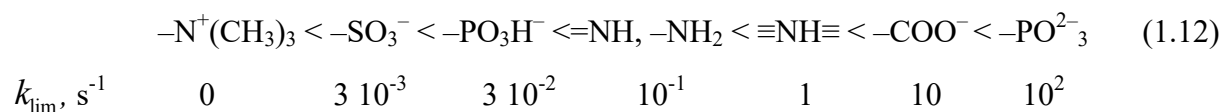
These proton-transfer reactions take place in a thin, about 2 nm of thickness, reaction layer of the membrane adjoining to the depleted solution. In the case of CEM, the protons produced by reaction (1.7) leave the reaction layer for the membrane bulk, under the action of applied current, while the hydroxyl anions produced by reaction (1.8) migrate into the adjacent depleted solution. In BMs, the protonation and deprotonation reactions take place at the junction of the cation- and anion-exchange layers [55-57].

The backward reactions of recombination in reactions (1-7, 1-8, 1-9, 1-10) are normally rapid, the rate constants k_{-n} ($n=1,2,3,4$) are of the order of 10^{10} ($\text{M}^{-1} \text{s}^{-1}$) [58], while the forward reactions of dissociation depend strongly on the nature of the functional groups. The dissociation rate constants at equilibrium can be expressed in the following form, e.g. for reactions (1.7) and (1.8):

$$k_1 = K_a k_{-1}; \quad k_2 = \frac{K_w}{K_a} k_{-2} \quad (1.11)$$

where K_a is the acid-dissociation equilibrium constant. Following Simons [59], note that if $\text{p}K_a$ is close to 7, k_1 and k_2 are of approximately equal magnitude. When $\text{p}K_a$ increases by 1 unit (K_a decreases in 10 times), k_1 decreases and k_2 increases in 10 times, hence, reaction (1.7) becomes rate limiting. If $\text{p}K_a$ decreases by several units, k_1 increases and k_2 decreases in corresponding number of times, and reaction (1-8) becomes rate limiting.

It is possible to range the ion-exchange groups (fixed to a membrane matrix) in the order of increasing water splitting as follows [55, 57]:



Here k_{lim} is the rate constant corresponds to the step limiting reaction.

At the same time, water splitting reaction gives rise to another mechanism of the overlimiting transfer. This is the effect of exaltation of limiting current [60]. Yu.I. Kharkats [61] explored the effect of exaltation of limiting current in relation to EMS for the first time. The emergence of the H^+ and OH^- ions in the vicinity of the membrane surface perturbs electric field and is capable of increasing (exalting) transfer of counter-ions of a salt. For example, the OH^- ions generated at the interface depleted diffusion layer/CEM surface attract the cations from the bulk solution towards the membrane interface. Taking into account the effect of exaltation the flux density of salt counter-ions, j_1 , is described:

$$j_1 = \frac{2D_1C_0}{\delta} + \frac{D_1}{D_w} J_w \quad (1.13)$$

Here index 1 is the counter-ion; D_w and J_w are the diffusion coefficient and the flux density of the products of the water splitting reaction that are generated near the surface of a membrane (in the case of a CEM, these are the OH^- ions).

The increase in the flux of salt counter-ions due to the effect of exaltation of limiting current in EMS is relatively small. For example, it is about $0.2j_1^{\text{lim}}$ when the flux of OH^- ions reaches the values equal to j_1^{lim} . In practice, the increment flux of salt counter-ions is much higher [62, 63], therefore, it can not be explained only by the effect of exaltation of limiting current.

1.3.2.2 Gravitational convection

Gravitational convection arises due to the non-uniform distribution of solution density, which causes Archimedean volume force bringing the liquid in motion [64, 65] (Fig. 1-14). Solution is more diluted near the membrane then in the bulk. Moreover, its temperature is elevated due to Joule heat within a layer with high electric resistance. As a result, near the surface, the Archimedean buoyant force acts upon a parcel of fluid vertically upward, while in the bulk, the body force applied to a parcel of fluid acts in opposite direction. This couple of forces produces vortex motion of the fluid in the space near the membrane.

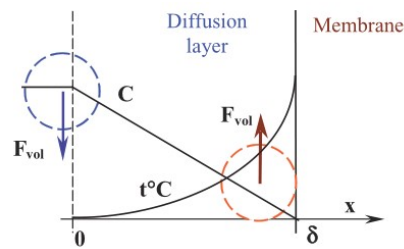


Fig. 1-14. Scheme of gravitational convection (adapted from [66]).

Consider a solution layer situated between two solid plates. When the plates are vertical and the density gradient in the solution is horizontal, the gravitational convection arises without threshold [64]. When the plates are horizontal and the density gradient is vertical, two cases are possible. If the lighter solution sublayer (depleted boundary layer) is on the top of the solution layer (hence, just under the top plate), no convection arises. If the lighter sublayer is at the bottom, there is a threshold in development of the gravitational convection determined by the Rayleigh number, Ra [64, 65]:

$$Ra = \frac{\Delta\rho}{\rho} \frac{gX_0^3}{\nu D} \quad (1.14)$$

Here g is the free-fall acceleration; ν is the viscosity; X_0 is the characteristic distance where the variation in the solution density, ρ , takes place; $\Delta\rho$ is the variation of ρ within X_0 .

If the region of solution density variation spreads from the one plate to the other, X_0 is equal to the distance between the plates. Otherwise, X_0 is less than the distance between the plates, being more close to the diffusion boundary layer (DBL) thickness near a plate [67, 68].

1.3.2.3 Electroconvection

EC is the main mechanism of the mass transfer enhancement through the IEM in ED for the treatment of dilute solutions in overlimiting regimes [65, 69-71]. EC is an entrainment of fluid molecules by ions forming a space charge region (SCR) at the surface of IEM under the electric field [72].

EC can develop according to different mechanisms depending on the applied voltage and other conditions (Fig. 1-15).

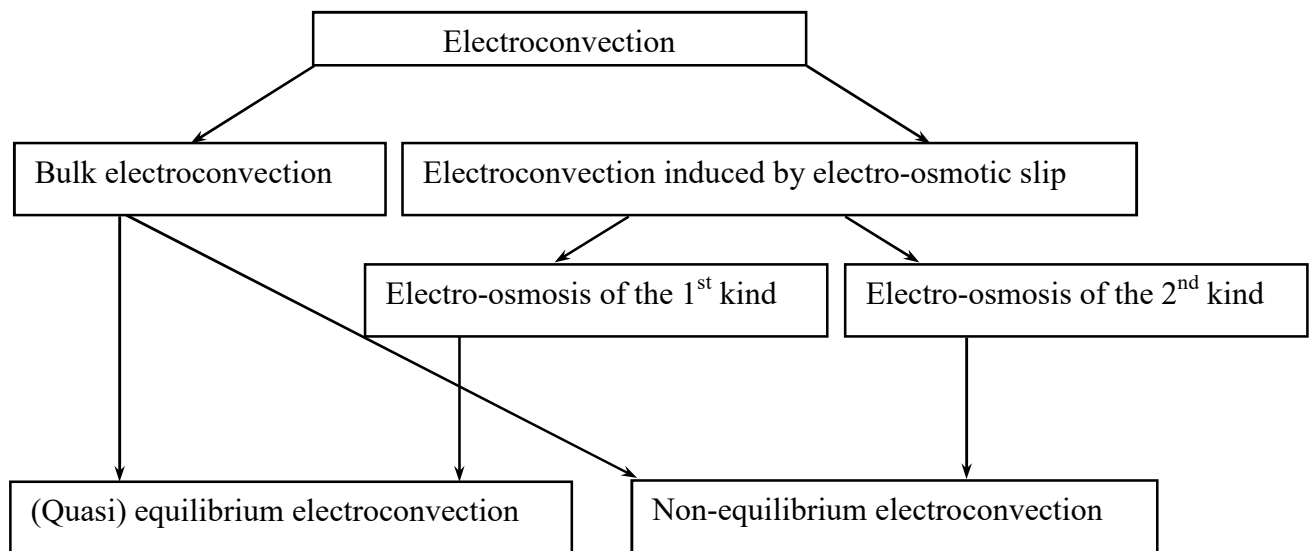


Fig. 1-15. Mechanisms of electroconvection.

Theoretically [73-75] there are two main mechanisms of EC:

- bulk EC caused by the action of an electric field upon the residual space charge of a (quasi) electroneutral strong electrolyte with a non-uniform concentration distribution;
- EC induced by electro-osmotic slip in SCR forming at the interface depleted solution/ion-selective membrane surface. Dukhin [76] and Mishchuk [77] proposed to distinguish two principal kinds of the current-induced electro-osmosis:
 - Electro-osmosis of the 1st kind occurs as the electrolyte slip caused by the action of the imposed tangential electric field upon the diffuse part of the electric double layer (EDL), which remains (quasi) equilibrium;
 - Electro-osmosis of the 2nd kind occurs as the electrolyte slip caused by the action of the imposed tangential electric field upon the extended non-equilibrium SCR of the EDL.

The bulk and the current-induced electro-osmosis may be (quasi) equilibrium and non-equilibrium. At small currents/voltages, when the EDL at the interface depleted solution/IEM surface is (quasi) equilibrium (the structure of its diffuse part preserves the Boltzmann ion distribution, shifted by the action of the external field [78]), there is a (quasi) equilibrium EC. In contrast to the (quasi) equilibrium EC [75], a non-equilibrium EC develops in the overlimiting current regimes. In this case, the electro-osmosis of the 1st kind transforms into the electro-osmosis of the 2nd kind [79, 80]. A feature of this kind of EC is the presence of an extended SCR (Fig. 1-16) that is located outside the EDL.

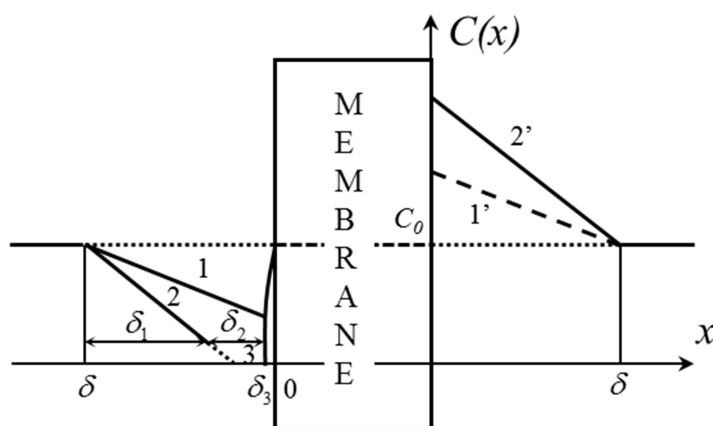


Fig. 1-16. Profiles of ion concentration: the distribution of electrolyte concentration near membrane surface at lower (curves 1, 1') and higher (curves 2, 2', 3) voltage; δ is the overall diffusion layer thickness; δ_1 , δ_2 and δ_3 are the thicknesses of the electrically neutral region, extended SCR and quasi-equilibrium SCR, respectively; C_0 is the bulk electrolyte concentration. The difference between counter-ions (curve 2) and co-ions (curve 3) concentrations near the left membrane side corresponds to the appearance of the SCR (adapted from [81]).

As mentioned above, the tangential electric field is required for the development of electro-osmosis of the 1st and 2nd kind. The tangential electric field can be due to the electrical and/or geometrical heterogeneity of the membrane surface [74, 82], as well as the non-uniform lateral concentration distribution [83]. Also, electro-osmotic slip can appear as a result of spontaneous perturbation of an initially homogeneous electric field [73]. In the case of forced flow of a solution in the electro dialysis chambers, the reason for the non-uniform concentration distribution is the partial desalination of the solution increasing as the solution moves along the chamber. It causes an increase in the solution resistance along the longitudinal coordinate and, as a consequence, the electric current lines condense near the entrance to the chamber [83].

EC induced by electro-osmotic slip can arise both in a no-threshold and threshold modes. In the first case, there is a stable EC due to the action of a stable tangential electric field upon the SCR, the main part of which is made up of a quasi-equilibrium EDL. This type of EC develops in the membrane system at relatively low currents/voltages (corresponding to the linear part of the I-V curve and to the part of the inclined plateau where the curve is smooth). Usually, the contribution of a stable EC to mass transfer is negligible. In the second case, a hydrodynamically unstable EC develops. The reason for the instability when a certain voltage threshold is reached is the appearance of a positive feedback between the fluctuation of the

local tangential force and the electro-osmosis slip velocity [73, 74, 84]. The tangential force is directed from the depleted solution region at the membrane surface to the region where the solution is enriched due to the rotation of the vortex, which brings a relatively concentrated solution out of the volume. If the force grows for some reason, it will lead to an increase in the rotation speed of the vortex and an increase in the electrolyte concentration at the surface, which in turn will cause an increase in the tangential electric force.

1.3.3 Methods for studying the concentration polarization in an electromembrane system

Voltammetry [39, 85, 86], chronopotentiometry [87, 88], chronoamperometry [89-91] impedance [92-94], optical methods [95-97], as well as methods for pH measurement [98, 99] and ion transport numbers [100-103] are used for IEM concentration polarization. Hereafter we give a short review of these methods with focusing attention on those methods, which will be used in our research.

Optical methods (laser interferometry, schlieren-method, etc.) are especially convenient for studying the CP in membrane systems. Even an insignificant change in concentration causes a sufficiently large change in the refractive index of the solution [104] and leads to a shift in the interference fringes. The most informative of these methods is laser interferometry based on recording an interference pattern between a wave reflected from the object under study and a reference wave. If an optical disturbance arises in the region of the reflected wave from the object, then, where the path difference reaches a value that is a multiple of the wavelength, a dark band appears. The method of laser interferometry allows one to determine the local electrolyte concentrations in desalination and concentration chambers of complex geometry. The minimum distance from the surface of the membrane on which measurements are possible is several micrometers ($\approx 10 \mu\text{m}$).

The most common methods of voltammetry and chronopotentiometry are the galvanostatic one [104]. The constant current is passed through the experimental cell until the steady values of potential are reached in the galvanostatic method. I-V curve obtained with a linear current sweep are called galvanodynamic curves. These methods are the most common tools for studying the electrochemical characteristics of membrane systems. As the IEMs are conductors of the second kind, they must be located between two polarizing electrodes to ensure the current flows into the EMS. There are quite a few modifications of equivalent electrical circuit for studying the CP in EMS. The most commonly used four-electrode cell (Fig. 1-17). In this setup, the cathode and anode are located parallel to the membranes and

limit the membrane package. The current is applied between the working (anode) and the counter (cathode) electrodes. The potential drop (PD) across the membrane under study, $\Delta\phi$, is measured using sense and reference Ag/AgCl electrodes. These electrodes are placed in the Luggin capillaries. The Luggin tips are installed at both sides of the membrane under study in its geometric center at a distance of about 0.5 mm from the surface. The PD between sense and reference Ag/AgCl electrodes in the electrolyte solution (without the membrane) is zero. To prevent the ingress of electrolysis products from the near-electrode to the premembrane chambers, they are separated by auxiliary CEM and AEM. In this case, the AEM separates the investigated membrane from the anode chamber, the CEM from the cathode membrane.

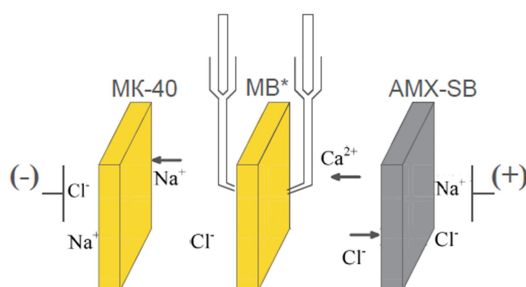


Fig. 1-17. Principal scheme of the four-electrode cell.

1.3.3.1 Voltammetry

The typical form of the I-V curve of the IEM and the methods for determining the limiting current density, i_{lim} are shown in Fig. 1-18. Three characteristic regions with different slopes to the potential axis can be distinguished on I-V curve of the IEM. The slope of the initial linear section is determined by the electrical resistance of the unpolarized membrane and the adjacent diffusion layers, as well as the solution layers enclosed between the external diffusion layer boundary and the tips of the Ag/AgCl electrodes. As well, the Donnan interfacial PDs having diffusion nature contribute to the overall voltage. The CP increases linearly with the current density, and therefore is often called the ohmic region [105], while it is not strictly correct, since the overall voltage involves also the diffusion PDs. This region is limited by the i_{lim}^{exp} value. At $i > i_{lim}^{exp}$ the increase in the resistance of the depleted diffusion layer caused by the concentration polarization leads to a nonlinear increase in the voltage with increasing applied current.

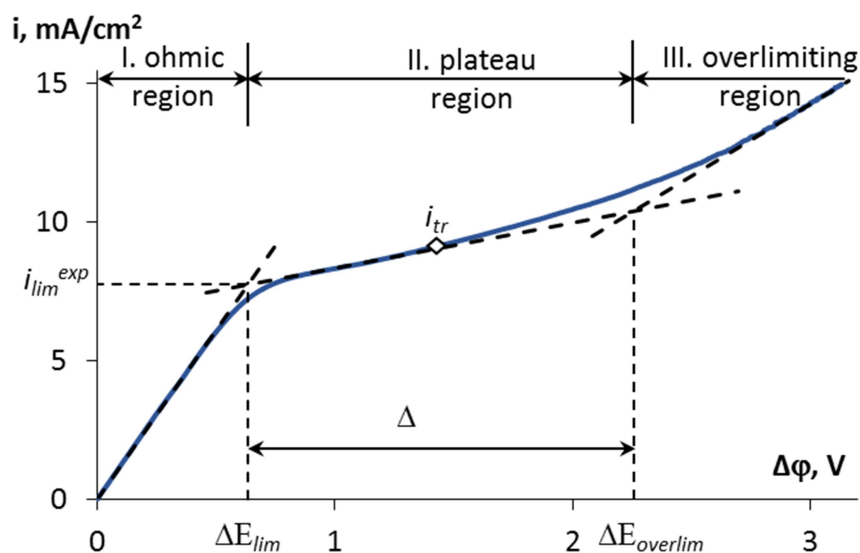


Fig. 1-18. Typical I-V curve.

A sharp increase in the PD in second region indicates that the salt concentration at the membrane/solution interface becomes small compared to the salt concentration in the bulk solution. This region is called "plateau" or "limiting current" region. It corresponds to the maximum ion transfer rate, controlled by diffusion through the diffusion layer. In membrane systems, there is always a current increase in this region, which is mainly due to a decrease in the thickness of the diffusion layer, caused by the development of various types of coupled convection. Another reason for the current increase in the second region can be a non-simultaneous achievement of the limiting state due to heterogeneity of a membrane surface. At the beginning, the limiting current is reached in the areas where the thickness of the diffusion layer is large, with a further increase in the PD the limiting state extends to regions with smaller thickness.

The third region corresponds to a higher growth rate of current density, which is usually associated with the development of water splitting reaction and/or the appearance of additional current carriers. The inflection point i_{tr} in plateau region corresponds to the transition state from the trend in the concentration polarization development in this region to a faster increase in current in the overlimiting region.

The characteristic point of the I-V curve is the intersection of the tangents drawn to the ohmic and plateau regions. The intersection point of the tangents i_{lim}^{exp} characterizes another transition state, when the linear section of increasing CP is replaced by an inclined plateau corresponding to the spread of the limiting state along the membrane surface [106] and the

development of coupled convection. Thus, $i_{\text{lim}}^{\text{exp}}$ characterizes the state when the limiting current density is reached at least on the conductive areas of the membrane surface.

The accuracy of determining the point i_r of the I-V curve can be increased [107] if one takes into account that the extremum of the first derivative of this curve corresponds to the inflection point.

1.3.3.2 Chronopotentiometry

Chronopotentiometry is one of the most informative methods for studying the bulk and surface properties of IEMs. It consists in measuring the PD in the membrane system as a function of time at a constant current density. This method was first applied to electrode systems in electrochemistry and subsequently, practically without changes, was used for the membrane study. The main advantage of chronopotentiometry in comparison with other dynamic methods (impedance, voltammetry) is a direct study of the contribution of different regions (layers, heterogeneities) of the membrane system to the overall PD.

The typical chronopotentiogram (ChP) for a system with a homogeneous IEM obtained with an overlimiting current regime is shown in Fig. 1-19. The ChP can be divided into several parts. At time zero the experiment is started but no current is applied yet and since the solutions on either side of the membrane are equal, the voltage drop remains zero. When the fixed current is switched on an instantaneous increase in PD occurs (Fig. 1-19). This increase is due to the initial ohmic resistance of the system composed of solution and membrane between the tips of the voltage measuring capillaries.

After the increase in voltage due to the ohmic resistance, part b commences corresponding to the slow growth of PD up to the inflection point 2. It is caused by a drop in the electrolyte concentration near the membrane from the side of the desalination chamber. In this case, the transport of electrolyte from the solution bulk to the membrane surface has an electrodiffusion character. At a certain time this is followed by a strong increase in PD (part c). The point at which this increase occurs is the transition time, τ , (point 2). After the inflection point 2, the convective transfer plays an important role in the delivery of ions. It should be noted that the inflection point occurs on the ChP only at $i > i_{\text{lim}}^{\text{exp}}$, otherwise there is no pronounced change in the delivery mechanism of the electrolyte with the connection of convective transfer. After point 3, the membrane system goes into a stationary state, in which no noticeable changes in the PD occur. The PD in part e is equal to the ohmic PD of the polarized membrane system after the current is turned off. The last segment of the curve describes the process of

relaxation of the membrane system, consisting in the resorption of the concentration gradients formed during the electrical current flow.

An important characteristic of non-stationary ion transport is transient time [108]. In mathematical models that do not take into account convective transport, this moment corresponds to the drop of the concentration at the membrane/solution boundary to zero, with the PD becoming equal to infinity. In real systems, at this point, the mechanism of ion delivery to the surface of the membrane changes. There are some difficulties in determining the transition time from the ChP. Krol and co-authors [108] proposed a method for determining τ from the intersection point of the tangents to the regions of slow and rapid growth of the PD in part c.

Also in the literature there is a method to find the transition time as the inflection point (point 2), located in the segment, where two mechanisms of electrolyte delivery are present. The first one is electrodiffusion, the second one, current-induced convection. The contribution of the convective component gradually increases after passing the inflection point. Increasing convective contribution allows system to reach a (quasi) steady state. It follows from this analysis, that the position of the inflection point gives a more accurate estimation of the transition time.

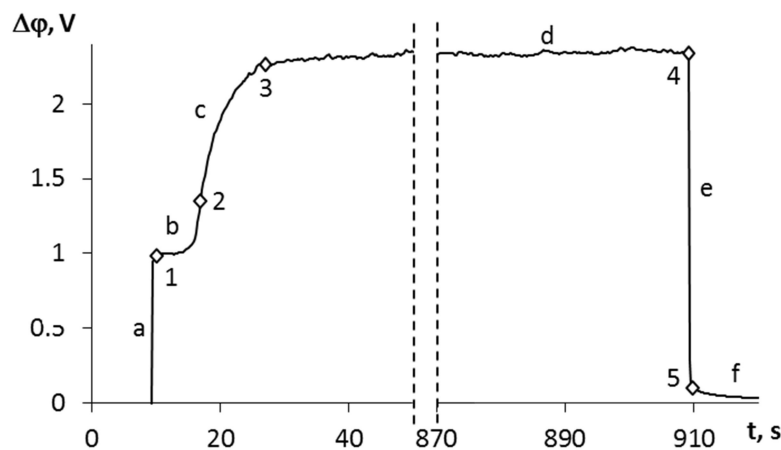


Fig. 1-19. Characteristic points of the chronopotentiogram.

It should be noted that for the homogeneous membrane under the electrodiffusion mechanism of ion transport within the framework of the semi-infinite diffusion model, Sand obtained an expression for the transition time in 1901 [109]

$$\tau = \frac{\pi D}{4} \left(\frac{C_0 z_i F}{\bar{i}_i - i_i} \right)^2 \frac{1}{i^2} \quad (1.15)$$

Here i is the applied current density. The transition time reaches a minimum with an ideally selective membrane $\bar{t}_i = 1$ and increases with increasing co-ions transfer through the membrane.

The determination of the connection between the transition time and the heterogeneity of the membrane surface is also of great interest. Thus, Krol and co-authors [108] experimentally determined the transition time for systems with heterogeneous membranes. This value turned out to be less than theoretical transition time (Eq. 1.15). The authors thought that the local current density at the conducting regions of the heterogeneous membrane is above the average over the surface.

The difference in the surface structure and internal structure of different types of membranes is reflected in their electrochemical properties, which can be seen on ChPs. If the surface is practically homogeneous, as in the case of AMX, the current lines are uniformly distributed over the surface (Fig. 1-20a), and the electrolyte concentration in the solution near the membrane boundary is approximately the same at all points of the surface.

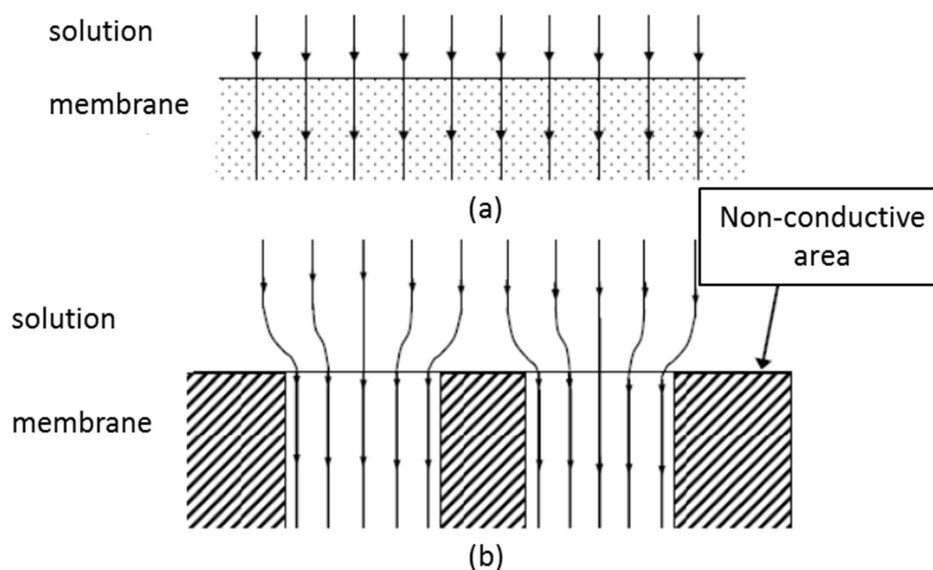


Fig. 1-20. Schematic distribution of current lines at the homogeneous (a) and heterogeneous (b) membrane surfaces (adapted from [110]).

The electric current lines condense on the conductive areas of heterogeneous membrane (Fig. 1-20b). The local current density is substantially higher than the average one over the surface, and the boundary concentration here is much lower than the average one. In this case, the electrolyte concentration near the conducting regions decreases more rapidly and the state corresponding to the transition time occurs in the system more rapidly. The different structure of the surface of the membrane also affects the form of the ChP (Fig. 1-21).

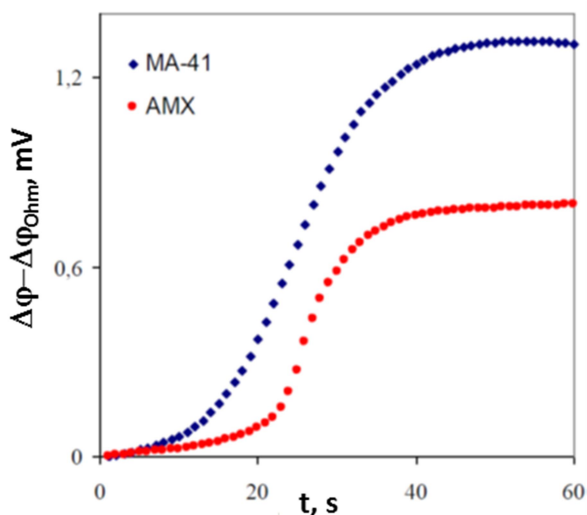


Fig. 1-21. Chronopotentiograms for heterogeneous (MA-41) and homogeneous (AMX) anion-exchange membranes in a 0.1 M solution NaCl. The membrane is in a vertical position, the current density is 17.2 mA cm^{-2} (adapted from [111]).

The PD begins to grow much earlier for homogeneous membrane surface than in the case of heterogeneous surface. When the boundary concentration on the conducting regions becomes sufficiently small, the delivery of the electrolyte begins to be carried out in a tangential direction. As a result, the PD through the heterogeneous membrane grows faster at first after the current is turned on in comparison with the homogeneous membrane, and slower near the inflection point, which explains the smoothed curve. Thus, chronopotentiometry makes it possible to characterize the electrical heterogeneity of the membrane surface.

1.3.3.3 Experimental cells for voltammetry and chronopotentiometry

The main demands for the lab-cells used for studying membrane properties are the data reproducibility and the opportunity to calculate the thickness of the diffusion boundary layer. A cell with a rotating membrane disk (RMD) [112] and cells with laminar solution flow [110, 111] are convenient for experimental and theoretical studies.

The central element of the RMD cell is a rotating glass tube (2) (Fig. 1-22). At the end portion of the tube an IEM (1) is attached. Inside the tube there are inlet (4) and outlet (5) solution capillaries and a polarizing platinum electrode (6), as well as one of the Luggin capillaries (7). The rotating glass tube with its polarizing platinum electrode and membrane forms the anode chamber. The bottom half-cell (3), which is the cathodic chamber contains a second platinum polarizing electrode (6) and the second Luggin capillary (7).

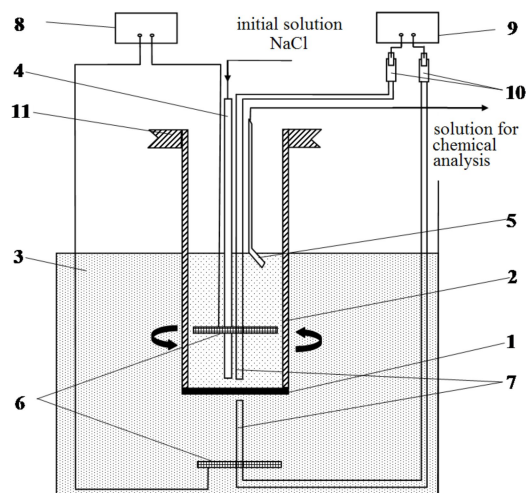


Fig. 1-22. Scheme of the RMD cell. 1 – anion-exchange membrane under investigation, 2 – top half-cell with a NaCl solution (anode chamber), 3 – bottom half-cell with a NaCl solution (cathode chamber), 4 – inlet solution capillary, 5 – outlet solution capillary, 6 – Pt polarizing electrodes, 7 – Luggina-Haber capillaries, 8 – galvanostat, 9 – millivoltmeter, 10 – Ag/AgCl reference electrodes, 11 – pulley (adapted from [112]).

The Luggin capillaries are located on opposite sides of the membrane on an axis passing through the centre of the membrane disc. Measurement of the current-voltage characteristics of the membrane system is carried out in galvanostatic mode, gradually increasing the current density with the galvanostat (8). The potential drop across the membrane is recorded on a millivoltmeter (9) with silver chloride electrodes (10). The rotation speed is varied from 100 to 500 rpm and measured using an optical-mechanical transducer coupled to the digital display unit. In this range of speeds a laminar fluid flow regime is observed.

The diagram of the measuring cell with a laminar flow is presented in Fig. 1-23 [110]. The chambers are formed by membranes (1) as well as by plastic (2) and elastic (3, 4) gaskets with a square aperture of 2×2 cm (5). The thickness of the plastic gaskets is 5 mm. The thickness of elastic gasket (3) and (4) is 0.5 and 0.95 mm, respectively. Hence, the distance between the neighbouring membranes, h , is about 7 mm. The chambers adjoining the membrane under study (A^*) are separated from the electrode chambers by a CEM (C) from the side of the platinum plane cathode (6) and by an AEM (A) from the side of the platinum plane anode (7). Two Luggin capillaries (8) are used for the sampling of solution from the layers adjoining the studied membrane from both sides. The face planes of the Luggin capillaries with diameter 0.8 mm are placed at the center of the membrane at the angle of 45° at a distance of about 0.5 mm from the membrane surface.

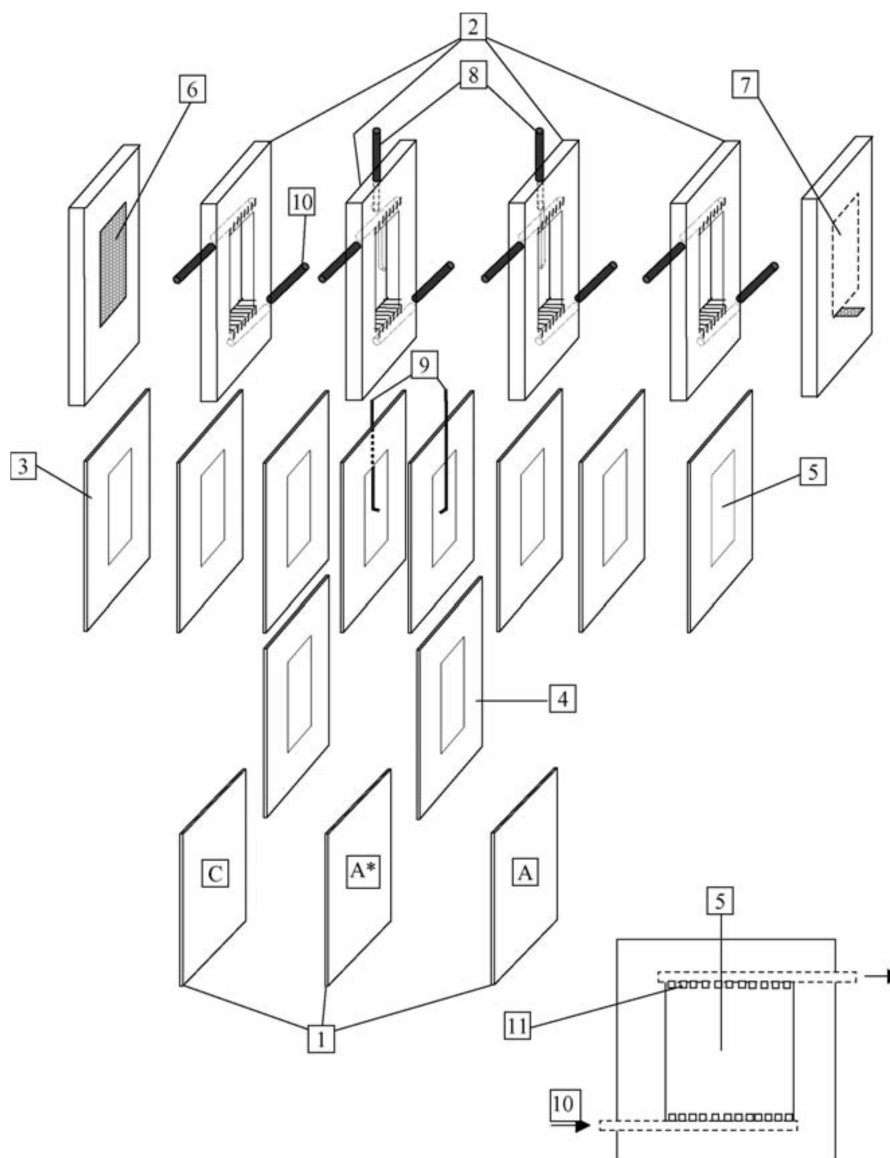


Fig. 1-23. The diagram of the experimental cell: membranes (1); plastic gaskets (2); elastic gaskets (3,4); square aperture (5); cathode (6); anode (7); plastic capillaries (8); Ag/AgCl chloride electrode or Luggin capillary (9); connecting pipe (10); stream spreader of a comb shape (11); the membrane studied (A*); a cation-exchange membrane (C); an anion-exchange membrane (A) (adapted from [110]).

The flow rate of this solution is not exceed 5 % of the solution flow rate through the desalination and concentration chambers. Two Ag/AgCl electrodes (9) used to measure the potential difference are placed in the Luggin capillaries. Each chamber is supplied with a solution through the connecting pipes (10) built into the plastic gaskets. Special guides for the solution in shape of comb (11) installed after inlet and before outlet connecting pipes provide laminar uniform flowing of solution between the membranes in the cell chambers. The cell is

settled in such a way that the plane of the membranes is vertical. The solution is passed from down to up of the cell.

In the case of the cell with the rotating disk the solution viscosity, ν , and the angular velocity of the disk rotation, ω , determine the DBL thickness:

$$\delta = 1.61\omega^{-1/2}\nu^{1/6}D^{1/3} \quad (1.16)$$

In the case of the cell with a laminar solution flow the thickness of DBL can be approximately calculated using the following equation deduced from the convection-diffusion model proposed by L ev eque [113]:

$$\delta = 1.02h\left(\frac{LDh}{h^2V}\right)^{1/3} \quad 10^{-4} < L \leq 0.02\frac{Vh^2}{D} \quad (1.17)$$

Here L is the length of desalination path; h is intermembrane distance in the desalination chamber; V is the flow velocity of solution through the desalination chamber.

A more accurate calculation may be made using the following equation [106]:

$$\text{Sh}_{av} = 1.85\left[\text{Re Sc}\left(\frac{2h}{L}\right)\right]^{1/3} - 0.4 \quad L \leq 0.02\frac{Vh^2}{D} \quad (1.18)$$

Where Sh_{av} is the Sherwood number,

$$\text{Re} = \frac{VX}{\nu} = \frac{2hV}{\nu}, \quad \text{Sc} = \frac{\nu}{D}, \quad (1.19)$$

are the Reynolds and Schmidt numbers. The Sherwood number may be presented in the form

$$\text{Sh}_{av} = \frac{2h}{\delta} \quad (1.20)$$

which allows the calculation of δ delta after calculation of Sh_{av} using Eq. (1.18).

Eq. (1.18) allows also calculation of the LCD when applying the Peers equation [114]:

$$i_{\text{lim}} = \frac{FDC_0}{(\bar{t}_i - t_i)\delta} \quad (1.21)$$

Substituting Eqs (1.18) and (1.20) in Eq. (1.21), we find:

$$i_{\text{lim}} = \frac{FDC_0}{h(\bar{t}_i - t_i)} \left[1.47 \left(\frac{h^2 V}{DL} \right)^{1/3} - 0.2 \right] \quad (1.22)$$

Volodina et al. [110] have shown that when using the lab-cell presented in Fig. 1-23 in the case of homogeneous membrane and negligible coupled effects of CP such as EC, gravitational convection and water splitting, the experimental and calculated values of i_{lim} using Eq. (1.22) are in a good agreement.

1.4 Fouling

Membrane fouling in separation processes results in loss of performance of a membrane due to the deposition of suspended or dissolved substances on its external surfaces, at its pore openings, or within its pores [115]. This process is one of the key problems for the modern chemical, agricultural, food, pharmaceutical processing and water treatment. The types of fouling on IEMs can be divided into four categories: colloidal, organic and biofouling, and scaling [116]. In our study, we focus on scaling phenomena.

1.4.1 Scale forming mechanisms

Scaling is a complex phenomenon including both crystallization and transport mechanisms. Thermodynamically, crystallization becomes possible when the activity of ions in solution is above their saturation limit and the solution is supersaturated. Also, kinetics of precipitation is a key determinant of the severity of scaling. When supersaturation exceeds a critical value, nucleation of crystal particles occurs, and then these particles grow. Higher concentration of nucleation sites accelerates crystallization kinetics. Heterogeneous nucleation, when “foreign” particles act as a “scaffold” for the crystal growth, takes place more quickly. Some of the most typical ones are small inclusions or scratches in the surface where the crystal is growing. If the solution region, where the product of ion concentrations exceeds the solubility product, is near the membrane/solution interface, the scale formation occurs on the membrane surface (surface crystallization). In the case where this region is far from the surface, the scale crystals are formed in the bulk of the processed solution (bulk crystallization) [117, 118]. A schematic representation of these crystallization processes is shown in Fig. 1-24. Scaling in membrane systems is a combination of these two extreme mechanisms and is affected by membrane morphology and process conditions.

Surface crystallization results in flux decline and surface blockage. Bulk crystallization may deposit on membrane surfaces as sediments/particles to form a cake layer that leads to flux decline. In addition, supersaturated scale itself forms conditions leading to scale growth and agglomeration. This is due to the random collision of ions with particles and secondary crystallization occurs on the surface of these foreign bodies present in the bulk phase [28, 30].

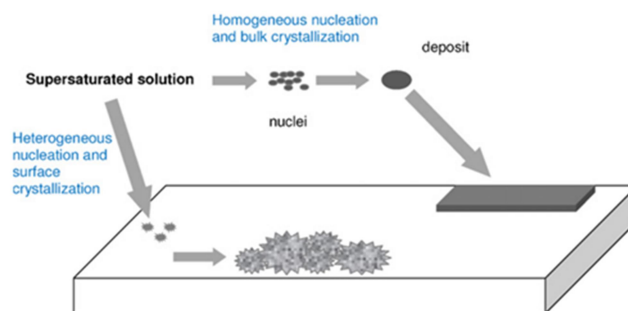
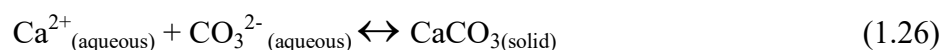


Fig. 1-24. Schematic illustration of scale formation schemes (adapted from [119]).

Simultaneous bulk and surface crystallization may also occur for high recovery operating conditions. The Mg^{2+} , Ca^{2+} , HCO_3^- , SO_4^{2-} ions are the main cause of scaling phenomenon in ED treatment [116, 120, 121]. Membrane structure, regimes of ED treatment, solution temperature also affect the precipitation [122]. As the temperature decreases, the solubility decreases and the solution becomes supersaturated, which leads to crystallization of the salt. Also, pH of the treated solution is one of the important factors for scale formation. OH^- ions cause formation of such precipitates as $\text{Mg}(\text{OH})_2$ and $\text{Ca}(\text{OH})_2$ [123]:



Higher pH shifts carbonic ions towards carbonate ions, which participate in scaling:



An additional factor affecting the scale formation is the ratio of the scaling ions due to the competition in their migration from the dilute chamber towards the concentrate and due to the cross-effects of different scaling ions on nucleation and crystal growth [124, 125].

Asraf-Snir et al. [126, 127] investigated the effect of IEM surface structure on gypsum scale formation. They found that in the case of heterogeneous anion-exchange MA-40 membrane,

the scale formation occurs mainly on the surface of conductive areas, which are ion-exchange resin beads incorporated in the polyethylene supporting matrix. The amount of deposit is essentially lower on the surface of a homogeneous anion-exchange AMV membrane [126, 127]. Moreover, the scale forms not only on the heterogeneous membrane surface, but within its macropores also.

1.4.2 Methods for studying scaling on ion-exchange membranes

1.4.2.1 Visualization of ion-exchange membranes scaling

Photo imaging, optical microscopy, scanning electron microscopy (SEM), confocal laser scanning microscopy (CLSM), atomic force microscopy (AFM) are ordinary methods for visualization of membrane fouling (Fig. 1-25). These methods may be used to identify the presence of membrane fouling, to reveal the fouling structure and distribution on the membrane surface or inside the membrane. The majority of membrane fouling investigations are performed with the use of SEM, biofouling is analysed by CLSM.

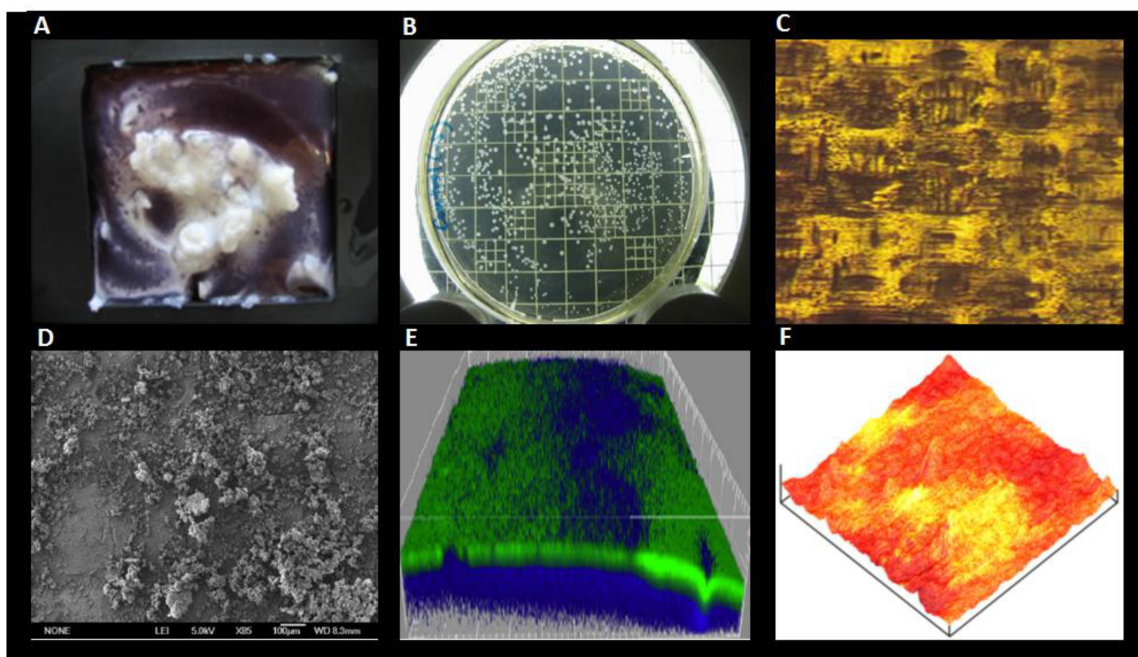


Fig. 1-25. Visualization of membrane fouling by photo imaging (A,B), optical microscopy (C), SEM (D), CLSM (E), AFM (F) (adapted from [116]).

1.4.2.2 Membrane characteristics depending on scaling in electrodialysis

1.4.2.2.a Membrane thickness, scaling content, membrane electrical conductivity

Membrane thickness, scaling content (SC), membrane electrical conductivity are the characteristics, which can be determined by direct methods [124]. SC can be calculated as follows:

$$SC = \frac{W_w - W_c}{W_c} * 100 \quad (1.27)$$

Here W_w and W_c is the dry weight of the working membrane after ED and control membrane, respectively.

There is a wide range of methods to measure the membrane electrical conductivity in the literature [9]. Belaid et al. [128] and Lteif et al. [129] developed a method using a clip-cell with two platinum electrodes to measure the conductance of the solution with membrane, G_{m+s} , and without membrane G_s (Fig.1-26). As the membrane conductance depends on the temperature, thermostat provides the constant temperature during experiment. The electrical resistance of the membrane can be calculated using Eq. 1.28.

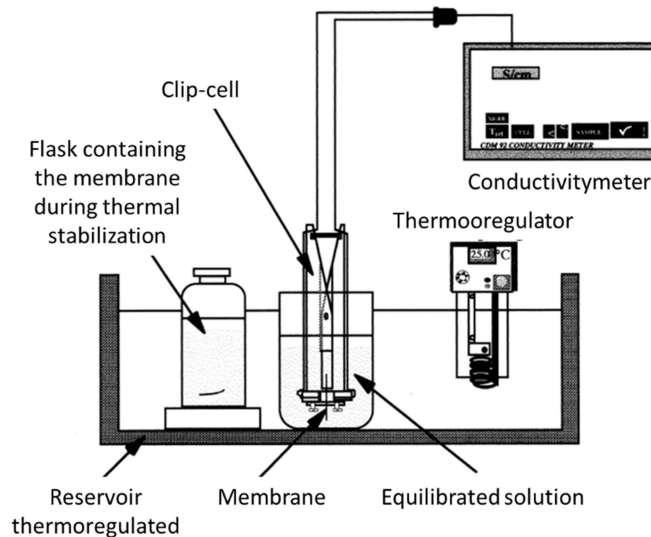


Fig. 1-26. Schematic representation of the system for measuring membrane conductance (adapted from [129]).

$$R_m = \frac{1}{G_m} = \frac{1}{G_{m+s}} - \frac{1}{G_s} \quad (1.28)$$

Here R_m is the transverse electric resistance of the membrane; G_m is the conductance of the membrane. Finally, the membrane electrical conductivity, κ , can be calculated as [129]

$$\kappa = \frac{L}{R_m S} \quad (1.29)$$

Here L is the membrane thickness; S is the electrode area.

Generally, scaling leads to the increase in membrane resistance by formation of surface scaling layer or internal membrane scaling and deposition of scale crystals on membrane ion-exchange groups [130]. The disadvantage of this method is that during immersion of the scaled membranes into the working solution (usually NaCl), the scaling could be detached from the membrane leading to the underestimation of results.

1.4.2.2.b Voltammetry and chronopotentiometry

Voltammetry and chronopotentiometry are the privilege methods to study electrochemical behavior of IEMs in the presence of scaling [70, 98]. The formation of scaling on the membrane surface or inside the membrane leads to the changes in shape of I-V curve. For example, the significant changes in the slope of the initial linear region, i_{lim} and the plateau length of scaled membrane in comparison with the pristine membrane [131].

As was mentioned above, the electrical resistance of the scaled membrane reduces in comparison with the pristine one, that is why the slope angle of the quasi-ohmic region became higher in the case of scaled membrane. The extended plateau is related to the formation of precipitates at the membrane surface. The decrease in i_{lim} for scaled membrane is attributed to the presence of area of different conductance on the surface of IEM. It is possible to obtain important information on operations of ED processes to minimize scaling effects. The disadvantages of this method are that it takes a lot of time and usually requires additional knowledge to interpret the results. Also, during the sample preparation and I-V curve registration, the weakly bounded scaling can be modified and/or detached.

Marti-Calatayud et al. [98] studied the process of scale formation on a homogeneous Nafion 117 (Du Pont) and heterogeneous HDX 100 cation-exchange membranes in mixed Na_2SO_4 and $\text{Fe}_2(\text{SO}_4)_3$ solutions by means of chronopotentiometric measurements. They showed that the increase with time of the quasi-steady state PD was related to the formation of precipitate on the depleted membrane surface (Fig. 1-27).

Moreover, in the case of Nafion 117 they discovered the second increase of PD. They supposed that this increase relates to the formation of a precipitate layer at the anodic side of

the membrane, which was visually confirmed at the end of the experiments. In the case of HDX membrane the PD increases immediately after the current is applied. This different response may indicate the presence in the heterogeneous membrane of some pores more prone to the formation of precipitates where this phenomenon starts from the beginning of the current pulse.

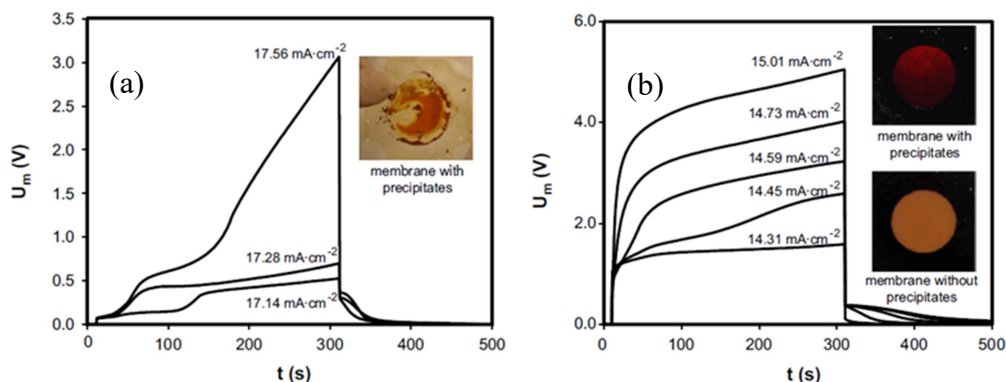


Fig. 1-27. Chronopotentiograms obtained with 0.02M $\text{Fe}_2(\text{SO}_4)_3$ solutions and in the overlimiting range of currents for (a) Nafion 117 and (b) HDX 100 (adapted from [98]).

Kang et al. [132] reported the decrease of the fraction of conducting region with deposited silica compounds from 10 to 25 % for different AEMs and with embedded hydroxide and oxide of Fe^{3+} from 7 to 27 % respectively for the Nafion 117 membrane.

1.4.2.2.c Contact angles

The membrane surface hydrophobicity can be investigated by the contact angle measurements [68, 133]. Usually, contact angles, θ , of different membranes are measured by goniometer with a measurement range of contact angle 0–180 °. The measurement procedure includes the registration of the contact angles between a drop of a liquid (distilled water) and a membrane surface [134]. A drop of liquid may be applied onto a dry membrane or onto a swollen membrane (sessile drop technique) mopped with a filter paper to remove the excessive water from the surface (Fig. 1-28a). Furthermore, membrane can be immersed into a liquid and a drop of another liquid (immersed method) [134] or air bubble (captive bubble method) [135] could be applied onto a membrane surface (Fig. 1-28b).

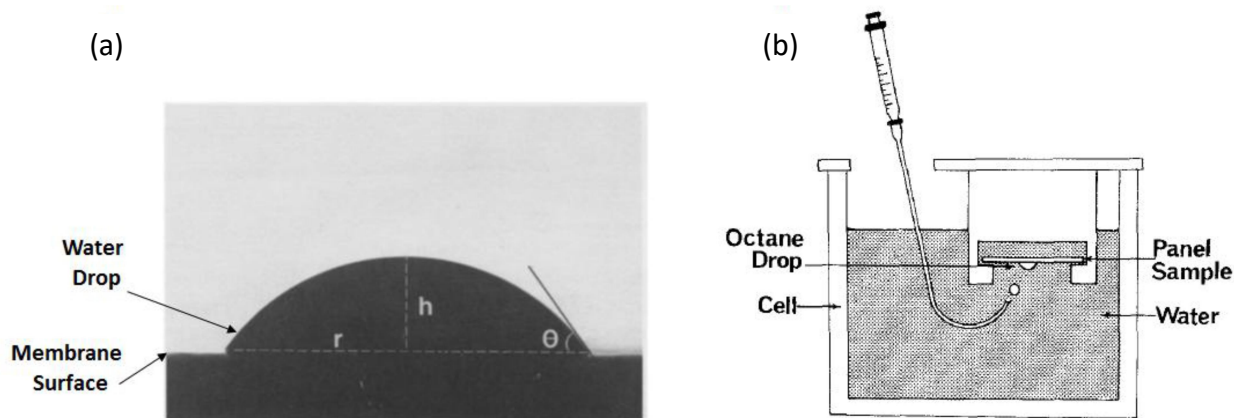


Fig. 1-28. Examples of contact angles measurement methods a) in air and b) in liquid (adapted from [134, 136]).

The studies of Bukhovets et al. [137] revealed the increase of the AEM hydrophobicity when membrane was fouled by phenylalanine. Similar increases in the AEM surface hydrophobicity were reported by Guo et al. [138] who conducted studies on polyacrylamide fouling and Lee et al. [139] who conducted studies on humate, SDBS and bovine serum albumin fouling. The simplicity and rapidity of the contact angles method is very attractive to analyze the scaling phenomena. However, the scaling can be partially removed during the mopping procedure aiming removal of excessive water at the surface. Furthermore, IEMs lose their inner water on the air and become dry quite quickly, which demands certain skills from researcher to accomplish an analysis in appropriate quick way.

However, as far as we know, there are no studies where the contact angle is measured on the membrane surface containing salt precipitates.

1.4.2.3 X-ray diffraction analysis

X-ray diffraction (XRD) is a method for the identification of atomic and molecular structure of a crystal. XRD diffractometer consists of a source of monochromatic X-rays, which are focused on a sample at some angle θ . The intensity of diffracted X-rays is analyzed by a detector, which is placed at 2θ from the source path. The diffraction happens when the X-rays strike the crystalline surface resulting in their partially scattering by atoms from different layers of crystalline lattice having a certain interlayer distance d . If X-ray beams diffracted by two different layers are in phase, constructive interference occurs and diffraction results in a peak on a diffractogram. However, if beams are out of phase, destructive interference occurs and there is no peak on a diffractogram. Hence, only crystalline solids will be detected by XRD while the limit is that amorphous materials will remain undetected [140].

The studies of XRD spectra allow revealing of the crystalline structures of precipitates formed on the IEMs treated by ED. The only pretreatment of a scaled membrane prior to XRD is drying. Casademont et al. [141] reported the transformation of calcium carbonate and hydroxides of Ca and Mg during the consecutive ED treatments. The more detailed studies using XRD of scaling formation mechanisms and effects of non-stationary electric fields were conducted by Cifuentes-Araya et al. [124]. These authors reported the formation of multilayer scaling composed of calcite, brucite and aragonite crystals during consecutive ED treatments.

1.4.3 Methods for prevention and control of ion-exchange membrane scaling

1.4.3.1 Ion-exchange membrane modification

Nowadays researches try to change the membrane surface properties such as surface charge, hydrophobic/hydrophilic balance and roughness.

Since the scaling agents are Ca^{2+} , Mg^{2+} and other multiply charged ions, the modification of a membrane surface by a layer selective to the transfer of singly charged ions is an option. It is known that the deposition of organic substances on the membrane surface can be reduced when the membrane is covered with a thin ion-conductive layer bearing a fixed charge opposite to the charge of the supporting membrane matrix [142]. As a result, the resistance of the composite membrane is increasing towards multiply charged counter-ions, which causes scaling. A similar effect is obtained by modification of the membrane surface with high-molecular surface active substances [143].

The above modification reduces the transfer of multicharged ions from the diluate to the concentrate chamber. This mitigates or prevents scaling in the concentrate chamber. However, in diluate chamber the situation may be even worse: the increased local concentration of multicharged ions at the depleted membrane surface together with possible increase in pH due to water splitting may provoke formation of hydrates of multicharged ions able to precipitate.

In practice, the casting of conductive perfluorinated resin solution of Nafion[®] or its Russian analogue MF-4SK on the surface of a CEM leads to the growth of limiting current density by 1.5 times in comparison with unmodified membrane [34-36]. This effect is explained by a better distribution of the current lines after the surface modification. Besides, the membrane surface becomes relatively more hydrophobic that is beneficial for EC [34-36, 144].

The positive effect of application a homogeneous film to the membrane surface is supported by theoretical studies of Rubinstein et al. [145]. The current lines are distorted in solution near an electrically heterogeneous surface: they are accumulated at the conductive areas causing higher CP [145], which should lead to increasing scale formation. It is shown [145] that

application of a homogeneous conductive layer on heterogeneous surface diminishes the effect of formation of funnel-shaped distribution of current lines in the solution near the membrane surface. Even a very thin and weakly charged conductive layer results in homogenization of current lines distribution over the membrane surface and in the near-surface solution. As a consequence, the CP at the membrane surface decreases and the LCD increases [145].

1.4.3.2 Cleaning agents

The cleaning agents are used to remove the scaling from the surface of IEMs or to prevent scaling formation during ED treatment. He et al [146] showed that the application of antiscalants helps to prevent membrane scaling by calcite and gypsum. The effects of antiscalants were investigated during the direct contact membrane distillation process implemented with porous hydrophobic polypropylene hollow fibers having a porous fluorosilicone coating on the fiber outside surface. Antiscalant K752, a polyacrylic acid and sodium polyacrylate based compound, is more effective in inhibiting CaSO_4 scaling, compared with other antiscalants tested, i.e., K797, GHR, GLF and GSI. However, a great amount of scaling deposits were observed on the membrane surface after de-ionized water washing [147]. Hydraulic cleaning was limited for the strong adhesion force between the scalants and the membrane surface. Acid cleaning may improve the removal efficiency as a result of the neutralization and/or hydrolysis reactions between hydrochloric acid and mineral deposits that would dissolve the scalants (calcium or magnesium hydroxide or their carbonates) into acid solution [147].

1.4.3.3 Pretreatment: Pressure-driven membrane processes

Microfiltration, ultrafiltration, nanofiltration and reverse osmosis are successfully used as a pretreatment step prior ED [148, 149]. The pressure gradient are used as a driving force and allow separation of particles according to their size or molecular weight.

There are two types of filtration dead-end filtration and cross flow filtration (Fig.1-29). In dead-end filtration, the stream of the feed solution flows perpendicularly to the membrane surface and only one flow leaves the membrane module. In crossflow filtration, the feed solution flows tangentially to the membrane surface, and there are two streams leaving the membrane module. For the majority of the modern pressure-driven membrane processes dead-end mode is in appropriate due to the severe accumulation of the rejected particles on the membrane surface leading to an abrupt decrease of the permeate flux. The tangential flow

can help to shear away the accumulated rejected particles and attain relatively high flux of permeate.

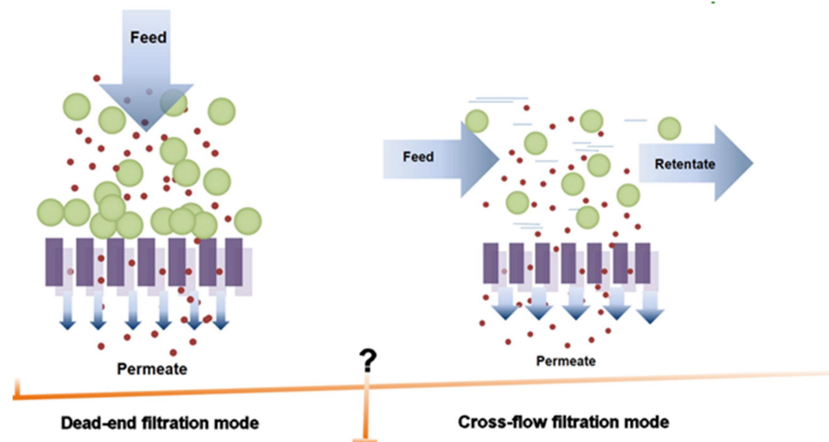


Fig. 1-29. Dead-end filtration and cross-flow filtration (adapted from [150]).

1.4.3.4 Mechanical action

The ultrasound has been demonstrated as an effective method to remove fouling materials from the membrane surface [147]. The actual physical phenomena involved in ultrasonic cleaning is cavitation, which can be defined as the formation, growth, and implosive collapse of bubbles combined with a large negative pressure applied to a liquid medium. This cavitation collapse produces a number of phenomena that result in the break and dislodgement of fouling layer from the membrane surface. 19.9 % of oxygen and 71.5 % of calcium were removed compared with the untreated membrane after 120 s ultrasonic cleaning [147].

The combination of acid cleaning with ultrasound showed that after 60 s of ultrasound treatment in 1 % HCl solution, the scale deposits observed on the treated CEM surface were almost removed. The physical and chemical membrane parameters indicated that the performance of cleaned membrane was restored [147].

1.4.3.5 Changing regimes of electro dialysis treatment

1.4.3.5.a Control of hydrodynamic conditions

Concentration polarization causes limitations in ED. Water splitting occurs at currents more than limiting current. This pH changes can lead to the scale formation on the IEM surface. In order to get the maximum ion flux per unit membrane area it is desirable to operate at the highest possible current density. Grossman et al. [151] increased the limiting current changing the hydrodynamic conditions. They showed that the changing in flow rate and using the

spacer material promoting turbulence mitigate the scaling on the IEM surface. The spacers design is important in terms of increasing current efficiency. Impact of air sparging on the ED process was shown in Ref. [152]. They compared the gas/liquid ratio in combination with various spacer configurations and the situation without feed spacer. The mass transfer increase was most effective in a spacer free cell where the mass transfer increased linearly with increasing gas/liquid ratio. Also, the spacer free cell combined the highest mass transfer increase with the lowest increase in cell resistance. This approach allows increasing solution turbulence, which may be also advantageous in the reduction of a membrane scale.

1.4.3.5.b Electrodialysis reversal

In the 1950's, Ionics started experiments with systems which showed a radical improvement in scale control [153]. They proposed to use electrodialysis reversal (EDR) process which results in the prevention of calcium carbonate and calcium sulfate scale formation. Also Japanese researchers have highly developed the scaling process. They used ED treatment for the production of sodium chloride from the sea-water [57, 154]. The key moment in the EDR is the changing of the electrode polarity and the flow direction at the same time [57]. The electric field is alternately reversed to dissolve salt scale deposited on the membranes. The desalination channels become concentration channels, and vice versa, concentration channels – desalination channels (Fig. 1-30). The disadvantage of this method is the productivity loss and the waste of the finished product when the electrode polarity is changing.

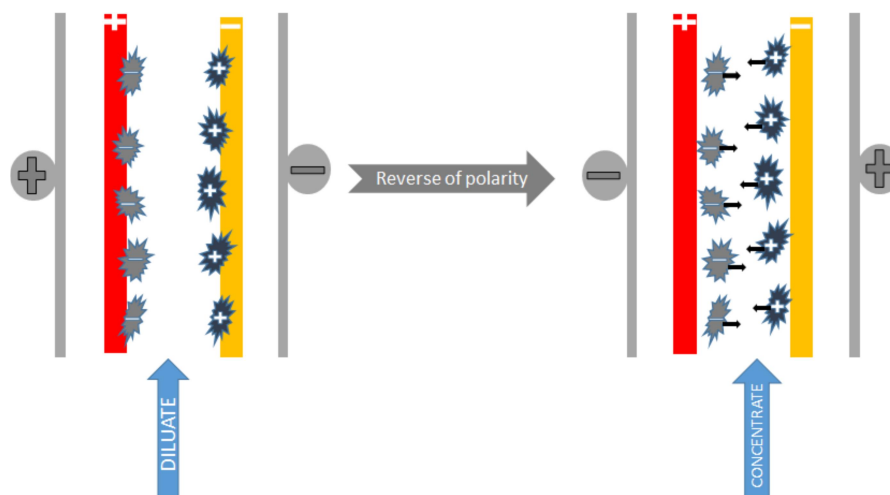


Fig. 1-30. Scheme of EDR and presence of foulants (adapted from [116]).

1.4.3.5.c Pulsed electric field

Pulsed electric field (PEF) modes are proposed as another effective way for combating the consequences of CP, such as the scaling formation at IEM interfaces [124]. In this mode the

pulse lapse (T_{on}) of current or voltage alternate with pause lapse (T_{off}) of certain duration. During the pause lapse the ions transport from the bulk solution to the membrane surface by means of diffusion and convection, so the effect of CP diminishes before the pulse lapse is applied [133, 155]. The rate of ED desalination is higher applying a non-stationary regime with short current or voltage pulses [124, 155]. The duration of pulse/pause lapses is very important for the ED intensification. Sostat et al. [156] compared the desalination rate of sodium chloride during ED under a constant applied voltage and PEF modes. They showed that the average current density and the desalination rate increase with increasing frequency of pulse lapses from 1 Hz to 100 Hz.

Also, the duration of pulse/pause lapses affects essentially the amount and the composition of the salt deposits [124, 157].

During pause lapses the concentration depolarization occurs. As a result the electric resistance of depleted solution reduces and the salt deposits dissolve, at least partially. EC plays an important role in this process. EC appears as a result of the action of electric field on the space electric charge at the membrane surface. The transfer of solution by EC intensifies the exchange between the near-surface solution layer and the bulk solution [158-161] and contributes to reducing scaling [162]. The duration of the current or the voltage pulses should be considerably shorter than the calculated characteristic time to build up the polarization layer. Subsequent studies conducted by Mikhaylin et al. revealed that short PEF modes (1 s - 3 s) allow better mitigation of concentration polarization and scaling phenomena [124]. Indeed, the application of the optimal pulse/pause mode of 2 s/0.5 s allows a 40 % decrease of the CEM scaling and complete inhibition of AEM scaling (just traces of AEM scaling were detected) in comparison with a continuous current mode [124].

Moreover, Uzdénova et al. [156] have shown that EC vortices persist after pulse lapses. The reason is that electro-osmotic fluid flows remain in the membrane system during pause lapse. These flows are due to the non-uniform distribution of counter-ion concentrations along the longitudinal coordinate inside the double electric layer. The longitudinal diffusion of the counter-ions inside the space charged region generates the flow of electric current, which in turn causes electro-osmotic slip of the liquid. Thus, a non-uniform distribution of the space electric force arises, which feeds the vortices.

1.4.3.5.d Overlimiting current regime

Recently it was shown that the use of overlimiting currents could improve ED performances [114]. It is possible if the overlimiting regime leads to the formation of electroconvection. Electroconvective vortices significantly reduce the scaling on the surface of IEMs. This effect

is due to increasing convection transfer, which enhances hydrodynamic effect on the scale and decreases water splitting [162, 163]. The latter results in lowering pH changes at the membrane surface, and, as consequence, mitigation of scaling. The effect of EC increases for IEMs with relatively hydrophobic surface [164] and in the case where PEF are applied [124]. Accordingly, the scaling is mitigated in these cases [155, 162].

Nevertheless, another coupled effect of concentration polarization can both mitigate and intensify scale formation. Casademont et al. [165-167] studied in details the pH influence on scaling on the IEM surfaces. It was reported that the membrane scaling formed by minerals of Ca^{2+} and Mg^{2+} on AEM surface mostly takes place at neutral pH values, however CEM surface was scaled at basic pH. Additionally to pH factor, the type of IEM (anion-exchange or cation-exchange) can play an important role in the scaling formation. Generation of OH^- ions by CEM provides conditions for the scaling formation, however H^+ ions generated by AEM may create a “proton barrier” preventing precipitation of minerals.

1.5 Conclusions

In the literature review presented in this chapter, we have considered the structure and main properties of ion-exchange membranes, the methods of their characterization, the approaches to their surface and volume modifications and their main applications in ion separation and energy production. Analysis of the literature shows that there are two main drawbacks of electro dialysis, which hinder its wider implementation. They are concentration polarization and scale formation. The both result in increasing resistance of the membrane system and causing higher energy losses. On the other hand, concentration polarization initiates coupled phenomena, which can produce positive or negative effects on the economics of electro dialysis process. Current-induced convection, mainly electroconvection in dilute solutions, allows enhancement of mass transfer: electroconvective vortexes contribute to the delivery of salt ions from the bulk solution to the membrane interface, as well as to the evacuation of the depleted solution from the interface to the bulk solution. However, water splitting at the membrane depleted interface is generally non-desirable effect. Generation of H^+ and OH^- ions leads to the decrease in current efficiency towards the transfer of salt ions. Besides, it results in pH changes of solution, which increase the risk of membrane fouling/scaling. The situation is complicated by the fact that these two effects affect each other. Since electroconvection contributes to the transfer of “fresh” solution to the membrane surface, it diminishes the water splitting rate and mitigates the scale formation on the ion-exchange membrane surface in the overlimiting current regimes.

The development of electroconvection is essentially affected by the nature of electrolyte solution. The understanding of this effect is important when trying to use electroconvection for optimizing electro dialysis treatment of natural multicomponent solutions inclined to scale formation. This effect was studied in stationary conditions (using voltammetry) by Choi and Moon. They have shown that the intensity of electroconvection increases with the increase of the degree of counter-ion hydration. However, it remains not clear, how the ability of counter-ions to involve the water volume in motion and membrane surface properties will influence the mechanism of electroconvection development in non-stationary conditions (chronopotentiometry).

In practice, there are several approaches for scaling mitigation. Pretreatment and electro dialysis reversal are sufficiently mature methods. Pretreatment step is used to remove the particles causing scale formation from the feed solution according to their size or weight by microfiltration, ultrafiltration and nanofiltration. The key moment in the electro dialysis reversal is the changing of the electrode polarity and the flow direction at the same time. The

disadvantage of this method is the loss in the current efficiency, capacity and final product during the operation of electrode polarity changing.

Another approach is modification of membrane surface by a layer, which is selective to the transfer of singly charged ions. The fluxes scaling agents, which are the Ca^{2+} , Mg^{2+} , SO_4^{2-} and other multiply charged ions, are reduced, so the concentration of these ions is low in the concentrate chamber and the scale does not form there. Recently it has been shown that polymerization of polyaniline on the surface of the cation-exchange membrane results in the appearance of selectivity for the transfer of singly charged ions and the decrease of water transport number. Modification of the membrane with polyaniline leads to a smoother surface, which should reduce the risk of nucleation of scale crystals of the membrane surface. However, the formation of an internal bipolar boundary between the cation- and anion-exchange layers lead to catalytic water splitting that can stimulate the rate of scale formation on the ion-exchange membrane. In that connection, it would be interesting to study how polyaniline modification of heterogeneous membranes affects the scaling process.

Pulsed electric field modes are proposed as another effective way for combating the non-desirable consequences of concentration polarization and scaling formation at ion-exchange membrane interfaces. It was shown that the duration of pulse and pause lapses of high frequency affects essentially the amount and the composition of the salt deposits. During pause lapses, the concentration depolarization occurs. As a result, the electric resistance of depleted solution reduces and the salt deposits dissolve, at least partially. It was also shown that the application of low frequency pulsed electric field modes (with the period about 1 min, Ruiz) allows mitigation of organic fouling. However, the influence of pulsed electric field with low frequency on the mineral scale formation on the membrane surface is not studied.

There are only few publications (Mikhaylin, Bazinet et al.) where the phenomenon of electroconvection is used for fighting scale formation. The literature analysis above shows that the beneficial effect of electroconvection may be increased when applying surface modification of commercial ion-exchange membranes. Thus, it is found in the publications by Belova, Belashova, Pismenskaya et al. that the casting of a thin homogeneous ion-conductive perfluorinated film of Nafion[®] or its Russian analogue MF-4SK on the surface of a heterogeneous cation-exchange membrane leads to the growth of the limiting current density by 1.5 times in comparison with the pristine membrane. Besides, when applying the modified membrane, one can obtain an essential growth of the overlimiting mass transfer and a decrease in the water splitting rate. This effect is explained by a better distribution of the current lines and a more hydrophobic surface after the membrane modification that is beneficial for electroconvection. Since intensification of electroconvection contributes to the

scaling mitigation, we can expect that the use of the ion-exchange membranes modified with a conductive perfluorinated film will essentially decrease the rate or totally prevent salt precipitation. Besides, we can expect that the effect of electroconvection on the scaling mitigation will be higher in the case where pulsed electric field modes are applied.

The literature analysis allows us to formulate the following problems, which are worth to be investigated and to study which our research will be directed.

- 1) The effect of electrolyte nature and membrane surface properties on the electroconvection development in non-stationary conditions (chronopotentiometry) in particular at times shorter than the transition time, which is very important in pulsed electric field modes.
- 2) The effect of homogenization and hydrophobization of a cation-exchange membrane by Nafion[®] film on its scaling in the presence of divalent ions during electro dialysis.
- 3) The process of water splitting at the depleted membrane interface and the search of possibilities how water splitting can be used for pH adjustment in desalination and concentration chambers without external addition of HCl to prevent the scale formation.
- 4) The effect of pulsed electric field with low frequency on the scale formation on the surface of pristine membrane and the membrane modified by Nafion[®] film.
- 5) The development of a method for the preparation of an anisotropic composite membrane by formation of a polyaniline layer within a cation-exchange membrane. Investigation of the electrochemical behavior of the composite membrane and the process of scale formation on its surface in the presence of divalent ions.

References

- [1] F. G. Helfferich, Ion exchange, Dover Publication Inc., New York (1962).
- [2] L. Liberti, J. R. Millar, Fundamentals and applications of ion exchange, MartinusNijhoff Publishers, Dordrecht (1985).
- [3] E. Sélégny, Charged gels and membranes, Springer Science & Business Media, Berlin (2012).
- [4] N. P. Berezina, Electrochemistry of membrane systems, Kuban State University, Krasnodar (2009).
- [5] F. Mark, The encyclopedia of polymer science and technology, Concise, third edition, John Wiley & Sons, Hoboken (2013).
- [6] Y. Mizutani, Structure of ion exchange membranes, *J. Membr. Sci.* 49 (1990) 121–144.
- [7] J. Ran, L. Wu, Y. He, Z. Yang, Y. Wang, C. Jiag, L. Ge, E. Bakangura, T. Xu, Ion exchange membranes: New developments and applications, *J. Membr. Sci.* 522 (2017) 267–291.
- [8] T. Sata, Ion Exchange Membranes: Preparation, Characterization, Modification and Application, The Royal Society of Chemistry, Gateshead (2004).
- [9] N. P. Berezina, N. A. Kononenko, O. A. Dyomina, N. P. Gnusin, Characterization of ion-exchange membrane materials: Properties vs structure, *Adv. Colloid Interface Sci.* 139 (2008) 3–28.
- [10] C. Larchet, L. Dammak, B. Auclair, S. Parchikov, V. Nikonenko, A simplified procedure for ion-exchange membrane characterization, *New J. Chem.* 28 (2004) 1260–1267.
- [11] N. Berezina, N. Gnusin, O. Dyomina, S. Timofeyev, Water electrotransport in membrane systems. Experiment and model description, *J. Membr. Sci.* 86 (1994) 207–229.
- [12] C. Larchet, B. Auclair, V. Nikonenko, Approximate evaluation of water transport number in ion-exchange membranes, *Electrochim. Acta* 49 (2004) 1711-1717.
- [13] H. Strathmann, Chapter 3 – Preparation and Characterization of Ion-Exchange Membranes, Ion-Exchange Membrane Separation Processes, *Membr. Sci. Techno.* 9 (2004) 89–146.
- [14] S. M. J. Zaidi, T. Matsuura, Polymer membranes for fuel cells, Springer (2009).
- [15] T. Sata, Properties of composite membranes formed from ion exchange membranes and conducting polymers 4. Change in membrane resistance during electrodialysis in the presence of surface active agents, *J. Phys. Chem.* 97 (1993) 6920–6923.

- [16] T. Sata, T. Funakoshi, K. Akai, Preparation and transport properties of composite membranes composed of cation exchange membranes and polypyrrole, *Macromol.* 29 (1996) 4029–4035.
- [17] T. Sata, Y. Matsuo, T. Yamaguchi, K. Matsusaki, Preparation and transport properties of anion-exchange membranes containing viologen moieties as anion-exchange groups in the presence or absence of photoirradiation, *J. Chem. Soc., Faraday Trans.* 93 (1997) 2553–2560.
- [18] T. Sata, Y. Ishii, K. Kawamura, K. Matsusaki, Composite membranes prepared from cation exchange membranes and polyaniline and their transport properties in electro dialysis, *J. Electrochem. Soc.* 146 (1999) 585–591.
- [19] S. Oae, J. Doi, *Organic sulfur chemistry*, CRC Press (1992).
- [20] B. Bahar, A.R. Hobson, J.A. Kolde, D. Zuckerbrod, Ultra-thin integral composite membrane, 5,547,551 U.S. Patent (1996).
- [21] D. B. Xing, S. H. Zhang, C. X. Yin, B. G. Zhang, X. G. Jian, Effect of amination agent on the properties of quaternized poly(phthalazinone ether sulfone) anion exchange membrane for vanadium redox flow battery application, *J. Membr. Sci.* 354 (2010) 68–73.
- [22] N. P. Berezina, S. A. Shkirskaya, M. V. Kolechko, O. V. Popova, I. N. Senchikhin, V. I. Roldugin, Barrier Effects of Polyaniline Layer in Surface Modified MF-4SK/Polyaniline Membranes, *Russ. J. Electrochem.* 47 (2011) 995–1005.
- [23] N. Agmon, The Grotthuss mechanism, *Chem. Phys. Lett.* 244 (1995) 456–462.
- [24] V. F. Ivanov, O. L. Gribkova, S. V. Novikov, A. A. Nekrasov, A. A. Isakova, A. V. Vannikov, G. B. Meshkov, I. V. Yaminsky, Redox heterogeneity in polyaniline films: from molecular to macroscopic scale, *Synth. Met.* 152 (2005) 153–156.
- [25] H. Farrokhzad, M. R. Moghbeli, T. Van Gerven, B. Van der Bruggen, Surface modification of composite ion exchange membranes by polyaniline, *React. Funct. Polym.* 86 (2015) 161–167.
- [26] A. T. K. Tran, Y. Zhang, J. Lin, P. Mondal, W. Ye, B. Meesschaert, L. Pinoy, B. Van der Bruggen, Phosphate pre-concentration from municipal wastewater by selectrodialysis: Effect of competing components, *Sep. Purif. Technol.* 141 (2015) 38–47.
- [27] T. Rottiers, B. Van der Bruggen, L. Pinoy, Synthesis and transport of impurities in electro dialysis metathesis: Production of choline dihydrogen phosphate, *J. Membr. Sci.* (2017) <https://doi.org/10.1016/j.memsci.2017.07.042>.
- [28] R. Simons, Preparation of a high performance bipolar membrane, *J. Membr. Sci.* 78 (1993) 13–23.

- [29] G. Eigenberger, H. Strathmann, A. Grabovskiy, Membrane assembly, electro dialysis device and method for continuous electro dialytic desalination, Germ. Patent WO 2005/009596 A1, B01D 61/44 (2005).
- [30] I. G. Wenten, Khoiruddin, Recent developments in heterogeneous ion-exchange membrane: preparation, modification, characterization and performance evaluation, *J. Eng. Sci. Technol.* 11 (2016) 916 – 934.
- [31] V. I. Zabolotskii, S. A. Loza, M. V. Sharafan, Physicochemical Properties of Profiled Heterogeneous Ion-Exchange Membranes, *Russ. J. Electrochem.* 41 (2005) 1053–1060.
- [32] N. V. Sheldeshov, V. I. Zabolotskii, S. A. Loza, Electric conductivity of profiled ion exchange membranes, *Pet. Chem.* 54 (2014) 664–668.
- [33] C. Larchet, V. I. Zabolotsky, N. Pismenskaya, V. V. Nikonenko, A. A. Tskhay, K. Tastanov, G. Pourcelly, Comparison of different ED stack conceptions when applied for drinking water production from brackish waters, *Desalination* 222 (2008) 489–496.
- [34] E. D. Belashova, N. A. Melnik, N. D. Pismenskaya, K. A. Shevtsova, A. V. Nebavsky, K. A. Lebedev, V. V. Nikonenko, Overlimiting mass transfer through cation-exchange membranes modified by Nafion film and carbon nanotubes, *Electrochim. Acta* 59 (2012) 412–423.
- [35] N. D. Pis'menskaya, V. V. Nikonenko, N. A. Mel'nik, G. Pourcelli, G. Larchet, Effect of the ion-exchange-membrane/solution interfacial characteristics on the mass transfer at severe current regimes, *Russ. J. Electrochem.* 48 (2012) 610–628.
- [36] N. Pismenskaya, N. Melnik, E. Nevakshenova, K. Nebavskaya, V. Nikonenko, Enhancing ion transfer in overlimiting electro dialysis of dilute solutions by modifying the surface of heterogeneous ion-exchange membranes, *Int. J. Chem. Eng.* 2012 (2012) 528290.
- [37] Y. Zhao, H. Liu, K. Tang, Y. Jin, J. Pan, B. Van der Bruggen, J. Shen, C. Gao, Mimicking the cell membrane: bioinspired simultaneous functions with monovalent anion selectivity and antifouling properties of anion exchange membrane, *Nat. Sci. Rep.* 6 (2016) 37285.
- [38] P. Sivaraman, J.G. Chavan, A.P.Thakur, V.R.Hande, A.B. Samui, Electrochemical modification of cation exchange membrane with polyaniline for improvement in permselectivity, *Electrochim. Acta* 52 (2007) 5046–5052.
- [39] G. Vázquez-Rodríguez, L. M. Torres-Rodríguez, A. Montes-Rojas, Synthesis and characterization of commercial cation exchange membranes modified electrochemically by polypyrrole: Effect of synthesis conditions on the transport properties, *Desalination* 416 (2017) 94–105.

- [40] H. Strathmann, Electrodialysis, a mature technology with a multitude of new applications, *Desalination* 264 (2010) 268–288.
- [41] J. R. Wilson, *Demineralization by Electrodialysis*, Butterworth, London (1960).
- [42] R. Pattle, Production of electric power by mixing fresh and salt water in the hydroelectric pile, *Nature* 174 (1954) 660.
- [43] A. Giwa, V. Dufour, F. Al Marzooqi, M. Al Kaabi, S.W. Hasan, Brine management methods: Recent innovations and current status, *Desalination* 407 (2017) 1–23.
- [44] L. M. Camacho, J. A. Fox, J. O. Ajedegba, Optimization of electrodialysis metathesis (EDM) desalination using factorial design methodology, *Desalination* 403 (2017) 136–143.
- [45] K. J. Liu, F. P. Chlanda, K. J. Nagasubramanian, Use of bipolar membranes for generation of acid and base: an engineering and economic analysis, *J. Membr. Sci.* 2 (1977) 109–124.
- [46] W. Vielstich, A. Lamm, H. Gasteiger, *Handbook of Fuel Cells: Fundamentals, Technology, Applications*, Wiley (2004).
- [47] R. K. A. Rasheed, Q. Liao, Z. Caizhi, S. Hwa Chan, A review on modelling of high temperature proton exchange membrane fuel cells (HT-PEMFCs), *Int. J. Hydrogen Energy* 42 (2017) 3142–3165.
- [48] N. Guerrero Moreno, M. Cisneros Molina, D. Gervasio, J. Pérez Robles, Approaches to polymer electrolyte membrane fuel cells (PEMFCs) and their cost, *Renew. Sustainable Energy Rev.* 52 (2015) 897–906.
- [49] G. Pourcelly, V.V. Nikonenko, N.D. Pismenskaya, A.B. Yaroslavtsev, Chapter 20 Applications of charged membranes in separation, fuel cells, and emerging processes, *Ionic interactions in natural and synthetic macromolecules*, Wiley (2012) 761–815.
- [50] B. Auclair, C. Larchet, L. Dammak, V. Nikonenko, M. Métayer, Correlation between transport parameters of ion-exchange membranes, *J. Membr. Sci.* 195 (2002) 89–102.
- [51] A. M. Peers, General discussion, *Disc. Faraday Soc.* 21 (1956) 124–125.
- [52] R. Simons, Water splitting in ion exchange membranes, *Electrochim. Acta* 30 (1984) 275–282.
- [53] C. Forgacs, N. Ishibashi, J. Leibovitz, J. Sinkovic, K.S. Spiegler, Polarization at ion-exchange membranes in electrodialysis, *Desalination* 10 (1972) 181–214.
- [54] R. Simons, Strong electric field effects on proton transfer between membrane-bound amines and water, *Nature* 280 (1979) 824 – 826.
- [55] V. I. Zabolotskii, N. V. Shel'deshov, N. P. Gnusin, Dissociation of water molecules in systems with ion-exchange membranes, *Russ. Chem. Rev.* 57 (1988) 801–808.

- [56] S. Mafé, P. Ramírez, A. Alcaraz, Electric field-assisted proton transfer and water dissociation at the junction of a fixed-charge bipolar membrane, *Chem. Phys. Lett.* 294 (1998) 406–412.
- [57] Y. Tanaka, *Ion exchange membranes fundamentals and applications*, second edition, Elsevier Science, 2015.
- [58] V. V. Nikonenko, M. Kh. Urtenov, On a generalization of the electroneutrality condition, *Russ. J. Electrochem.* 32 (1996) 195–198.
- [59] R. Simons, Electric field effects on proton transfer between ionizable groups and water in ion exchange membranes, *Electrochim. Acta* 28 (1984) 151–158.
- [60] B. B. Damaskin, O. A. Petrii, G. A. Tsirlina, *Elektrokhimiya*, Moscow: Khimiya, 2001.
- [61] Yu. I. Kharkats, *Elektrokhimiya*, 21 (1985) 974.
- [62] V. I. Zabolotsky, V. V. Nikonenko, N. D. Pismenskaya, On the role of gravitational convection in the transfer enhancement of salt ions in the course of dilute solution electro dialysis, *J. of Membr Sci.* 119 (1996) 171–181.
- [63] V. I. Zabolotsky, V. V. Nikonenko, N. D. Pismenskaya, E. V. Laktionov, M. Kh. Urtenov, H. Strathmann, M. Wessling, G. H. Koops, Coupled transport phenomena in overlimiting current electro dialysis, *Sep. Purif. Technol.* 14 (1998) 255–267.
- [64] E. Guyon, J-P. Hulin, L. Petit, In *Hydrodynamique physique. Matière Condensée*, CNRS (Eds), Paris: Savoirs Actuels InterEditions, 2001.
- [65] V. M. Volgin, A. D. Davydov, Natural-convective instability of electrochemical systems: A review, *Russ. J. Electrochem.* 42 (2006) 567–608.
- [66] V. V. Nikonenko, A. B. Yaroslavtsev, G. Pourcelly, 9. Ion transfer in and through charged membranes: structure, properties, and theory, *Ionic interactions in natural and synthetic macromolecules* (2012) 267–336.
- [67] I. Rubinstein, B. Zaltzman, O. Kedem, Electric fields in and around ion-exchange membranes, *J. Membr Sci.* 125 (1997) 17–21.
- [68] N. D. Pismenskaya, V. V. Nikonenko, E. I. Belova, G. Yu. Lopatkova, Ph. Sstat, G. Pourcelly, K. Larshe, Coupled convection of solution near the surface of ion-exchange membranes in intensive current regimes, *Russ. J. Electrochem.* 43 (2007) 307–327.
- [69] Y. Tanaka, Concentration polarization in ion-exchange membrane electro dialysis: The events arising in an unforced flowing solution in a desalting cell, *J. Membr. Sci.* 244 (2004) 1–16.
- [70] M. C. Martí-Calatayud, M. García-Gabaldón, V. Pérez-Herranz, Effect of the equilibria of multivalent metal sulfates on the transport through cation-exchange membranes at different current regimes, *J. Membr. Sci.* 443 (2013) 181–192.

- [71] A. Pismenskiy, M. Urtenov, A. Kovalenko, S. Mareev, Electrodesalination process in conditions of mixed convection, *Desalin. Water Treat.* 56 (2015) 3211–3213.
- [72] R. F. Probstein, *Physicochemical Hydrodynamics*, Wiley (1994).
- [73] I. Rubinstein, B. Zaltzman, Electro-osmotically induced convection at a permselective membrane, *Phys. Rev. E.* 62 (2000) 2238–2251.
- [74] I. Rubinshtein, B. Zaltzman, J. Pretz, C. Linder, Experimental verification of the electroosmotic mechanism of overlimiting conductance through a cation exchange electrodesalination membrane, *Russ. J. Electrochem.* 38 (2002) 853–863.
- [75] I. Rubinstein, B. Zaltzman, Equilibrium electroconvective instability, *Phys. Rev. Lett.* 114 (2015) 114502-1–114502-5.
- [76] S. S. Dukhin, Electrokinetic phenomena of the second kind and their applications, *Adv. Colloid Interface Sci.* 35 (1991) 173–196.
- [77] A. V. Delgado, *Interfacial electrokinetics and electrophoresis*, Marcel Dekker Inc., New York (2002).
- [78] V. G. Levich, To the theory of non-equilibrium double layer, *Proc. USSR Acad. Sci.* 124 (1959) 869–872.
- [79] N. A. Mishchuk, Electro-osmosis of second kind near heterogeneous ion-exchange membranes, *Colloids Surf. A: Physicochem. Eng. Asp.* 140 (1998) 75–89.
- [80] N. A. Mishchuk, P.V. Takhistov, Electroosmosis of the second kind, *Colloids Surf. A: Physicochem. Eng. Asp.* 95 (1995) 119–131.
- [81] N. A. Mishchuk, Concentration polarization of interface and non-linear electrokinetic phenomena, *Adv. Colloid Interface Sci.* 160 (2010) 16–39.
- [82] F. Maletzki, H.W. Rösler, E. Staude, Ion transfer across electrodesalination membranes in the overlimiting current range: stationary voltage current characteristics and current noise power spectra under different conditions of free convection, *J. Membr. Sci.* 71 (1992) 105–116.
- [83] M. K. Urtenov, A.M. Uzdenova, A.V. Kovalenko, V.V. Nikonenko, N.D. Pismenskaya, V.I. Vasil'eva, P. Sistat, G. Pourcelly, Basic mathematical model of overlimiting transfer enhanced by electroconvection in flow-through electrodesalination membrane cells, *J. Membr. Sci.* 447 (2013) 190-202.
- [84] M. B. Andersen, K.M. Wang, J. Schiffbauer, A. Mani, Confinement effects on electroconvective instability, *Electrophoresis* 38 (2017) 702–711.
- [85] M. García-Gabaldón, V. Pérez-Herranz, E. Ortega, Evaluation of two ion-exchange membranes for the transport of tin in the presence of hydrochloric acid, *J. Membr. Sci.* 371 (2011) 65–74.

- [86] H. Tiana, Y. Li, H. Shao, H.-Z. Yu. Thin-film voltammetry and its analytical applications: A review, *Anal. Chim. Acta* 855 (2015) 1-12.
- [87] S. A. Mareev, D. Yu. Butylskii, N.D. Pismenskaya, V.V. Nikonenko, Chronopotentiometry of ion-exchange membranes in the overlimiting current range. Transition time for a finite-length diffusion layer: modeling and experiment, *J. Membr. Sci.* 500 (2016) 171–179.
- [88] T. Scarazzato, Z. Panossian, M. García-Gabaldón, E.M. Ortega, D.C.R. Espinosa, Evaluation of the transport properties of copper ions through a heterogeneous ion-exchange membrane in etidronic acid solutions by chronopotentiometry, *J. Membr. Sci.* 535 (2017) 268–278.
- [89] R. Madhusudana Rao, R. Rengaswamy, A distributed dynamic model for chronoamperometry, chronopotentiometry and gas starvation studies in PEM fuel cell cathode, *Chem. Eng. Sci.* 61 (2006) 7393–7409.
- [90] M. Grzeszczuk, M. Chmielewski, Influence of electrodeposition potential on composition and ion exchange of polypyrrole films in aqueous hexafluoroaluminate featured by EQCM molar mass to charge factors, *J. Electroanal. Chem.* 681 (2012) 24–35.
- [91] A. A. Moya, P. Sístat, Chronoamperometric response of ion-exchange membrane systems, *J. Membr. Sci.* 444 (2013) 412–419.
- [92] Zh. Xie, St. Holdcroft, Polarization-dependent mass transport parameters for orr in perfluorosulfonic acid ionomer membranes: an EIS study using microelectrodes, *J. Electroanal. Chem.* 568 (2004) 247–260.
- [93] A. A. Moya, The differential capacitance of the electric double layer in the diffusion boundary layer of ion-exchange membrane systems, *Electrochim. Acta* 178 (2015) 249–258.
- [94] F. Roghmans, M. C. Martí-Calatayud, S. Abdu, R. Femmer, M. Wessling, Electrochemical impedance spectroscopy fingerprints the ion selectivity of microgel functionalized ion-exchange membranes, *Electrochemistry Communications* 72 (2016) 113–117.
- [95] V. A. Shaposhnik, V. A. Kuzminykh, O. V. Grigorchuk, V. I. Vasil'eva, Analytical model of laminar flow electro dialysis with ion-exchange membranes, *J. Membr. Sci.* 133 (1997) 27–37.
- [96] V. I. Vasil'eva, O. V. Grigorchuk, V. A. Shaposhnik, Limiting current density in electromembrane systems with weak electrolytes, *Desalination* 192 (2006) 401–407.
- [97] V. I. Vasil'eva, V. A. Shaposhnik, O. V. Grigorchuk, I. P. Petrunya, The membrane-solution interface under high-performance current regimes of electro dialysis by means of laser interferometry, *Desalination* 192 (2006) 408–414.

- [98] M. C. Martí-Calatayud, D. C. Buzzi, M. García-Gabaldón, A. M. Bernardes, J. A. S. Tenório, V. Pérez-Herranz, Ion transport through homogeneous and heterogeneous ion-exchange membranes in single salt and multicomponent electrolyte solutions, *J. Membr. Sci.* 466 (2014) 45–57.
- [99] V. I. Zabolotskiy, A. Yu. But, V. I. Vasil'eva, E. M. Akberova, S. S. Melnikov, Ion transport and electrochemical stability of strongly basic anion-exchange membranes under high current electro dialysis conditions, *J. Membr. Sci.* 526 (2017) 60–72.
- [100] M. L. Vázquez-Garzón, G. Bonotto, L. Marder, J. Z. Ferreira, A. M. Bernardes, Transport properties of tartrate ions through an anion-exchange membrane, *Desalination* 263 (2010) 118–121.
- [101] F. Q. Mir, A. Shukla, Sharp decline in counter-ion transport number of electro dialysis ion exchange membrane on moderate increase in temperature, *Desalination* 372 (2015) 1–6.
- [102] M. B. Kristensen, A. Bentien, M. Tedesco, J. Catalano, Counter-ion transport number and membrane potential in working membrane systems, *J. Colloid and Interface Sci.* 504 (2017) 800–813.
- [103] M. B. Kristensen, A. Bentien, M. Tedesco, J. Catalano, Counter-ion transport number and membrane potential in working membrane systems, *J. Colloid and Interface Sci.* 504 (2017) 800–813.
- [104] J. A. Plambeck, *Electroanalytical chemistry: Basic principles and applications*, John Wiley & Sons Inc, New York (1982).
- [105] J. J. Krol, M. Wessling, H. Strathmann, Concentration polarization with monopolar ion exchange membranes: current-voltage curves and water dissociation, *J. Membr. Sci.* 162 (1999) 145–154.
- [106] V. I. Zabolotsky, V. V. Nikonenko, *Ion transport in membranes*, Moscow, Nauka (1996).
- [107] J.-H. Choi, J.-S. Park, S.-H. Moon, Direct measurements of concentration distribution within the boundary layer of an ion-exchange membrane, *J. Colloid. Interface Sci.* 251 (2002) 311–317.
- [108] J. J. Krol, M. Wessling, H. Strathmann, Chronopotentiometry and overlimiting ion transport through monopolar ion exchange membranes, *J. Membr. Sci.* 162 (1999) 155–164.
- [109] H. J. S. Sand, On the concentration at the electrodes in a solution, *Phil. Mag.* 1 (1901) 45–79.
- [110] E. Volodina, N. Pismenskaya, V. Nikonenko, C. Larchet, G. Pourcelly, Ion transfer across ion-exchange membranes with homogeneous and heterogeneous surfaces, *J. Colloid Interface Sci.* 285 (2005) 247–258.

- [111] E. I. Belova, G. Y. Lopatkova, N. D. Pismenskaya, V. V. Nikonenko, C. Larchet, G. Pourcelly, Effect of Anion-exchange Membrane Surface Properties on Mechanisms of Overlimiting Mass Transfer, *J. Phys. Chem. B* 110 (2006) 13458–13469.
- [112] V.I. Zabolotskiy, A. Yu. But, V.I. Vasil'eva, E.M. Akberova, S.S. Melnikov, Ion transport and electrochemical stability of strongly basic anion-exchange membranes under high current electro dialysis conditions, *J. Membr. Sci.* 526 (2017) 60–72.
- [113] M. A. Lévêque, Les lois de la transmission de chaleur par convection, *Annales des Mines* 13 (1928) 201-239.
- [114] V. V. Nikonenko, A. V. Kovalenko, M. K. Urtenov, N. D. Pismenskaya, J. Han, P. Sistat, G. Pourcelly, Desalination at overlimiting currents: State-of-the-art and perspectives, *Desalination* 342 (2014) 85–106.
- [115] W. J. Koros, Y. H. Ma, T. Shimidzu, Terminology for membranes and membrane processes, *Pure Appl. Chem.* 68 (1996) 1479–1489.
- [116] S. Mikhaylin, L. Bazinet, Fouling on ion-exchange membranes: Classification, characterization and strategies of prevention and control, *Adv. Colloid Interface Sci.* 229 (2016) 34–56.
- [117] S. Lee, C.-H. Lee, Effect of operating conditions on CaSO₄ scale formation mechanism in nanofiltration for water softening, *Water Res.* 34 (2000) 3854–3866.
- [118] S. Lee, C.H. Lee, Scale formation in NF/RO: mechanism and control, *Water Sci. Technol.* 51 (2005) 267–275.
- [119] A. Antony, J. How Low, St. Gray, A. E. Childress, P. Le-Clech, Greg Leslie, Scale formation and control in high pressure membrane water treatment systems: A review, *J. Membr. Sci.* 383 (2011) 1–16.
- [120] S. Y. Choi, J. W. Yu, J. H. Kweon, Electrodialysis for desalination of brackish groundwater in coastal areas of Korea. *Desalin. Water Treat.* 51 (2013) 6230–6237.
- [121] S. Van Geluwe, L. Braeken, T. Robberecht, M. Jans, C. Creemers, B. Van der Bruggen Evaluation of electro dialysis for scaling prevention of nanofiltration membranes at high water recoveries, *Resources, Conservation and Recycling* 56 (2011) 34–42.
- [122] A. C. M. Franklin, Prevention and control of membrane fouling: practical implications and examining recent innovations, *Membraan Applicatie Centrum Twente* (2009).
- [123] N. Gence, N. Ozbay, pH dependence of electrokinetic behavior of dolomite and magnesite in aqueous electrolyte solutions. *Appl. Surf. Sci.* 252 (2006) 8057–8061.
- [124] N. Cifuentes-Araya, G. Pourcelly, L. Bazinet, Multistep mineral fouling growth on a cation-exchange membrane ruled by gradual sieving effects of magnesium and carbonate ions and its delay by pulsed modes of electro dialysis, *J. Colloid Interface Sci.* 372 (2012) 217–230.

- [125] S. Mikhaylin, V. Nikonenko, G. Pourcelly, L. Bazinet, Intensification of demineralization process and decrease in scaling by application of pulsed electric field with short pulse/pause conditions, *J. Membr. Sci.* 468 (2014) 389–399.
- [126] M. Asraf-Snir, J. Gilron, Y. Oren, Gypsum scaling on anion exchange membranes during donnan exchange, *J. Membr. Sci.* 455 (2014) 384–391.
- [127] M. Asraf-Snir, J. Gilron, Y. Oren, Gypsum scaling on anion exchange membranes in electro dialysis, *J. Membr. Sci.* 520 (2016) 176–186.
- [128] N. N. Belaid, B. Ngom, L. Dammak, C. Larchet, B. Auclair, Conductivité membranaire: interpretation et exploitation selon le modèle à solution interstitielle hétérogène, *Eur. Polym. J.* 35 (1999) 879–897.
- [129] R. Lteif, L. Dammak, C. Larchet, B. Auclair Conductivité électrique membranaire: étude de l'effet de la concentration, de la nature de l'électrolyte et de la structure membranaire, *Eur. Polym. J.* 35 (1999) 1187–1195.
- [130] M. Araya-Farias, L. Bazinet, Electro dialysis of calcium and carbonate high-concentration solutions and impact on membrane fouling, *J. Colloid Interface Sci.* 286 (2005) 639–646.
- [131] H-J. Lee, M-K. Hong, S-D. Han, J. Shim, S-H. Moon, Analysis of fouling potential in the electro dialysis process in the presence of an anionic surfactant foulant, *J. Membr. Sci.* 325 (2008) 719–726.
- [132] M-S. Kang, Y-J. Choi, H-J. Lee, S-H. Moon, Effects of inorganic substances on water splitting in ion-exchange membranes: I. Electrochemical characteristics of ion-exchange membranes coated with iron hydroxide/oxide and silica sol, *J. Colloid Interface Sci.* 273 (2004) 523–532.
- [133] V. V. Nikonenko, N. D. Pismenskaya, E. I. Belova, P. Sizat, P. Huguet, G. Pourcelly, C. Larchet, Intensive current transfer in membrane systems: Modelling, mechanisms and application in electro dialysis, *Adv. Colloid Interface Sci.* 160 (2010) 101–123.
- [134] W. C. Hamilton, A technique for the characterization of hydrophilic solid surfaces, *J. Colloid Interface Sci.* 40 (1972) 219–222.
- [135] Y. Yuan, T. R. Lee, Contact angle and wetting properties, *Surface Science Techniques* 51 (2013) 3–34.
- [136] W. Zhang, M. Wahlgren, B. Sivik, Membrane Characterization by the Contact Angle Technique: II. Characterization of UF-Membranes and Comparison between the Captive Bubble and Sessile Drop as Methods to obtain Water Contact Angles, *Desalination* 72 (1989) 263–273.

- [137] A. Bukhovets, T. Eliseeva, Y. Oren, Fouling of anion-exchange membranes in electro dialysis of aromatic amino acid solution, *J. Membr. Sci.* 364 (2010) 339–343.
- [138] H. Guo, L. Xiao, S. Yu, H. Yang, J. Hu, G. Liu, Y. Tang, Analysis of anion exchange membrane fouling mechanism caused by anion polyacrylamide in electro dialysis, *Desalination* 346 (2014) 46–53.
- [139] H-J. Lee, M-K. Hong, S-D. Han, S-H. Cho, S-H. Moon, Fouling of an anion exchange membrane in the electro dialysis desalination process in the presence of organic foulants, *Desalination* 238 (2009) 60–69.
- [140] A. Guinier, X-ray diffraction in crystals, imperfect crystals, and amorphous bodies, Courier Corporation (1994).
- [141] C. Casademont, Gr. Pourcelly, L. Bazinet, Bilayered Self-Oriented Membrane Fouling and Impact of Magnesium on CaCO₃ Formation during Consecutive Electro dialysis Treatments, *Langmuir* 26 (2009) 854–859.
- [142] T. Sata, Studies on anion exchange membranes having permselectivity for specific anions in electro dialysis — effect of hydrophilicity of anion exchange membranes on permselectivity of anions, *J. Membr. Sci.* 167 (2000) 1–31.
- [143] V. D. Grebenyuk, R. D. Chebotareva, S. Peters, V. Linkov, Surface modification of anion-exchange electro dialysis membranes to enhance anti-fouling characteristics, *Desalination* 115 (1998) 313–329.
- [144] K. A. Nebavskaya, V. V. Sarapulova, K. G. Sabbatovskiy, V. D. Sobolev, N. D. Pismenskaya, P. Sistat, M. Cretin, V. V. Nikonenko, Impact of ion exchange membrane surface charge and hydrophobicity on electro convection at underlimiting and overlimiting currents, *J. Membr. Sci.* 523 (2017) 36–44.
- [145] I. Rubinstein, B. Zaltzman, T. Pundik, Ion-exchange funneling in thin-film coating modification of heterogeneous electro dialysis membranes, *Phys. Rev. E Stat. Nonlin. Soft. Matter. Phys.* 65 (2002) 041507.
- [146] F. He, K. K. Sirkar, J. Gilron, Effects of antiscalants to mitigate membrane scaling by direct contact membrane distillation, *J. Membr. Sci.* 345 (2009) 53–58.
- [147] Q. Wang, P. Yang, W. Cong, Cation-exchange membrane fouling and cleaning in bipolar membrane electro dialysis of industrial glutamate production wastewater, *Sep. Purif. Technol.* 79 (2011) 103–113.
- [148] Q. Chen, C. Xue, W-M. Zhang, W-G. Song, L-J. Wan, K-S. Ma, Green Production of Ultrahigh-Basicity Polyaluminum Salts with Maximum Atomic Economy by Ultrafiltration and Electro dialysis with Bipolar Membranes, *Ind. Eng. Chem. Res.* 53 (2014) 13467–13474.

- [149] S. Mikhaylin, V. Nikonenko, G. Pourcelly, L. Bazinet, Hybrid bipolar membrane electro dialysis/ultrafiltration technology assisted by pulsed electric field for casein production, *Green Chem.* (2015) doi: 10.1039/c5gc00970g.
- [150] I. H. Tsibranska, B. Tylkowski, Concentration of ethanolic extracts from *Sideritis* ssp. L. by nanofiltration: Comparison of dead-end and cross-flow modes, *Food and Bioprod. Process.* 91 (2013) 169–174.
- [151] G. Grossman, A. A. Sonin, Experimental study of the effects of hydrodynamics and membrane fouling in electro dialysis, *Desalination* 10 (1972) 157–180.
- [152] J. Balster, D. F. Stamatialis, M. Wessling, Towards spacer free electro dialysis, *J. Membr. Sci.* 341 (2009) 131–138.
- [153] W. E. Katz, The electro dialysis reversal process, *Desalination* 28 (1979) 31–40.
- [154] L. K. Wang, Membrane and desalination technologies, *Handbook of environmental engineering* 13 (2010) 525-556.
- [155] N. A. Mishchuk, L. K. Koopal, F. Gonzalez-Caballero, Intensification of electro dialysis by applying a non-stationary electric field, *Colloid Surf. A* 176 (2001) 195–212.
- [156] A. M. Uzdenova, A. V. Kovalenko, M. K. Urtenov, V. V. Nikonenko, Effect of electroconvection during pulsed electric field electro dialysis. Numerical experiments, *Electrochem. Commun.* 51 (2015) 1–5.
- [157] N. Cifuentes-Araya, G. Pourcelly, L. Bazinet, Impact of pulsed electric field on electro dialysis process performance and membrane fouling during consecutive demineralization of a model salt solution containing a high magnesium/calcium ratio, *J. Colloid Interface Sci.* 361 (2011) 79–89.
- [158] I. Rubinstein, B. Zaltzman, Electro-convective versus electroosmotic instability in concentration polarization, *Adv. Colloid Interface Sci.* 134–135 (2007) 190–200.
- [159] R. Kwak, G. Guan, W.K. Peng, J. Han, Microscale electro dialysis: concentration profiling and vortex visualization, *Desalination* 308 (2013) 138–146.
- [160] V. V. Nikonenko, V. I. Vasil'eva, E. M. Akberova, A. M. Uzdenova, M. K. Urtenov, A. V. Kovalenko, N. P. Pismenskaya, S. A. Mareev, G. Pourcelly, Competition between diffusion and electroconvection at an ion-selective surface in intensive current regimes, *Adv. Colloid Interface Sci.* 235 (2016) 233-246.
- [161] M. Davidson, M. Wessling, A. Mani, On the dynamical regimes of pattern-accelerated electroconvection, *Sci. Rep.* 6 (2016) doi:10.1038/srep22505.
- [162] S. Mikhaylin, V. Nikonenko, N. Pismenskaya, G. Pourcelly, S. Choi, H. J. Kwon, J. Han, L. Bazinet, How physico-chemical and surface properties of cation-exchange membrane

affect membrane scaling and electroconvective vortices: Influence on performance of electrodialysis with pulsed electric field, *Desalination* 393 (2016) 102–114.

[163] E. Belova, G. Lopatkova, N. Pismenskaya, V. Nikonenko, C. Larchet, Role of water splitting in development of electroconvection in ion-exchange membrane systems, *Desalination* 199 (2006) 59–61.

[164] N. D. Pismenskaya, V. V. Nikonenko, N. A. Melnik, K. A. Shevtsova, E. I. Belova, G. Pourcelly, D. Cot, L. Dammak, C. Larchet, Evolution with time of hydrophobicity and microrelief of a cation-exchange membrane surface and its impact on overlimiting mass transfer, *J. Phys. Chem. B* 116. (2012) 2145–2161.

[165] C. Casademont, G. Pourcelly, L. Bazinet, Effect of magnesium/calcium ratios in solutions treated by electrodialysis: Morphological characterization and identification of anion-exchange membrane fouling, *J. Colloid Interface Sci.* 322 (2008) 215–223.

[166] C. Casademont, G. Pourcelly, L. Bazinet, Effect of magnesium/calcium ratio in solutions subjected to electrodialysis: Characterization of cation-exchange membrane fouling, *J. Colloid Interface Sci.* 315 (2007) 544–554.

[167] C. Casademont, M. Araya-Farias, G. Pourcelly, L. Bazinet, Impact of electro-dialytic parameters on cation migration kinetics and fouling nature of ion-exchange membranes during treatment of solutions with different magnesium/calcium ratios, *J. Membr. Sci.* 325 (2008) 570–579.

Chapter 2

Effect of electrolyte nature and membrane surface properties on the development of electroconvection

Presentation of the article

In the previous chapter, we have presented general information about ion-exchange membranes, the main applications of ion-exchange membranes and the limitations of electro dialysis process. It has been shown that the application of overlimiting currents in electro dialysis can increase the mass transfer in electromembrane system due to intensification of electroconvection. As the electroconvective vortexes deliver the “fresh” solution from the bulk to the membrane interface, the water splitting is reduced and the scale formation on the membrane surface can be prevented or mitigated.

Choi and Moon [1] showed that the intensity of electroconvection depends on the nature of electrolyte, namely, on the degree of counter-ion hydration. More the counter-ion hydration number, more intensive is electroconvection. These results were obtained in steady state of membrane system using voltammetry. However, the influence of counter-ion nature on the dynamics of electroconvection development in non-stationary conditions is not studied. Nevertheless, non-stationary conditions are widely used in electro dialysis, namely, in pulse electric field modes. It is important to know how fast electroconvection is developing, at which current density/voltage the effect of electroconvection on mass transfer becomes significant, and how these parameters depend on the electrolyte nature.

On the other hand, it is known that the effect of electroconvection increases when heterogeneous membrane is surface-modified by a thin homogeneous ion-conductive perfluorinated film of Nafion[®] or its Russian analogue MF-4SK in NaCl solutions. Hence, this type of membrane modification seems promising for mass transfer intensification and for mitigation of scaling, taking into account the ability of electroconvection to reduce the rate and amount of scale formation shown by Mikhaylin et al. [2]. However, electroconvection in the systems with this type of membranes in the solutions containing scaling agents is not studied yet.

The main task of the study presented in this chapter is the effect of electrolyte nature and membrane surface properties on the dynamics of electroconvection development. By means of chronopotentiometry and voltammetry the influence of different counter-ions Na⁺, Ca²⁺ and Mg²⁺ is investigated in the article when using a commercial heterogeneous cation-exchange MK-40 membrane and its modification by a MF-4SK layer. Investigations are carried out in a four-compartment flow-through electro dialysis cell.

This study allows us to conclude that the potential drop across the membranes at a fixed value of i/i_{lim} decreases in the order Na⁺>Ca²⁺>Mg²⁺ in both stationary and non-stationary regimes. This order agrees with that found by Choi and Moon [1] in the case of steady state.

Additionally, we have established that at a fixed i/i_{lim} ratio, electroconvection develops faster in the case of Mg^{2+} and Ca^{2+} ; the value of time at which electroconvection becomes significant in the case of Na^+ is greater. In the case of Mg^{2+} and Ca^{2+} at a constant overlimiting current this time is about 3-7 s, which is less than the transition time. In the case of Na^+ this time is close to the transition time. The latter is necessary to attain a concentration at the membrane surface close to zero and varies in the range of 4-23 s.

In all studied case, at a fixed i/i_{lim} ratio, the potential drop is less and electroconvection is higher in the case of modified membrane. The latter is necessary to attain a concentration at the membrane surface close to zero.

Thus, in the case of Mg^{2+} and Ca^{2+} ions, the electroconvection is more intense and the oscillations appear at times shorter than the transition time, which gives us reason to assume that the “fight” against sedimentation will be successful.

**Effect of counterion hydration number on the
development of electroconvection at the surface of
heterogeneous cation-exchange membrane modified
with an MF-4SK film**

Petroleum Chemistry (56) 2016 440-449

V. V. Gil^a, M. A. Andreeva^{a, b}, N. D. Pismenskaya^a, V. V. Nikonenko^a, C. Larchet^b, and L. Dammak^b

^a *Kuban State University, ul. Stavropol'skaya 149, Krasnodar, Russia*

^b *Institut de Chimie et des Matériaux Paris-Est, UMR7182 CNRS–Université Paris-Est, 2 Rue Henri Dunant, 94320 Thiais, France*

Abstract

The transport of sodium, calcium, and magnesium ions through the heterogeneous cation-exchange membrane MK-40, surface modified with a thin (about 15 μm) homogeneous film MF-4SK. By using chronopotentiometry and voltammetry techniques, it has been shown that the combination of relatively high hydrophobicity of the film surface with its electrical and geometrical (surface waviness) heterogeneity creates conditions for the development of electroconvection, which considerably enhances mass transfer in overlimiting current regimes. The electroconvection intensity substantially depends on the degree of counter-ion hydration. Highly hydrated calcium and magnesium ions involve in motion a much larger volume of water as compared with sodium ions. When constant overlimiting direct current is applied to the membrane, electroconvective vortices in 0.02 M CaCl_2 and MgCl_2 solutions are generated already within 5-8 s, a duration that is the transition time characterizing the change of the transfer mechanism in chronopotentiometry.

The generation of vortices is manifested by potential oscillations in the initial portion of chronopotentiograms; no oscillation has been observed in the case of 0.02 M NaCl solution. More intense electroconvection in the case of doubly charged counter-ions also causes a reduction in the potential drop ($\Delta\phi$) at both short times corresponding to the initial portion of chronopotentiograms and long times when the quasi-steady state is achieved. At a fixed ratio of current to its limiting value, $\Delta\phi$ decreases in the order $\text{Na}^+ > \text{Ca}^{2+} > \text{Mg}^{2+}$.

2.1 Introduction

Overlimiting current regimes are increasingly being used in electro dialysis of dilute solutions [3]. A positive economic effect [4] under such conditions is achieved via stimulation of mass transfer by electroconvection [4-7], which not only increases the useful transport of salt ions [8], but also prevents membrane scaling [2].

Several electroconvection (EC) mechanisms are discussed in the literature [9]. Globally, electroconvection, i.e., fluid transport driven by an electric force, occurs when the force acts on both space charge in the region of a microscopic electric double layer (EDL) (electro-osmosis phenomenon) and the residual space charge in the stoichiometrically electroneutral macroscopic bulk solution [9-11]. On the other hand, the state of EDL can be either (quasi)equilibrium at a current density i below the limiting current density i_{lim} or nonequilibrium when $i > i_{lim}$. Accordingly, there are equilibrium and nonequilibrium electroconvection modes [9]. When $i < i_{lim}$, the EDL structure remains the same as for $i = 0$, with the EDL thickness being inversely proportional to the root of counter-ion concentration at the interface of EDL with electrically neutral solution, C_{1s} [12]. At $i > i_{lim}$, when C_{1s} is on the order of 10^{-6} mol/L, the quasi-equilibrium EDL having a thickness of about a hundred nanometers adds a nonequilibrium extended space charge region (SCR) with a thickness of several microns [13, 14]. Dukhin and Mishchuk [15, 16] proposed to call electro-osmosis at $i < i_{lim}$ (equilibrium EC) electro-osmosis of the first kind and that at $i > i_{lim}$, electro-osmosis of the second kind. With underlimiting currents in the case of a homogeneous, smooth, ideally ion-selective surface, EC is stable and its influence on mass transfer is negligible. According to published data [6, 15-17], intense EC is developed near an ion-selective surface (ion-exchange beads, membranes, etc.) if the following two conditions are observed: there are the extended SCR and tangential electric force. The tangential force emerges if the surface has electrical or geometrical heterogeneity: the surface resistance varies along the longitudinal coordinate or the surface has convexities or cavities. However, as shown theoretically by Urtenov et al. [18], EC in the channels of a forced-flow electro dialyzer develops even in the case of smooth homogeneous membranes. At currents $i \approx i_{lim}$, the mechanism of the phenomenon is similar to the Dukhin-Mishchuk mechanism. However, the cause of the tangential bulk electric force is nonuniformity of the concentration field, rather than electric or geometric irregularity of the surface. The heterogeneity of the concentration field is due to the fact that the solution is desalted as it flows between the membranes. This mechanism gives

rise to stable vortices in the surface layer of the depleted solution. The vortices facilitate arrival of the fresh solution to the membrane surface and the removal of the depleted solution from the surface into the bulk, a factor that explains the increase in the counter-ion transport velocity and the excess current density over its limiting value. The Dukhin-Mishchuk regime pertains to the potential range corresponding to the sloping plateau of the current-voltage curve, in which there are no noticeable oscillations. As the potential drop increases to a certain threshold, this EC mechanism is replaced by the Rubinstein-Zaltzman convective instability mechanism [19]. In this case, EC vortices become significantly larger and more unstable over time, thereby causing current oscillation at a constant potential drop (or potential drop oscillations at a fixed value of current).

Existing theoretical models [9, 18-22] suggest that the electric body force responsible for the transfer of water is proportional to the product of the field strength and space charge density. The expression for this force does not contain parameters that reflect the interaction of ions and water molecules. In particular, this expression does not account for the influence of the nature of space-charge-forming ions. However, the experimental data obtained by Choi et al. [1] indicate that current-voltage curve parameters, such as the plateau length, substantially depend on the nature of the electrolyte. Analysis of the current-voltage curves led the cited authors [23] to the conclusion that the electroconvection intensity increases with an increase in the Stokes radius of the counter-ion. This is an important conclusion, because it gives the opportunity to predict the behavior of membrane systems indifferent electrolytes under intensive current regimes.

In particular, this information can help to evaluate the risk of scaling on the surface and in the bulk of the membrane during treatment of solutions containing hardness ions (Ca^{2+} , Mg^{2+} , etc.).

However, the concepts of electroconvection emergence mechanisms, which can be different depending on the ability of counter-ion to engage a volume of water in movement, have been poorly developed. In particular, it is unclear how the nature of the counter-ion will affect the dynamics of mass transfer and electroconvection over time. In this study, the main tool of experimental research was the technique of chronopotentiometry. We show that in the presence of strongly hydrated Ca^{2+} and Mg^{2+} ions, electroconvection is not only more intense under steady state conditions, but onsets at shorter times after switching on direct current.

2.2 Experimental

2.2.1 Protocol

Investigations were carried out in a four-compartment, flow-through electro dialysis (ED) cell, in which the desalination channel (DC) was formed by an AMX anion-exchange membrane (Astom, Tokuyama Soda, Japan) and an MK-40_{MOD} cation-exchange membrane. The procedures for measuring current–voltage characteristics and chronopotentiograms are detailed in [23]. A specific feature of the cell design is that the cell provides a laminar flow regime in the intermembrane space. In this case, it is possible to theoretically calculate the limiting current density in the cell and the effective thickness of the diffuse layer using the Leveque equation (see. Eq. (2.5) in Results and Discussion section).

Experiments were carried out with three different solutions (NaCl, CaCl₂, and MgCl₂) of the same concentration (0.02 M), which were alternately pumped through the desalination channel. A 0.02 M NaCl solution was circulated through the buffer and electrode compartments. The pumping rate of the solution through all the compartments was the same, $V = 0.4 \text{ cm s}^{-1}$; the intermembrane distance was $h = 6.5 \text{ mm}$; and the polarized membrane area was $S = 4 \text{ cm}^2$. Luggin capillaries, connected with Ag/AgCl electrodes, were brought to the geometric centers of polarizable sites of the test membrane and spaced at about 0.8 mm from its surface.

2.2.2 Ion-exchange membranes

The membrane MK-40_{MOD} was prepared by forming on the surface of a heterogeneous MK-40 membrane (Shchekinoazot, Russia) of a thin (about 15 μm thickness) homogeneous film by casting an LF-4SK solution kindly provided by S.V. Timofeev (Plastpolymer). The LF-4SK is a solution of tetrafluoroethylene copolymer with sulfonated perfluorovinyl ether in isopropyl alcohol. Solvent evaporation gives a film identical to the MF-4SK membrane. The procedure for preparing the modifying film and main characteristics of the resulting bilayer membrane are presented in [8]. From these data it follows that the exchange capacity, diffusion permeability, and conductivity of the original (MK-40) and modified (MK-40_{MOD}) membranes are identical within the measurement errors. What have changed are the chemical composition, most (80 %) of the surface of the swollen MK-40 membrane is coated with polyethylene, used as a filler binder. Particles of KU-2 ion-exchange resin, which provide selective conductivity of the membrane, form crests on the polyethylene surface of about 3 μm in height (Fig. 2-1a). The MF-4SK film covering the MK-40_{MOD} surface does not

contain nonconductive areas ($\hat{S} = 100\%$), but it is not perfectly smooth (Fig. 2-1b). There are projections and depressions on the surface, with the height difference between them determined with a Zeiss AxioCam MRc5 light microscope being about $2\ \mu\text{m}$; the distance between adjacent crests is $5\text{--}10\ \mu\text{m}$.

Coating the MK-40 membrane with the MF-4SK film leads to an increase in the contact angle (measured for the swollen state as described in [24]) from 55° to $64^\circ (\pm 3^\circ)$.

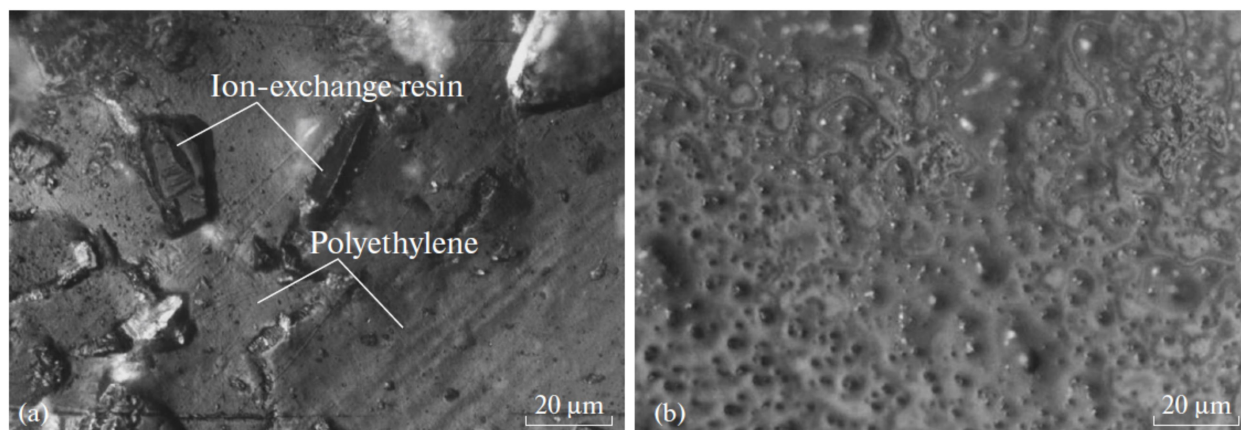


Fig. 2-1. Image of the surface of swollen MK-40 (a) and MK-40_{MOD} (b) membranes as obtained with a Zeiss AxioCam MRc5 light microscope.

2.2.3 Materials

The solutions were prepared using distilled water ($400\ \text{k}\Omega\ \text{cm}$) and the following chemicals: NaCl (R.P.NORMAPURTM, VWR International), $\text{CaCl}_2 \cdot 2\text{H}_2\text{O}$, and $\text{MgCl}_2 \cdot 6\text{H}_2\text{O}$ (LABOSI, Fisher Scientific s.a.).

Values for the diffusion coefficients (D_i), Pauling crystal radii (r_{cr}), Stokes radii determined from the Einstein–Stokes relation (r_{St}), and the hydration numbers of the Na^+ , Ca^{2+} , and Mg^{2+} cations and the Cl^- anion in aqueous solution are presented in Table 2-1. The electrolyte diffusion coefficients (D) and cation transport numbers (t_i) are also listed there. All the transport characteristics are given for infinitely dilute solutions and a temperature of 20°C , at which the experiments were conducted. The values for the crystal radii and ion hydration numbers were borrowed from [25]. To determine D_i , D , r_{St} , and t_i at 20°C , the temperature dependence of equivalent conductivity at infinite dilution was used [25].

Water molecules in the primary shell of Mg^{2+} are stronger bonded to the ion as compared with Ca^{2+} [26], a difference that is manifested in a lower value of the average length of the Mg–O bond compared to Ca–O. These bond lengths are respectively 2.07 and $2.45\ \text{\AA}$ [27]. The

length of the hydrogen bond between oxygen atoms in the primary and secondary shells of the Mg^{2+} or Ca^{2+} ions is 2.74 or 2.88 Å, respectively [27], values that also indicate a greater strength of water binding by magnesium ions. These data, as well as the hydration numbers and Stokes radii of cations (Table 2-1) show that the ability of the cations to structure water increases in the following order: $\text{Na}^+ < \text{Ca}^{2+} < \text{Mg}^{2+}$.

Ion					Electrolyte		
	$D_i, 10^5 \text{ cm}^2 \text{ s}^{-1}$	$r_{cr}, \text{ Å}$	$r_{St}, \text{ Å}$	hydration number		$D, 10^5 \text{ cm}^2 \text{ s}^{-1}$	t_i of cation
Na^+	1.18	0.97	2.1	5	NaCl	1.43	0.395
Ca^{2+}	0.70	0.99	3.5	8	CaCl_2	1.18	0.436
Mg^{2+}	0.62	0.65	4.0	10	MgCl_2	1.10	0.406
Cl^-	1.80	1.81	1.4	2			

Table 2-1. Some characteristics of ions and electrolyte solutions containing the ions (at 20°C).

2.3. Results and discussion

2.3.1 Chronopotentiometry

Fig. 2-2 exemplifies a chronopotentiogram (CP) of one of the test systems (MK-40_{MOD} in 0.02 M CaCl_2 solution), which shows some characteristic sections and points that are used in data processing. Explanations are given in the figure caption.

To compare between chronopotentiograms of different membrane systems, it is convenient to use the difference of total potential drop $\Delta\varphi$ and ohmic potential drop $\Delta\varphi_{ohm}$ in the unpolarized membrane system instead of the total potential drop per sec. [28]:

$$\Delta\varphi' = \Delta\varphi - \Delta\varphi_{ohm} \quad (2.1)$$

The value of $\Delta\varphi_{ohm}$ is found by extrapolation to the time $t = 0$ (current switching on time) in the $\Delta\varphi - \sqrt{t}$ coordinates [29]. The value of $\Delta\varphi'$ is sometimes called reduced potential difference.

When a membrane system reaches a (quasi-)steady state, the potential $\Delta\varphi_{st}$ slightly changes with time (Fig. 2-2). The values of $\Delta\varphi_{st}$ and i were used to construct galvanostatic current-voltage curves (CVCs).

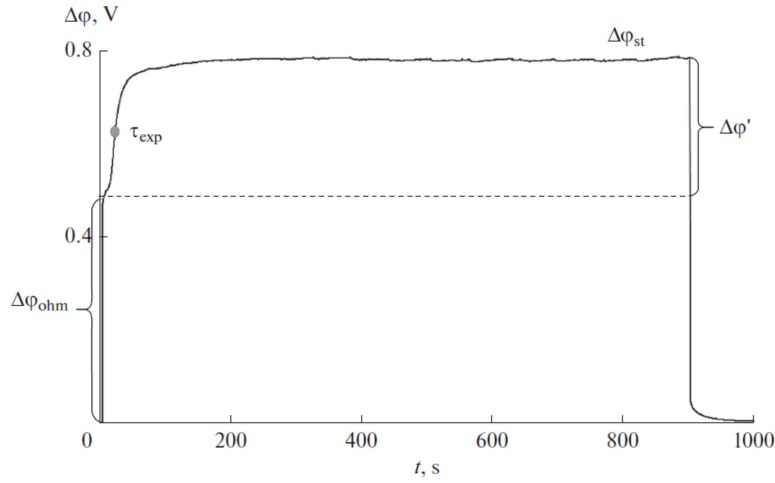


Fig. 2-2. Chronopotentiogram of the MK-40_{MOD} membrane in 0.02 M CaCl₂ solution at a current density of $i = 4.8 \text{ mA}\cdot\text{cm}^2$: $\Delta\varphi_{ohm}$ is the ohmic potential drop immediately after turning on the power, $\Delta\varphi_{st}$ is the potential drop at the time the membrane system reaches the steady state, $\Delta\varphi'$ is the reduced potential difference defined by Eq. (2.1), and τ_{exp} is the transition time determined from the inflection point on the chronopotentiometric curve.

In terms of the simple mathematical model proposed by Sand [30], assuming local electroneutrality and the absence of convection, the counter-ion concentration at the membrane surface C_{1s} depends upon the time t elapsed since the switching on the direct current with a density i , as a function of \sqrt{t}

$$C_{1s} = C_1 - \frac{2i(T_i - t_i)}{z_1 F D} \sqrt{\frac{Dt}{\pi}} \quad (2.2)$$

where C_1 is the counter-ion concentration (in $\text{mol}\cdot\text{L}^{-1}$) in the bulk of the stirred solution; T_1 and t_1 are the counter-ion transport numbers in the membrane and the solution, respectively; z_1 is the counter-ion charge; and F is Faraday's number.

According to Eq. (2.2), C_{1s} decreases with time, resulting in increased potential drop (DP) across the membrane. When C_{1s} becomes small relative to C_1 , the potential drop dramatically

increases (Fig. 2-2). The smallness of C_{1s} and a large value of $\Delta\phi$ cause the appearance of additional transport mechanisms other than electrically driven diffusion occurring at low values of $\Delta\phi$. Such additional mechanisms can be the dissociation of water (which generates additional charge carriers, the H^+ and OH^- ions), as well as conjugated convection, gravitational convection [31], and electroconvection. As shown in our earlier study [7], electroconvection whose mechanism is briefly described in the introduction gives the largest contribution in this system. Electroconvection provides mixing of the depleted solution at the membrane surface, which slows the PD growth over time. Slowing down the growth of the potential drop causes the appearance of an inflection point in the chronopotentiogram. The time corresponding to the inflection point is called transition time, τ . The quantity τ is an important parameter because it defines the time required to achieve a nearly zero value of the near-to-surface concentration of electrolyte and to change the transport mechanism. The equation for calculating τ was derived by Sand [30] from Eq. (2.2), in which C_{1s} is set to be zero [32, 33]:

$$\tau = \frac{\pi D}{4} \left(\frac{Fz_1 C_1}{T_1 - t_1} \right)^2 \frac{1}{i^2} \quad (2.3)$$

Equation (2.3) holds if electrolyte transport at the membrane surface is determined by electrodiffusion. To eliminate the effect of the finite thickness of the diffuse layer, the current density at which this equation is applicable should be greater than the limiting value by a factor of at least 1.5 [34].

The EC intensity increases with $\Delta\phi$, so the system goes into the (quasi-)stationary state over time when value of $\Delta\phi$ only slightly changes with time.

The stationary value of the limiting current density i_{lim} is defined as the maximum value of i achieved during electrodiffusion transport in the absence of associated effects. According to Pierce equation [5],

$$i_{lim} = \frac{z_1 C_1 F D}{\delta(T_1 - t_1)} \quad (2.4)$$

where δ is the thickness of the Nernst diffusion boundary layer.

In the case of a channel formed by smooth membranes and laminar flow of solution, i_{lim} can be calculated by the Leveque equation obtained in terms of the convection-diffusion model [35]:

$$i_{\text{lim}}^{\text{theor}} = \frac{z_1 C_1 F D}{h(T_1 - t_1)} \left[1.47 \left(\frac{h^2 V}{LD} \right)^{1/3} - 0.2 \right] \quad (2.5)$$

Here, L is the length of the desalination path (2 cm).

Substituting Eq. (2.4) into Eq. (2.2) gives

$$C_{1s} = C_1 \left(1 - \frac{2}{\pi} \frac{i}{i_{\text{lim}}} \right) \frac{\sqrt{Dt}}{\delta} \quad (2.6)$$

Since the potential drop across the membrane upon electrodiffusion transport is largely determined by the value of C_{1s} , the form of the initial portion of CP for different electrolytes should be almost identical if the i/i_{lim} ratio and for the two systems take the same values.

Fig. 2-3 and 2-4a show chronopotentiograms of the test membrane systems under comparable conditions: reduced potential differences $\Delta\phi'$ (see Eq. (2.1)) for different electrolytes are compared for the same values of i/i_{lim} . Fig. 2-4b presents the data in the $\Delta\phi' - \sqrt{Dt}/\delta$ coordinates. As can be seen from Fig. 2-4b, the chronopotentiograms for all the three systems at short times $t < t_m$ are generalized by a single curve in accordance with the foregoing. However, the patterns of the curves become different at $t > t_m$.

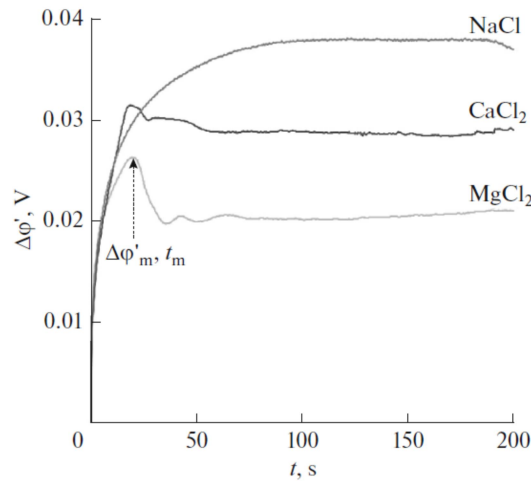


Fig. 2-3. Chronopotentiograms of the MK-40_{MOD} membrane, as measured for different electrolytes at $i/i_{\text{lim}}^{\text{theor}} = 0.8$. The data were obtained at current densities of $i = 1.5 \text{ mA}\cdot\text{cm}^{-2}$ (NaCl), $i = 2.8 \text{ mA}\cdot\text{cm}^{-2}$ (CaCl₂), and $i = 2.5 \text{ mA}\cdot\text{cm}^{-2}$ (MgCl₂); the values of $i_{\text{lim}}^{\text{theor}}$ are given in Table 2-2.

In the case of NaCl, there is a monotonic increase in the potential drop, which is qualitatively consistent with the Sand theory. In the case of MgCl₂ or CaCl₂, there is a local PD maximum at a time $t = t_m$. The minimum current density at which the local maximum is detectable is 0.8 with t_m being 19 s for both electrolytes (Fig. 2-3). Note that the transitional state is not achieved yet at this underlimiting current. As the current increases, t_m decreases: in particular, $t_m \approx 3$ s at $i / i_{\text{lim}}^{\text{theor}} = 2.2$ for MgCl₂ (Fig. 2-4b), which is substantially shorter than the transition time $\tau = 13$ s.

The nonmonotonic pattern of the time dependence for the potential drop in the initial portion of the chronopotentiogram develops as potential oscillation with the increasing time.

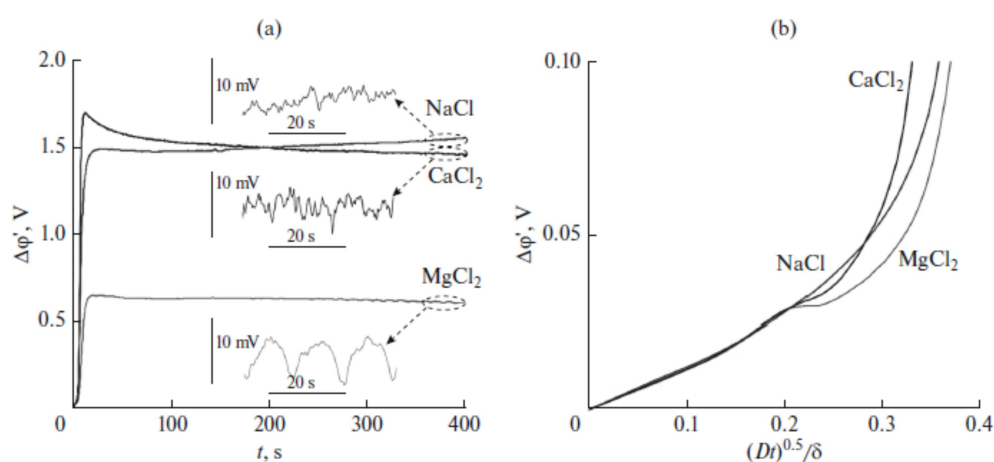


Fig. 2-4. Chronopotentiograms of the MK-40_{MOD} membrane, as measured for different electrolytes at $i / i_{\text{lim}}^{\text{theor}} = 2.2$. The data were obtained at current densities of $i = 4.5 \text{ mA cm}^{-2}$ (NaCl), $i = 7.7 \text{ mA cm}^{-2}$ (CaCl₂), and $i = 7.0 \text{ mA cm}^{-2}$ (MgCl₂).

This oscillation is clearly seen when the quasi-stationary state is reached; that is, when the time average PD value, $\Delta\phi'_{st}$, becomes constant (Fig. 2-4a). The value of $\Delta\phi'_{st}$ (minus initial ohmic PD) increases in the order $\text{Mg}^{2+} < \text{Ca}^{2+} < \text{Na}^+$, whereas the PD oscillation amplitude, on the contrary, decreases on passing from Mg^{2+} to Na^+ (Fig. 2-4a).

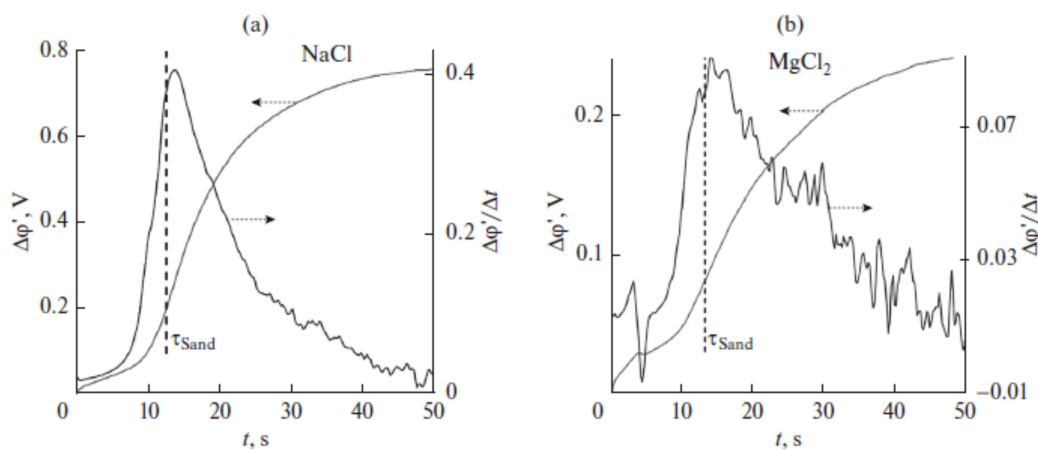


Fig. 2-5. Initial portions of chronopotentiograms of the MK-40_{MOD} membrane in 0.02 M solutions of (a) NaCl and (b) MgCl₂ and the same curves shown in the differential form. The data were obtained at $i/i_{\text{lim}}^{\text{theor}}=1.7$; $i=3.5 \text{ mA cm}^{-2}$ (NaCl) and $i=5.3 \text{ mA cm}^{-2}$ (MgCl₂).

The PD fluctuations can be shown in a more illustrative manner if the initial CP portion of the chronopotentiogram is represented in the differential form (Fig. 2-5b). The values of corresponding to the first local maximum are in the range of 20–30 mV over the entire current range examined (Fig. 2-6).

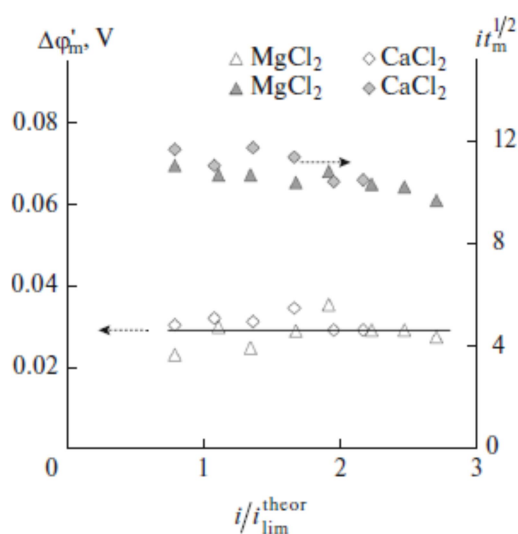


Fig. 2-6. Plot of values for the first local maximum of reduced CP potential difference (open symbols) and the time taken to reach the maximum (closed symbols) versus the current density normalized to the limiting current density calculated by Eq. (2.5).

As has been already noted, t_m rapidly decreases with an increase in applied current (Figs. 2-3–2-5). However, the value of $it_m^{0.5}$ is almost independent of i (Fig. 2-6). This behavior can be

explained if we take into account Eq. (2.6), which suggests that C_s depends upon $it^{0.5}$. The onset of the first PD oscillation is presumably due to reaching a certain threshold value of C_s at the membrane/solution interface. Calculation of the surface-average value $C_{s_{av}}$ using Eq. (2.6) for $i/i_{lim} = 0.8$ and $t = 19$ s (conditions corresponding to the maximum in Fig. 2-3) yields $C_{s_{av}} = 0.011$ mol L⁻¹. The resulting value is too high to allow the formation of the extended SPR. However, Rubinstein and Zaltzman [9] showed that for the development of electroconvection at underlimiting currents, the electrochemical potential gradient along the membrane surface is important and not so much the average concentration $C_{s_{av}}$. This gradient may take relatively large values for the test membrane, since the membrane surface is electrically and geometrically irregular. In particular, the presence of crests and troughs can lead to a significantly large value of the tangential electrical force acting on the equilibrium space charge along the “slope” of the crest necessary for EC development [6]. However, PD oscillations in the case of NaCl were not observed at times shorter than τ (Figs. 2-3–2-5). Thus, it can be stated that a necessary condition for the appearance of such oscillations at underlimiting currents is not only the presence of the tangential body force, but also the presence of a sufficiently large hydration shell, as in the case of Ca²⁺ and Mg²⁺ ions.

2.3.2 Current-Voltage Characteristics

Fig. 2-7 shows reduced current-voltage curves for the test membranes in 0.02 M NaCl, CaCl₂, and MgCl₂ solutions, as derived from chronopotentiograms in the form of dependence of the time-average potential drop in the steady state, $\Delta\phi_{st}$, upon current density (Figs. 2-3, 2-4a).

Table 2-2 presents values for the limiting current density calculated by Eq. (2.5), i_{lim}^{theor} and the data obtained by the graphic processing of CVCs. The value of i_{lim}^{exp} was determined by extrapolating the tangent to the inclined CVC “plateau” to the ordinate axis. The “plateau” length $\Delta\phi'_p$ was found from the value of the potential drop at the point of intersection of the tangents to the inclined “plateau” and to the segment of the rapid current rise [1]. The thickness of the diffusion layer (δ) was evaluated using Eq. (2.5) and Pierce equation (2.4). From these data it follows that the “plateau” length decreases and the slope of the “plateau” increases in the order of Na⁺ < Ca²⁺ < Mg²⁺, that is, with an increase in the water-structuring capacity of the cations and, hence, the capacity to engage large volumes of water in their movement. These results are in good agreement with those obtained by Choi et al. [1], who

associated the revealed relationship with the enhancement of electroconvection by increasing the Stokes radius of the counter-ion.

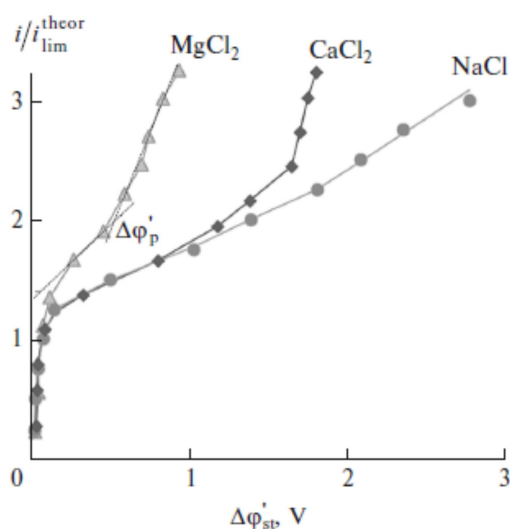


Fig. 2-7. Current-voltage curves for the MK-40_{MOD} membrane in 0.02 M NaCl, CaCl₂, and MgCl₂ solutions. The reduced potential difference was determined using Eq. (2.1). The value of $\Delta\phi'_p$ shows the intersection of the tangents to the inclined “plateau” and to the segment of the fast current rise.

In [8, 23] we have shown that the application of a homogeneous hydrophobic cation-exchange film onto the surface of a heterogeneous cation-exchange membrane promotes the development of electroconvection and enhances mass transfer.

Counter-ion	Theoretical values		Experimental values			
	δ , μm	$i_{\text{lim}}^{\text{theor}}$, mA cm^{-2}	$i_{\text{lim}}^{\text{exp}}$, mA cm^{-2}	$i_{\text{lim}}^{\text{exp}} / i_{\text{lim}}^{\text{theor}}$	$\Delta\phi'_p$, V	CVC plateauslope, mS cm^{-2}
Na ⁺	248	2.0	2.4	1.2	1.8	1.2
Ca ²⁺	233	3.5	4.2	1.2	1.6	2.1
Mg ²⁺	228	3.1	4.1	1.4	0.5	3.7

Table 2-2. Parameters of current-voltage curves for the test membrane systems.

The effect of surface properties of ion-exchange membranes on their electrochemical behavior at overlimiting currents, depending on the degree of development of electroconvection, was also studied by other investigators. Zhil'tsova et al. [36] visualized convective instability

zones due to oscillating EC vortices near two membranes, using laser interferometry. Commercial MK-40 and modified membranes were studied; the latter was similar to MK-40_{MOD}, but it was prepared with the use of a Nafion film, not the MF-4SK. It was shown that at a fixed current density, the size of the EC instability zone near the MK-40_{MOD} is greater and the potential drop across the membrane is smaller compared with those in the case of MK-40. The cause of EC intensification at the surface of the modified membrane is an easier slip of the liquid along the hydrophobic surface [37]. The second reason behind the growth of EC near the modified membrane may be optimization of the “funnel” effect. This effect, described by Rubinstein and coworkers [38], consists in that electric current lines at the surface of an electrically inhomogeneous membrane are concentrated in conductive areas. This concentration leads to two outcomes. One is that local current density through the conductive areas is substantially higher than the surface-average density, thereby causing a significant reduction in salt concentration at the surface and a greater potential drop compared with those at the homogeneous surface. The other is the stimulation of electroconvection by the tangential electric force formed at the boundary between the conducting and nonconducting areas when the current lines are curved. More intense electroconvection reduces both the resistance of the system and the potential drop. In the case of MK-40, in which the proportion of the conductive surface is very small, the first effect is dominant, and the potential difference across this membrane at a low excess of the limiting current is higher than that across the homogeneous membrane. In the case of MK-40_{MOD}, in contrast, the second effect makes a greater contribution; the PD across a membrane of this type is substantially smaller than that across the unmodified membrane.

The scenario of development of early oscillations in the equilibrium EC mode when the concentration polarization of the membrane is relatively low and the extended SCR is not formed, was described in the recent theoretical paper by Rubinstein and Zaltzman [9]. They associated periodic oscillations of current at a fixed potential drop with the evolution of EC vortices at the membrane surface in the system with an unforced flow of the solution. A surface part corresponding to the maximum size of a vortex was considered. The larger the vortex size, the more effectively it stirs the solution at the surface. This decreases the resistance of the solution adjacent to the membrane and increases the current density. At the same time, the evolution of the vortex structure involves the formation of another, adjacent vortex rotating in the opposite direction. Developing, this second vortex increases in size and captures part of the space that has been originally occupied by the first vortex. As a result, the size of the first vortex decreases. After some time when the both vortices have similar sizes making in total the maximum size of the first vortex, their contribution in the mixing of the

near-membrane solution becomes minimal. The resistance in this state becomes maximal, and the current density is reduced to its minimum. Then, the initial vortex disappears and a new vortex that rotates in the opposite direction appears instead. The current density reaches a maximum value again. Note that the oscillation pattern and period (several seconds) calculated in [9] are similar to those observed in our experiment (Fig. 2-4a).

According to Rubinstein and Zaltzman [9], the threshold current/PD value for equilibrium electroconvection may be well below the threshold required for the onset of nonequilibrium EC, which appears in the presence of the extended SCR. This fact, as well as the similarity of the oscillation parameters predicted by Rubinstein and Zaltzman and found in the experiment, suggests that the potential oscillations observed at low potential drops in the initial portions of CP are due to instability of equilibrium EC [9]. Electroconvection of this type occurs in all the test systems. However, the size of vortices emerged in the case of NaCl is so small that their appearance does not affect the form of the initial portion of CP (Figs. 2-3–2-5). Indirect evidence for their presence is the excess of τ_{exp} values over τ_{Sand} (Fig. 2-5a). In fact, Ca^{2+} and, especially, Mg^{2+} ions structure water much stronger than do Na^+ ions (Table 2-1). Therefore, the EC vortices formed in their presence much stronger stir the solution, a difference that is manifested in the oscillations recorded.

The mechanism of CP oscillations observed at large times of $t > \tau$, when the system reaches a quasi-stationary state, differs from the oscillation mechanism at $t < \tau$. As mentioned above, additional current transport mechanisms that ensure the achievement of the steady state at a finite potential drop develop in the vicinity of the transition time. Under our experimental conditions, electroconvection plays a determining role. At $t \approx \tau$, ($i > i_{\text{lim}}$), the near-surface electrolyte concentration reaches a threshold value sufficient for the development of a nonequilibrium extended SCR at the membrane surface. In this case, unstable EC appears in accordance with the Rubinstein-Zaltzman mechanism. After reaching the quasi-stationary state, vortex clusters consisting of several opposing vortices are continuously formed at the membrane surface [18, 39]. Dominating are the vortices, the rotation direction of which on their outer boundary is concerted with the direction of the forced fluid flow. Inside the cluster, there is the depleted solution, which is being vigorously stirred [5, 22]. Under the influence of the forced flow, the clusters drift from the entrance of the desalination channel to its exit. When the cluster gets in between the Luggin capillaries (which are used to measure the potential difference), the resistance in the gap between the capillaries increases and the PD takes a relatively high value. In between two clusters, the solution has a higher concentration [39], so when the intercluster gap occurs between the capillaries, the PD value is relatively

low. The motion of the clusters is responsible for oscillations with a relatively low frequency, about 0.25 Hz in the case of NaCl; this means that a cluster passes between the capillaries every 4 seconds. At the same time, smaller vortices within the clusters are responsible for high-frequency oscillation with a smaller amplitude. In the case of Ca^{2+} ions, the PD oscillations that can be attributed to the emergence of EC by the Rubinstein-Zaltzman mechanism are detected at times (potential drops) slightly exceeding τ_{sand} . In the system with MgCl_2 , these oscillations appear near $t = \tau_{sand}$, thereby significantly affecting the shape of CP in the vicinity of the transition time (Fig. 2-5b). On passing from NaCl to the divalent cations, the frequency of low-frequency oscillations decreases to 0.13 Hz (CaCl_2) or 0.08 Hz (MgCl_2) and the oscillation amplitude increases (Fig. 2-4a).

It is noteworthy that the thickness of equilibrium EDL in the case of singly charged counter-ions (Na^+) is greater than that in the case of doubly charged (Ca^{2+} , Mg^{2+}) ions. This factor can diminish the effect of the bulkier hydration shell of the doubly charged ions on electroconvection. Indeed, at current densities close to i_{lim} (Fig. 2-7) and for short chronopotentiometry times (Fig. 2-4) when the equilibrium EC dominates, the behavior of the membrane in the CaCl_2 solution is closer to that in the NaCl, rather than the MgCl_2 solution. However, at $i > i_{lim}$ and $t > \tau$ when EC becomes nonequilibrium, the factor of increasing the size of the hydration shell is dominant, resulting in a lower value of the pressure drop in the system with CaCl_2 compared to NaCl at a given i/i_{lim} ratio.

2.4 Conclusions

The influence of the nature of counter-ions (Na^+ , Ca^{2+} , Mg^{2+}) on chronopotentiograms and the current-voltage characteristics of the MK-40_{MOD} membrane, prepared from a commercial MK-40 membrane by applying a MF-4SK thin film on its surface, has been studied. The resulting bilayer membrane is characterized by not only electrical heterogeneity, but also significant waviness and comparatively high hydrophobicity of the surface, properties that promotes electroconvection.

It has been shown that at a fixed i/i_{lim} ratio, the potential drop across the membrane varies in the order $\text{Na}^+ > \text{Ca}^{2+} > \text{Mg}^{2+}$, as can be explained by the influence of electroconvection, which is the most intense in the case of Mg^{2+} and minimal in the case of Na^+ . The resulting electroconvection intensity series is consistent with the data obtained previously by Choi et al. [1] and is supposed to be due to the effect of the degree of hydration of the counter-ion: the

greater the degree of ion hydration (maximal for Mg^{2+} and minimal for Na^+), the more intense is the electroconvection.

A characteristic feature of the nonstationary transport of the strongly hydrated counter-ions Ca^{2+} and Mg^{2+} is that the chronopotentiogram exhibits potential drop oscillations a few seconds after switching on the electric current ($i \geq 0.8i_{\text{lim}}$). The time of appearance of the first local maximum is approximately half of the transition time, and the value of the reduced potential difference at maximum is 20–30 mV. The pattern and period of oscillations, as well as the values of potential drop at which the oscillations are detected, suggest that these oscillations are due to equilibrium electroconvection that develops according to the mechanism of electro-osmosis of the first kind.

The oscillations observed at higher potential differences are due to the instability of the Rubinstein-Zaltzman nonequilibrium electroconvection. Assembling of nascent vortices in clusters and their drift by the action of forced convection from the entrance of the desalination channel to its exit cause low-frequency oscillations in the quasi-stationary portions of the chronopotentiograms. The period and amplitude of the oscillations increase in the following order: $\text{Na}^+ < \text{Ca}^{2+} < \text{Mg}^{2+}$, that is, with an increase in the hydration of counter-ions.

2.5 Acknowledgments

This work was supported by the Russian Science Foundation, project no. 14-19-00401 (measurement and general analysis of voltammograms and chronopotentiogram, electroconvection mechanism); the Russian Foundation for Basic Research, project no. 13-08-96518 (surface homogenization effect); and project no. 15-58-16005-NCNIL (chronopotentiometry at small potential drops).

References

- [1] J.-H. Choi, H.-J. Lee, S.-H. Moon, Effects of electrolytes on the transport phenomena in a cation-exchange membrane, *J. Colloid Interface Sci.* 238 (2001) 188–195.
- [2] S. Mikhaylin, V. Nikonenko, N. Pismenskaya, G. Pourcelly, S. Choi, H.J. Kwon, J. Han, L. Bazinet, How physico-chemical and surface properties of cation-exchange membrane affect membrane scaling and electroconvective vortices: Influence on performance of electrodialysis with pulsed electric field, *Desalination* 393 (2016) 102–114.
- [3] H. Strathmann, Electrodialysis, a mature technology with a multitude of new applications, *Desalination* 264 (2010) 268–288.
- [4] V. V. Nikonenko, A. V. Kovalenko, M. K. Urtenov, N. D. Pismenskaya, J. Han, P. Sistat, G. Pourcelly, Desalination at overlimiting currents: State-of-the-art and perspectives, *Desalination* 342 (2014) 85–106.
- [5] R. Kwak, G. Guan, W. K. Peng, J. Han, Microscale electrodialysis: Concentration profiling and vortex visualization, *Desalination* 308 (2013) 138–146.
- [6] N. A. Mishchuk, Concentration polarization of interface and non-linear electrokinetic phenomena, *Adv. Colloid Interface Sci.* 160 (2010) 16–39.
- [7] V. V. Nikonenko, N. D. Pismenskaya, E. I. Belova, P. Sistat, P. Huguet, G. Pourcelly, C. Larchet, Intensive current transfer in membrane systems: Modelling, mechanisms and application in electrodialysis, *Adv. Colloid Interface Sci.* 160 (2010) 101–123.
- [8] N. Pismenskaya, N. Melnik, E. Nevakshenova, K. Nebavskaya, V. Nikonenko, Enhancing ion transfer in overlimiting electrodialysis of dilute solutions by modifying the surface of heterogeneous ion-exchange membranes, *Int. J. Chem. Eng.* 2012 (2012) 528290.
- [9] I. Rubinstein, B. Zaltzman, Equilibrium electroconvective instability, *Phys. Rev. Lett.* 114 (2015) 114502-1–114502-5.
- [10] V. M. Volgin, A. P. Grigin, A. D. Davydov, Numerical solution of the problem of the limiting current for the copper electrodeposition from a solution of cupric sulfate and sulfuric acid in conditions of natural convection, *Russ. J. Electrochem.* 39 (2003) 335-349.
- [11] I. Rubinstein, B. Zaltzman, Extended space charge in concentration polarization, *Adv. Colloid Interface Sci.* 159 (2010) 117–129.
- [12] V. G. Levich, *Physicochemical Hydrodynamics*, PrenticeHall, Englewood Cliffs, NJ, 1962.
- [13] I. Rubinstein, L. Shtilman, Voltage against current curves of cation exchange membranes, *J. Chem. Soc., Faraday Trans.* 75 (1979) 231–246.

- [14] M. A. Urtenov, E. V. Kirillova, N. M. Seidova, V. V. Nikonenko, Decoupling of the Nernst–Planck and Poisson equations. Application to a membrane system at overlimiting currents, *J. Phys. Chem. B* 111 (2007)14208–14222.
- [15] S. S. Dukhin, Electrokinetic phenomena of the second kind and their applications, *Adv. Colloid Interface Sci.* 35 (1991)173–196.
- [16] N. A. Mishchuk, P. V. Takhistov, Electroosmosis of the second kind, *Colloids Surf. A* 95 (1995)119–131.
- [17] S. S. Dukhin, N. A. Mishchuk, Unlimited increase in the current through an ionite granule, *Kolloid. Zh.* 49(1987)1197–1198.
- [18] M. K. Urtenov, A. M. Uzdenova, A. V. Kovalenko, V. V. Nikonenko, N. D. Pismenskaya, V. I. Vasil'eva, P. Sistat, G. Pourcelly, Basic mathematical model of overlimiting transfer enhanced by electroconvection in flow-through electro dialysis membrane cells, *J. Membr. Sci.* 447 (2013) 190-202.
- [19] I. Rubinstein, B. Zaltzman, Electro-osmotically induced convection at a permselective membrane, *Phys. Rev. E.* 62 (2000) 2238–2251.
- [20] S. V. Pham, Z. Li, K. M. Lim, J. K. White, J. Hanet, Direct numerical simulation of electroconvective instability and hysteretic current-voltage response of a permselective membrane, *Phys. Rev. E* 86 (2012) 046310.
- [21] V. S. Shelistov, E. A. Demekhin, G. S. Ganchenko, Electrokinetic instability near charge-selective hydrophobic surfaces, *Phys. Rev. E* 90(2014)013001.
- [22] R. Kwak, V. S. Pham, K. M. Lim, J. Han, Shear flow of an electrically charged fluid by ion concentration polarization: Scaling laws for electroconvective vortices, *Phys. Rev. Lett.* 110 (2013)114501.
- [23] E. D. Belashova, N. A. Melnik, N. D. Pismenskaya, K. A. Shevtsova, A. V. Nebavsky, K. A. Lebedev, V. V. Nikonenko, Overlimiting mass transfer through cation-exchange membranes modified by Nafion film and carbon nanotubes, *Electrochim. Acta* 59 (2012) 412–423.
- [24] N. D. Pismenskaya, V. V. Nikonenko, N. A. Melnik, K. A. Shevtsova, E. I. Belova, G. Pourcelly, D. Cot, L. Dammak, C. Larchet, Evolution with time of hydrophobicity and microrelief of a cation-exchange membrane surface and its impact on overlimiting mass transfer, *J. Phys. Chem. B* 116. (2012) 2145–2161.
- [25] R. A. Robinson, R. H. Stokes, *Electrolyte Solutions*, 2-nd edition, Dover, New York, 2003.
- [26] T. Badessa, V. Shaposhnik, The electro dialysis of electrolyte solutions of multi-charged cations, *J. Membr. Sci.* 498 (2016)86–93.

- [27] M. Pavlov, P. E. M. Siegbahn, M. Sandstrom, Hydration of beryllium, magnesium, calcium, and zinc ions using density functional theory, *J. Phys. Chem. A* 102 (1998)219–228.
- [28] H.-W. Rosler, F. Maletzki, E. Staude, Ion transfer across electro dialysis membranes in the overlimiting current range: Chronopotentiometric studies, *J. Membr. Sci.* 72 (1992)171–179.
- [29] C. Larchet, S. Nouri, B. Auclair, L. Dammak, V. Nikonenko, Application of chronopotentiometry to determine the thickness of diffusion layer adjacent to an ion-exchange membrane under natural convection, *Adv. Colloid Interface Sci.* 139 (2008)45–61.
- [30] H. J. S. Sand, On the concentration at the electrodes in a solution, *Phil. Mag.* 1 (1901) 45–79.
- [31] Z. Galus, *Teoretyczne podstawy elektroanalizy chemicznej*, Panstwowe Wydawnictwo naukowe, Warsaw, 1971.
- [32] D. Lerche, H. Wolf, Quantitative characterisation of current-induced diffusion layers at cation-exchange membranes. I. investigations of temporal and local behaviour of concentration profile at constant current density, *Bioelectrochem. Bioenerg.* 2(1975)293–302.
- [33]. J. J. Krol, M. Wessling, H. Strathmann, Chronopotentiometry and overlimiting ion transport through monopolar ion exchange membranes, *J. Membr. Sci.* 162 (1999) 155–164.
- [34] S. A. Mareev, D. Yu. Butylskii, N. D. Pismenskaya, V. V. Nikonenko, Chronopotentiometry of ion-exchange membranes in the overlimiting current range. Transition time for a finite-length diffusion layer: modeling and experiment, *J. Membr. Sci.* 500 (2016)171–179.
- [35] J. S. Newman, *Electrochemical Systems*, Prentice Hall, Englewood Cliffs, NJ, 1973.
- [36] V. I. Vasil'eva, A. V. Zhiltsova, M. D. Malykhyn, N. D. Pismenskaya, N. A. Melnik, Influence hydrophobic surface of the sulfocation exchange membrane to development of instability electroconvective in stratified electro systems, *Sci. J. Proc. Voronezh. Univ.* 2 (2013) 35–38.
- [37] S. R. Maduar, A. V. Belyaev, V. Lobaskin, O. I. Vinogradova, Electrohydrodynamics near hydrophobic surfaces, *Phys. Rev. Lett.* 114 (2015) 118301.
- [38] I. Rubinstein, B. Zaltzman, T. Pundik, Ion-exchange funneling in thin-film coating modification of heterogeneous electro dialysis membranes, *Phys. Rev. E Stat. Nonlin. Soft Matter. Phys.* 65 (2002) 041507.
- [39] A. M. Uzdenova, A. V. Kovalenko, M. K. Urtenov, V. V. Nikonenko, Effect of electroconvection during pulsed electric field electro dialysis. Numerical experiments, *Electrochem. Commun.* 51 (2015) 1–5.

Chapter 3

Effect of homogenization and hydrophobization of a cation-exchange membrane surface on its scaling in the presence of calcium and magnesium chlorides during electro dialysis

Presentation of the article

The main task of this chapter is to study the influence of homogenization and hydrophobization of cation-exchange membrane on its scaling in the presence of divalent ions during electro dialysis.

In the previous chapter, it has been shown that the casting of a thin homogeneous ion-conductive perfluorinated MF-4SK film on the surface of a heterogeneous cation-exchange membrane leads to the growth of the limiting current density and electroconvection intensification in comparison with the pristine membrane, in particular, in the presence of divalent ions. This effect is explained by a better distribution of the current lines in the boundary solution and a more hydrophobic surface after the membrane modification, which is beneficial for electroconvection.

As the effect of electroconvection contributes to the scaling mitigation, we can expect that the use of the ion-exchange membranes modified with a perfluorinated film (which is Nafion[®] in this study) will essentially decrease the rate or totally prevent salt precipitation.

The main experimental techniques are chronopotentiometry and voltammetry. Chronopotentiograms and I-V curves are measured for a commercial MK-40 and a modified MK-40_{MOD} membranes in MgCl₂ and CaCl₂ electrolyte solutions of two (0.02 M and 0.04 M) concentrations. The modification is carried out by casting a homogeneous Nafion[®] film onto the MK-40 membrane surface. Another MK-40 membrane and a homogeneous anion-exchange AMX membrane are used as auxiliary membranes.

This study allows us to conclude that the current density is higher and water splitting is lower for the MK-40_{MOD} membrane, due to a stronger electroconvection in the depleted solution at the surface of this membrane. The formation of scaling is observed only in the case of MK-40/0.04 M MgCl₂ system at current densities in the range from $1.1i_{lim}^{th}$ to $1.4i_{lim}^{th}$. The crystals of the Mg(OH)₂ are found on the surface of ion-exchange particles embedded into the MK-40 membrane. At $i > 1.4i_{lim}^{th}$ the water splitting becomes dominating at the AMX membrane, thus providing a low *pH* in the overall desalination chamber, hence, creating the conditions where the hydroxide deposition does not occur. No salt deposit is detected at any currents in the case of CaCl₂ solutions, evidently because of an essentially higher value of the solubility product for Ca(OH)₂ in comparison with Mg(OH)₂. No scaling is either detected in the case of the MK-40_{MOD} membrane.

Thus, the surface of the MK-40_{MOD} membrane (relatively more hydrophobic and less electrically heterogeneous) provides a better distribution of current lines enhancing the ion

transport. Electroconvection vortices mix the depleted solution and add to maintain the ion concentrations higher than the solubility product. In conditions where water splitting becomes dominating at the auxiliary anion-exchange membrane, pH in the overall desalination chamber reduces. As a consequence of these two effects, the hydroxide deposition does not occur.

Effect of homogenization and hydrophobization of a cation-exchange membrane surface on its scaling in the presence of calcium and magnesium chlorides during electro dialysis

Journal of Membrane Science (540) 2017 183–191

M.A. Andreeva^{a,b}, V.V. Gil^b, N.D. Pismenskaya^b, V.V. Nikonenko^b, L. Dammak^a, C. Larchet^a, D. Grande^a, N.A. Kononenko^b

^a*Institut de Chimie et des Matériaux Paris-Est (ICMPE) UMR 7182 CNRS – Université Paris-Est, 2 Rue Henri Dunant, 94320 Thiais, France.*

^b*Kuban State University, 149 Stavropolskaya st., 350040 Krasnodar, Russia.*

Abstract

In this paper, two cation-exchange membranes, *i.e.* MK-40 and MK-40_{MOD}, were studied by chronopotentiometry and voltammetry, MK-40_{MOD} being obtained by covering the heterogeneous surface of a commercial MK-40 membrane with a homogeneous 20 μm thick Nafion[®] film. Electrodialysis process was realized in an electrodialysis flow-through laboratory cell, in which the cation-exchange membrane under study formed a desalination chamber with an auxiliary anion-exchange (Neosepta AMX-SB) membrane. 0.02 M and 0.04 M solutions of CaCl_2 , MgCl_2 and NaCl were used. The current densities were changed in the range from $0.25 i_{\text{lim}}^{\text{th}}$ to $2.5 i_{\text{lim}}^{\text{th}}$, where the theoretical limiting current density, $i_{\text{lim}}^{\text{th}}$, was calculated using the Leveque equation. The potential drop over the modified MK-40_{MOD} membrane and the water splitting at this membrane turned out to be lower in all studied cases. Formation of scaling was observed only in the case of the MK-40/0.04 M MgCl_2 system at current densities in the range from $1.1 i_{\text{lim}}^{\text{th}}$ to $1.4 i_{\text{lim}}^{\text{th}}$. For these current densities, the (quasi)steady state value of potential drop slowly increased with time and the crystals of $\text{Mg}(\text{OH})_2$ were found on the ion-exchange particles embedded onto the MK-40 membrane surface facing the desalination chamber. At higher currents, stronger electroconvection at this membrane and higher water splitting at the AMX-SB membrane (the latter providing lower pH in the desalination chamber) prevented scaling. No scaling was found on the modified membrane at any current. It is due to the Nafion[®] film, which is relatively more hydrophobic than pristine MK-40 and which provides a “better” distribution of current lines near the surface, thus enhancing electroconvection and decreasing water splitting.

3.1 Introduction

Electrodialysis (ED) with ion-exchange membranes (IEMs) is one of the efficient methods for water desalination and solution concentration [1, 2]. It is reasonable to use this method in combination with reverse osmosis (RO) in brackish water desalination [3, 4]. Ultrapure water and ultra-concentrated electrolyte solutions can be obtained by means of this hybrid process. Conventional ED can also be coupled with bipolar membrane ED to generate bases and acids from salts [5], or even protein recovery from the tofu whey [6]. Two other important ED applications are developed: casein production in milk industry [7, 8] and tartaric stabilization of wines [9].

In ED, due to different ion transport numbers in the membrane and solution, concentration polarization (CP) occurs [10]. This phenomenon can result in salt precipitation on the membrane surface facing the concentration and/or desalination chambers [7, 10, 11]. The scaling layer reduces the effective surface area of the membrane, which causes additional resistance to the flow and mass transfer. The scaling phenomenon can be aggravated by membrane fouling in presence of organic matters (proteins, sugars, polyphenols, tannins...) [12, 13].

CaCO_3 and CaSO_4 are generally the main salts, which form a precipitate on the membrane surfaces during ED of seawater [14]. The fouling layer consisting of CaCO_3 , $\text{Mg}(\text{OH})_2$, and $\text{Ca}(\text{OH})_2$ forms on cation-exchange membrane (CEM) interfaces during electromembrane processes used in dairy industry [15]. In the 1950's, Ionics started experiments with systems which showed a radical improvement in scaling control [16]. They proposed to use ED reversal process (EDR), which results in the prevention of calcium carbonate and calcium sulfate scale formation. It was found that EDR may be successfully applied to the production of sodium chloride from the seawater [10, 17]. The key moment in the EDR is the changing of the electrode polarity and the flow direction at the same time [1, 10, 16]. The desalination chambers become concentration chambers, and vice versa. The disadvantage of this method is the loss in the current efficiency, capacity and in the final product during the operation of electrode polarity changing.

Pulsed electric field (PEF) modes are proposed as another effective way for combating the consequences of CP, such as the scaling formation at IEM interfaces [18, 19]. In this regime the pulses of current or voltage alternate with pauses. Karlin et al. [20], Sistas et al. [21], Mikhaylin et al. [7] showed that the duration of pulse and pause lapses affects essentially the amount and the composition of the salt deposits. During pause lapses, the concentration depolarization occurs. As a result, the electric resistance of depleted solution reduces [22] and

the salt deposits dissolve, at least partially. Electroconvection (EC) plays an important role in this process. EC appears as a result of the action of electric field on the space electric charge at the membrane surface. The transfer of solution by EC intensifies the exchange between the near-surface solution layer and the bulk solution [23-26] and contributes to reducing scaling [27].

A modification of a membrane surface by a layer selective to the transfer of singly charged ions is another option, which can be used for mitigation of the scaling and fouling. It is known that the deposition of organic substances on the membrane surface can be reduced when the membrane is covered with a thin ion-conductive layer bearing a fixed charge opposite to the charge of the supporting membrane matrix [28]. As a result, the resistance of the composite membrane is increasing towards multiply charged counter-ions, which causes scaling. A similar effect is obtained by modification of the membrane surface with high-molecular surface active substances [29].

Asraf-Snir et al. [30, 31] investigated the effect of IEM surface structure on gypsum scale formation. They found that in the case of heterogeneous anion-exchange MA-40 membrane, the scale formation occurs mainly on the surface of conductive areas, which are ion-exchange resin beads incorporated in the polyethylene supporting matrix. The amount of deposit is essentially lower on the surface of a homogeneous anion-exchange AMV membrane [30, 31]. Moreover, the scale forms not only on the heterogeneous membrane surface, but within its macropores also. Based on the latter results [30, 31], it can be expected that coating a homogeneous conductive film on a heterogeneous membrane surface could improve its resistance towards fouling.

In practice, the casting of conductive perfluorinated resin solution of Nafion[®] or its Russian analogue MF-4SK on the surface of a cation-exchange membrane leads to the growth of limiting current density by 1.5 times in comparison with unmodified membrane [32-34]. This effect is explained by a better distribution of the current lines after the surface modification. Besides, the membrane surface becomes relatively more hydrophobic that is beneficial for EC [34, 35].

The positive effect of application a homogeneous film to the membrane surface is supported by theoretical studies of Rubinstein et al. [36]. The current lines are distorted in solution near an electrically heterogeneous surface: they are accumulated at the conductive areas causing higher CP [36], which should lead to increasing scale formation. It is shown [36] that application of a homogeneous conductive layer on heterogeneous surface diminishes the effect of formation of funnel-shaped distribution of current lines in the solution near the membrane surface. Even a very thin and weakly charged conductive layer results in

homogenization of current lines distribution over the membrane surface and in the near-surface solution. As a consequence, the CP at the membrane surface decreases and the limiting current density increases [36].

In the present paper, we study the effect of surface modification of a heterogeneous cation-exchange MK-40 membrane with a thin film of Nafion[®] on the scale formation. From the literature reviewed above, it can be expected that the application of a thin homogeneous and relatively hydrophobic layer on the surface of a heterogeneous membrane would produce a double effect: it will reduce CP due to homogenization of the current density distribution over the membrane surface, and will stimulate EC. As a consequence, the rate of salt precipitation should be lower than that at the pristine heterogeneous membrane.

Despite the extensive literature in this field, the effect of modification of heterogeneous membranes by a thin conductive homogeneous layer on scaling process has not been studied yet. We will explore this effect in calcium and magnesium chloride solutions of different concentrations.

3.2 Experimental

3.2.1 Ion-exchange membranes

Two cation-exchange membranes were used in this study. The MK-40 membrane (Shchekinoazot, Russia) is a heterogeneous membrane containing sulfonic acid fixed groups. It is produced by hot pressing from the mixture of dispersed cation-exchange resin KU-2 and polyethylene as a binder filler. About 80 % of the MK-40 surface is covered by polyethylene [37] (Fig. 3-1a). The size of ion-exchange KU-2 resin particles is 10 to 50 μm . These particles form “hills” of 5 to 6 μm height on the membrane surface mainly covered by polyethylene. The height of hills was determined by focusing the optical microscope consecutively on the tops and bottoms of the membrane surface relief (Fig. 3-1b). The MK-40_{MOD} membrane (Fig. 3-1c) is obtained by coating the MK-40 membrane surface with a homogeneous film obtained from a Nafion[®] perfluorinated resin solution after evaporation of the solvent in an oven at 80 °C [33]. The film thickness in the dry state is 12-15 μm (Fig. 3-1d). The copolymer film covering the surface of the MK-40_{MOD} membrane does not include non-conductive macroscopic regions, but it is not perfectly smooth. The difference in height between peaks and valleys for this membrane is about 2 μm .

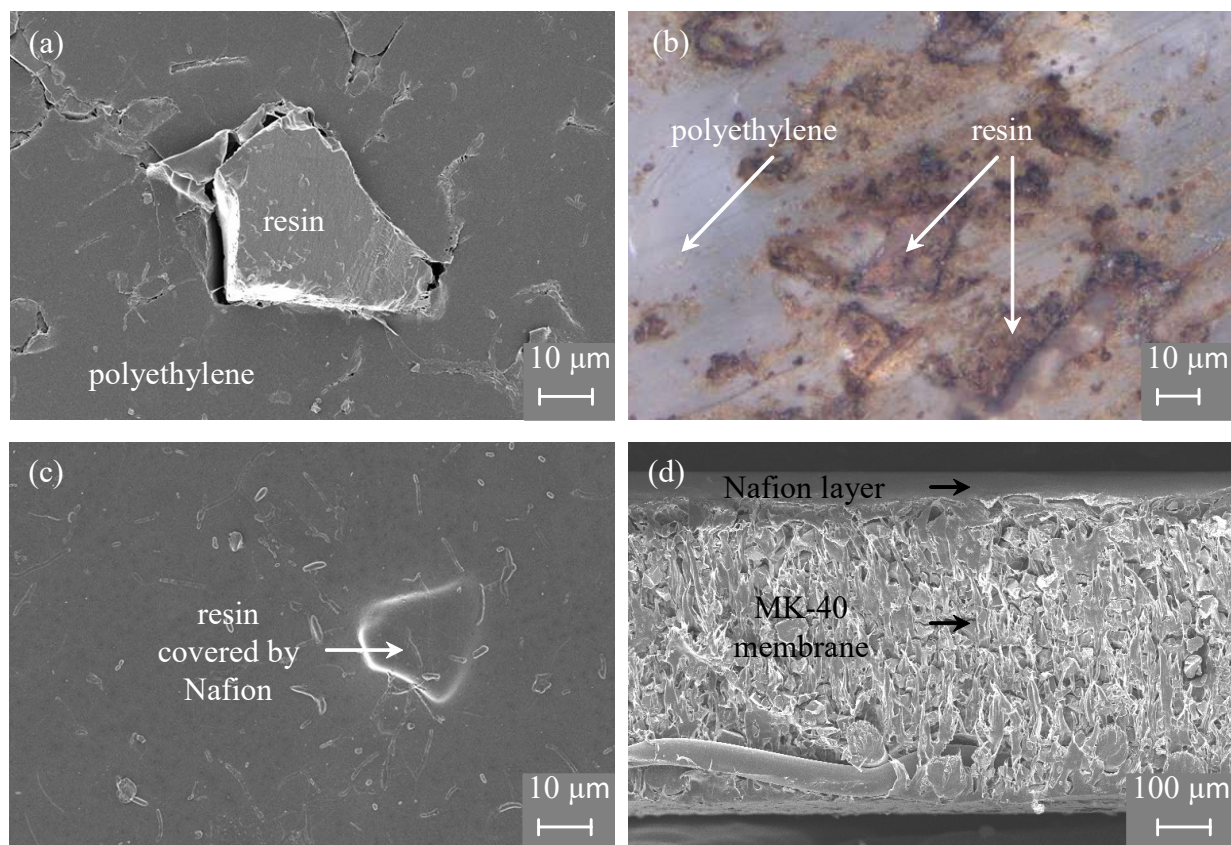


Fig. 3-1. SEM images of MK-40 membrane surface in dry (a) and swollen (b) states, the surface (c) and cross section (d) of MK-40_{MOD} membrane in the dry state.

The bulk and surface properties of the MK-40 and the MK-40_{MOD} membranes were previously described elsewhere [33]. After modification, the ion-exchange capacity, electrical conductivity and diffusion permeability vary only slightly, within the margin of experimental error. In contrast, the conductive surface fraction of MK-40_{MOD} becomes 100 % instead of 20 % for the pristine membrane, and the contact angle increases from 55 ° to 64 ° (± 3 °) [33, 34]. The contact angle characterizes hydrophobic/hydrophilic balance of an ion-exchange membrane surface. It depends on the fixed ions, which attract water molecules, and on the matrix polymer material not containing fixed charged groups. Generally, the morphology of ion-exchange membranes (or the resins constituting the main part of them) may be presented as a system of hydrophilic conducting channels confined within a hydrophobic polymer phase [38]. When comparing the surface of Nafion and MK-40, one can distinguish there hydrophobic and hydrophilic areas. The perfluorinated matrix of Nafion is rather hydrophobic. The contact angle of Teflon having the same chemical structure as the Nafion matrix is 115 °. The surface fraction of pore mouths forming hydrophilic areas of the surface can be evaluated as about 20 % (equal to the water content in the membrane). Two main components of MK-40 membrane are polystyrene (making the matrix in KU-2 cation-

exchange resin) and polyethylene. Polyethylene covers about 80% of the MK-40, however, its contact angle (about 92°) is essentially lower than that of Teflon. The contact angle of polystyrene is 86° , however, the exchange capacity (5.0 meq/g dry) and water content (43-53 %) of KU-2 [39] are much higher than respective parameters of Nafion (0.83 meq g^{-1} dry and 22 % [40]). Thus, the surface areas occupied by the particles of KU-2 on the MK-40 are quite hydrophilic. As a result, the surface of MK-40 is more hydrophilic than that of Nafion.

3.2.2 Protocol

A flow-through four-chamber ED cell shown in Fig. 3-2 was used in the study. The central desalination chamber (3) was formed by an auxiliary anion-exchange Neosepta[®] AMX-SB membrane (Astom, Japan) (AEM) and the tested (M^*) MK-40 or MK-40_{MOD} membrane. The intermembrane distance in this chamber, h , was 6.5 mm. The experiment was carried out at 20°C .

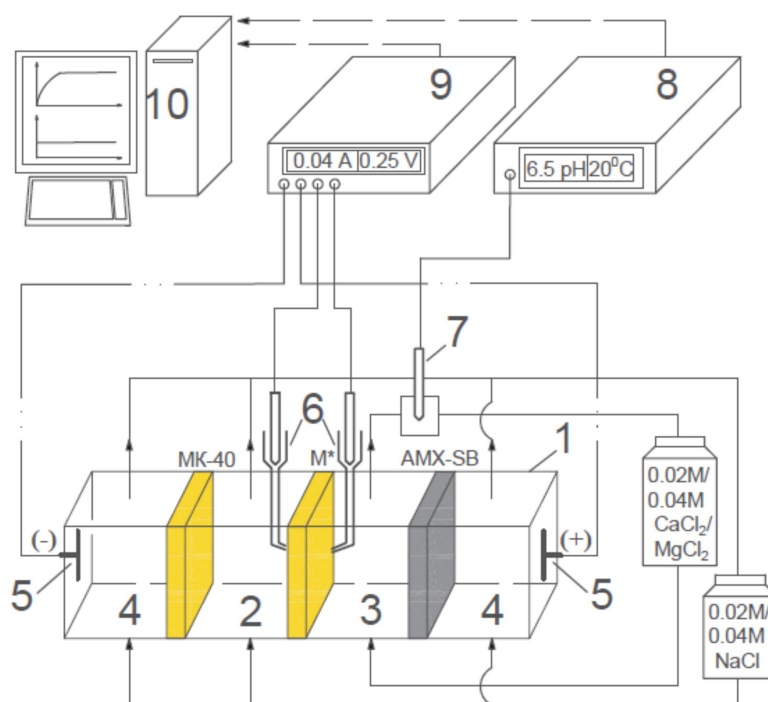


Fig. 3-2. Principal scheme of the experimental setup. ED cell (1) consists of one concentration (2), one desalination (3) and two electrode chambers (4), two platinum polarizing electrodes (5) and two Ag/AgCl electrodes inserted in Luggin capillaries (6). A flow pass cell with a pH electrode (7) and a pH meter pHM120 MeterLab (8) are used for pH measurements. The current was set and the potential difference was measured using a potentiostat-galvanostat PARSTAT 2273 (9); the data were registered using a PC (10).

The potential drop (PD), $\Delta\phi$, was measured between the tips of two Luggin capillaries installed from both sides of the membrane under study in its geometric center at a distance of about 0.5 mm from the surface. The procedure for obtaining chronopotentiograms (ChPs) and current-voltage (I-V) curves is described elsewhere [34, 37].

The membrane behavior was studied in 0.02 M CaCl₂, 0.04 M CaCl₂, 0.02 M MgCl₂, and 0.04 M MgCl₂ solutions. These solutions were pumped through the desalination chamber at a flow rate of 30 mL min⁻¹. All other chambers were fed with a NaCl solution of the same concentration as the solution feeding the desalination chamber (Fig. 3-2). The effective membrane area was 4 cm². For preparation of the solutions, we used NaCl (R.P. NORMAPURTM, VWR International), CaCl₂·2H₂O, and MgCl₂·6H₂O (LABOSI, Fisher Scientific s.a.), and demineralized water at 4MΩ (Millipore Elix 3).

3.3. Results and discussion

3.3.1 Theoretical value of the limiting current density

The theoretical value of the limiting current density, $i_{\text{lim}}^{\text{th}}$, was found using the Leveque equation obtained in the framework of the convection-diffusion model [41]:

$$i_{\text{lim}}^{\text{th}} = \frac{z_i c_i^0 F D}{h(T_i - t_i)} \left(1.47 \left(\frac{h^2 V}{L D} \right)^{1/3} - 0.2 \right) \quad (3.1)$$

Here z_i and c_i^0 are the counter-ion charge and concentration in the feed solution, respectively; F is the Faraday constant; T_i and t_i are the counter-ion effective transport number in the membrane and the transport number in the solution respectively; V is the flow velocity of solution through the desalination chamber; L is the length of desalination path; D is the electrolyte diffusion coefficient.

In the studied cases $V = 0.38 \text{ cm s}^{-1}$, $L = 2 \text{ cm}$, $t_{\text{Ca}^{2+}} = 0.436$, $t_{\text{Mg}^{2+}} = 0.406$, $D_{\text{CaCl}_2} = 1.18 \times 10^{-5} \text{ cm}^2 \text{ s}^{-1}$, $D_{\text{MgCl}_2} = 1.10 \times 10^{-5} \text{ cm}^2 \text{ s}^{-1}$. The electrolyte diffusion coefficients and transport numbers are found from the limiting molar conductivities of the individual ions at 20°C [42], see Appendix. The MK-40 and MK-40_{MOD} membranes, for which the limiting current density is calculated, are assumed to be perfectly permselective, $T_i = 1$. Indeed, according to Larchet et al. [43], the MK-40 membrane has a high exchange capacity (1.64 meq g⁻¹ dry membrane); the effective transport number of Na⁺ in this membrane bathed in a 1 M NaCl solution is equal to 0.98. Since we use essentially more dilute solutions (the maximum concentration is

0.04 M), and the permselectivity increases with decreasing solution concentration, assumption $T_i = 1$ seems reasonable. The same assumption ($T_i = 1$) is accepted for the anion-exchange Neosepta AMX membrane, which is a homogeneous membrane with a relatively high exchange capacity (1.4-1.7 meq/g [44]). The values of i_{lim}^{th} calculated using Eq. (1) are presented in Table 3-1.

Generally, the application of Eq. (3.1) shows a good agreement of i_{lim}^{th} with the experimental values, i_{lim} , in the case of a homogeneous membrane with flat surface [37].

Solution	$i_{lim}^{th,CEM}$, mA cm ⁻²	$i_{lim}^{th,AEM}$, mA cm ⁻²
0.02M CaCl ₂	3.5	4.5
0.04M CaCl ₂	6.9	8.9
0.02M MgCl ₂	3.1	4.6
0.04M MgCl ₂	6.2	9.1

Table 3-1. Theoretical value of limiting current density of CEM, $i_{lim}^{th,CEM}$, and AEM, $i_{lim}^{th,AEM}$, in different electrolytes at 20⁰C.

3.3.2 Chronopotentiometry

ChPs were obtained in 0.02 M and 0.04 M MgCl₂ solutions, as well as in 0.02 M and 0.04 M CaCl₂ solutions. The applying current density, i , was in the range of 0.25 i_{lim}^{th} to 2.5 i_{lim}^{th} . A typical ChP at $i < i_{lim}^{th}$ (obtained for a MK-40 membrane in 0.04 M CaCl₂ at $i = 1.7 i_{lim}^{th}$) is presented in Fig. 3-3. The characteristic points shown in Fig. 3-3 were used in data processing. There are three stages of $\Delta\phi$ variation with time (Fig. 3-3). Immediately after switching on a direct current, there is an ohmic potential drop, $\Delta\phi_{Ohm}$, which is a PD response where no concentration gradient occurs. The second stage corresponds to a PD growth with a rate increasing in time. This stage relates to decreasing electrolyte concentration at the depleted membrane interface, c_s^I , and to the corresponding increase at the enriched interface, c_s^{II} , both governed by electrodiffusion processes. With increasing time, c_s^I goes down, and $\Delta\phi$ increases with a rate proportional to $\ln c_s^{II}/c_s^I$ [45]. When the concentration gets sufficiently low, along with electrodiffusion, current-induced convection (EC in the experiment conditions) arises. This leads to reducing the rate of c_s^I decrease. As a

consequence, the rate of $\Delta\phi$ increase slows down, and finally, $\Delta\phi$ tends to a quasi-steady state value (stage III). An inflection point divides stages II and III, it relates to the so-called transition time (τ_{SAND} in Fig. 3-3). The value of τ_{SAND} relates to the change in the mechanism of ion transport, namely to the appearance of current-induced convection [46]:

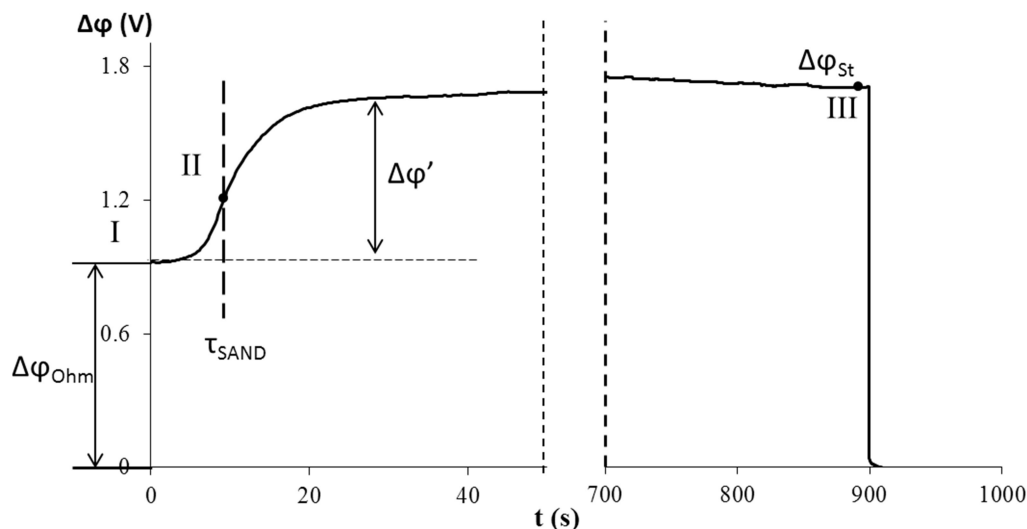


Fig. 3-3. Chronopotentiogram of an MK-40 membrane: $\Delta\phi$ vs. t , in a 0,04M CaCl_2 solution at current density 11.5 mA cm^{-2} . $\Delta\phi_{Ohm}$ is the ohmic potential drop just after the current is switched on; $\Delta\phi_{St}$ is the potential drop at the steady-state; $\Delta\phi' = \Delta\phi - \Delta\phi_{Ohm}$ is the reduced potential drop; τ_{SAND} is the transition time. Stages I, II, and III are described in the text.

Figs. 3-4a-b show ChPs measured at different current densities for an unmodified MK-40 and a modified MK-40_{MOD} membranes in 0.04 M MgCl_2 and 0.04 M CaCl_2 solutions. At current densities lower than i_{lim}^{th} , the ChP has no inflection point: the rate of PD growth decreases monotonously with time. The steady state corresponds to the condition where the electrolyte diffusion, which increases with time, balances the difference between the ion migration transport in the membrane and solution. At higher currents, slight oscillations of PD in quasi-steady state are observed. In the case of 0.04 M CaCl_2 solution, the time averaged steady-state value of PD remains approximately constant. However, in MK-40/0.04 M MgCl_2 system, the steady-state value of PD slowly increases with time during one experiment run (900 seconds), in the current density range from $1.1 i_{lim}^{th}$ to $1.4 i_{lim}^{th}$. The case of $i = 1.4 i_{lim}^{th}$ is shown in Fig. 3-4a. At more intensive currents, $i > 1.4 i_{lim}^{th}$, the growth of PD does not occur (the case of $i = 2.5 i_{lim}^{th}$ is shown in Fig. 3-4a). Instead, PD oscillations of higher amplitude are observed.

It is noteworthy that in all cases the oscillations are higher and the PD is lower in the system with MK-40_{MOD} membrane. There is no growth of steady state PD over this membrane in all solutions.

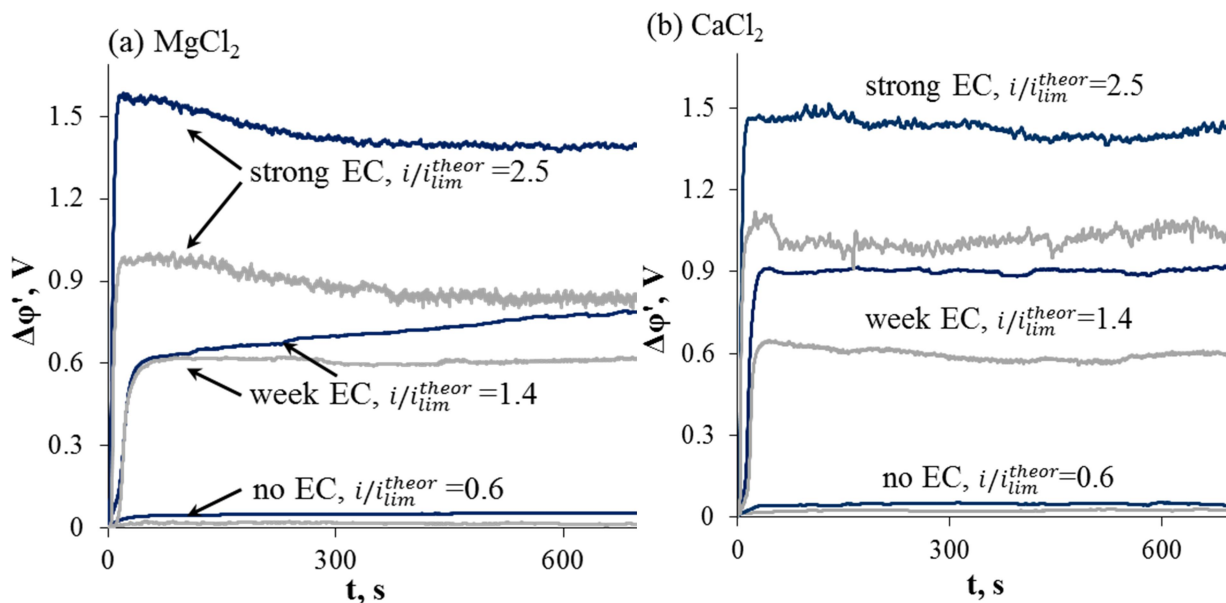


Fig. 3-4. Chronopotentiograms of MK-40 (dark blue (darker) lines) and MK-40_{MOD} (grey (lighter) lines) membranes measured in 0.04 M MgCl₂ (a) and 0.04 M CaCl₂ (b) solutions at $i/i_{lim}^{th} = 0.6, 1.4$ and 2.5.

The oscillations in the obtained ChPs can be explained by electroconvective instability, which occurs above a certain threshold value of $\Delta\phi'$ [47]. The greater the current density, the more intensive the electroconvection oscillations. These oscillations are higher in case of MK-40_{MOD} membrane showing that EC is stronger near the modified membrane.

EC is also stronger in the MgCl₂ solution than in CaCl₂ solution at the same i/i_{lim}^{th} ratio, all other conditions being equal. It follows from the fact that at the same i/i_{lim}^{th} value, the PD is higher in CaCl₂ solution than that in MgCl₂. This effect has been discovered by Choi et al. [48] and confirmed by Gil et al. [49]. It was shown [48, 49] that the value of $\Delta\phi'$ increased in the series $Mg^{2+} < Ca^{2+} < Na^{+}$. The EC intensification was related to increasing the Stokes radius of counter-ions: the Stokes radius (and the hydration number) of Mg²⁺ (0.346 nm [50]) is higher than that of Ca²⁺ (0.308 nm [50]).

More intensive EC at the surface of the MK-40_{MOD} membrane is explained by an easier slip of liquid along the hydrophobic surface [51]. The relative hydrophobicity of the MK-40_{MOD} surface is higher than that of MK-40: the contact angle of MK-40_{MOD} is equal to 64°⁰, while that of MK-40 is equal to 55°⁰ [33]. Besides, the growth of EC near the modified membrane

may be explained by “better” distribution of electric current lines disturbed by the “funnel” effect [36]. The electric current lines condense on the conductive areas of the electrically non-uniform membrane surface. This produces two effects:

- on the one hand, higher local current density through the conductive areas of a heterogeneous membrane results in a significant decrease of the salt concentration at these areas and, as a consequence, to a higher PD (higher concentration polarization) in comparison with a homogeneous membrane at a given current; and
- on the other hand, distortion of the current lines at the borders of conductive and nonconductive areas leads to appearance of an electric tangential force stimulating EC, which enhances ion transport.

Hence, there is an optimum value of electrical surface heterogeneity where the ion transport through the membrane attains its maximum under a given PD. A theoretical analysis based on the coupled 2D Nernst-Planck-Poisson-Navier-Stokes equations was recently made by Davidson et al. [52]. They found that when a fixed pattern period size and a fixed voltage (≈ 0.5 V) are chosen, a maximum current density is attained for a membrane whose surface contains 40 % of conductive and 60 % of non-conductive areas. This finding agrees qualitatively with our results: the surface of MK-40 membrane contains about 20 % of conductive areas [37], hence, the factor of high CP seems dominant over EC. The conductive permselective film applied on the MK-40 reduces heterogeneity in the current and concentration longitudinal distribution, hence, mitigates CP, while the tangential electric force remains sufficiently high to generate intensive EC.

3.3.3 pH changes

The pH difference ($\Delta pH = pH_{out} - pH_{in}$) between the outlet and inlet solution measured as a function of time for the desalination chamber is shown in Fig. 3-5. The ΔpH value depends on the difference in water splitting (WS) rate at the CEM and AEM. The H^+ ions formed at the CEM go into the membrane, the OH^- ions generated at this membrane move towards the bulk solution. The OH^- ions formed at the AEM go into the membrane, the H^+ ions move towards the bulk solution [53]. Thus, ΔpH depends on the difference between the H^+ and OH^- ion fluxes directed from the corresponding membrane surface into the bulk solution. When the flux of H^+ ions is higher than that of OH^- , the solution in desalination chamber becomes acidic. Otherwise, it becomes basic. As in all the experiments the same auxiliary membrane (AMX-SB) is used, the ΔpH value allows one to compare the WS rate at the different CEM samples under study.

The obtained data show that pH of the desalinated solution does not change or becomes acidic for both $MgCl_2$ and $CaCl_2$ solutions (Fig. 3-5). Therefore, the generation rate of H^+ ions going towards the bulk solution from the AEM is greater than or equal to the generation rate of OH^- ions moving towards the bulk solution from the CEM.

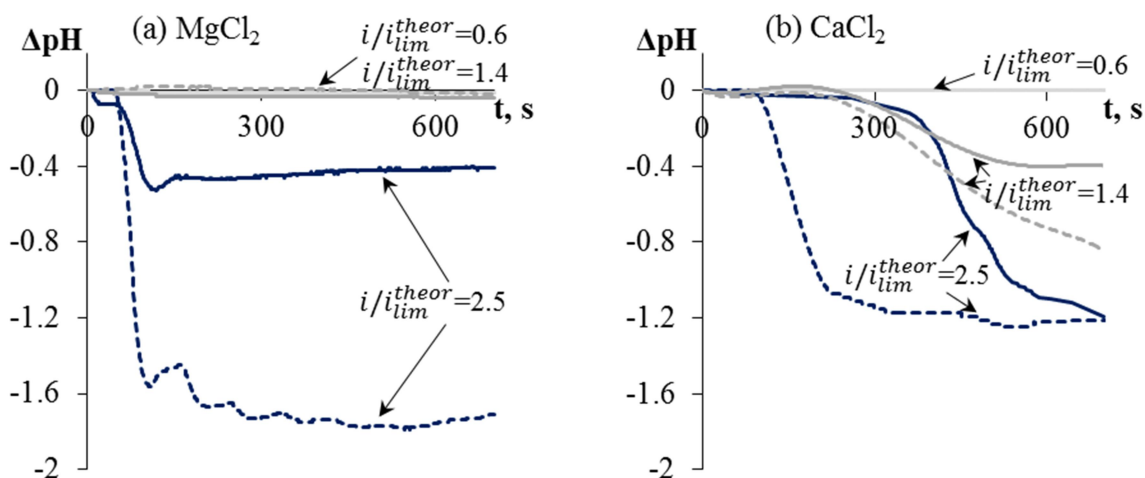


Fig. 3-5. Time dependence of pH difference between the outlet and inlet solution passing through the desalination chamber in cases of MK-40//AMX-SB (solid lines) and MK-40_{MOD}//AMX-SB (dashed lines) measured in 0.04 M $MgCl_2$ (a) and 0.04 M $CaCl_2$ (b) solutions.

The desalinated solution acidifies more in the case of modified membrane for both electrolytes. That means the WS rate at the modified membrane is lower than that at the unmodified one. It is noteworthy that both MK-40 and MK-40_{MOD} membranes contain functional groups of the same nature ($R-SO_3^-$). These groups are characterized by a weak catalytic activity toward the WS [54, 55]. Taking into account this fact, the difference in WS rate can be explained by the impact of two factors. First, the MK-40_{MOD} membrane provides a more uniform distribution of current lines near the membrane surface, which leads to reducing CP. Second, more intensive EC at the MK-40_{MOD} surface promotes better mixing of the solution and higher near-surface concentration of salt counter-ions.

Water splitting at the membrane interface becomes noticeable, when the concentration of salt ions at the membrane surface is comparable with the concentration of water ions, H^+ and OH^- , i.e. lower than about 10^{-5} M [56]. The current density relating to this event is close to i_{lim}^{th} . At $i > i_{lim}^{th}$, the salt concentration at the interface is sufficiently low for the water ions might compete in current transfer. However, the rate of WS is a function of the catalytic activity of the functional groups. The $R-SO_3^-$ groups of CEMs used in the study have low catalytic

activity, as we mentioned above, while the catalytic activity of the secondary and tertiary amino groups present in the AMX-SB is essentially higher [54, 57]. As a consequence, the rate of WS is generally higher at the AMX-SB, when a current density $i > i_{\text{lim}}^{\text{th,AEM}}$ is applied. It is noteworthy that $i_{\text{lim}}^{\text{th,AEM}} = 1.3 i_{\text{lim}}^{\text{th,CEM}}$ in CaCl_2 and $i_{\text{lim}}^{\text{th,AEM}} = 1.5 i_{\text{lim}}^{\text{th,CEM}}$ in MgCl_2 solution (Table 3-1). When the current density $i = 1.4 i_{\text{lim}}^{\text{th,CEM}}$ is applied, the overlimiting current occurs at the AEM in the case of CaCl_2 solution, but it is lower than $i_{\text{lim}}^{\text{th,AEM}}$ in the case of MgCl_2 solution. For this reason, at $i = 1.4 i_{\text{lim}}^{\text{th,CEM}}$, the solution in desalination chamber is acidified, when the CaCl_2 solution is used, and its pH value remains nearly constant in the case of MgCl_2 (Fig. 3-5b).

Stronger acidification of MgCl_2 solution in comparison with CaCl_2 at $i = 2.5 i_{\text{lim}}^{\text{th,CEM}}$ is explained by lower WS at the CEM in the case of MgCl_2 . Apparently, this is associated with more intensive EC in the MgCl_2 solution.

3.3.4 Scaling formation

The increase with time of the quasi-steady state PD in the case of MK-40/ MgCl_2 system in the range from $1.1 i_{\text{lim}}^{\text{th}}$ to $1.4 i_{\text{lim}}^{\text{th}}$ current densities (Fig. 3-4a) is associated with the scaling formation of $\text{Mg}(\text{OH})_2$ on the CEM surface. Marti-Calatayud et al. [58] studied the process of scale formation on cation-exchange membranes in mixed Na_2SO_4 and $\text{Fe}_2(\text{SO}_4)_3$ solutions by means of chronopotentiometric experiments. They showed that the increase with time of the quasi-steady state PD was related to the formation of precipitate on the depleted membrane surface.

Fig. 3-6b shows crystals on the ion-exchange particle embedded onto the MK-40 membrane surface. Formation of the $\text{Mg}(\text{OH})_2$ deposit is due to the following reaction:



with participation of a part of the OH^- ions generated at the CEM surface.

A similar reaction with formation of CaOH_2 is possible. However, $\text{Mg}(\text{OH})_2$ is much less soluble than $\text{Ca}(\text{OH})_2$: indeed, the solubility product, K_{sp} , at $T=25^\circ\text{C}$ in the case of $\text{Ca}(\text{OH})_2$ is equal to $6 \times 10^{-6} \text{ mol}^3 \text{ L}^{-3}$ [59], while in the case of $\text{Mg}(\text{OH})_2$ its value is equal to $1.8 \times 10^{-11} \text{ mol}^3 \text{ L}^{-3}$ [59].

Scaling formation of $\text{Mg}(\text{OH})_2$ or $\text{Ca}(\text{OH})_2$ depends on the balance of water dissociation rates at CEM and AEM. When the water dissociation rate at CEM is small and that at AEM is high,

the solution is significantly acidified (the case of MK-40_{MOD}/MgCl₂ $i = 2.5i_{lim}^{th}$ (Fig. 3-5a)) and no deposit is formed. In this case, a part of H⁺ ions generated in the space charge region at the AMX-SB depleted surface is delivered to the MK-40 surface by the electric field. The solution near the MK-40 surface gets more acidic, that prevents the formation of Mg(OH)₂ or Ca(OH)₂ scaling.

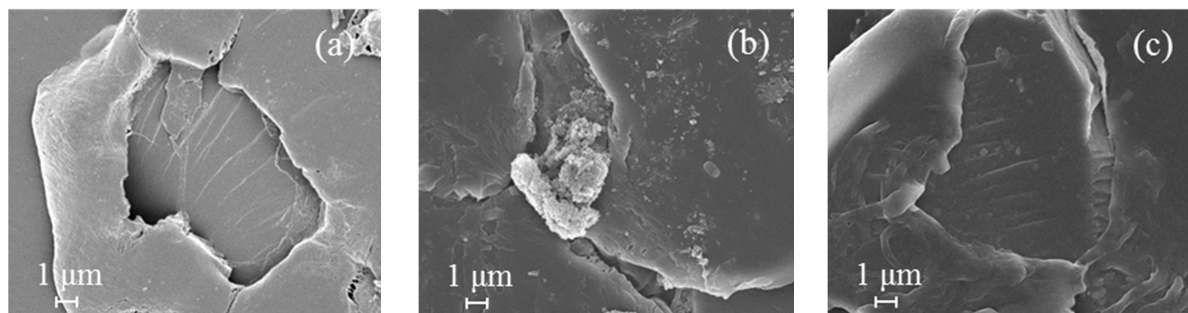


Fig. 3-6. SEM images of the surface of dry MK-40 membrane before (a) and after 5h electro dialysis of 0.04M MgCl₂ (b) solution and 0.04M CaCl₂ (c) at $i = 1.4i_{lim}^{th}$.

No deposit formation in the case of Ca(OH)₂ was observed at any current density (Fig. 3-6c). If the WS rate at both membranes is the same (the case of MK-40/MgCl₂ $i = 1.4i_{lim}^{th}$ (Fig. 3-5a)), deposit formation is possible. Effectively, in this case after 5 h of current flowing, we observe deposit of crystals on the MK-40 surface facing the desalination chamber (Fig.3-6b). It is noteworthy that the deposit forms on the surface of ion-exchange particles, which are conductive parts of the membrane surface and where WS reaction occurs. There is no deposit on the surface covered by polyethylene. This result is in a good agreement with the results obtained by Oren et al. [30, 31], who observed the formation of gypsum at the surface of ion-exchange resin particles embedded in a heterogeneous anion-exchange MA-40 membrane and facing the concentration compartment in dialysis [30] and electro dialysis processes [31].

3.3.5 Voltammetry

Fig. 3-7 shows the I-V curves obtained in CaCl₂ and MgCl₂ solutions of different concentrations. The I-V curves are found from the ChPs of tested membranes measured at different current densities. The value of potential drop related to a current density is the quasi-steady state PD averaged in time, $\Delta\phi'_{St}$.

Pismenskaya et al. [33] investigated the effect of modification of MK-40 membrane by a thin Nafion film on water splitting rate and mass transfer characteristics at different concentrations of NaCl solution. They found that when the value of potential drop ($\Delta\phi$) per cell pair was

fixed, the water splitting rate was lower and the mass transfer coefficient of salt counterion were higher in the case of modified MK-40_{MOD} membrane. The water splitting rate decreased with increasing concentration and at 0.02 M NaCl (the maximum concentration in study [33]) at $\Delta\varphi=2.5\text{V}$ (the maximum voltage used in this study) the effective transport number of H^+ in both MK-40 and MK-40_{MOD} membranes were lower than 0.05. Thus, the current density flowing through a cation-exchange membrane may be considered as a measure of the salt counterion mass transfer characteristic.

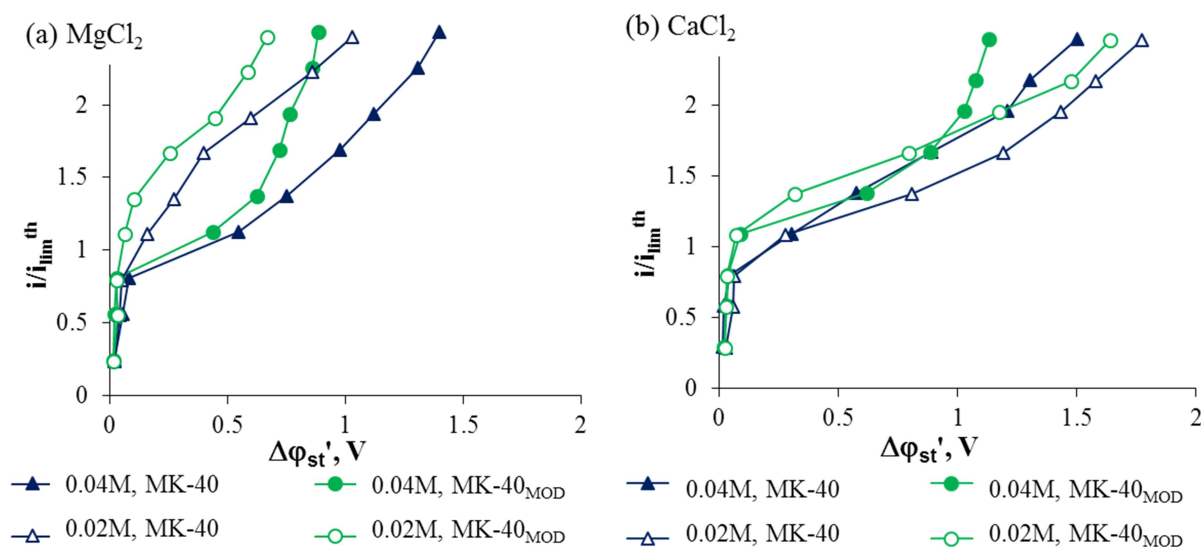


Fig. 3-7. Current-voltage curves for MK-40 and MK-40_{MOD} membranes in MgCl_2 (a) and CaCl_2 (b) solutions of different concentrations.

As it can be seen in Fig. 3-7, there are three regions on the I-V curves, which are generally distinguished in literature [47, 60]. An initial linear region is followed by a plateau of limiting current density, and then by a region of a higher growth of current density. The moderate growth of current density in the plateau region is associated with stable EC, while the higher growth in the final region of the curve, with unstable EC and/or with WS [47, 60, 61].

Fig. 3-7 shows that the experimental limiting current density, i_{lim} (which can be evaluated by the intersection of the tangents drawn to the first and the second regions of the I-V curve), and the overlimiting current density are always lower for the MK-40 membrane in comparison with the MK-40_{MOD} membrane. The value of i_{lim} for the MK-40_{MOD} membrane is about 1.5 times higher than that for the MK-40 membrane. As it was discussed above, this membrane behavior is explained by too low fraction of the surface conductive areas of the MK-40 membrane. The Nafion[®] film on the MK-40_{MOD} membrane surface makes the distribution of current lines near the surface closer to the optimum, thus decreasing CP and enhancing EC.

Additionally, higher hydrophobicity of the Nafion film surface in comparison to the MK-40 surface contributes to stronger EC. Belashova et al. [34] observed also a nearly 1.5-fold increase of the limiting current density across a MK-40 membrane covered with a 20 μm Nafion[®] film, in comparison with the unmodified MK-40 membrane.

In all studied cases, the plateau length is greater and the plateau slope is lower in the case of Ca^{2+} , in comparison with the case of Mg^{2+} . This is in a good agreement with the aforementioned results reported by Choi et al. [48] and Gil et al. [49].

The comparison of I-V curves obtained for two different concentrations shows that the experimental limiting current density i_{lim} is higher than the theoretical value $i_{\text{lim}}^{\text{th}}$ in the case of 0.02 M concentration, and i_{lim} is lower than $i_{\text{lim}}^{\text{th}}$ in the case of 0.04 M concentration, for both membranes. More generally, the plateau of limiting current lies higher in the case of 0.02 M concentration than in the case of 0.04 M concentration. This behavior is explained by higher stable electroconvection in more dilute solutions. Indeed, in the region of currents/voltages not far from the limiting current state, there are no oscillations of PD in the chronopotentiograms, as it can be seen in Fig. 3-4 for $i \leq 1.4i_{\text{lim}}^{\text{th}}$. Stable electroconvection in this current region was observed also by studying the development of concentration profiles with time using laser interferometry [62, 25]. In this current region, EC strongly depends on the parameters of the (quasi)equilibrium electrical double layer (EDL) [35, 63]. In 0.02 M solutions, the thickness of the EDL is higher than that in the 0.04 M solutions. The higher the EDL thickness, the more intensive the EC. In the final region of I-V curve, where its slope is higher and there are oscillations in the ChPs (Fig. 3-4, $i = 2.5i_{\text{lim}}^{\text{th}}$), EC is unstable. Its intensity is mainly determined by the extended space charge region, which is independent of the equilibrium EDL parameters [35, 63]. Since EC depends only slightly on the equilibrium EDL, the difference between the I-V curve obtained for 0.02 M and 0.04 M solutions is not so great. In this current region, the balance of surface hydrophobicity/hydrophilicity plays an important role: EC increases with increasing the relative surface hydrophobicity [34, 35].

3.4 Conclusions

Chronopotentiograms and current-voltage curves were measured for commercial MK-40 and modified MK-40_{MOD} membranes in MgCl_2 and CaCl_2 electrolyte solutions of two (0.02 M and 0.04 M) concentrations. The modification was carried out by casting a homogeneous Nafion[®] film onto the MK-40 membrane surface.

In all studied cases, the current density was higher and water splitting was lower for the MK-40_{MOD} membrane. This effect is explained by a stronger electroconvection in the depleted solution at this membrane. The reason is that the surface of the modified membrane is relatively more hydrophobic and less electrically heterogeneous, thus providing a better distribution of current lines enhancing the ion transport. For both membranes, electroconvection is higher in the MgCl₂ solutions than in the CaCl₂ solutions. That is associated with higher hydration of Mg²⁺ cations in comparison with Ca²⁺ analogues.

Formation of scaling was observed only in one case of MK-40/0.04 M MgCl₂ system at current densities in the range from $1.1i_{\text{lim}}^{\text{th}}$ to $1.4i_{\text{lim}}^{\text{th}}$. In this current range, the (quasi) steady state value of PD slowly increased with time, and crystals of the Mg(OH)₂ were found on the ion-exchange particles embedded onto the MK-40 membrane surface. At $i < 1.1i_{\text{lim}}^{\text{th}}$ and $i < 1.4i_{\text{lim}}^{\text{th}}$, the steady state PD did not vary with time, and no salt deposit was observed on the MK-40 surface. No growth of steady state PD with time and no salt deposit were detected at any currents in the case of CaCl₂ solutions, evidently because of an essentially higher value of the solubility product for Ca(OH)₂ in comparison with Mg(OH)₂. No scaling was either detected in the case of the MK-40_{MOD} membrane.

Two factors affect the scaling: EC and local *pH* value. EC mixes the depleted solution and adds to maintain the ion concentrations higher than the solubility. Increasing *pH* reduces the solubility. In the case of MK-40/0.04 M MgCl₂, $i = 1.4i_{\text{lim}}^{\text{th}}$, EC is stable and relatively low, and the WS rate is nearly the same at CEM and AEM ($\Delta pH \approx 0$). At $i > 1.4i_{\text{lim}}^{\text{th}}$, EC is stronger and unstable, and the rate of WS is higher at the AEM resulting in a reduced *pH* near the CEM. EC should sweep down the deposit of crystals on the CEM surface, if only they could appear in the conditions of lower *pH*. In the case of MK-40_{MOD}, EC is more intensive than in the case of MK-40 membrane. This more intensive EC results in higher near-surface salt counter-ion concentration, due to better mixing of solution. Moreover, reduced CP leads to lower WS rate at the CEM, hence to lower concentration of OH⁻ ions at the depleted membrane interface. WS becomes dominating at the AEM, thus providing a low *pH* in the overall desalination chamber, hence, the conditions where the hydroxide deposition does not occur.

3.5 Acknowledgments

This investigation was realized in the frame of a joint French-Russian PHC Kolmogorov 2017 project of the French-Russian International Associated Laboratory "Ion-exchange membranes

and related processes" with the financial support of Minobrnauki (Ref. N° RFMEFI58617X0053), Russia, and CNRS, France (project N° 38200SF).

3.6 Appendix

The value of the electrolyte diffusion coefficient is found using the equation

$$D = \frac{(z_+ + |z_-|)D_+D_-}{z_+D_+ + |z_-|D_-} \quad (3.3)$$

where z_+ and z_- are the charge numbers of cation and anion, respectively; D_+ and D_- are the diffusion coefficients of cation and anion, respectively. The later are calculated using the following equation

$$D_i = \frac{RT}{F^2} \left(\frac{\lambda_i^0}{|z_i|} \right) \quad (3.4)$$

where R is the gas constant; T is the temperature; λ_i^0 is the limiting molar conductivities of the individual ions at 20⁰C.

The transport numbers of Ca²⁺ and Mg²⁺ in solution are found using the equation

$$t_i = \frac{z_i D_i}{z_i D_i - z_A D_A} \quad (3.5)$$

where subscript A relates to the anion in the solution.

References

- [1] H. Strathmann, Electrodialysis, a mature technology with a multitude of new applications, *Desalination* 264 (2010) 268–288.
- [2] J. Ran, L. Wu, Y. He, Zh. Yang, Y. Wang, Ch. Jiang, L. Ge, E. Bakangura, T. Xu, Ion exchange membranes: new developments and applications, *J. Membr. Sci.* 522 (2017) 267–291.
- [3] Y. Oren, E. Korngold, N. Daltrophe, R. Messalem, Y. Volkman, L. Aronov, M. Weismann, N. Bouriakov, P. Glueckstern, J. Gilron, Pilot studies on high recovery BWRO-EDR for near zero liquid discharge approach, *Desalination* 261 (2010) 321–330.
- [4] Y. Zhang, K. Ghyselbrecht, B. Meesschaert, L. Pinoy, B. Van der Bruggen, Electrodialysis on RO concentrate to improve water recovery in wastewater reclamation, *J. Membr. Sci.* 378 (2011) 101–110.
- [5] K. Ghyselbrecht, A. Silva, B. Van der Bruggen, K. Boussu, B. Meesschaert, L. Pinoy, Desalination feasibility study of an industrial NaCl stream by bipolar membrane electrodialysis, *J. Environ. Manage.* 140 (2014) 69–75.
- [6] W. Ben Ounis, C.P. Champagne, J. Makhlof, L. Bazinet, Utilization of tofu whey pre-treated by electromembrane process as a growth medium for *Lactobacillus plantarum* LB17, *Desalination* 229 (2008) 192–203.
- [7] S. Mikhaylin, V. Nikonenko, G. Pourcelly, L. Bazinet, Intensification of demineralization process and decrease in scaling by application of pulsed electric field with short pulse/pause conditions, *J. Membr. Sci.* 468 (2014) 389–399.
- [8] S. Mikhaylin, V. Nikonenko, G. Pourcelly, L. Bazinet, Hybrid bipolar membrane electrodialysis/ultrafiltration technology assisted by a pulsed electric field for casein production, *Green Chem.* 18 (2016) 307–314.
- [9] K.N. Kontogiannopoulos, S.I. Patsios, A.J. Karabelas, Tartaric acid recovery from winery lees using cation exchange resin: optimization by response surface methodology, *Sep. Purif. Technol.* 165 (2016) 32–41.
- [10] Y. Tanaka, *Ion exchange membranes fundamentals and applications*, second edition, Elsevier Science, 2015.
- [11] T. Sata, M. Tsujimoto, T. Yamaguchi, K. Matsusaki, Change of anion exchange membranes in an aqueous sodium hydroxide solution at high temperatures, *J. Membr. Sci.* 112 (1996) 161–170.

- [12] R. Ghalloussi, W. Garcia-vasquez, L. Chaabane, L. Dammak, C. Larchet, N. Bellakhal, M. Rakib, Decline of ion exchange membranes after utilization in electrodialysis for food applications, *Phys. Chem. News* 65 (2012) 66–72.
- [13] R. Ghalloussi, L. Chaabane, L. Dammak, D. Grande, Ageing of ion-exchange membranes used in an electrodialysis for food industry: SEM, EDX and limiting current investigations, *Desalin. Water Treat.* 56 (2015) 2561–2566.
- [14] N. Hanzawa, T. Yuyama, K. Suzuki, M. Nakayama, Studies on durability of ion exchange membrane (IV): Long term electro-dialytic concentration test, *Scientific Papers of the Odawara Salt Experiment Station, Japan Monopoly Corporation, Odawara, Japan* 11, 1966, pp. 1–13.
- [15] N. Cifuentes-Araya, G. Pourcelly, L. Bazinet, Multistep mineral fouling growth on a cation-exchange membrane ruled by gradual sieving effects of magnesium and carbonate ions and its delay by pulsed modes of electrodialysis, *J. Colloid Interface Sci.* 372 (2012) 217–230.
- [16] W. E. Katz, The electrodialysis reversal process, *Desalination* 28 (1979) 31–40.
- [17] J. P. Chen, L. K. Wang, L. Yang, Y.-M. Zheng, Desalination of seawater by thermal distillation and electrodialysis technologies, in: L. K. Wang, J. P. Chen, Y.-T. Hung, N. K. Shamma (Eds.), *Membrane and desalination technologies*, Humana Press, New York, 2011, pp. 525–558.
- [18] N. A. Mishchuk, L. K. Koopal, F. Gonzales-Caballero, Intensification of electrodialysis by applying a non-stationary electric field, *Colloids Surf., A* 176 (2001) 195–212.
- [19] B. Ruiz, P. Sizat, P. Huguet, G. Pourcelly, M. Araya-Farias, L. Bazinet, Application of relaxation periods during electrodialysis of a casein solution: impact on anion-exchange membrane fouling, *J. Membr. Sci.* 287 (2007) 41–50.
- [20] Y. V. Karlin, V. N. Kropotov, Electrodialysis separation of Na^+ and Ca^{2+} in a pulsed current mode, *Russ. J. Electrochem.* 31 (1995) 517.
- [21] P. Sizat, P. Huguet, B. Ruiz, G. Pourcelly, S. A. Mareev, V.V. Nikonenko, Effect of pulsed electric field on electrodialysis of a NaCl solution in sub-limiting current regime, *Electrochim. Acta* 164 (2015) 267–280.
- [22] A. M. Uzdenova, A. V. Kovalenko, M. K. Urtenov, V. V. Nikonenko, Effect of electroconvection during pulsed electric field electrodialysis. Numerical experiments, *Electrochem. Commun.* 51 (2015) 1–5.
- [23] I. Rubinstein, B. Zaltzman, Electro-convective versus electroosmotic instability in concentration polarization, *Adv. Colloid Interface Sci.* 134–135 (2007) 190–200.
- [24] R. Kwak, G. Guan, W.K. Peng, J. Han, Microscale electrodialysis: concentration profiling and vortex visualization, *Desalination* 308 (2013) 138–146.

- [25] V. V. Nikonenko, V. I. Vasil'eva, E. M. Akberova, A. M. Uzdenova, M. K. Urtenov, A. V. Kovalenko, N. P. Pismenskaya, S. A. Mareev, G. Pourcelly, Competition between diffusion and electroconvection at an ion-selective surface in intensive current regimes, *Adv. Colloid Interface Sci.* 235 (2016) 233–246.
- [26] M. Davidson, M. Wessling, A. Mani, On the dynamical regimes of pattern-accelerated electroconvection, *Scientific Reports* 6 (2016) doi:10.1038/srep22505.
- [27] S. Mikhaylin, V. Nikonenko, N. Pismenskaya, G. Pourcelly, S. Choi, H. J. Kwon, J. Han, L. Bazinet, How physico-chemical and surface properties of cation-exchange membrane affect membrane scaling and electroconvective vortices: Influence on performance of electrodialysis with pulsed electric field, *Desalination* 393 (2016) 102–114.
- [28] T. Sata, Studies on anion exchange membranes having permselectivity for specific anions in electrodialysis — effect of hydrophilicity of anion exchange membranes on permselectivity of anions, *J. Membr. Sci.* 167 (2000) 1–31.
- [29] V. D. Grebenyuk, R. D. Chebotareva, S. Peters, V. Linkov, Surface modification of anion-exchange electrodialysis membranes to enhance anti-fouling characteristics, *Desalination* 115 (1998) 313–329.
- [30] M. Asraf-Snir, J. Gilron, Y. Oren, Gypsum scaling on anion exchange membranes during donnan exchange, *J. Membr. Sci.* 455 (2014) 384–391.
- [31] M. Asraf-Snir, J. Gilron, Y. Oren, Gypsum scaling on anion exchange membranes in electrodialysis, *J. Membr. Sci.* 520 (2016) 176–186.
- [32] N. D. Pis'menskaya, V.V. Nikonenko, N. A. Mel'nik, G. Pourcelli, G. Larchet, Effect of the ion-exchange-membrane/solution interfacial characteristics on the mass transfer at severe current regimes, *Russ. J. Electrochem.* 48 (2012) 610–628.
- [33] N. Pismenskaya, N. Melnik, E. Nevakshenova, K. Nebavskaya, V. Nikonenko, Enhancing ion transfer in overlimiting electrodialysis of dilute solutions by modifying the surface of heterogeneous ion-exchange membranes, *Int. J. Chem. Eng.* 2012 (2012) 528290.
- [34] E. D. Belashova, N. A. Melnik, N. D. Pismenskaya, K. A. Shevtsova, A. V. Nebavsky, K. A. Lebedev, V. V. Nikonenko, Overlimiting mass transfer through cation-exchange membranes modified by Nafion film and carbon nanotubes, *Electrochim. Acta* 59 (2012) 412–423.
- [35] K. A. Nebavskaya, V. V. Sarapulova, K. G. Sabbatovskiy, V. D. Sobolev, N. D. Pismenskaya, P. Sistat, M. Cretin, V. V. Nikonenko, Impact of ion exchange membrane surface charge and hydrophobicity on electroconvection at underlimiting and overlimiting currents, *J. Membr. Sci.* 523 (2017) 36–44.

- [36] I. Rubinstein, B. Zaltzman, T. Pundik, Ion-exchange funneling in thin-film coating modification of heterogeneous electro dialysis membranes, *Phys. Rev. E Stat. Nonlin. Soft. Matter. Phys.* 65 (2002) 041507.
- [37] E. Volodina, N. Pismenskaya, V. Nikonenko, C. Larchet, G. Pourcelly, Ion transfer across ion-exchange membranes with homogeneous and heterogeneous surfaces, *J. Colloid Interface Sci.* 285 (2005) 247–258.
- [38] K. D. Kreuer, S. J. Paddison, E. Spohr, M. Schuster, Transport in proton conductors for fuel-cell applications: simulations, elementary reactions, and phenomenology, *Chem. Rev.* 104 (2004) 4637.
- [39] GOST 20298-74, Ion-exchange resins. Cation exchangers. Specifications, Moscow, 1991.
- [40] S. Koter, P. Piotrowski, J. Kerres, Comparative investigations of ion-exchange membranes, *J. Membr. Sci.* 153 (1999) 83–90.
- [41] J. S. Newman, *Electrochemical systems*, Prentice Hall, Englewood Cliffs, N.J., 1973.
- [42] A. Adamson, *Textbook of Physical Chemistry*, second edition, Elsevier Inc., 1973.
- [43] C. Larchet, B. Auclair, V. Nikonenko, Approximate evaluation of water transport number in ion-exchange membranes, *Electrochim. Acta* 49 (2004) 1711–1717.
- [44] T. Xu, Ion exchange membranes: State of their development and perspective, *J. Membr. Sci.* 263 (2005) 1–29.
- [45] Ph. Sizat, A. Kozmai, N. Pismenskaya, Ch. Larchet, G. Pourcelly, V. Nikonenko, Low-frequency impedance of an ion-exchange membrane system, *Electrochim. Acta* 53 (2008) 6380–6390.
- [46] J. J. Krol, M. Wessling, H. Strathmann, Chronopotentiometry and overlimiting ion transport through monopolar ion exchange membranes, *J. Membr. Sci.* 162 (1999) 155–164.
- [47] I. Rubinstein, B. Zaltzman, Electro-osmotically induced convection at a permselective membrane, *Phys. Rev. E Stat. Phys. Plasmas Fluids Relat. Interdiscip. Topics* 62 (2000) 2238–2251.
- [48] J.-H. Choi, H.-J. Lee, S.-H. Moon, Effects of electrolytes on the transport phenomena in a cation-exchange membrane, *J. Colloid Interface Sci.* 238 (2001) 188–195.
- [49] V. V. Gil, M. A. Andreeva, N. D. Pismenskaya, V. V. Nikonenko, C. Larchet, L. Dammak, Effect of counterion hydration numbers on the development of electroconvection at the surface of heterogeneous cation-exchange membrane modified with an MF-4SK film, *Petrol. Chem.* 56 (2016) 440–449.
- [50] V. S. Bagotzky, *Fundamentals of Electrochemistry*, Plenum Press, New York, 1993.

- [51] S. R. Maduar, A. V. Belyaev, V. Lobaskin, O. I. Vinogradova, Electrohydrodynamics near hydrophobic surfaces, *Phys. Rev. Lett.* 114 (2015) 118301.
- [52] Sc. M. Davidson, M. Wessling, A. Mani, On the dynamical regimes of pattern-accelerated electroconvection, *Scientific Reports* 6 (2016) 22505.
- [53] V. V. Nikonenko, N. D. Pismenskaya, E. I. Belova, Ph. Sizat, P. Hugué, G. Pourcelly, Ch. Larchet, Intensive current transfer in membrane systems: modelling, mechanisms and application in electro dialysis, *Adv. Colloid Interface Sci.* 160 (2010) 101–123.
- [54] R. Simons, Strong electric field effects on proton transfer between membrane-bound amines and water, *Nature*, 280 (1979) 824–826.
- [55] V. I. Zabolotskii, N. V. Shel'deshov, N. P. Gnusin, Dissociation of water molecules in systems with ion-exchange membranes, *Russ. Chem. Rev.* 57 (1988) 801.
- [56] E. Belova, G. Lopatkova, N. Pismenskaya, V. Nikonenko, Ch. Larchet, Role of water splitting in development of electroconvection in ion-exchange membrane systems, *Desalination* 199 (2006) 59–61.
- [57] V. Zabolotskii, N. Sheldeshov, S. Melnikov, Heterogeneous bipolar membranes and their application in electro dialysis, *Desalination* 342 (2014) 183–203.
- [58] M. C. Martí-Calatayud, D. C. Buzzi, M. García-Gabaldón, A. M. Bernardes, J. A. S. Tenório, V. Pérez-Herranz, Ion transport through homogeneous and heterogeneous ion-exchange membranes in single salt and multicomponent electrolyte solutions, *J. Membr. Sci.* 466 (2014) 45–47.
- [59] L. G. Sillen, A.E. Martell, Stability constants of metal-ion complexes, second edition, Chemical Society, London, 1964.
- [60] J. Balster, M. H. Yildirim, D. F. Stamatialis, R. Ibanez, R. G. H. Lammertink, V. Jordan, M. Wessling, Morphology and microtopology of cation-exchange polymers and the origin of the overlimiting current, *J. Phys. Chem. B* 111 (2007) 2152–2165.
- [61] M. K. Urtenov, A. M. Uzdenova, A. V. Kovalenko, V. V. Nikonenko, N. D. Pismenskaya, V. I. Vasil'eva, P. Sizat, G. Pourcelly, Basic mathematical model of overlimiting transfer enhanced by electroconvection in flow-through electro dialysis membrane cells, *J. Membr. Sci.* 447 (2013) 190–202.
- [62] V. I. Vasil'eva, A. V. Zhil'tsova, M. D. Malykhin, V. I. Zabolotskii, K. A. Lebedev, R. K. Chermit, M. V. Sharafan, Effect of the chemical nature of the ionogenic groups of ion-exchange membranes on the size of the electroconvective instability region in high-current modes, *Rus. J. Electrochem.* 50 (2014) 120–128.
- [63] I. Rubinstein, B. Zaltzman, Equilibrium electroconvective instability, *Phys. Rev. Lett.* 114 (2015) 114502.

Chapter 4

Effect of electroconvection, pH adjustment and pulsed electric field on membrane scaling in electro dialysis

Presentation of the article

In the previous chapter, it has been shown that the casting of a thin homogeneous ion-conductive perfluorinated Nafion[®] film on the surface of a heterogeneous MK-40 membrane leads to intensification of electroconvection, reduction of water splitting and prevention of scaling in individual MgCl₂ and CaCl₂ solutions. When water splitting at the auxiliary AMX membrane is dominant (higher than that at the CEM under study), the desalination solution is acidified, as a result, the scale does not form on the membrane surface in acid medium.

According to the literature review, the use of pulsed electric field modes of high frequency allows reduction of scale formation. However, the effect of pulsed electric field of low frequency is not yet studied.

The main task of this chapter is to study the influence of electroconvection, pH adjustment and pulsed electric field application on the kinetics of membrane scaling. Scale formation on the surface of a heterogeneous cation-exchange MK-40 membrane and its modification MK-40_{MOD} is investigated by means of chronopotentiometry and voltammetry. The study is made in the range of current densities from $0.25 i_{\text{lim}}^{\text{exp}}$ to $2.5 i_{\text{lim}}^{\text{exp}}$, where $i_{\text{lim}}^{\text{exp}}$ is the experimentally determined limiting current density. The modification is obtained by casting a homogeneous cation-conducting Nafion[®] film on the surface of MK-40 membrane. In order to obtain a significant scale on the studied membranes, a mixed solution with relatively high concentration of Ca²⁺, Mg²⁺ and hydrocarbonates is used. The mineral composition of this solution models a thrice-concentrated milk. Two electric current regimes are used: constant current and four modes of pulsed electric field. In all cases the total working time (not including the time of pause lapses) is the same: 75 min or 105 min.

Scale is found not only on the MK-40 and MK-40_{MOD} membranes, but also on the auxiliary anion-exchange MA-41 membrane. In all cases, the scale forms on the surfaces facing the diluate chamber of the cell. The MK-40 membrane surface is scaled with CaCO₃, Ca(OH)₂ and Mg(OH)₂ compounds at $1.0 i_{\text{lim}}^{\text{exp}} \leq i \leq 2.0 i_{\text{lim}}^{\text{exp}}$. The scale amount on the MK-40_{MOD} is essentially lower; it forms at $1.0 i_{\text{lim}}^{\text{exp}} \leq i \leq 1.5 i_{\text{lim}}^{\text{exp}}$ and contains only CaCO₃. A small amount of CaCO₃ is detected on the auxiliary MA-41 membrane, when it is used together with the MK-40 membrane. Negligible precipitation is found on the MA-41 membrane paired with the MK-40_{MOD} membrane. At $i > 2.0 i_{\text{lim}}^{\text{exp}}$ (for MK-40) and $i > 1.5 i_{\text{lim}}^{\text{exp}}$ (for MK-40_{MOD}), no scale is observed in the studied membrane systems. It can be assumed that higher electroconvection and higher contribution of water splitting at the MA-41 membrane, which adjusts the pH of the depleted solution in a slightly acid range, act together to prevent scaling.

The use of pulsed electric field mode with sufficiently high relaxation time allows essential reduction of membrane scaling. During a pause, the concentration profiles tend to return to the state relative to $i=0$ that decreases the solubility product involving the concentration of OH^- ions. Besides, water splitting rate in this mode is lower, hence, the role of the auxiliary anion-exchange membrane, which produces H^+ ion into the diluate chamber, increases and pH in this chamber is more acid.

Mitigation of membrane scaling in electrodialysis by electroconvection enhancement, pH adjustment and pulsed electric field application

Journal of Membrane Science (549) 2018 129–140

M.A. Andreeva^{a,b}, V.V. Gil^b, N.D. Pismenskaya^b, L. Dammak^a, N.A. Kononenko^b, C. Larchet^a, D. Grande^a, V.V. Nikonenko^b

^a*Institut de Chimie et des Matériaux Paris-Est (ICMPE) UMR 7182 CNRS – Université Paris-Est, 2 Rue Henri Dunant, 94320 Thiais, France.*

^b*Kuban State University, 149 Stavropolskaya st., 350040 Krasnodar, Russia.*

Abstract

Scale formation on the surface of a heterogeneous cation-exchange MK-40 membrane and its modification MK-40_{MOD} was studied during electro dialysis of a solution whose mineral composition models a thrice concentrated milk. The modification was obtained by casting a homogeneous cation-conducting Nafion[®] film on the surface of MK-40 membrane used as a substrate. A 0.04 M NaCl solution circulated through the concentrate compartment of a laboratory flow-through cell. Constant current and pulsed electric field modes were applied; the current densities in overlimiting current range were used. The amount of scale was characterized by the potential drop across the membrane and using the scanning electronic microscopy. Scale was found on the membrane surfaces of both cation-exchange membranes and the auxiliary anion-exchange MA-41 membrane facing the diluate compartment of the cell. The MK-40 membrane surface was scaled with CaCO₃, Ca(OH)₂ and Mg(OH)₂ compounds. The scale amount on the MK-40_{MOD} was essentially lower and it contained only CaCO₃. A small amount of CaCO₃ was detected on the auxiliary MA-41 membrane, when it was used together with the MK-40 membrane. Negligible precipitation was found on the MA-41 membrane paired with the MK-40_{MOD} membrane. At currents 1.5 to 2 times higher than the limiting current, higher electroconvection and higher contribution of water splitting at the MA-41 membrane, which adjusted the pH of the depleted solution in a slightly acid range, act together to prevent scaling. Lower scaling of the MK-40_{MOD} membrane is explained by its more appropriate surface properties: the thin Nafion[®] layer forming the surface is smooth, homogeneous and relatively hydrophobic. These three properties together with a heterogeneous substrate aid an earlier onset of electroconvective instability; enhanced electroconvection partially suppresses water splitting at the cation-exchange membrane, which allows slight acidification of the diluate solution due to a more pronounced water splitting at the anion-exchange membrane. The use of pulsed electric fields with sufficiently high relaxation time allows essential reduction of membrane scaling.

4.1 Introduction

Electrodialysis (ED) is widely used in the treatment of natural and waste waters, solutions for the food industry, such as dairy products and wine [1-3], and nutrient recovery [4]. Zero liquid discharge systems are actively developing [5] due to the toughening of ecological requirements for discharge of slightly concentrated solutions. The optimal technological scheme is when the concentrate obtained after water treatment by nanofiltration and reverse osmosis is further concentrated using ED [5-7]. The presence of Mg^{2+} , Ca^{2+} , CO_3^{2-} , SO_4^{2-} and other multivalent ions in solutions treated by ED leads to the scale formation on the surface from both sides of ion-exchange membranes (IEMs) facing concentrate and diluate compartments [8-11]. This scale causes an increase in the electrical and hydraulic resistance of the membrane stack causing a growth of energy consumption [8]. Interruption of industrial process in order to regenerate or replace the scaled membranes leads to additional costs. Therefore, the membrane scaling is one of the key obstacles to wider ED implementation.

The scaling on the IEM relates to the deviation from solubility equilibrium. Deposition of particles on a membrane is mainly due to the presence of Mg^{2+} , Ca^{2+} , Ba^{2+} cations and CO_3^{2-} and SO_4^{2-} anions in the processed solutions [12, 13]. If the solution region where the product of ion concentrations exceeds the solubility product is near the membrane/solution interface, the scale formation occurs on the membrane surface. In the case where this region is far from the surface, the scale crystals are formed in the bulk of the processed solution [11]. Water splitting at the depleted interface of a cation-exchange membrane (CEM) produces OH^- ions, which increase pH of the near-surface solution and causes formation of such precipitates as $Mg(OH)_2$ and $CaCO_3$ in the diluate compartment. Note that while electrodialysis metathesis and selectrodialysis [14-16] allow one to exclude the simultaneous presence of divalent anions and divalent cations in concentrate compartments of ED stack (hence, to reduce the risk of scaling there), these ions are still present in the diluate compartments. And even when only divalent cations, such as Ca^{2+} or Mg^{2+} are in the feed solution, scale formation is yet possible on the diluate side of the CEM [17].

The rate of scale formation, its structure and ability to retain on the surface of an IEM is largely determined by the ratio of calcium and magnesium ions in the processed solutions [18, 19]. The presence of Mg^{2+} ions inhibits the scale growth of $CaCO_3$ [18]. The alkaline media contributes to the formation of scale due to the formation of hydroxides having a very low solubility product. On the contrary, in an acidic media, $CaCO_3$ scale can dissolve. Water splitting at the membrane/depleted solution interface leads to an increase of the pH in the near-surface solution of CEM and, as a consequence, to the scale (of $Mg(OH)_2$, $CaCO_3$ and

other compounds [17, 20]) growth on its surface facing the desalination compartment. At the same time, the "proton-barrier" [21] created by the anion-exchange membrane (AEM) partially prevents the scaling of salts on the AEM side facing the desalination compartment [17, 21].

The electrical and geometric heterogeneity of the membrane surface also influences the scale formation on the IEM. Some types of geometric heterogeneity or surface roughness (which is understood as the deviation from flatness) may provoke scaling. Membranes with a rough surface are more exposed to scaling as compared to the membranes with a smooth surface [22]. IEMs are conventionally classified as homogeneous and heterogeneous. Homogeneous membranes are generally fabricated using the "paste method" [23]. The fine powder of styrene, divinylbenzene and poly(vinyl chloride) is coated onto the cloth of a reinforcing material and heated to prepare the base membrane. Then the ion-exchange groups are introduced by appropriate after-treatments [23]. The micro- and mesopores in the range from several nm to several tens of nm are obtained in such membranes [24]. Heterogeneous membranes are fabricated from the powder of ion-exchange resins and polyethylene as filler. After hot pressing, polyethylene forms continuous network providing mechanical strength; ion-exchange resin particles having micro- and mesopores (with the size in the range from 5 to 50 μm) form the ion pathways. Generally, homogeneous IEMs have very little or no macropores, while heterogeneous IEMs contain considerable amount (of the order of 10 % by vol.) of macropores, which are mainly localized in the contacts between resin particles and polyethylene. A series of studies [8, 25, 26] showed that the scaling occurs more intensively in the case of heterogeneous membranes compared to the homogeneous ones. In the case of homogeneous membranes, the scale is mainly localized on their surface [8], whereas in the case of heterogeneous membranes it is formed not only on the surface, but also inside the macropores [8, 27]. When heterogeneous membranes, such as Russian MA-40 or MK-40 membranes, are used in ED, the scale is localized on the surface of ion-exchange resin particles incorporated into polyethylene, which serves as a filler-binder [8, 28]. The partial blocking of the ion conductive pathways on the membrane surface leads to an increase in the local current density across the conducting surface areas. Rubinstein et al. [29] theoretically studied the "funnel effect": distortion of the electric current lines due to their accumulation in the ion conductive pathways on the membrane surface. This effect leads to increasing concentration polarization (CP) at the ion-conductive surface area. An equation connecting the limiting current density with the parameters of membrane surface heterogeneity (the fraction and the size of ion-conductive regions) had been obtained by Batrunas et al. [30] and verified experimentally by Zabolotsky et al. [31].

It is established [10, 17] that the development of electroconvection (EC) significantly reduces the scaling on the surface of IEMs. This effect is due to increasing convection transfer, which enhances hydrodynamic effect on the scale and decreases water splitting [17, 32]. The latter results in lowering pH changes at the membrane surface, and, as consequence, mitigation of scaling. The effect of EC increases for IEMs with relatively hydrophobic surface [17, 33], and in the case where pulsed electric field (PEF) are applied [10, 34]. Accordingly, the scaling is mitigated in these cases [10, 17].

Thus, the review above shows that despite the great attention paid to the problem of the scale formation in the literature, there is no satisfactory solution to the problem. In this paper we study the impact of membrane surface properties and PEF on the rate of scale formation in a feed solution imitating trice concentrated milked. In comparison with our precedent study [17], where individual calcium and magnesium chlorides were used, a more concentrated solution is chosen now in order to amplify the scaling phenomenon. The amount of scale formed on the membrane surface is characterized by the value of potential drop across the membrane [17, 35]. In addition to use a specially prepared membrane, MK-40_{MOD}, which has shown its effectiveness in mitigation of scaling [17], we apply PEF with the period of pulses in the range from 2 to 30 minutes, which is essentially greater than in other studies [9, 10, 11, 19, 20, 21]. We show that electroconvection together with optimization of pH and application of PEF produces an essential effect on the rate of scale formation on the membranes in the desalination compartment. For the first time, the pH value of the solution in desalination compartment is adjusted by the choice of the membranes and the current density.

4.2 Experimental

4.2.1. Membranes

Two cation-exchange membranes, a heterogeneous commercial MK-40 (Shchekinoazot, Russia) and its modification MK-40_{MOD} (Figs. 4-1a-b) are studied. The MK-40 membrane has polystyrene-based polymer matrix with fixed sulfonic acid groups. About 80 % of the MK-40 surface is covered by polyethylene [28, 36] used as the binder filler for the membrane reinforcement. Particles of KU-2 cation-exchange resin, which provide selective conductivity of the membrane, protrude over the polyethylene surface and form “hills” of about 6 μm in height [33]. The thickness of the swollen MK-40 membrane in the Mg^{2+} form is about 515 μm .

The MK-40_{MOD} membrane is obtained by casting a Nafion[®] water-isopropyl-alcohol solution onto the MK-40 membrane as substrate. After evaporation of the solvent, a thin perfluorinated

cation-exchange homogeneous layer is formed on the MK-40 membrane surface (Fig. 4-1c). More details may be found in [36, 37]. The thickness of the Nafion[®] film in the Mg²⁺ form is 25 μm when the membrane is swollen (obtained using a micrometer by the difference in the thickness of the pristine and modified membranes). Its thickness of the film is about 15 μm in dry state as shown in Fig. 4-1 (SEM images are obtained for dried membranes). The conductive surface fraction of the MK-40_{MOD} membrane is 100 %, however the film is not perfectly smooth. The difference in height between peaks and valleys for this membrane is about 2 microns. The contact angle of the MK-40 membrane is 55°, that of the MK-40_{MOD} is 15% greater [36]. The surface of the MK-40_{MOD} membrane is less hydrophilic in comparison with the MK-40 membrane.

A heterogeneous anion-exchange commercial MA-41 (Shchekinoazot, Russia) (Fig. 4-1d) membrane is used as the auxiliary membrane in chronopotentiometric and voltammetry measurements. The structure of this membrane is similar to that of the MK-40 membrane, the difference is that the fixed groups of this membrane are quaternary ammonium groups with a noticeable presence of tertiary and secondary amines. This membrane is characterized by stable properties and moderated water splitting rate. Its stability is important for long-term experiments.

The pair of MK-40 membrane and its modification is chosen for the following reasons. The MK-40 membrane is inexpensive, its properties are stable when it is used in ED processes; however its performance is not so high as that of homogeneous commercial IEMs. In particular, under the same current density, the concentration polarization of this membrane (evaluated by the voltage) is higher in comparison with homogeneous membranes. On the other hand, as it was shown earlier [36, 38, 39], modification of MK-40 with a thin perfluorinated cation-exchange layer, such as Nafion[®], results in decreasing the concentration polarization/voltage and water splitting. The MK-40_{MOD} membrane remains cost effective, as the thickness of the expensive Nafion[®] layer is small. The main cause of better membrane performance of the modified membrane according to [36, 38, 39] is lower electrical and geometric surface heterogeneity (which decreases the non-uniformity in current density distribution) and stronger electroconvection. The fact that the MK-40_{MOD} membrane has these improved properties allows us to anticipate its good scaling resistance.

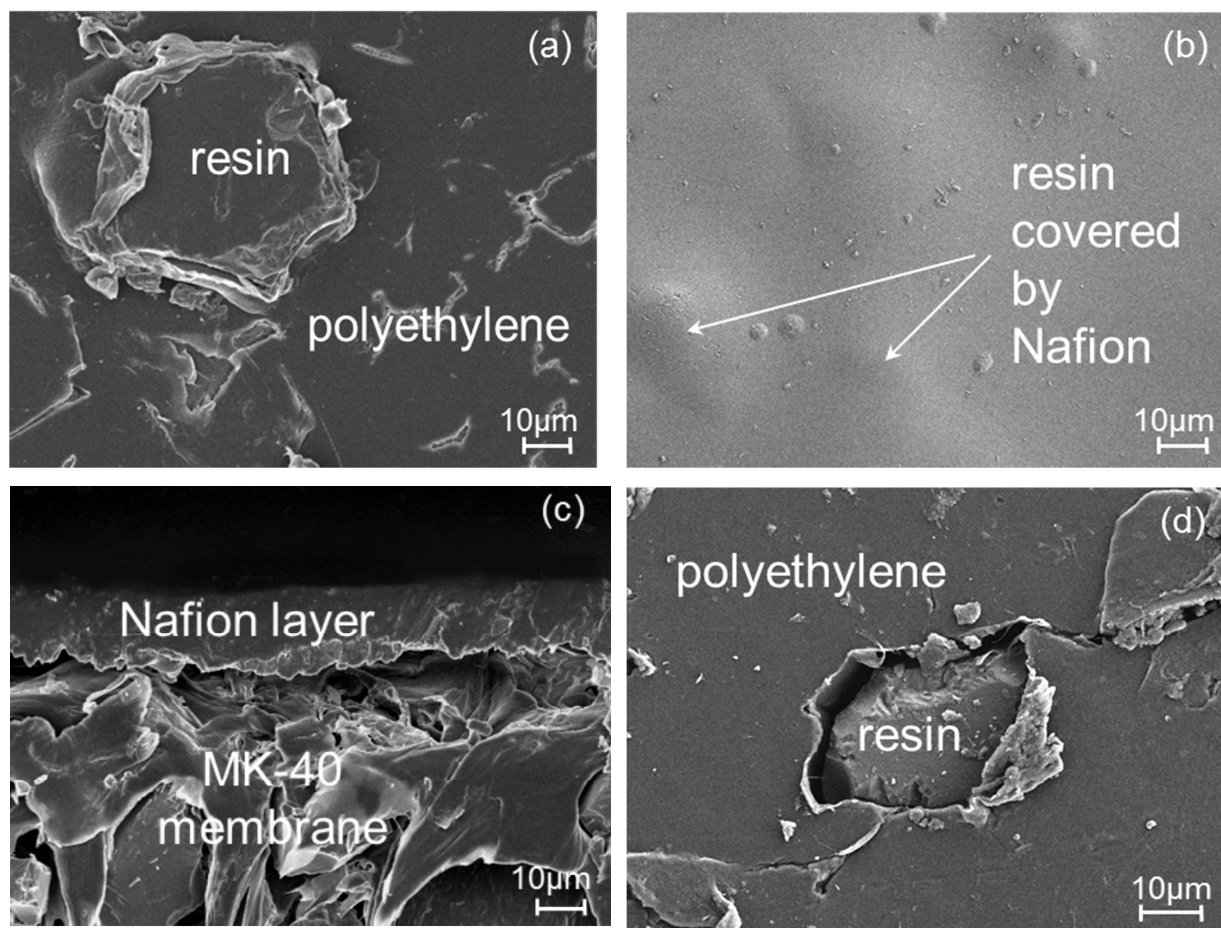


Fig. 4-1. SEM images of the membrane surfaces in a dry state: MK-40 (a), MK-40_{MOD} (b), MA-41 (d) and the cross section of MK-40_{MOD} membrane (c).

4.2.2. Electrodialysis cell and experimental setup

The flow-through four-compartment electrodialysis cell used in this study and similar to that applied in our earlier studies [17, 40] is shown in Fig. 4-2. The desalination compartment is formed by a cation-exchange membrane (M^*) and an auxiliary anion-exchange membrane. The MK-40 or MK-40_{MOD} membrane is used as the M^* membrane, and the MA-41 membrane as the auxiliary one. The intermembrane distance in this compartment, h , is 6.4 mm, the membrane area available to electric current passage is $2 \times 2 \text{ cm}^2$. The study is performed with a mixed salt solution used for feeding the central desalination compartment (compartment 2 in Fig. 4-2). This solution is composed of Na_2CO_3 (1000 mg L^{-1}), KCl (800 mg L^{-1}), $\text{CaCl}_2 \cdot 2\text{H}_2\text{O}$ (4116 mg L^{-1}) and $\text{MgCl}_2 \cdot 6\text{H}_2\text{O}$ (2440 mg L^{-1}). In this solution, the Mg/Ca molar concentrations ratio is $2/5$ and the total concentration of CaCl_2 and MgCl_2 is 0.04M . The pH of the solution is adjusted to 6.5 by adding HCl . The mineral composition of this solution corresponds approximately to that of trice concentrated milk. This composition is chosen because the dairy products (such as milk whey) are often subjects of ED processing

(demineralization). The main components are also present in seawater, other natural and waste waters. The component concentration is so that the rate of scale formation on the membrane is in the range of relatively easy measurements.

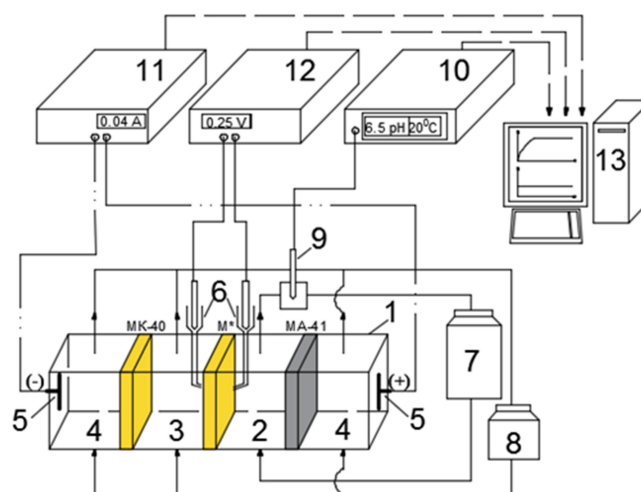


Fig. 4-2. Principal scheme of the experimental setup. ED cell (1) consists of one desalination (2), one auxiliary (3) and two electrode compartments (4), two platinum polarizing electrodes (5) and two Ag/AgCl electrodes inserted in Luggin capillaries (6). A mixed salt solution (7) composed of Na_2CO_3 , KCl , CaCl_2 and MgCl_2 feeds the desalination compartment; NaCl solution (8) circulates through the auxiliary and two electrode compartments. A flow cell with a pH electrode (9) and a pH meter pHM120 MeterLab (10) are used for pH measurements. The current is supplied by KEITHLEY 220 current source (11), the potential difference is measured using HEWLETT PACKARD 34401A multimeter (12); the data are registered using a PC (13).

The auxiliary compartment (compartment 3 in Fig. 4-2) formed by an auxiliary MK-40 membrane and the tested (M^*) membrane, and two electrode compartments (compartments 4 in Fig. 4-2) are fed with a 0.04 M NaCl solution. The anode and the cathode are platinum polarizing electrodes. All three compartments are fed in parallel each with a rate of 30 mL min^{-1} . The concentration of this solution is taken the same as the total concentration of the solution feeding the desalination compartment in order to minimize the diffusion transport of auxiliary solution components into compartment 2. The electrically driven transport of cations from the anode compartment into the desalination compartment is restrained by the MA-41 anion-exchange membrane. The volume of the auxiliary solution circulating through compartments 3 and 4 was 8 L. The volume of the solution circulating through desalination compartment 2 was 5 L; the rate of its flow was also 30 mL min^{-1} . The volumes of both solutions were so that during one experimental run (maximum 5 hours of current flowing) the

decrease/increase in component concentrations was negligible. Indeed, the current was 42 mA; during 5 hours, the decrease/increase of a component in the circulating solution according to the Faraday law does not exceed 10 mmol, while more than 400 mmol (in terms of a singly charged anion, such as Cl^-) were initially in 5 L of the feeding solution.

Before chronopotentiometry measurements, the membranes were equilibrated for 24 h with the solutions to be used subsequently.

4.2.3. Chronopotentiometric and voltammetry measurements

Chronopotentiograms (ChPs) and voltammograms (I-V curve) are obtained using the flow-through electro dialysis cell presented in Fig. 4-2. A KEITHLEY 220 current source is used to supply the current between the polarizing electrodes. The potential drop (PD) across the membrane under study, $\Delta\phi$, is measured using Ag/AgCl electrodes. These electrodes are placed in the Luggin capillaries. The Luggin tips are installed at both sides of the membrane under study in its geometric center at a distance of about 0.5 mm from the surface. PD is registered by a HEWLETT PACKARD 34401A multimeter. I-V curves are obtained from ChPs by taking (quasi) steady state time-averaged values of PD related to a fixed current density in the range up to 18 mA cm^{-2} while the PD remains $< 4\text{V}$. The experiment is carried out at 20°C .

Two electric current modes are used in chronopotentiometric measurements: constant current and four pulsed electric field modes. In all cases total working time is the same (75 min or 105 min). In PEF mode the phase of constant current application (pulse lapse, T_{on}) is alternated with the phase of zero current (pause lapse, T_{off}). The following regimes of PEF mode are used: $T_{\text{on}}/T_{\text{off}}=15\text{min}/15\text{min}$, $T_{\text{on}}/T_{\text{off}}=15\text{min}/7.5\text{min}$, $T_{\text{on}}/T_{\text{off}}=5\text{min}/5\text{min}$, $T_{\text{on}}/T_{\text{off}}=1\text{min}/1\text{min}$. It was impossible to apply lower values of T_{on} and T_{off} because of limitations of the available software.

4.2.4. Analysis methods

4.2.4.1 Scanning electron microscopy and X-ray elemental analysis

Visualization of the membrane structure is made by a scanning electron microscope (Merlin, Carl Zeiss Microscopy GmbH) equipped with an energy dispersive spectrometer. The energy dispersive spectrometer conditions are 6 kV accelerating voltage with a 9.9-mm working distance. The dried membrane samples are coated with a thin layer of platinum in order to make them electrically conductive and to improve the quality of the microscopy photographs. The membrane sample preparation for X-ray analysis is the same like for SEM.

4.2.4.2 pH

The pH value of the diluate solution is measured using a flow cell (Fig. 4-2) with a pH meter pHM120 MeterLab with a pH electrode.

4.3. Results and discussion

4.3.1 I-V curves

Fig. 4-3 shows the I-V curves obtained as described above for MK-40 and MK-40_{MOD} membranes in the model salt solution. It can be observed three general regions of the I-V curve (Fig. 4-3). An initial linear region at low currents is followed by a plateau of limiting current density, i_{lim} . When approaching i_{lim} , the electrolyte interfacial concentration gets nearly zero that initiates coupled effects of membrane CP: current-induced convection (generally, electroconvection and gravitational convection) and water splitting [17]. EC arises due to the action of the electric field on the electric space charge in the boundary depleted solution. Gravitational convection, which develops due to the non-uniform distribution of solution density, is more likely to occur in relatively concentrated solutions (0.1 mol L^{-1} or more) and wide compartments [41].

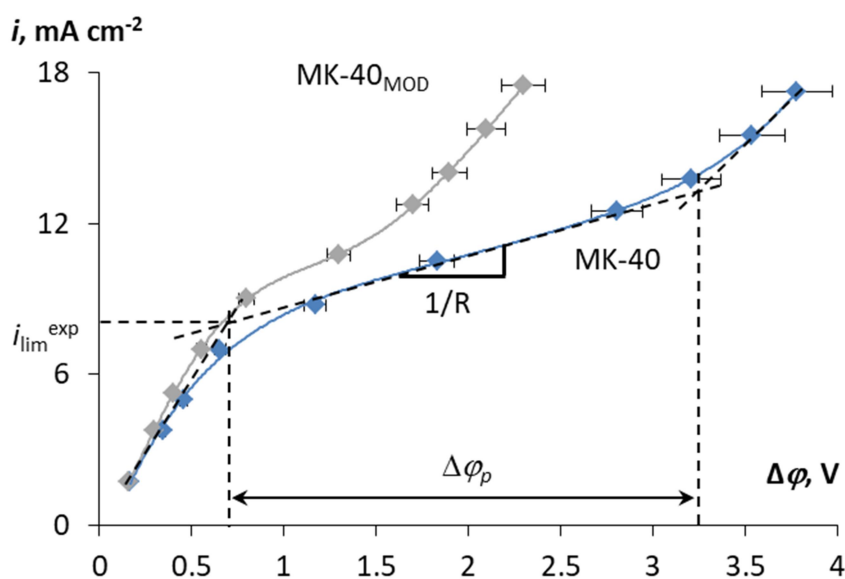


Fig. 4-3. I-V curves of the MK-40 (dark blue line) and MK-40_{MOD} (grey line) membranes in the model solution. $\Delta\phi_p$ is the "plateau" length; $1/R$ is the "plateau" slope; i_{lim}^{exp} is the limiting current density determined (for the MK-40 membrane) by the intersection point of tangents.

Table 4-1 presents some characteristics of experimental I-V curves of MK-40, MK-40_{MOD} and MA-41 membranes: the experimental limiting current density, i_{lim}^{exp} , the plateau length and the plateau slope determined as shown in Fig. 4-3.

membrane	i_{lim}^{exp}	Plateau length, $\Delta\phi_p$, V	Plateau slope, $1/R$, mA cm ⁻² V ⁻¹
MK-40	7.9±0.1	2.8±0.1	2.0±0.1
MK-40 _{MOD}	8.8±0.1	1.1±0.1	3.1±0.1
MA-41	9.3±0.1		1.7±0.1

Table 4-1. Some parameters of I-V curves of MK-40, MK-40_{MOD} and MA-41 membranes in the mixed model solution at 20⁰C.

Comparing parameters of I-V curves shows that the plateau length is less while the limiting current density i_{lim}^{exp} and the plateau slope are higher in the case of MK-40_{MOD} membrane in comparison with the MK-40. Similar results were obtained earlier [17, 36, 38, 39]. Belashova et al. [39] observed a nearly 1.5-fold increase of the limiting current density across a MK-40 membrane after covering its surface with a 20 μ m Nafion[®] film in a 0.02 M NaCl solution. Close values of plateau length and plateau slope were found for the MK-40 and MK-40_{MOD} membranes in 0.02 M and 0.04 M individual solutions of MgCl₂ and 0.04 M CaCl₂ [17]. Pismenskaya et al. [36, 38] have found similar parameters of the I-V curves in NaCl solutions of different concentrations, and additionally established the fact that the water splitting rate is essentially lower at the MK-40_{MOD} membrane in comparison with the MK-40. All these results were explained by stronger electroconvection near the MK-40_{MOD} membrane [17, 36, 39]. Indeed, according to [42-46], earlier onset of unstable non-equilibrium electroconvection leads to a shorter length of the plateau region; higher i_{lim}^{exp} and plateau slope relate to higher stable equilibrium and non-equilibrium electroconvection, which develop in the corresponding current range. A more intensive unstable non-equilibrium electroconvection gives rise to a steeper slope of current density curve following the inclined plateau. Thus, the comparison of parameters of I-V curves show that EC near the MK-40_{MOD} membrane is stronger than that near the MK-40 one.

There are two factors caused by electrical heterogeneity of membrane surface, which affect mass transfer rate. The first one is the funnel effect [29] leading to higher concentration polarization/higher potential drop at a given current density. The second one is the occurrence of tangential electric field, which enhances EC, hence, reduces CP. In the case of MK-40 membrane, the conductive surface area is quite low (about 20% [28]), the size of a conductive

spot, an ion-exchange resin particle, is small (about $30\ \mu\text{m}$ [39]) compared to the diffusion layer thickness (about $200\ \mu\text{m}$ in the cell under study), hence, the CP due to the funnel effect is considerable. The homogeneous conductive Nafion[®] film on the MK-40_{MOD} membrane surface essentially reduces the CP caused by funnel effect. However, the current lines near the Nafion[®] surface remain sufficiently distorted and the tangential electric field produces effective EC. The distance between the EC vortices near an electrically heterogeneous surface is determined by the length of repeating fragment of heterogeneity on the surface [47, 48] (Fig. 4-4). This length is about $100\ \mu\text{m}$ for the MK-40 membrane used in this study [39]. The electrical conditions near the “gates” for ion passage (in particular, the value of tangential electric field and the length and thickness of the space charge region near the surface) determine the size of vortices. Thus, the homogeneous conductive film on the MK-40_{MOD} membrane allows “optimization” of electric current lines in the depleted near-surface solution (Fig. 4-4).

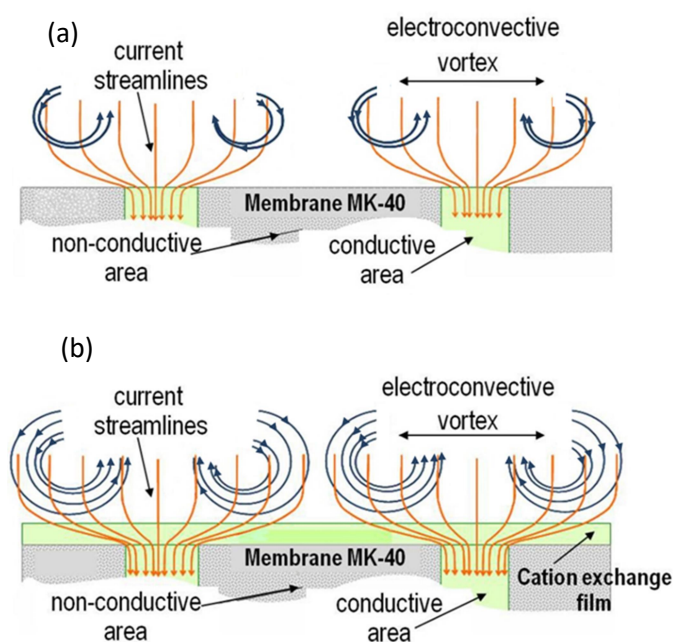


Fig. 4-4. Schematic distribution of electric current lines near the surface of MK-40 (a) and MK-40_{MOD} (b) membranes. Due to low fraction of conductive area and narrow “gates” for ion passage, the funnel effect [29] results in high concentration polarization of MK-40 while electroconvection is low. The increased “gates” and more hydrophobic surface of MK-40_{MOD} membranes lead to lower concentration polarization and higher electroconvection. Adapted from [38].

Theoretically this type of optimization was studied by Davidson et al. [48] and Zabolotsky et al. [49], who simulated mass transfer near an ion-selective heterogeneous surface involving

alternating conductive and non-conductive regions. It was found via simulation based on the Nernst-Planck-Poisson-Navier-Stokes equations that at low fractions of conductive regions, the mass transfer is low due to funnel effect. At very high fractions of conductive regions the mass transfer is also low due to reduced tangential electric field. Hence, there is an optimum value of the conductive area fraction where electric field involves a sufficiently high tangential component causing a strong electroosmotic flow, while the growth of CP caused by the funnel effect remains low. In our case, an effective tangential electric field is formed due to the electrically heterogeneous MK-40 membrane serving as a substrate. Note that Balster et al. [44] and Wesslilng et al. [50] produced and then studied ion-exchange membranes with tailored microheterogeneous surface, which showed quite elevated electroconvection. Korzhova et al. [51] deposited spots of non-conductive hydrophobic fluoropolymer on the homogeneous membrane, which screened 8 or 12% of the membrane surface, and resulted in up to a 1.5-fold growth of the limiting and overlimiting current density and reduced water splitting. In particular, the surface modification allows an earlier onset of unstable electroconvection leading to an essential decrease of the plateau length.

The surface of MK-40_{MOD} membrane covered with a fluoropolymer film is relatively more hydrophobic than that of the MK-40 membrane: the contact angles of the MK-40 and MK-40_{MOD} membranes are 55° and 63°, respectively. Hydrophobization of membrane surface facilitates water slipping along the surface, which contributes to enhancing EC [33, 51-53].

4.3.2 Chronopotentiograms

Fig. 4-5 shows the ChP of MK-40_{MOD} membrane and its derivative obtained in the model solution at $i=17.5 \text{ mA cm}^{-2}$ ($i=2 i_{\text{lim}}^{\text{exp}}$). The shape of the curve is typical for IEMs in a binary solution of monovalent ions at $i \geq i_{\text{lim}}$ [54, 55]. An immediate increase of PD is observed after switching-on the direct current. It is related to the ohmic potential drop, $\Delta\varphi_{\text{Ohm}}$, over the membrane and two adjacent solutions where the concentrations are not yet affected by CP. At $i < i_{\text{lim}}$ the value of PD does not increase significantly during one experimental run. At $i \geq i_{\text{lim}}$ the electrolyte concentration at the depleted membrane interface gradually decreased with time, the process is governed by electrodiffusion. As a result, the sharp increase in PD is observed on the ChPs. When the electrolyte concentration at the depleted membrane interface gets sufficiently low, along with electrodiffusion, current-induced convection arises. As a consequence, the rate of PD growth slows down, and finally, PD tends to a quasi-steady state value, $\Delta\varphi_{\text{St}}$. The transition time, τ , related to the inflection point on the ChP corresponds to

the appearance of an additional mechanism of ion transport, namely, the current-induced convection [54, 55].

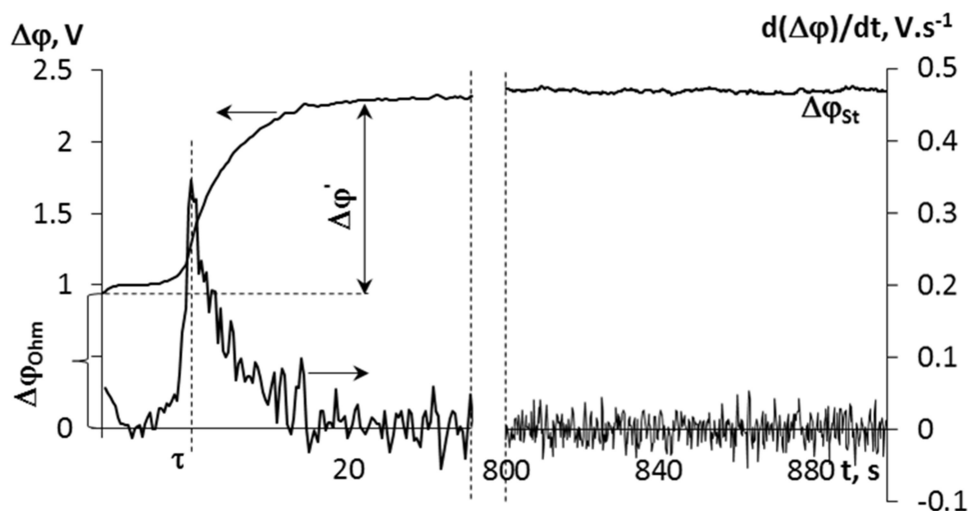


Fig.4-5. Chronopotentiogram of the MK-40_{MOD} membrane in the model solution, $\Delta\phi$ vs. t , and its derivative, $d(\Delta\phi)/dt$ vs t , in the model solution at $i=17.5 \text{ mA cm}^{-2}$. $\Delta\phi_{\text{ohm}}$ is the ohmic potential drop just after the current is switched on; $\Delta\phi_{\text{St}}$ is the potential drop at the steady-state; $\Delta\phi' = \Delta\phi - \Delta\phi_{\text{ohm}}$ is the reduced potential drop; τ is the transition time.

Figs. 4-6a-b show ChPs for the pristine MK-40 and modified MK-40_{MOD} membranes measured in the model salt solution at different current densities. In all considered cases, there are oscillations of the potential drop across the cation-exchange membrane under study. The potential drop is always lower and the PD oscillations are always higher in the case of MK-40_{MOD} membrane, which should be due to stronger electroconvection near this membrane. At low current density (Fig. 4-6a, $i=5.3 \text{ mA cm}^{-2}$, $i < i_{\text{lim}}$) the observed PD oscillations can be explained by equilibrium electroconvective instability [56]; however, they may be also due to early stages of crystal growth on the membrane surface. The latter cause might be especially relevant at overlimiting currents where scale formation becomes visible on the membrane surface. Equilibrium EC instability arises when a tangential gradient of electrochemical potential occurs near the depleted membrane surface [56]. This gradient can appear due to electrical and/or geometrical heterogeneity of the membrane surface [52]. The PD oscillations at low potential drops ($<0.1 \text{ V}$ without ohmic contribution) were observed earlier in NaCl [40, 51] and individual CaCl_2 and MgCl_2 [17, 40] solutions in conditions where no scale formation occurs.

Fig. 4-6c shows the ChPs obtained in a 0.1 M NaCl solution at $i=5.3 \text{ mA cm}^{-2}$ and $i=12.8 \text{ mA cm}^{-2}$. This experiment is made in order to find out the character of oscillations in a

solution with nearly the same equivalent concentration and a close limiting current density ($i_{\text{lim}}^{\text{NaCl}}=9.0 \text{ mA cm}^{-2}$) as in the model solution, where, however, no scale formation occurs.

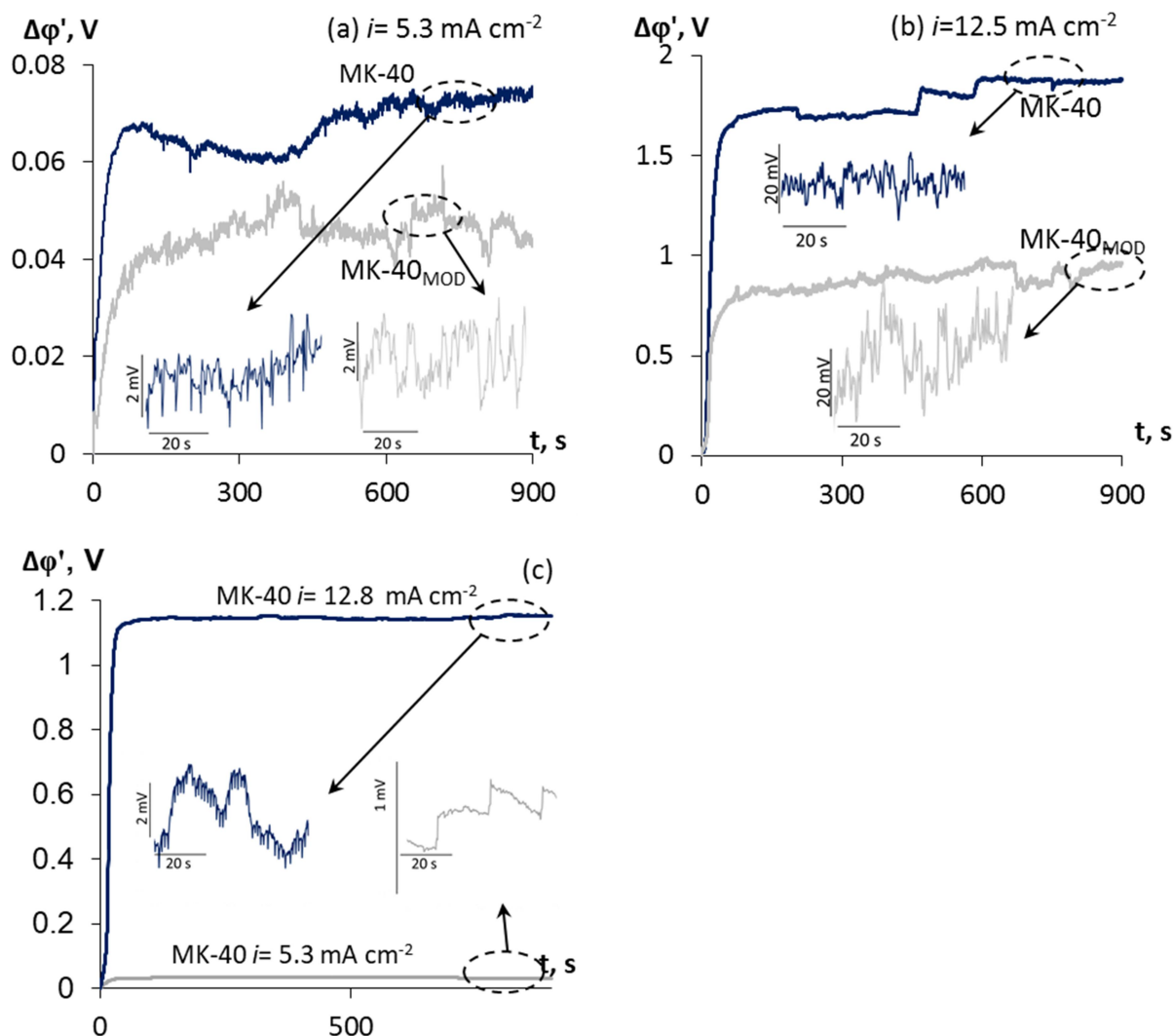


Fig. 4-6. Chronopotentiograms of the MK-40 and MK-40_{MOD} membrane measured in the model solution at $i=5.3 \text{ mA cm}^{-2}$ ($i < i_{\text{lim}}^{\text{exp}}$) (a) and $i=12.5 \text{ mA cm}^{-2}$ ($i > i_{\text{lim}}^{\text{exp}}$) (b) and in a 0.1 M NaCl solution at $i=5.3 \text{ mA cm}^{-2}$ and $i=12.8 \text{ mA cm}^{-2}$ (c)

It can be seen that oscillations in this solution occur at both current densities. Though, when comparing them with those in the model solution, one can see that the amplitude of oscillations in the 0.1 M NaCl solution is essentially lower. While it is known that EC is more intensive in Ca^{2+} and Mg^{2+} containing solutions than in NaCl solutions in comparable conditions [17, 40, 43], the large difference between the size of oscillations makes one think about the initial stage of crystal formation as the cause of stronger PD oscillations in the model solution. Apparently, scale formation and destruction are the main phenomena behind the relatively steep PD increases and decreases, respectively, both of the order of 100 mV

seen in Fig. 4-6b at $i=12.5 \text{ mA cm}^{-2}$ in the model solution. No PD variations of this type can be seen in the case of 0.1 M NaCl solution, Fig. 4-6c.

Lower potential drop and shorter plateau length of the I-V curves (Fig. 4-3), higher amplitude of potential oscillations seen on the chronopotentiograms (Figs. 4-6a-b) in the case of MK-40_{MOD} in comparison to MK-40 allows us to state that the intensity of EC is higher in the case of MK-40_{MOD} under the same current density. This statement is supported by the results of Zhiltsova, Vasil'eva et al [57], who visualized convective instability zones emerged due to oscillating EC vortices near MK-40 and MK-40_{MOD} membranes, using laser interferometry. The laser interferometry technique allows obtaining concentration profiles near an ion-selective interface due to the fact that interference fringe patterns depend on the liquid density. The convective instability zone near the membrane surface is determined by the boundary dividing a zone where oscillations of concentration profile occur and a zone where these oscillations are absent [58-60]. It was shown [57] that at a fixed overlimiting current density, the size of the EC instability zone near the MK-40_{MOD} is greater and the potential drop across the membrane is smaller compared with those in the case of MK-40 (Fig. 4-7). Note that direct optical observation of electroconvective vortices and measurement of the size of EC vortices (for other membranes and using other techniques) were performed by Rubinstein et al. [61], Yossifon et al. [62], Kwak et al. [63] and de Valenca et al. [64].

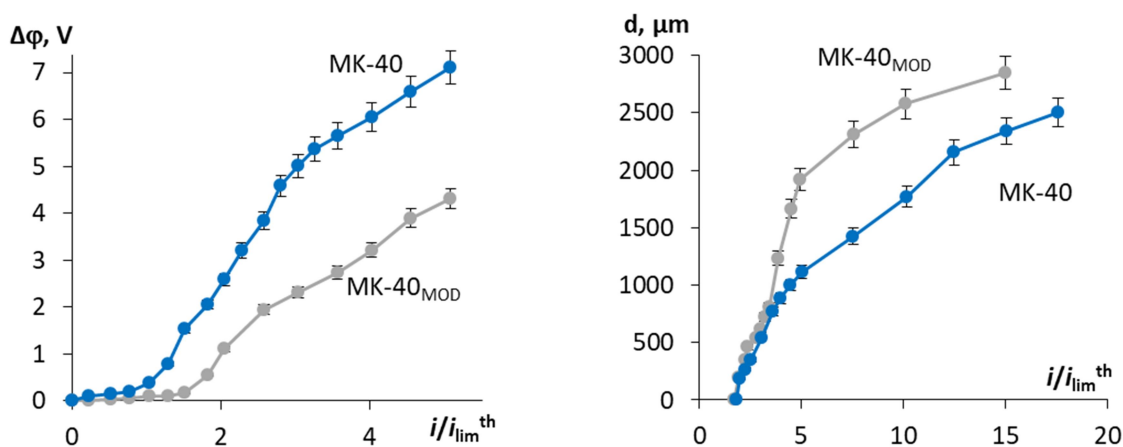


Fig. 4-7. I-V curves (a) and the current density dependences of the size d of convection instability zone near the MK-40 and MK-40_{MOD} membranes in a membrane channel (the length is 4.2 cm, the intermembrane distance is 5 mm); a 0.02 M NaCl is fed with a velocity 0.2 mm s^{-1} . The data are obtained using an interferometric setup of the Mach-Zehnder type.

The value of d is defined as the distance from the membrane surface on which the concentration profile has an unstable, oscillatory character. The curves are performed using experimental data from Ref. [57].

4.3.3 Scaling formation in constant current mode

It can be seen that PD across the membrane, in the case of both MK-40 and MK-40_{MOD} membranes, slowly increases with time after reaching the quasi-steady state. This growth occurs for the MK-40 at $7.9 \text{ mA cm}^{-2} \leq i \leq 15.5 \text{ mA cm}^{-2}$ ($i_{\text{lim}}^{\text{exp}} \leq i \leq 2 i_{\text{lim}}^{\text{exp}}$) and at $8.8 \text{ mA cm}^{-2} \leq i \leq 13.3 \text{ mA cm}^{-2}$ ($i_{\text{lim}}^{\text{exp}} \leq i \leq 1.5 i_{\text{lim}}^{\text{exp}}$) for the MK-40_{MOD} membrane. Marti-Calatayud et al. [35], who have studied the chronopotentiometry of IEMs in iron-containing solutions, related the increase of PD with time to the precipitation formation. In order to understand where the precipitation is localized, the scanning electron microscopy (SEM) images of the surfaces of the membranes at the end of a 5-hour experiment run at $i=10.5 \text{ mA cm}^{-2}$ are obtained (Figs. 8a-i). Both surfaces facing the diluate and concentrate compartments are studied.

For all membranes, no precipitation is found on the concentrate side, where a 0.04 M NaCl solution circulates. Note that this solution passes through the concentrate and two electrode compartments in parallel, then return to the tank 8, as shown in Fig. 4-2. Due to relatively large volume of this solution (8 L), during 5 h of an experimental run, the salt concentration increases only by 6% while the pH of this solution changes from 6.5 to 7.3.

However, the scale formation on the diluate side is established for both MK-40 and MK-40_{MOD} cation-exchange membranes as well as for the MA-41 anion-exchange membrane used to form the desalination compartment (Fig. 4-2). The amount of precipitation at all current densities is less on the MK-40_{MOD} membrane than on the MK-40 membrane. According to X-ray elemental analysis of the membrane surface facing diluate solution, the presence of two main scale-forming ions, Ca^{2+} and Mg^{2+} in the form of CaCO_3 , $\text{Ca}(\text{OH})_2$ and $\text{Mg}(\text{OH})_2$ (Figs. 4-8a-e) is established on the MK-40 membrane. Only Ca^{2+} in the form of CaCO_3 is found on the MK-40_{MOD} membrane (Figs. 4-8g-h). CaCO_3 is detected also on the MA-41 membrane surface facing the desalination compartment (Figs. 4-8f, i). In all cases the amount of the scale on the MA-41 is less than that found on the cation-exchange membrane under study. This amount is negligible in the case where the MA-41 membrane is used together with the MK-40_{MOD} membrane (Fig. 4-8i).

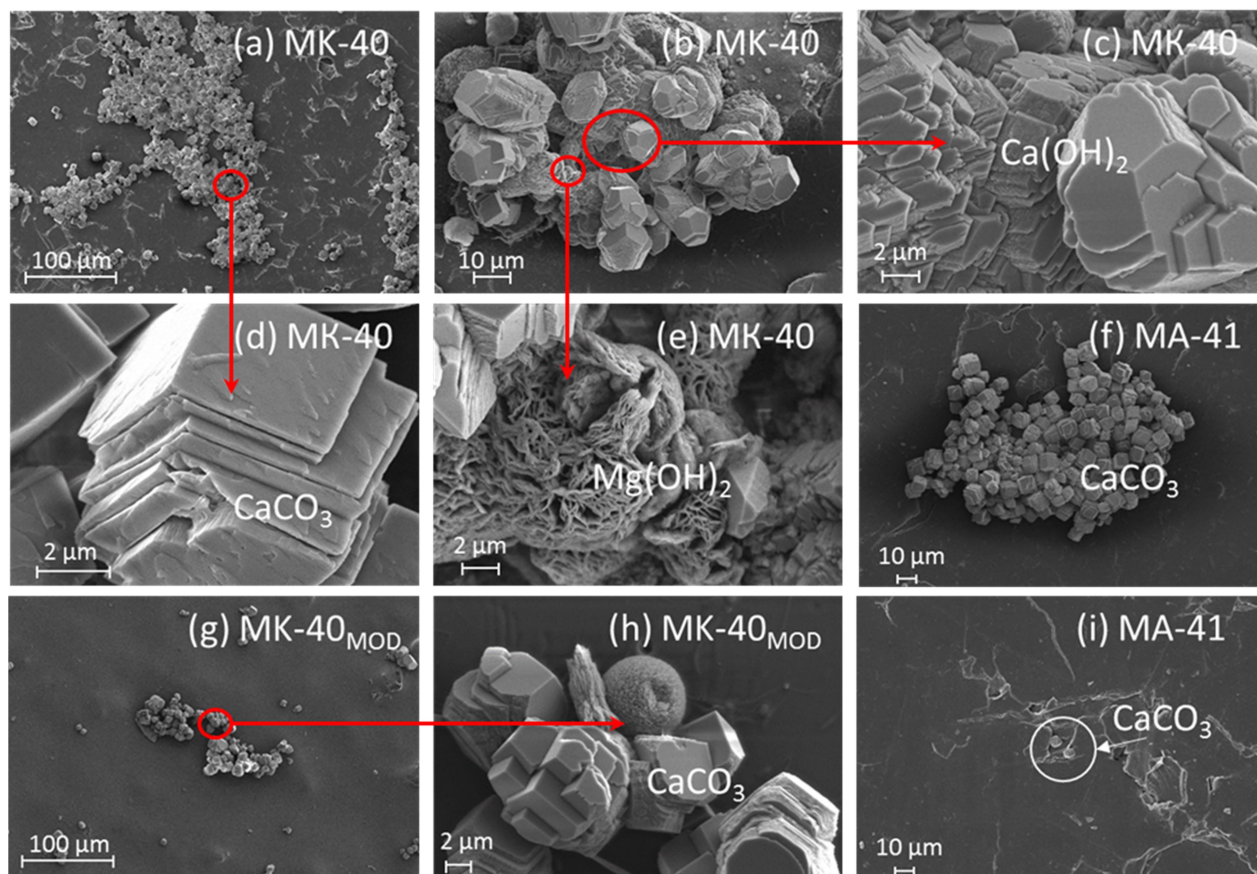


Fig. 4-8. SEM images of the surface of dry MK-40 (a- e), MK-40_{MOD} (g-h) and MA-41 (f, i) membrane after 5 h continuous electro dialysis of model solution at $i=10.5 \text{ mA cm}^{-2}$. (f) and (i) show the cases where the MA-41 membrane is used together with the MK-40 (f) or MK-40_{MOD} (i) membrane.

4.3.4 Water splitting and effect of pH

The scale formation depends on the local values of pH and concentration of the scale-forming ions, the Ca^{2+} and Mg^{2+} in our case. To estimate the local pH values, we have measured the *pH* of the diluate solution in the flow cell (cell 9 in Fig. 4-2) as a function of time; the results are shown in Fig. 4-9. *pH* value in the desalination compartment depends on the difference between the OH^- ion flux (generated at the CEM under study) and the H^+ ion flux (generated at the MA-41 anion-exchange membrane); both fluxes are directed from the corresponding membrane surface into the bulk solution. When the flux of OH^- ions is higher than that of H^+ , the diluate solution becomes basic. Otherwise, it becomes acidic. The reported *pH* values are bulk quantities dependent on the average effect of water splitting at the CEM and AEM. However, as in all the experiments the same auxiliary MA-41 membrane is used, the *pH* value of diluate solution allows one to compare the water splitting rate at the different membranes under study.

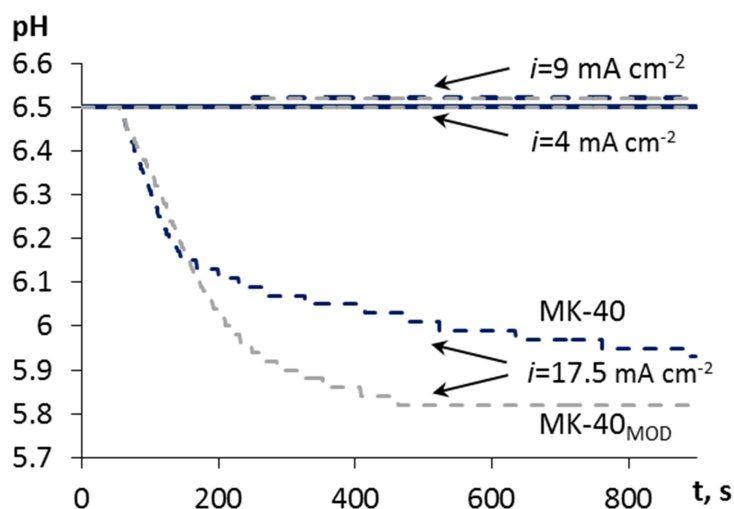
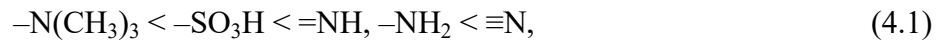


Fig. 4-9. Time dependence of the pH of diluate for the MK-40//MA-41 (dark blue line) and MK-40_{MOD}//MA-41 (grey line) membrane pairs at $i = 4 \text{ mA cm}^{-2}$, 9 mA cm^{-2} , 17.5 mA cm^{-2} .

Since at $i < i_{\text{lim}}$ the concentration of salt ions at the membrane surface is much higher than that of water ions, hence, the H^+ and OH^- ions cannot compete with the salt ions, there is no water splitting [28]. This statement is justified by the fact that there is no pH variation of the diluate solution at $i=4 \text{ mA cm}^{-2}$ (Fig. 4-9). Even at $i=9 \text{ mA cm}^{-2}$ no essential pH variation is observed. Insignificant alkalization of the diluate is observed at $7.9 \text{ mA cm}^{-2} \leq i \leq 15.5 \text{ mA cm}^{-2}$ ($i_{\text{lim}}^{\text{exp}} \leq i \leq 2 i_{\text{lim}}^{\text{exp}}$) in the case of MK-40 membrane and at $8.8 \text{ mA cm}^{-2} \leq i \leq 13.3 \text{ mA cm}^{-2}$ ($i_{\text{lim}}^{\text{exp}} \leq i \leq 1.5 i_{\text{lim}}^{\text{exp}}$) in the case of MK-40_{MOD} membrane. Accordingly, it can be stated that the water splitting rate for the above conditions is higher at the CEM than at the AEM. The explanation follows from the fact that the limiting current density of the MA-41 membrane in the model solution determined from the experimental I-V curve for this membrane is 9.3 mA cm^{-2} , which is about 1.2 times higher than that of the MK-40 membrane (Table 4-1). The higher value of i_{lim} for the AEM is due to the larger diffusion coefficient of dominant anion (Cl^-) than dominant cations (Ca^{2+} and Mg^{2+}). Note that in the case of NaCl, $i_{\text{lim}}^{\text{AEM}} / i_{\text{lim}}^{\text{CEM}} = 1.5$. When the current density is higher than $i_{\text{lim}}^{\text{CEM}}$, but lower or slightly higher than $i_{\text{lim}}^{\text{AEM}}$, the water splitting rate is higher at the CEM. However, when the current density is sufficiently high, water splitting at the AEM becomes determinant and the solution in the diluate compartment is acidified. This situation occurs at $i > 13.3 \text{ mA cm}^{-2}$ ($i > 1.4 i_{\text{lim}}^{\text{AEM}}$) in the case of MK-40_{MOD} membrane and at $i > 15.5 \text{ mA cm}^{-2}$ ($i > 1.7 i_{\text{lim}}^{\text{AEM}}$) in the case of MK-40.

According to the range of catalytic activity of ionogenic groups towards the water splitting reaction [65],



the MK-40 and MK-40_{MOD} membranes (containing the $-\text{SO}_3^-$ groups) are considered as the membranes with a weak catalytic activity. The MA-41 membrane has two types of fixed ion-exchange groups: the strongly basic quaternary ammonium ($-\text{N}^+(\text{CH}_3)_3$) and the weakly basic secondary ($=\text{NH}$) and tertiary amine ($\equiv\text{N}$) groups. The latter have strong catalytic activity towards water splitting, which explains higher catalytic effect of the MA-41 membrane (and the most other anion-exchange membranes [66]), as well as acidification of the solution in the desalination compartment at relatively elevated currents. Note also that Choi and Moon [67] showed that at high current densities, the quaternary ammonium groups initially present in an AMX anion-exchange membrane are partially converted into the secondary and tertiary amines. Zabolotskiy et al. [58, 68] found that in particular, this process occurs in the case of MA-41 membrane. These changes lead to an increase in water splitting rate at the depleted solution/MA-41 membrane interface.

Thus the stronger catalytic activity of ionogenic groups of the MA-41 membrane than those of the MK-40 and MK-40_{MOD} membranes explains the higher rate of water splitting at this membrane as well as the overall course of curves shown in Fig. 4-9: under a similar degree of CP (which can be estimated by the i/i_{lim} ratio), the water splitting rate is higher at the MA-41 membrane in comparison to the MK-40 and MK-40_{MOD} membranes.

The water splitting rate at the MK-40_{MOD} membrane is lower than that at the pristine one in view of the fact that the diluate acidifies more in the case of MK-40_{MOD} membrane (the case of $i=17.5 \text{ mA cm}^{-2}$ is shown in Fig. 4-9). This difference in the water splitting rate can be explained by the impact of two factors. First, the modified membrane provides a more uniform distribution of current lines near the membrane surface, which leads to reducing CP. Second, more intensive EC at the modified surface promotes better mixing of the solution and higher near-surface concentration of salt ions. At higher currents, higher water splitting rate at the MA-41 membrane prevents scaling in the desalination compartment.

Fig. 4-10 shows numerically simulated concentration profiles and the $(C_{\text{Mg}}(C_{\text{OH}})^2)$ concentration product in the diffusion boundary layer adjacent to a CEM in the case where a $\text{Mg}(\text{Cl})_2$ solution is fed in the desalination compartment. It can be seen that due to water splitting at the CEM, the OH^- ions are generated and their concentration passes through a maximum. As well, the $(C_{\text{Mg}}(C_{\text{OH}})^2)$ product reaches a maximum within the diffusion layer, as the concentration of Mg^{2+} decreases when approaching the membrane surface. The simulation shows that this behavior occurs even when the bulk solution (at $x=0$) is slightly acid. With increasing concentration of H^+ ions in the solution bulk, the concentration of OH^- ions in the

diffusion layer decreases, however, in a certain pH range the rate of water splitting at the CEM may be sufficient to obtain the $(C_{Mg}(C_{OH})^2)$ product value higher than the $Mg(OH)_2$ solubility product.

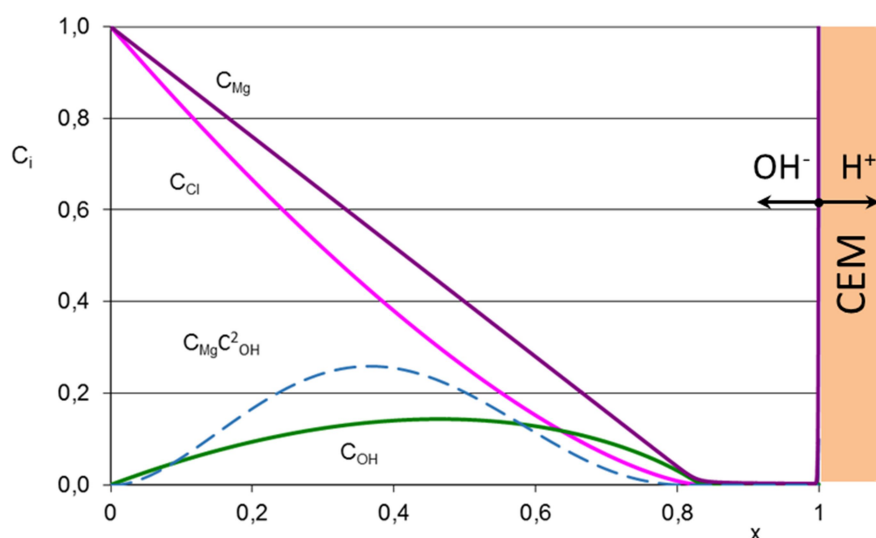


Fig. 4-10. Concentration profiles obtained using the mathematical model based on the Nernst-Planck-Poisson equations developed by Urtenov et al. [69] (EC does not taken into account); the solid lines show the equivalent fractions of ions (C_i), the dashed line shows the product $(C_{Mg}(C_{OH})^2 \times 50)$ near a cation-exchange membrane (CEM). Arrows show the direction of H^+ and OH^- ion fluxes generated at the depleted CEM surface. Adapted from [40].

4.3.5 Scale formation in PEF modes

ChPs measured in the model salt solution at $i = 10.5 \text{ mA cm}^{-2}$ in the constant current and PEF modes are presented in Figs. 4-10a-d. In PEF modes, during the pulse lapse the current density is also equal to 10.5 mA cm^{-2} . When counting the duration of an experimental run (75 min or 105 min), the ‘off’ time (when $i=0$) is not taken into account (Figs. 4-11b-d). Figs. 11a-d show also the value of pH of the diluate solution measured in the flow cell shown in Fig. 4-2 as a function of time. As Fig. 4-11a shows, the increase of $\Delta\phi'$ during one experiment run in the constant current mode is about 0.6 V for the MK-40 membrane, while it is only about 0.1 V in the case of MK-40_{MOD} membrane. Another effect is the growth of pH of the diluate solution, which circulates across the desalination compartment (compartment 2 in Fig. 4-2) and an intermediate tank (tank 7 in Fig. 4-2) in batch mode. As discussed above, this growth is explained by higher rate of water splitting at the CEM in the specified current range ($i_{lim}^{CEM} < i < k i_{lim}^{AEM}$, where in the constant current mode $k=1.4$ for MK-40_{MOD} and 1.7 for MK-40).

The scale blocks the ion pathways on the membrane surface, which enhances water splitting. There are two causes for this effect: 1) the local current density through the conductive area as well as CP strongly increase due to the reduction of conductive surface fraction; 2) the scale can contain compounds, which catalyze water splitting. The metal hydroxides, the $\text{Mg}(\text{OH})_2$ especially, are known as the catalyzers of water splitting [65, 70, 71]. Thus, it can be expected that water splitting rate increases during an experimental run, which in turn increases the rate of scaling.

More intensive EC and more uniform distribution of current density at the surface of MK-40_{MOD} membrane result in lower CP in comparison with the MK-40 membrane. As the result, water splitting and scaling are lower on the MK-40_{MOD} membrane surface. This conclusion is valid for all current regimes: under a constant current (Figs. 4-8a-g) and when applying PEF (Figs. 4-11a-c). The time-averaged value of PD for both MK-40 and MK-40_{MOD} membranes in the PEF mode is lower than that in the constant current mode in all studied cases, provided that the current density is the same. The least value of averaged PD is found for the minimum period studied (2 min), when $T_{\text{on}}=T_{\text{off}}=1$ min. With growing amount of the scale on the membrane surface, PD across the membrane increases. Thus, one can expect lower amount of the scale in the PEF conditions; it is the lowest in the case of the shortest period used in the study.

In the case of MK-40 membrane at $i = 10.5 \text{ mA cm}^{-2}$, pH of the diluate increases with time in the PEF mode; this increase is equal or lower than that found in the constant current mode (Figs. 4-11a,c,d). In the case of MK-40_{MOD} membrane, the behavior of pH in the constant current and PEF modes is quite different. While in the constant current mode, $i = 10.5 \text{ mA cm}^{-2}$, the pH of the diluate grows with time and its acidification occurs only at $i > 13.3 \text{ mA cm}^{-2}$, in the PEF mode at $i = 10.5 \text{ mA cm}^{-2}$ the value of pH remains nearly constant (regime $T_{\text{on}}/T_{\text{off}}=15/7.5$) or even decreases with time (regime $T_{\text{on}}/T_{\text{off}}=15/15$) (Fig. 4-11b). This shows that the rate of water splitting at the MK-40_{MOD} membrane is essentially lower in the PEF mode. Note that lower water splitting rate in the PEF mode was also detected by Malek et al. [72] and Mikhaylin et al. [20].

There is a delay in pH variation at the beginning of the experiment; this delay is well seen in Fig. 4-11d, where it is close to 10 min. There are several reasons for this. First, pH is measured in the flow cell, which is at a distance about 60 cm from the desalination compartment outlet; thus it takes about 9 s for the outlet solution to reach the flow cell. Second, after switching-on the current, a certain time (the transition time) should pass before the electrolyte concentration at the membrane surface attains a sufficiently low value where water splitting begins; the transition time may be determined by the inflection point of the

chronopotentiogram and/or evaluated using the Sand equation. This time at current density 10.5 mA cm^{-2} is equal approximately to 20 s. Finally, this delay may be due to the time needed for accumulation of the precipitate on the membrane surface. This process can take several minutes. Indeed, initially water splitting causing precipitation may be low. However, the presence of the scale on membrane surface stimulates water splitting as explained above. Hence, the rate water splitting increases with time following increasing amount of precipitate on the membrane surface. As Figs. 4-11a-d show, in the case of MK-40, the maximum delay occurs at short period PEF ($T_{\text{on}}/T_{\text{off}} = 1/1$ and $5/5$), Fig. 11d. According to the analysis above, it should be due to the fact that in these conditions the rate of scale formation is the lowest among the studied cases. Note that in the case of MK-40_{MOD}, in the $T_{\text{on}}/T_{\text{off}} = 15/7$ regime where the diluate is acidifies no $\text{Mg}(\text{OH})_2$ is detected.

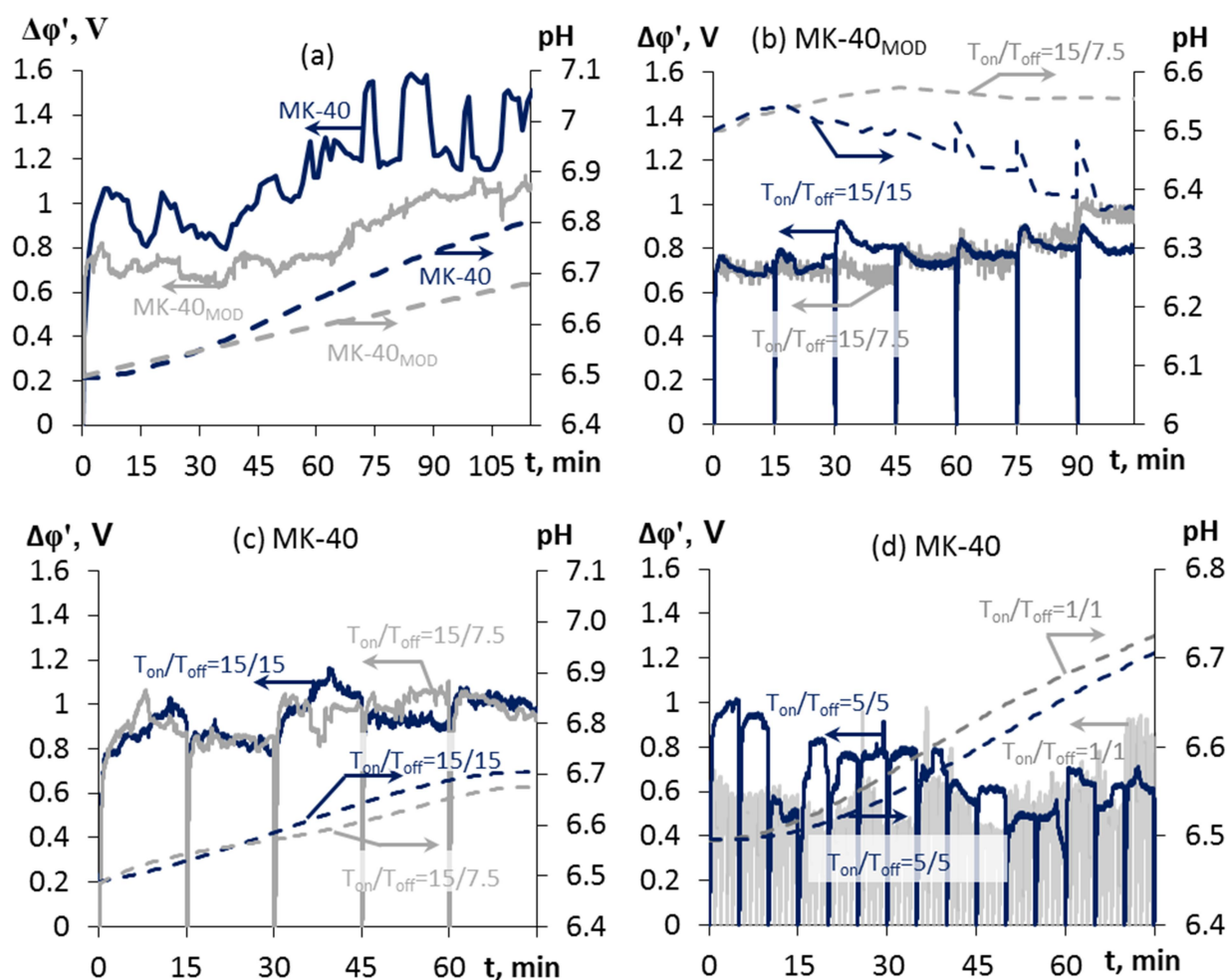


Fig. 4-11. Chronopotentiograms and corresponding pH measured for the MK-40 and MK-40_{MOD} membrane system in the constant current (a) and PEF (b-d) modes. In both modes, when the current flows its density $i = 10.5 \text{ mA cm}^{-2}$. Parameters of the PEF mode are indicated near the curves.

Apparently, the main reason for lower PD and lower water splitting rate in the PEF mode is the fact that during the pause lapse, a relaxation of the concentration profile occurs at the membrane surface. This relaxation can be complete or partial, depending on the ratio of the pause duration to the relaxation time; the latter may be approximated by the Sand transition time. Hence, the species concentrations return to their values in the bulk solution, and the product of ion concentrations becomes lower than the solubility product. The reason for the scale formation ceases, and in the case where the precipitation is reversible, the scale may dissolve.

One can remark larger scattering in PD in the case of short PEF period, when $T_{\text{on}}/T_{\text{off}} = 5/5$ and even more when $T_{\text{on}}/T_{\text{off}} = 1/1$ (Fig. 4-11d) in comparison to higher period (Fig. 4-11c). This should be due to a lower stability of the scale under short PEF periods. When a short current pulse is applied, a small amount of precipitate only a germ may be formed. During the pause the precipitate adherence to the surface weakens. After applying a new pulse, electroconvective flow could wash off the precipitate. Weak adherence of the precipitate may be also due to the fact that the maximum of concentration product of the scale-forming ions is located not on the membrane surface, but at a distance comparable with the diffusion boundary layer thickness. The simulation of concentration profiles in the case of $\text{Mg}(\text{OH})_2$ is shown in Fig. 4-10.

EC is an important factor in scale formation. Generation of additional liquid flow near the surface enhances solution mixing, which results in higher salt ion concentration at the depleted interface. This leads to 1) lower PD, and 2) lower water splitting – since the appearing water ions will have greater difficulty in competing with the salt ions in charge transfer [28]. As we have mentioned above, the MK-40_{MOD} membrane initiates stronger EC, which is due to relatively higher surface hydrophobicity and electrically more uniform surface layer providing “better” distribution of current lines (Fig. 4-4), in the sense of stimulating EC. Another factor, which contributes to lower scaling of the MK-40_{MOD} membrane in comparison to the MK-40 membrane, is the smooth surface of the former and the rough surface of the latter. The membranes with smooth surfaces are less susceptible to fouling than those with rough surface [73, 74]. Colloidal particles preferentially accumulate at the valleys of the rough membrane surface [75]. As a result, valleys become blocked and the formed precipitate acts as the center of crystallization. Our recent study [17] shows that the scaling of $\text{Mg}(\text{OH})_2$ crystals starts on the surface of ion-exchange resin particles embedded onto the heterogeneous MK-40 membrane surface. These data are consistent with the results of Asraf-Snir et al. [8, 27], which found the crystals of CaSO_4 on the surface of resin particles of a heterogeneous MA-40 membrane at initial stages of scaling, while no scale was detected on

the surface occupied by polyethylene. The amount of deposition on the membrane is much larger in this study, the resin particles are screened by the scale (Figs. 4-8a-h). Apparently, initially the scaling occurs on the resin particles. Further, the precipitate grows up and passes over the surface covered with polyethylene.

4.4 Conclusions

The scale formation on the surface of two cation-exchange membranes, a heterogeneous MK-40 and its modification MK-40_{MOD}, during ED of a solution containing the scale-forming cations, Ca²⁺, Mg²⁺ and CO₃²⁻ is investigated. The membrane modification is carried out by casting a homogeneous Nafion[®] film onto the MK-40 membrane surface. Deposition of CaCO₃ is detected on the surface of MK-40, MK-40_{MOD} and an auxiliary MA-41 membrane, the latter used to form the diluate compartment. Mg(OH)₂ and Ca(OH)₂ are found only on the surface of MK-40 membrane. The amount of scale is less in the case where the desalination compartment is formed by the pair of MK-40_{MOD} and MA-41 membranes. No precipitation is seen on the concentration side of all membranes where a NaCl solution was circulated. The scale is detected in the range $8.8 \text{ mA cm}^{-2} \leq i \leq 13.3 \text{ mA cm}^{-2}$ ($i_{\text{lim}}^{\text{exp}} \leq i \leq 1.5 i_{\text{lim}}^{\text{exp}}$) for MK-40_{MOD} membrane and $7.9 \text{ mA cm}^{-2} \leq i \leq 15.5 \text{ mA cm}^{-2}$ ($i_{\text{lim}}^{\text{exp}} \leq i \leq 2 i_{\text{lim}}^{\text{exp}}$) for MK-40. In the case, where a sufficiently high current density is applied, the water splitting rate at the MA-41 membrane is higher than that at the CEM. It provides an acidification of the solution throughout the desalination compartment and the reduction or the prevention of the scale formation.

The degree of the membrane surface screening by scale can be characterized by the value of the potential drop across the membrane, $\Delta\phi$, which increases with increasing amount of scale. The rate of scaling determines the rate of potential drop growth with time observed on the chronopotentiograms in quasi-steady state.

The mitigation of scaling on the MK-40_{MOD} membrane with modified surface is explained by three effects. The first one is the higher electroconvection at this membrane, which in addition to the increase in mass transfer helps to wash out the scale from the membrane surface. The second one is the reduction of water splitting, which allows adjusting pH in a slightly acid range due to the contribution of the anion-exchange membrane. The third effect is the reduction of the crystallization centers due to homogeneous surface of the MK-40_{MOD}. These centers are formed on a heterogeneous surface in the areas where the current lines are concentrated.

Another important factor allowing mitigation of scaling is the use of PEF mode. During the pause lapse, a relaxation of the concentration profile occurs at the membrane surface. The species concentrations return partially or completely to their values in the bulk solution, and the product of ion concentrations becomes lower than the solubility product, which causes (partial) dissolving the scale.

4.5 Acknowledgments

This investigation was realized in the frame of a joint French-Russian PHC Kolmogorov 2017 project of the French-Russian International Associated Laboratory "Ion-exchange membranes and related processes" with the financial support of Minobrnauki (Ref. N° RFMEFI58617X0053), Russia, using scientific equipment of the Core Facility "Environmental Analytical Center" of the Kuban State University (unique identifier RFMEFI59317X0008) and CNRS, France (project N° 38200SF). M. Andreeva thanks the French Embassy in Moscow, the Paris-Est University and the ICMPE CNRS for giving the possibility to carry out this work.

References

- [1] H. Strathmann, Electrodialysis, a mature technology with a multitude of new applications, *Desalination* 264 (2010) 268–288.
- [2] J. Ran, L. Wu, Y. He, Zh. Yang, Y. Wang, Ch. Jiang, L. Ge, E. Bakangura, T. Xu, Ion exchange membranes: new developments and applications, *J. Membr. Sci.* 522 (2017) 267–291.
- [3] W. Ben Ounis, C. P. Champagne, J. Makhlouf, L. Bazinet, Utilization of tofu whey pre-treated by electromembrane process as a growth medium for *Lactobacillus plantarum* LB17, *Desalination* 229 (2008) 192–203.
- [4] E. Thompson Brewster, C. M. Mehta, J. Radjenovic, D. J. Batstone, A mechanistic model for electrochemical nutrient recovery systems, *Water Res.* 94 (2016) 176–186.
- [5] Y. Oren, E. Korngold, N. Daltrophe, R. Messalem, Y. Volkman, L. Aronov, M. Weismann, N. Bouriakov, P. Glueckstern, J. Gilron, Pilot studies on high recovery BWRO-EDR for near zero liquid discharge approach, *Desalination* 261 (2010) 321–330.
- [6] S.-H. Joo, B. Tansel, Novel technologies for reverse osmosis concentrate treatment: A review, *J. Environmental Manag.* 150 (2015) 322–335.
- [7] A. T. K. Tran, Y. Zhang, N. Jullok, B. Meesschaert, L. Pinoy, B. Van der Bruggen, RO concentrate treatment by a hybrid system consisting of a pellet reactor and electrodialysis, *Chem. Engineering Sci.* 79. (2012) 228–238.
- [8] M. Asraf-Snir, J. Gilron, Y. Oren, Gypsum scaling of anion exchange membranes in electrodialysis, *J. Membr. Sci.* 520 (2016) 176–186.
- [9] N. Cifuentes-Araya, G. Pourcelly, L. Bazinet, Impact of pulsed electric field on electrodialysis process performance and membrane fouling during consecutive demineralization of a model salt solution containing a high magnesium/calcium ratio, *J. Colloid Interface Sci.* 361 (2011) 79–89.
- [10] S. Mikhaylin, V. Nikonenko, N. Pismenskaya, G. Pourcelly, S. Choi, H. J. Kwon, J. Han, L. Bazinet, How physico-chemical and surface properties of cation-exchange membrane affect membrane scaling and electroconvective vortices: Influence on performance of electrodialysis with pulsed electric field, *Desalination* 393 (2016) 102–114.
- [11] N. Cifuentes-Araya, C. Astudillo-Castro, L. Bazinet, Mechanisms of mineral membrane fouling growth modulated by pulsed modes of current during electrodialysis: Evidences of water splitting implications in the appearance of the amorphous phases of magnesium hydroxide and calcium carbonate, *J. Colloid Interface Sci.* 426 (2014) 221–234.

- [12] A. C. M. Franklin, Prevention and control of membrane fouling: practical implications and examining recent innovations, Membraan Applicatie Centrum Twente B.V., 2009.
- [13] Q. H. She, R. Wang, A. G. Fane, C. Y. Y. Tang, Membrane fouling in osmotically driven membrane processes: A review, *J. Membr. Sci.* 499 (2016) 201–233.
- [14] R. Bond, B. Batchelor, T. Davis, B. Klayman, Zero liquid discharge desalination of brackishwater with an innovative form of electrodialysis metathesis, *Fla Water Resour. J.* (2011) 38–44.
- [15] T. Rottiers, B. Van der Bruggen, L. Pinoy, Synthesis and transport of impurities in electrodialysis metathesis: Production of choline dihydrogen phosphate, *J. Membr. Sci.*, 2017. <https://doi.org/10.1016/j.memsci.2017.07.042>.
- [16] A. T. K. Tran, Y. Zhang, J. Lin, P. Mondal, W. Ye, B. Meesschaert, L. Pinoy, B. Van der Bruggen, Phosphate pre-concentration from municipal wastewater by selectrodialysis: Effect of competing components, *Sep. Purif. Technol.* 141 (2015) 38–47.
- [17] M. A. Andreeva, V. V. Gil, N. D. Pismenskaya, V. V. Nikonenko, L. Dammak, C. Larchet, D. Grande, N. A. Kononenko, Effect of homogenization and hydrophobization of a cation-exchange membrane surface on its scaling in the presence of calcium and magnesium chlorides during electrodialysis, *J. Membr. Sci.* 540 (2017) 183–191.
- [18] T. Chen, A. Neville, M. Yuan, Influence of Mg^{2+} on $CaCO_3$ formation-bulk precipitation and surface deposition, *Chem. Eng. Sci.* 61 (2006) 5318–5327.
- [19] N. Cifuentes-Araya, G. Pourcelly, L. Bazinet, Multistep mineral fouling growth on a cation-exchange membrane ruled by gradual sieving effects of magnesium and carbonate ions and its delay by pulsed modes of electrodialysis, *Journal of Colloid and Interface Science* 372 (2012) 217–230.
- [20] S. Mikhaylin, V. Nikonenko, G. Pourcelly, L. Bazinet, Intensification of demineralization process and decrease in scaling by application of pulsed electric field with short pulse/pause conditions, *J. Membr. Sci.* 468 (2014) 389–399.
- [21] N. Cifuentes-Araya, G. Pourcelly, L. Bazinet, Water splitting proton-barriers for mineral membrane fouling control and their optimization by accurate pulsed modes of electrodialysis, *J. Membr. Sci.* 447 (2013) 433–441.
- [22] E. M. V. Hoek, S. Bhattacharjee, M. Elimelech, Effect of membrane surface roughness on colloid-membrane DLVO interactions, *Langmuir* 19. (2003) 4836–4847.
- [23] Y. Mizutani, R. Yamane, H. Ihara, H. Motura, Studies of ion exchange membranes. XVI. The preparation of ion exchange membranes by the "Paste Method", *Bull. Chem. Soc. Jpn.*, 36 (1963) 361–366.

- [24] Y. Mizutani, K. Hirayama, S. Nago, Preparation of microporous membranes by paste method, *J. Membr. Sci.* 135 (1997) 129-133.
- [25] I. Atamanenko, A. Kryvoruchko, L. Yurlova, Study of the scaling process on membranes, *Desalination* 167 (2004) 327–334.
- [26] M. Turek, P. Dydo, J. Was, High efficiency electro dialysis reversal of concentrated calcium sulfate and calcium carbonate solutions , *Desalination* 205 (2007) 62–66.
- [27] M. Asraf-Snir, J. Gilron, Y. Oren, Gypsum scaling on anion exchange membranes during Donnan exchange, *J. Membr. Sci.* 455 (2014) 384–391.
- [28] E. Volodina, N. Pismenskaya, V. Nikonenko, C. Larchet, G. Pourcelly, Ion transfer across ion-exchange membranes with homogeneous and heterogeneous surfaces, *J. Colloid Interface Sci.* 85. (2005) 247–258.
- [29] I. Rubinstein, B. Zaltzman, T. Pundik, Ion-exchange funneling in thin-film coating modification of heterogeneous electro dialysis membranes, *Phys. Review E.* 65 (2002) 041507.
- [30] G. Baltrunas, R. Valiunas, G. Popkirov, Identification of electrode surface blocking by means of thin-layer cell: 1. The model // *Electrochim. Acta* 52 (2007) 7091–7096.
- [31] M. V. Sharafan, V. I. Zabolotskii, V. V. Bugakov, Electric mass transport through homogeneous and surface-modified heterogeneous ion-exchange membranes at a rotating membrane disk, *Russ. J. Electrochem Russian Journal of Electrochemistry* 45 (2009) 1162–1169.
- [32] E. Belova, G. Lopatkova, N. Pismenskaya, V. Nikonenko, C. Larchet, Role of water splitting in development of electroconvection in ion-exchange membrane systems, *Desalination* 199 (2006) 59–61.
- [33] N. D. Pismenskaya, V. V. Nikonenko, N. A. Melnik, K. A. Shevtsova, E. I. Belova, G. Pourcelly, D. Cot, L. Dammak, C. Larchet, Evolution with time of hydrophobicity and microrelief of a cation-exchange membrane surface and its impact on overlimiting mass transfer, *J. Phys. Chem. B* 116. (2012) 2145–2161.
- [34] A. M. Uzdenova, A. V. Kovalenko, M. K. Urtenov, V. V. Nikonenko, Effect of electroconvection during pulsed electric field electro dialysis. Numerical experiments, *Electrochem. Commun.* 51 (2015) 1–5.
- [35] M. C. Martí-Calatayud, D. C. Buzzi, M. García-Gabaldón, A. M. Bernardes, J. A. S. Tenório, V. Pérez-Herranz, Ion transport through homogeneous and heterogeneous ion-exchange membranes in single salt and multicomponent electrolyte solutions, *J. Membr. Sci.* 466 (2014) 45–57.

- [36] N. Pismenskaya, N. Melnik, E. Nevakshenova, K. Nebavskaya, V. Nikonenko, Enhancing ion transfer in overlimiting electro dialysis of dilute solutions by modifying the surface of heterogeneous ion-exchange membranes, *Int. J. Chem. Eng.* 2012 (2012) 528290.
- [37] N. D. Pis'menskaja, V. V. Nikonenko, N. A. Melnik, S. V. Timofeev, Method of making heterogeneous cation-exchange membrane, Patent RU(11) 2 489 200(13) C1.
- [38] N. D. Pis'menskaya, V. V. Nikonenko, N. A. Mel'nik, G. Pourcelli, G. Larchet, Effect of the ion-exchange membrane/solution interfacial characteristics on the mass transfer at severe current regimes, *Russ. J. Electrochem.* 48 (2010) 610-628.
- [39] E. D. Belashova, N. A. Melnik, N. D. Pismenskaya, K. A. Shevtsova, A. V. Nebavsky, K. A. Lebedev, V. V. Nikonenko, Overlimiting mass transfer through cation-exchange membranes modified by Nafion film and carbon nanotubes, *Electrochim. Acta.* 59 (2012) 412–423.
- [40] V. V. Gil, M. A. Andreeva, N. D. Pismenskaya, V. V. Nikonenko, C. Larchet, L. Dammak, Effect of counterion hydration numbers on the development of electroconvection at the surface of heterogeneous cation-exchange membrane modified with an MF-4SK film, *Petrol. Chem.* 56 (2016) 440–449.
- [41] V. I. Zabolotsky, V. V. Nikonenko, N. D. Pismenskaya, On the role of gravitational convection in the transfer enhancement of salt ions in the course of dilute solution electro dialysis, *J. Membr. Sci.* 119 (1996) 171–181.
- [42] I. Rubinstein, B. Zaltzman, Electro-osmotically induced convection at a permselective membrane, *Phys. Rev. E Stat. Phys. Plasmas Fluids Relat. Interdiscip. Topics* 62 (2000) 2238–2251.
- [43] J.-H. Choi, H.-J. Lee, S.-H. Moon, Effects of electrolytes on the transport phenomena in a cation-exchange membrane, *J. Colloid Interface Sci.* 238 (2001) 188–195.
- [44] J. Balster, M. H. Yildirim, D. F. Stamatialis, R. Ibanez, R. G. H. Lammertink, V. Jordan, M. Wessling, Morphology and microtopology of cation-exchange polymers and the origin of the overlimiting current, *J. Phys. Chem. B* 111 (2007) 2152–2165.
- [45] M. K. Urtenov, A. M. Uzdenova, A. V. Kovalenko, V. V. Nikonenko, N. D. Pismenskaya, V. I. Vasil'eva, P. Sistas, G. Pourcelly, Basic mathematical model of overlimiting transfer enhanced by electroconvection in flow-through electro dialysis membrane cells, *J. Membr. Sci.* 447 (2013) 190–202.
- [46] G. S. Ganchenko, E. N. Kalaydin, J. Schiffbauer, E. A. Demekhin, Modes of electrokinetic instability for imperfect electric membranes, *Phys. Rev. E* 94 (2016) 063106.

- [47] V. I. Zabolotsky, V. V. Nikonenko, N. D. Pismenskaya, E. V. Laktionov, M. Kh. Urtenov, H. Strathmann, M. Wessling, G. H. Koops, Coupled transport phenomena in overlimiting current electrodialysis, *Sep. Purif. Technol.* 14 (1998) 255–267.
- [48] M. Davidson, M. Wessling, A. Mani, On the dynamical regimes of pattern-accelerated electroconvection, *Sci. Rep.* 6 (2016) doi:10.1038/srep22505.
- [49] V. I. Zabolotsky, L. Novak, A. V. Kovalenko, V. V. Nikonenko, M. H. Urtenov, K. A. Lebedev, A. Y. But, Electroconvection in systems with heterogeneous ion-exchange membranes, *Petrol. Chem.* 57 (2017) 779–789.
- [50] M. Wessling, L. Garrigos Morcillo, S. Abdu, Nanometer-thick lateral polyelectrolyte micropatterns induce macroscopic electro-osmotic chaotic fluid instabilities, *Sci. Rep.* 4 (2014) doi:10.1038/srep042944294.
- [51] E. Korzhova, N. Pismenskaya, D. Lopatin, O. Baranov, L. Dammak, V. Nikonenko, Effect of surface hydrophobization on chronopotentiometric behavior of an AMX anion-exchange membrane at overlimiting currents, *J. Membr. Sci.* 500 (2016) 161–170.
- [52] V. S. Shelistov, E. A. Demekhin, G. S. Ganchenko, Electrokinetic instability near charge-selective hydrophobic surfaces, *Phys. Rev. E* 90 (2014) 013001.
- [53] K. A. Nebavskaya, V. V. Sarapulova, K. G. Sabbatovskiy, V. D. Sobolev, N. D. Pismenskaya, P. Sizat, M. Cretin, V. V. Nikonenko, Impact of ion exchange membrane surface charge and hydrophobicity on electroconvection at underlimiting and overlimiting currents, *J. Membr. Sci.* 523 (2017) 36–44.
- [54] J. J. Krol, M. Wessling, H. Strathmann, Chronopotentiometry and overlimiting ion transport through monopolar ion exchange membranes, *J. Membr. Sci.* 162 (1999) 155–164.
- [55] N. Pismenskaia, P. Sizat, P. Huguet, V. Nikonenko, G. Pourcelly, Chronopotentiometry applied to the study of ion transfer through anion exchange membranes, *J. Membr. Sci.* 228 (2004) 65–76.
- [59] I. Rubinstein, B. Zaltzman, Equilibrium electroconvective instability, *Phys. Rev. Lett.* 114 (2015) 114502.
- [57] A. V. Zhiltsova, V. I. Vasil'eva, M. D. Malykhyn, N. D. Pismenskaya, N. A. Melnik, Influence of a sulfocation-exchange membrane surface hydrophobicity on the development of electroconvective instability, *Sci. J. Proc. Voronezh. Univ.* 2 (2013) 35–38.
- [58] V. I. Vasil'eva, A. V. Zhil'tsova, M. D. Malykhin, V. I. Zabolotskii, K. A. Lebedev, R. Kh. Chermit, M. V. Sharafan, Effect of the chemical nature of the ionogenic groups of ion-exchange membranes on the size of the electroconvective instability region in high current modes, *Russ. J. Electrochem.* 50 (2014) 120–128.

- [59] V. A. Shaposhnik, V. I. Vasil'eva, O. V. Grigor'chuk, The interferometric investigations of electromembrane processes, *Adv. Colloid Interface Sci.* 139 (2008) 74-82.
- [60] V. V. Nikonenko, V. I. Vasil'eva, E. M. Akberova, A. M. Uzdenova, M. K. Urtenov, A. V. Kovalenko, N. P. Pismenskaya, S. A. Mareev, G. Pourcelly, Competition between diffusion and electroconvection at an ion-selective surface in intensive current regimes, *Adv. Colloid Interface Sci.* 235 (2016) 233-246.
- [61] S. M. Rubinstein, G. Manukyan, A. Staicu, I. Rubinstein, B. Zaltzman, R. G. H. Lammertink, F. Mugele, M. Wessling, Direct observation of a nonequilibrium electro-osmotic instability, *Phys. Rev. Lett.* 101 (2008) 236101.
- [62] G. Yossifon, H.-C. Chang, Selection of nonequilibrium overlimiting currents: Universal depletion layer formation dynamics and vortex instability, *Phys. Rev. Lett.* 101 (2008) 254501.
- [63] R. Kwak, G. Guan, W. K. Peng, J. Han, Microscale electro dialysis: Concentration profiling and vortex visualization, *Desalination* 308 (2012) 138-146.
- [64] J. C. de Valena, R. M. Wagterveld, R. G. H. Lammertink, P. A. Tsai, Dynamics of microvortices induced by ion concentration polarization, *Phys. Rev. E* 92 (2015) 031003(R).
- [65] V. I. Zabolotskii, N. V. Shel'deshov, N. P. Gnusin, Dissociation of water molecules in systems with ion-exchange membranes, *Russ. Chem. Rev.* 57 (1988) 801–808.
- [66] R. Simons, Strong electric field effects on proton transfer between membrane-bound amines and water, *Nature*, 280 (1979) 824–826.
- [67] J.-H. Choi, S.-H. Moon, Structural change of ion-exchange membrane surfaces under high electric fields and its effects on membrane properties, *J. Colloid Interface Sci.* 265 (2003) 93–100.
- [68] V. I. Zabolotskiy, A. Yu. But, V. I. Vasil'eva, E. M. Akberova, S. S. Melnikov, Ion transport and electrochemical stability of strongly basic anion-exchange membranes under high current electro dialysis conditions, *J. Membr. Sci.* 526 (2017) 60–72.
- [69] M. A. K. Urtenov, E. V. Kirillova, N. M. Seidova, V. V. Nikonenko, Decoupling of the Nernst–Planck and Poisson equations. Application to a membrane system at overlimiting currents, *J. Phys. Chem. B* 111 (2007) 14208–14222.
- [70] R. Simons, Electric field effects on proton transfer between ionizable groups and water in ion exchange membranes, *Electrochim. Acta* 29 (1984) 151–158.
- [71] Y. Tanaka, *Ion exchange membranes fundamentals and applications*, second edition, Elsevier Science, 2015.

- [72] P. Malek, J. M. Ortiz, B. S. Richards, A. I. Schäfer, Electrolytic removal of NaCl from water: Impacts of using pulsed electric potential on ion transport and water dissociation phenomena, *J. Memb. Sci.* 435 (2013) 99–109.
- [73] L. Suresh, J. Y. Walz, Effect of surface roughness on the interaction energy between a colloidal sphere and a flat plate, *J. Colloid Interface Sci.* 183 (1996) 199–213.
- [74] M. Elimelech, X. Zhu, A. E. Childress, S. Hong, Role of membrane surface morphology in colloidal fouling of cellulose acetate and composite aromatic polyamide reverse osmosis membranes, *J. Membr. Sci.* 127 (1997) 101–109.
- [75] D. Rana, T. Matsuura, Surface modifications for antifouling membranes, *Chem. Rev.* 110 (2010) 2448–2471.

Chapter 5

Effect of surface modification of cation-exchange membrane with polyaniline on polarization characteristics and scale formation

In the literature review, electro dialysis metathesis was considered as an effective approach to fight scaling. The design of electro dialysis stack is organized in a way that there are two concentrate chambers: in one of them, singly charged cations (such as Na^+) and multicharged anions (SO_4^{2-}); in the other one, multicharged cations (such as Ca^{2+}) and singly charged anions (Cl^-). In order to improve this process, monovalent-ion-selective membranes are used. A modification of membrane surface by a layer selective to the transfer of singly charged ions is a largely used option. It has been shown in literature that polymerization of polyaniline (PANI) on the cation-exchange membrane surface results in the decrease of water transport number and appearance of permselectivity towards the transfer of singly charged ions. Thus, the membranes modified with PANI present a high interest for metathesis electro dialysis. Potentially, these membranes may be used as monovalent-cation-selective ones. However, their behavior was not studied from the point of view of possible scaling.

The aim of the study described in this chapter is the preparation of a cation-exchange membrane modified with a thin surface layer of PANI and the investigation of kinetics of scale formation on this membrane in the same solution as used in the previous chapter (a model of trice-concentrated milk). The chapter involves two sections. The first one is devoted to the development of the principles of preparation of a PANI modified membrane in an applied electric field on the basis of a perfluorinated cation-exchange MF-4SK membrane. In the second section, we use the obtained knowledge for preparing a composite PANI membrane using as the substrate a cost effective heterogeneous cation-exchange MK-40 membrane. Then the kinetics of scaling process on the obtained membrane is investigated.

Presentation of the article 1

There are various methods for preparation of composite materials based on PANI and ion-exchange membrane. They can be divided into two groups: template synthesis of PANI directly in the matrix of membrane and introduction of the pre-prepared commercial PANI into the membrane at the stage of its formation, for example when casting the film from the suspension. For example, the powder of PANI particles is blended with liquid PVDF when preparing heterogeneous anion exchange membranes by casting the obtained solution on glasses followed by either wet phase inversion or dry phase inversion. In the case of template synthesis, the matrix of ion-exchange membrane serves as a template, which determines the structure of the resulting PANI phase and its spatial arrangement.

The aim of this work is to examine the possibility of obtaining modified composites based on the perfluorinated sulfocation-exchange MF-4SK membrane and PANI under the conditions of an external electric field and to study their electrochemical behavior.

The MF-4SK membrane is modified by synthesizing PANI within the membrane in the near-surface layer in a four-chamber cell under the external electric field. A 0.01 M aniline solution in 0.05 M HCl is fed into the cell chamber on the anode side. Aniline reacts with strong acids to form anilinium (or phenylammonium) ion ($C_6H_5-NH_3^+$). A 0.002 M potassium dichromate solution or a 0.005 M $(NH_4)_2S_2O_8$ solution in 0.05 M HCl is introduced on the cathode side. A 0.05 M HCl solution is fed in the electrode chambers. The phenylammonium cations, formed as the result of aniline protonation, are transferred, in accordance with the direction of electric current through the cation-exchange membrane. The dichromate or persulfate anions, in turn, migrate to the membrane surface, where the oxidative polymerization of aniline occurs. Thus, a PANI layer forms in the near-surface layer within the membrane surface on the cathode side. Since PANI has anion-exchange properties, and the non-modified part of MF-4SK cation-exchange ones, a two-layer structure with a bipolar boundary is formed. The thickness of the anion-exchange layer is much less than that of the cation-exchange one. This conditions some particular properties of the MF-4SK/PANI membrane. One of them is the asymmetry of I-V curves similar to that of bipolar membranes. Another peculiarity is the presence of two limiting current densities. The first limiting current, called pseudo-limiting current, $i_{pseudo-lim}^{exp}$, is due to the formation of depleted (in relation to mobile ions) layer at the bipolar junction / boundary within the membrane. The second one, i_{lim}^{exp} , which is higher than $i_{pseudo-lim}^{exp}$ and close to the limiting current of the non-modified membrane is due to saturation of the diffusion across the depleted diffusion layer in solution.

**Effect of surface modification of perfluorinated
membranes with polyaniline on their polarization
behavior**

Russian Journal of Electrochemistry (51) 2015 538-545

N. V. Loza, S. V. Dolgoplov, N. A. Kononenko, M. A. Andreeva and Yu. S. Korshikova

Kuban State University, ul. Stavropol'skaya 149, Krasnodar, Russia

Abstract

The possibility of obtaining composite membranes based on MF-4SK and polyaniline with an anisotropic structure and asymmetric current-voltage curves in an external electric field was considered. The polarization behavior of the obtained composite membranes was studied. As the current density increased during the synthesis of polyaniline, the conductivity of the membranes decreased; the hysteresis on the cyclic current-voltage curve, as well as the asymmetry of the parameters of the current-voltage curves, increased; and pseudo-limiting current appeared due to the formation of a bipolar internal boundary.

5.1 Introduction

Composite materials based on polyaniline (PANI) and perfluorinated membranes are very promising for use in various electrochemical and sensor devices [1]. Various methods for the preparation of these materials were developed. They can be divided into two large groups: template synthesis of polyaniline directly in the matrix of the membrane and introduction of commercial polyaniline [2-5]. Both groups of methods have their own advantages and disadvantages. When commercial polymer is introduced in the membrane at the stage of its formation, for example, during film casting from a suspension containing polyaniline and an F-4SK solution, it is difficult to have polyaniline uniformly distributed in the membrane. Moreover, forming a continuous path of charge transfer along the chain of conjugated carbon-carbon bonds requires contact between the polyaniline particles. This can only be achieved by increasing the polyaniline content in the membrane phase, which adversely affects the strength characteristics of the composite material [6]. One of the advantages of this method is the optimum conductive properties of the modifier. Synthesis of polyaniline directly in the phase and/or on the membrane surface seems more promising. The oxidative polymerization of aniline directly in the transport channels of the membrane matrix creates conditions for a continuous path for electric- and mass transfer along the polyaniline chain across the membrane. However, an obvious disadvantage of this group of methods is the impossibility of creating the conditions of synthesis that would provide the maximum electron conductivity of polyaniline [7, 8].

There are many variants of the template synthesis of polyaniline. An essential condition of this synthesis is monomer and oxidant concentration in the phase or near the membrane surface at which polymerization starts. This can be achieved in various ways: by keeping the membrane in solutions containing the monomer and oxidant in sequence [9]; sequential diffusion of the polymerizing solutions across the membrane into water; and counter-diffusion of the monomer and oxidant across the membrane [10]. To prepare composites with uniform distribution of PANI in the MF-4SK polymer base matrix, iron (III) chloride or ultraviolet radiation is used [11]. Materials in which polyaniline is distributed mainly on the surface of the composite are obtained by treatment with oxidants such as persulfate, permanganate, or dichromate anions, etc., which are co-ions relative to the MF-4SK membrane. Due to their anisotropic structure and asymmetric transport properties, these composites are most promising for use in various devices and electrochemical processes. The preparation of these materials in a concentration field using high reagent and supporting acid concentrations was described in [5]. It can be assumed that the use of an electric field will accelerate the

preparation of the material and reduce the concentrations of the polymerizing solutions, as was the case with the preparation of bulk-modified composites in the presence of FeCl_3 [12].

The aim of this work was to examine the possibility of obtaining surface-modified composites based on the MF-4SK membrane and polyaniline under the conditions of an external electric field and to study their electrochemical behavior.

5.2 Experimental

5.2.1 Preparation of anisotropic MF-4SK/Polyaniline composites under the conditions of an external electric field

The perfluorinated sulfocationite membrane MF-4SK (Plastpolymer) was the base membrane for the preparation of composites. The membrane was modified by synthesizing polyaniline on the membrane surface in a four-chamber cell while applying direct current. A 0.01 M aniline solution in 0.05 M HCl was fed into the cell chamber on the anode side and a 0.002 M potassium dichromate solution or a 0.005 M $(\text{NH}_4)_2\text{S}_2\text{O}_8$ solution in 0.05 M HCl was introduced on the cathode side. A 0.05 M HCl solution was fed in the near-electrode chambers. The synthesis was carried out at different polarization current densities (i , A m^{-2}) for 60 min (Table 5-1). The phenylammonium cations were transferred, in accordance with the direction of electric current, across the MF-4SK cation-exchange membrane into the concentration chamber (Fig. 5-1). The dichromate or persulfate anions, in turn, migrated to the membrane surface, where the oxidative polymerization of aniline occurred. Thus, a polyaniline layer formed on the membrane surface on the cathode side.

Sample	Current density during PANI synthesis, A m^{-2}	Composition of polymerizing solutions in near-membrane chambers on the side of	
		cathode	anode
MF-4SK/PANI-1	246		
MF-4SK/PANI-100-1	100	0.002 M $\text{K}_2\text{Cr}_2\text{O}_7$ + 0.05 M HCl	0.01 M $\text{C}_6\text{H}_5\text{NH}_2$ + 0.05 M HCl
MF-4SK/PANI-200-1	200		
MF-4SK/PANI-300-1	300		
MF-4SK/PANI-100-2	100	0.005 M $(\text{NH}_4)_2\text{S}_2\text{O}_8$ + 0.05 M HCl	
MF-4SK/PANI-200-2	200		
MF-4SK/PANI-300-2	300		

Table 5-1. Conditions for the preparation of MF-4SK/PANI composites.

The green color typical for polyaniline in the form of emeraldine appeared after 20 min of synthesis when potassium dichromate was used and after 30 min in the case of ammonium persulfate.

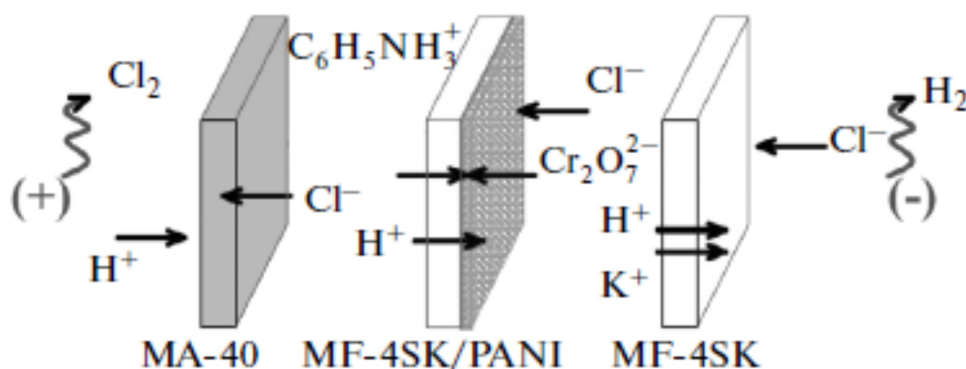


Fig. 5-1. Diagram of the formation of a polyaniline layer on the surface of the MF-4SK membrane under the conditions of an external electric field.

All the composite membrane samples had different color intensities. Fig. 5-2 shows the electronic absorption spectra of the samples, which exhibit absorption maxima typical for the emeraldine form of polyaniline: a maximum around 300 nm corresponding to the $\pi-\pi^*$ electron transitions in the benzene rings of polyaniline and a broad band at 800 nm corresponding to the localized polarons or radical cations [13]. Visual comparison of the composites obtained in the presence of ammonium persulfate and potassium dichromate at the same current density showed that the intensity of coloring was higher for the latter in all cases. This is indirect evidence for the larger amount of polyaniline in the membrane when potassium dichromate is used as an oxidant that initiates polymerization of aniline, though its redox potential is smaller than that of ammonium persulfate. This assumption is confirmed by the fact that the optical density at the absorption maxima for the MF-4SK/PANI-100-1 composite is higher than for MF-4SK/PANI-100-2. This unexpected result can be explained by the fact that during the preparation of composites, synthesis of polyaniline occurs concurrently with its oxidative destruction [14]. In general, the yield of PANI depends on the rate ratio of these two processes. We can assume that under the action of a stronger oxidizer (ammonium persulfate), the destruction is much faster and the amount of PANI in the membrane ultimately decreases. A comparative study of composites based on carbon nanotubes and polyaniline obtained in the presence of sodium persulfate and potassium dichromate was performed in [15]; it was noted that the yield of PANI was higher in the latter case. The authors explained this by the decomposition of sodium persulfate in water to

thiosulfate, liberating molecular oxygen. However, it was also noted that the PANI layer obtained in the presence of sodium persulfate was more uniform and conductive compared with that synthesized in the presence of potassium dichromate.

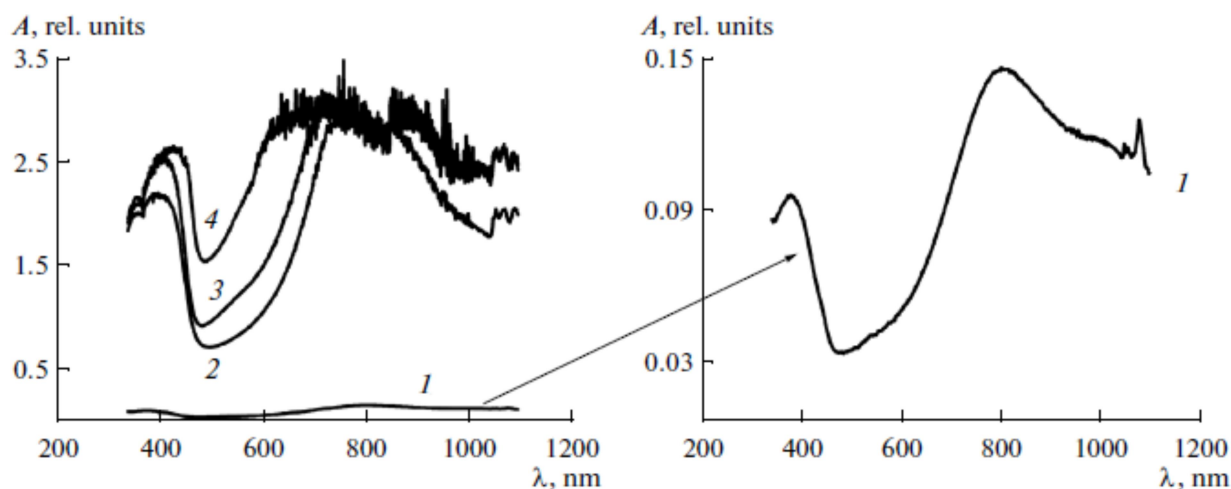


Fig. 5-2. Electronic absorption spectra of MF-4SK-PANI composites obtained under the conditions of an external electric field using (1)–(3) ammonium persulfate and (4) potassium dichromate as an oxidant of aniline: (1) MF-4SK/PANI-100-2, (2) MF-4SK/PANI-200-2, (3) MF-4SK/PANI-300-2, and (4) MF-4SK/PANI-100-1.

In each series of MF-4SK/PANI composites, we visualized an increase in the color intensity at increasing current density in the course of their preparation. According to Fig. 5-2, the optical density at the absorption maxima on the electronic absorption spectra increases with the current density during the preparation of anisotropic cation-exchange composite membranes. According to the Bouguer–Lambert–Beer law, the optical density at the absorption maximum is proportional to the content of the corresponding component in the sample.

Thus, it was shown that a polyaniline layer can be obtained on the surface of the MF-4SK membrane under the conditions of an external electric field. The amount of polyaniline in the membrane increases with current density during the preparation of the composites irrespective of the nature of the oxidant. The use of the potassium dichromate oxidant allows synthesis of samples with deeper coloring and hence with a larger amount of polyaniline in the emeraldine form.

5.2.2 Polarization behavior of anisotropic MF-4SK/PANI composites

The current-voltage curves (CVCs) were measured in the same cell in which the composites were prepared. The cell (Fig. 5-3) consisted of two near-electrode chambers with platinum polarizing electrodes with an area of 7.1 cm^2 and two near-membrane chambers. To prevent the transfer of the electrolysis products from near-electrode to near-membrane chamber, we used auxiliary anion- and cation-exchange membranes to separate the membrane under study from the anode and cathode chambers, respectively. The given rate of electrolyte circulation in the chambers (14 mL min^{-1}) was maintained using a peristaltic pump. Direct current was applied at a specified scan rate to the polarizing electrodes using an Autolab Pgstat302n potentiostat/galvanostat. The change in the potential difference on the membrane was recorded using Luggin–Haber capillaries connected with the membrane and the silver/silver chloride electrodes. The silver chloride electrodes were connected to the potentiostat/galvanostat, from which the signal was fed to a computer, which allowed real-time recording of the experimental ΔE value.

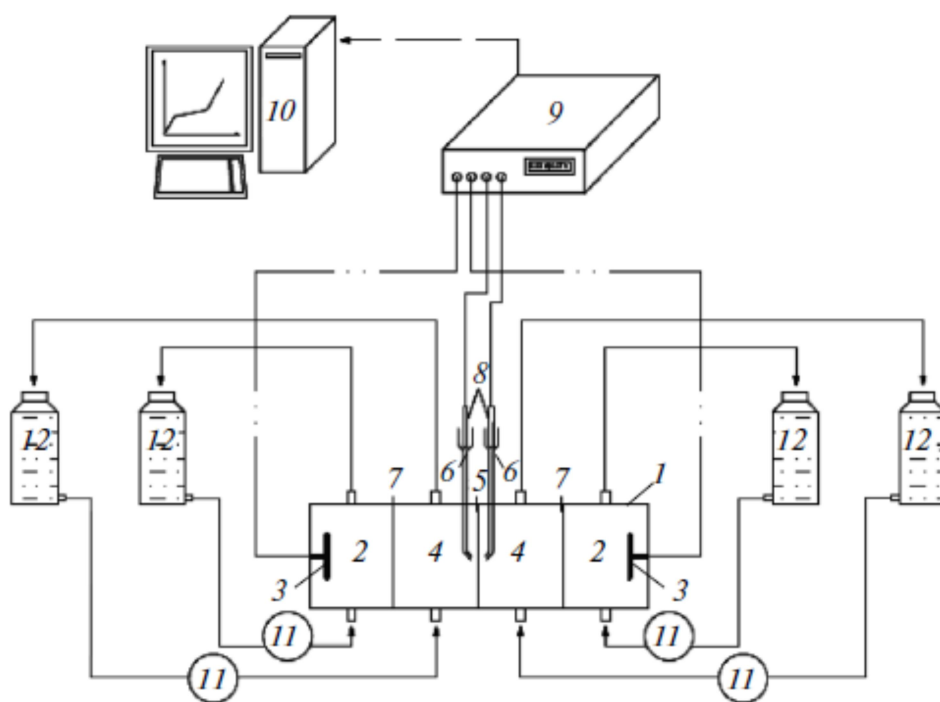


Fig. 5-3. Diagram of a unit for measuring the CVCs of the membrane system: (1) measurement cell, (2) near-electrode chambers, (3) platinum polarizing electrodes, (4) near-membrane chambers, (5) membrane under study, (6) Luggin–Haber capillaries, (7) auxiliary membranes, (8) silver/silver chloride electrodes, (9) Autolab pgstat302n potentiostat/galvanostat, (10) PC, (11) Heidolph pumpdrive 5101 peristaltic pump, and (12) vessels for solutions.

The parameters of CVCs were determined by the tangent method using numerical differentiation in the Microsoft Excel program. The tangent method is used to find the equations of linear regression of the sections corresponding to the ohmic, limiting, and overlimiting states of the electromembrane system (EMS) on the current-voltage curve. The slopes of the ohmic region, the limiting current plateau, and the overlimiting state region were determined as the coefficients a of the linear equations of the tangent lines of the form $y = ax + b$. The criterion of optimization of the number of points used for drawing the tangent lines was the accuracy of approximation (R^2). Then we determined all the characteristic points of CVCs by solving a set of two equations. These calculations were performed for all the curves in the series. The results of calculation were averaged and the confidence intervals and errors were determined for all quantities. Numerical differentiation was used because the differential curves for the CVCs of the membrane have a pronounced peak at currents close to the limiting current (i_{lim}) determined by the tangent method. Both methods allow us to determine i_{lim} with an error of less than 5 %.

When studying the polarization behavior of the obtained composites, it was noted that the CVCs changed during the experiment. Based on the experimental data, the total charge to be passed through the EMS to obtain reproducible results was determined. According to Fig. 5-4, reproducible results can be obtained after the 12th measurement, which corresponds to 2000–2500 C. This charge can be passed through the EMS in the course of sequential measurements of CVCs and by preliminarily keeping the membrane at a certain current. For example, at $I = 200$ mA, the keeping time of the sample should be 3 h.

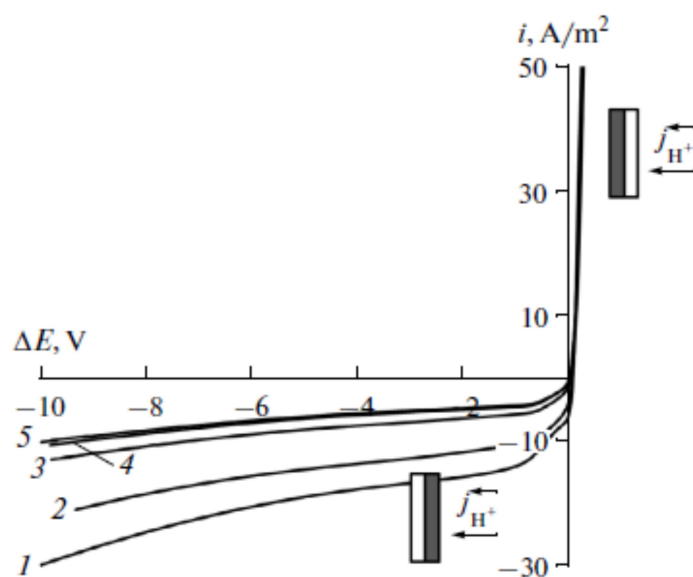


Fig. 5-4. CVCs of the MF-4SK/PANI-1 composite in 0.05 M HCl measured in sequence; measurement no. (1) 1, (2) 5, (3) 10, (4) 12, and (5) 13.

The measurement of cyclic CVCs at the standard scan rate usually used for measurements ($1 \times 10^{-4} \text{ A s}^{-1}$) showed that the polarization curves of the composites had a pronounced hysteresis, while the measurement of cyclic CVCs on the original MF-4SK membrane at the same scan rate had no such effect. The degree of this effect depends on the current density at which the samples were synthesized.

To determine the reason for the hysteresis, we studied the chronopotentiograms of the composites at different current densities (Fig. 5-5). An analysis of the results showed that the time of reaching the constant voltage drop on the composite membrane is at least 17 min. Therefore, to reduce the hysteresis, it is necessary to decrease the current scan rate during CVC measurements for membranes.

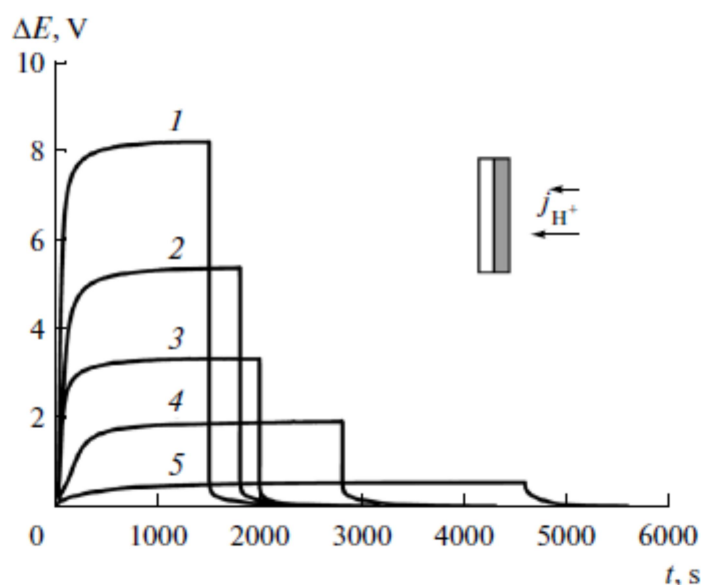


Fig. 5-5. Chronopotentiograms of the MF-4SK/PANI-1 anisotropic composite measured in 0.05 M HCl at different polarizing currents i , A dm^{-2} : (1) 11.3, (2) 7.0, (3) 6.5, (4) 2.8, and (5) 1.3.

An analysis of the experimental CVCs measured at different scan rates of the polarizing current (Fig. 5-6) showed that the polarization behavior of the composite orientated by its nonmodified side toward the flow of counter-ions is independent of the scan rate of current in the range 0.4×10^{-5} to $4.6 \times 10^{-5} \text{ A s}^{-1}$. However, when the composite is orientated by its polyaniline layer toward the flow of counter-ions, the shape and parameters of CVCs depend strongly on this value. The hysteresis of the polarization curve decreases with the scan rate. The hysteresis of CVCs was not completely eliminated during the experiment because of high time consumption. Thus, at a scan rate of $0.4 \times 10^{-5} \text{ A s}^{-1}$, the total time of measurement of one cyclic CVC was ~ 7 h. Therefore, in further experiments, we used the range of scan rates that allowed the minimum hysteresis on the CVC.

Thus, in order to obtain reproducible results with a minimum hysteresis, the following procedure for measuring the CVCs of composite membranes was suggested. After the synthesis, direct current with a density of 280 A m^{-2} should be passed through the system for 3 h. Thereafter, the CV curves should be measured using the current scan rates from 0.9×10^{-5} to $4.6 \times 10^{-5} \text{ A s}^{-1}$ depending on the sample preparation conditions. The scan rate can be higher ($4.6 \times 10^{-5} \text{ A s}^{-1}$) for the samples obtained at the minimum current density (100 A m^{-2}), but minimum ($0.9 \times 10^{-5} \text{ A s}^{-1}$) for the samples with the densest polyaniline layer obtained at the maximum current density (300 A m^{-2}) and having the most pronounced hysteresis of CVCs.

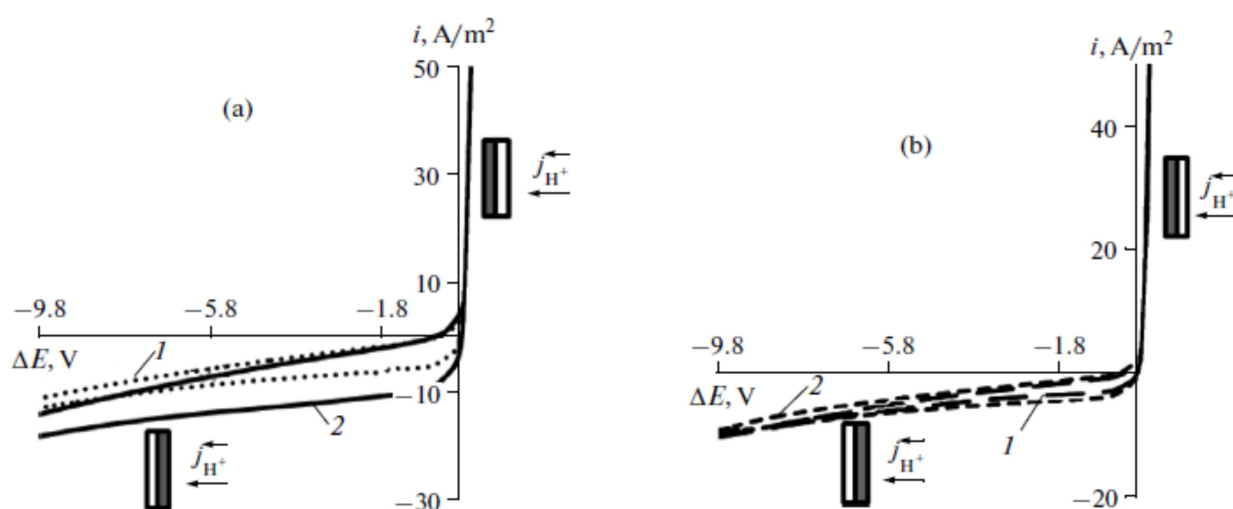


Fig. 5-6. CVCs of the MF-4SK/PANI-1 anisotropic composite measured in 0.05 M HCl at (a) high ((1) $1.5 \times 10^{-5} \text{ A s}^{-1}$ and (2) $4.6 \times 10^{-5} \text{ A s}^{-1}$) and (b) low ((1) $0.4 \times 10^{-5} \text{ A s}^{-1}$ and (2) $0.8 \times 10^{-5} \text{ A s}^{-1}$) scan rates of the polarizing current.

The developed procedure was used to study the polarization behavior of a series of anisotropic composites MF-4SK/PANI obtained at current densities of 100, 200, and 300 A m^{-2} . According to the data presented in Fig. 5-7, the CV curves are asymmetric for all the samples depending on the orientation of the modifying polyaniline layer relative to the counter-ion flow. If the counter-ion flow meets the polyaniline layer, the limiting current and the conductivity of the EMS decrease in all cases, while the potentials of the start of the overlimiting state increase compared with that for the original membrane. For the reverse orientation of membranes, an increase in the current to 100 A m^{-2} did not lead to the limiting condition in the EMS and its conductivity was higher than in the case with the counter-ion flow meeting the modified composite surface. A similar form of polarization curves was observed for the anisotropic composites obtained by sequential diffusion of polymerizing solutions across the membrane into water [5, 10].

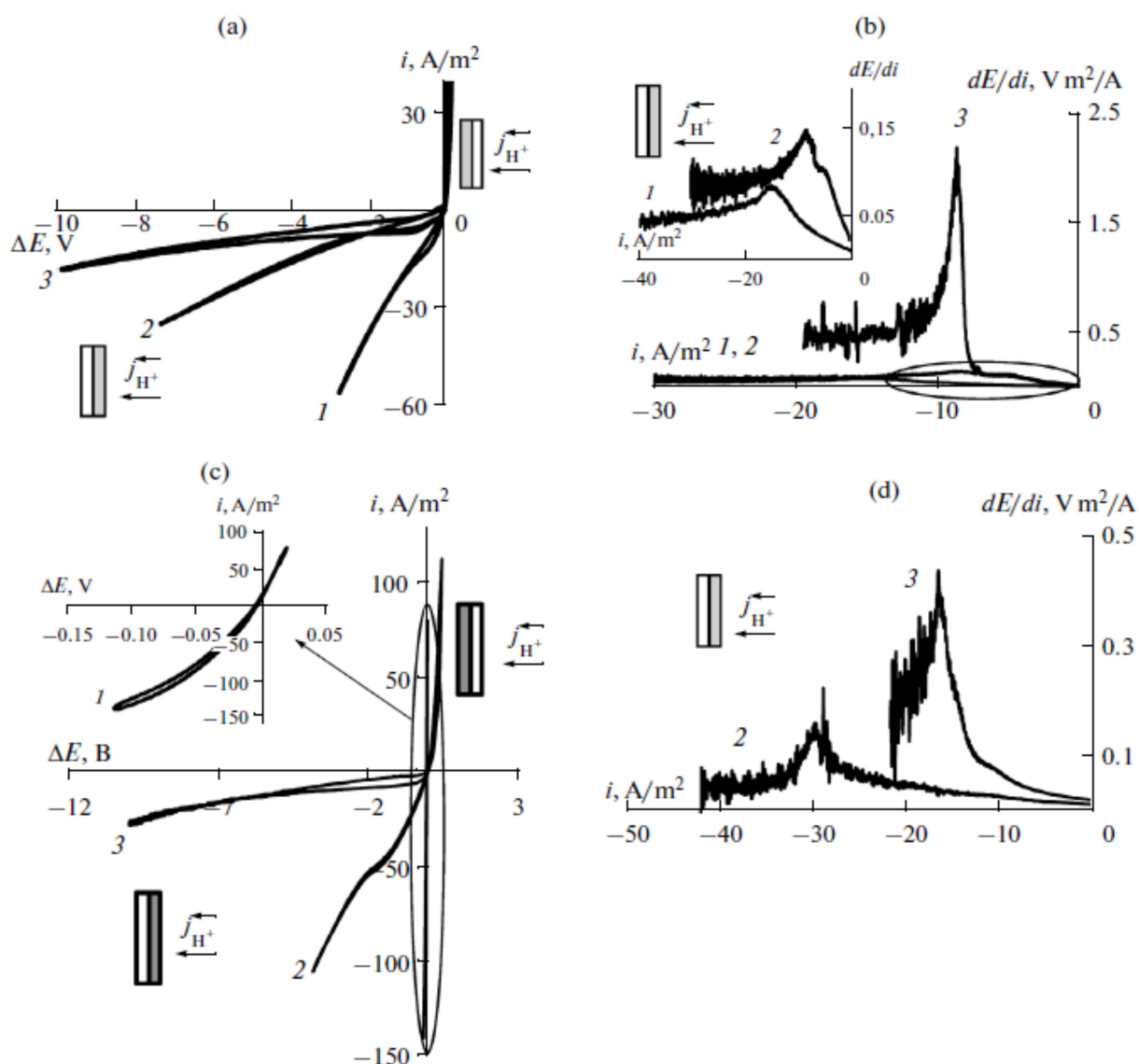


Fig. 5-7. (a), (c) Integrated and (b), (d) differential CVCs of the MF-4SK/PANI composites in 0.05 M HCl obtained at different current densities using (a), (b) potassium dichromate and (c), (d) ammonium persulfate as an oxidant of aniline. Current densities during the synthesis of the composites, A dm^{-2} : (1) 100, (2) 200, and (3) 300.

Thus, for the anisotropic MF-4SK/PANI samples, the general tendency of polarization behavior is the asymmetry of CVCs irrespective of the conditions of their synthesis and the oxidant used. We assumed that the reason for this is the presence of two layers formed in accordance with the asymmetric conditions of synthesis in the modified sample. Polyaniline having anion-exchange properties [16] is mainly localized in the surface layer of the sulfocationite membrane. This system is similar to the polyethylene terephthalate track membrane described in [17] and modified in aniline plasma under the conditions with only one open side of the membrane during plasmochemical polymerization in discharge. In this

case, a gradient of thickness of the deposited polyaniline layer appears in the pore channels, and carboxyl cationite–anionite layers with bipolar conductivity are formed. The formation of an internal bipolar boundary between the cation- and anion-exchange layers in a perfluorinated membrane can lead to catalytic dissociation of water. When the membrane is orientated toward the counter-ion flow by its polyaniline layer, the counter-ions cease to participate in current transport because they are partially neutralized by hydroxyl ions generated on the bipolar boundary, which should lead to the appearance of a pseudo-limiting state in the EMS (Fig. 5-8).

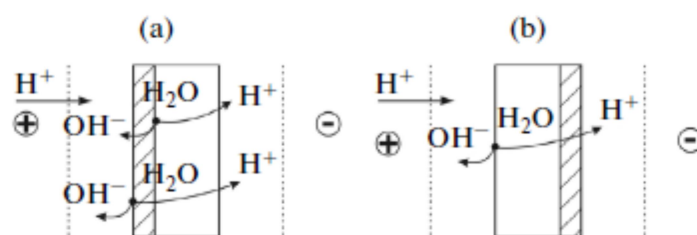


Fig. 5-8. Diagram of H⁺ and OH⁻ ion flows that appear in the EMS with the membrane orientated by its modified layer toward the (a) anode and (b) cathode (the modified layer is hatched).

This is confirmed by a detailed analysis of the region of small displacements of the potential from equilibrium (from 0 to 100 mV) on the CV curve. The effect of the appearance of the pseudo-limiting state and of the second inflection on the CV curve at low potentials (Fig. 5-7b) is directly related to the emergence of a PANI layer on the membrane surface. The higher the current density used in the PANI synthesis, the larger the second inflection on the CV curve and hence the greater the role of the internal bipolar boundary in the composite membrane. For the samples obtained at the minimum current density of 100 A m⁻², this effect is not observed on the polarization curves.

The influence of the internal bipolar contacts on the polarization behavior of the MF-4SK/PANI composite membrane was analyzed in [18]. The appearance of “fast ions” in the system due to the catalytic dissociation of water was confirmed by analyzing the frequency impedance spectrum.

The evaluation of the conductivity of the EMS from the slope of the ohmic region of CVCs showed that the asymmetry of this parameter is observed regardless of the measurement mode of the polarization curve, the orientation of the anisotropic membrane playing the determining role. Table 5-2 shows the calculated angular slopes of the ohmic region of CVCs and the asymmetry coefficients found as their ratio. According to Table 5-2, the EMS conductivity is

lower when the modified side of the membrane is directed toward the counter-ion flow. This effect is consistent with the data of [10, 19] for the composite membranes obtained during the diffusion of the polymerizing solutions. The different conductivities of the membrane system can be explained by different concentration profiles formed in this bilayer membrane. The concentration of counter-ions on the internal interface is higher when the counter-ion flow meets the nonmodified side of the membrane. Hence, the electric conductivity of the less conductive modified layer will be higher in this case. For the opposite orientation, the resistance of the modified layer and hence of the whole system is higher because of the lower concentration of counter-ions.

Sample	Angular slope of ohmic segment, $A V^{-1} m^{-2}$		
	nonmodified side directed toward the counter-ion flow	modified side directed toward the counter-ion flow	Asymmetry coefficient
MF-4SK/PANI-100-1	1207	48	25
MF-4SK/PANI-200-1	475	15	32
MF-4SK/PANI-300-1	475	38	12
MF-4SK/PANI-100-2	3490	2050	1.7
MF-4SK/PANI-200-2	690	42	16
MF-4SK/PANI-300-2	205	30	7

Table 5-2. Conditions for the preparation of MF-4SK/PANI composites.

The asymmetry of conductivity was described in the literature, for example, for metal–polymer composite membranes [20]. The authors of [17, 20, 21] noted a relationship between the straightening effect similar to the p – n transition in semiconductors and the change in the pore geometry of the membrane after the deposition of a modifier on one of its surfaces. As a result, a bipolar interface is formed between the initial membrane and the deposited layer, which have oppositely charged functional groups in electrolyte solutions. This diode effect or the effect of EMS conductivity switching was also found in the present study for composite anisotropic membranes prepared in an external electric field. The asymmetry coefficient of the slope of the ohmic region of the CVC was considerably higher for the samples obtained by using potassium dichromate (Table 5-2).

According to Table 5-2, as the current density increases during the synthesis of composite membranes orientated by their PANI layer toward the counter-ion flow, their conductivity at first decreases and then begins to increase if potassium dichromate is used. This may be due

to the appearance of a contribution of the intrinsic conductivity of PANI to the total conductivity of EMS. For the composites obtained in the presence of ammonium persulfate, however, the conductivity only decreased as the current density increased during the synthesis of PANI irrespective of the membrane orientation. One possible explanation for these differences in the polarization behavior of the composites is the fact that for the samples obtained at the same current densities, the amount of PANI in the composites is lower in the case of ammonium persulfate used as an oxidant than in the case of potassium dichromate.

5.3 Conclusions

Composite membranes based on MF-4SK and polyaniline with an anisotropic structure and asymmetric current-voltage curves can be obtained under the conditions of an external electric field. An analysis of various regions of the CVC curve of the composite membranes showed that as the current density increases during the synthesis of polyaniline, their conductivity decreases, the hysteresis on the cyclic current-voltage curve and the asymmetry of the CVC parameters increase, and the pseudo-limiting current appears due to the appearance of an internal bipolar boundary. Based on the analysis of the polarization behavior of the samples, we can determine their effective applications in various electrochemical devices. Materials with moderate asymmetry of the current-voltage curve and sufficiently high density of the limiting current are promising for use in electro dialysis because, as is known, modification of perfluorinated membranes with polyaniline increases their selectivity and reduces the diffusion and electroosmotic permeability [22–24]. Anisotropic composite membranes with a diode-like effect may be used as membrane switches or relays.

5.4 Acknowledgments

This study was financially supported by the Russian Foundation for Basic Research and the administration of the Krasnodar region (project nos. 14_08_31704_mol_a and 13_08_96540_r_yug_a).

References

- [1] R. A. Bullen, T. C. Arnot, J. B. Lakeman, F. C. Walsh, Biofuel cells and their development, *Biosens. Bioelectron.* 21 (2006) 2015–2045.
- [2] I. Y. Sapurina, M. E. Kompan, V. V. Malyshkin, V. V. Rosanov, J. Stejskal, Properties of proton-conducting Nafion-type membranes with nanometer-thick polyaniline surface layers, *Russ. J. Electrochem.* 45 (2009) 697–706.
- [3] P. A. Yurova, Y. A. Karavanova, Y. G. Gorbunova, A. B. Yaroslavtsev, Transport properties of asymmetric ion-exchange membranes based on MC-40, MF-4SC, and polyaniline, *Petroleum Chem.* 54 (2014) 551–555.
- [4] P. A. Yurova, Y. A. Karavanova, A. B. Yaroslavtsev, Diffusion characteristics of surface-modified ion-exchange membranes based on MK-40, MF-4SK, and polyaniline, *Petroleum Chem.* 52 (2012) 593–597.
- [5] S. Tan, D. Belanger, Characterization and transport properties of Nafion/Polyaniline composite membranes, *J. Phys. Chem. B* 109 (2005) 23480–23490.
- [6] A. B. Yaroslavtsev, V. V. Nikonenko, Ion-exchange membrane materials: Properties, modification, and practical application, *Nanotechnologies in Russia* 4 (2009) 137–159.
- [7] J. Stejskal, Polyaniline. Preparation of a conducting polymer, *Pure Appl. Chem.* 74 (2002) 857–867.
- [8] A. R. Blythe, D. Bloor, *Electrical Properties of Polymers*, Cambridge: Cambridge University Press, 2008.
- [9] N. P. Berezina, A. A.-R. Kubaisi, E. I. Griga, N. M. Alpatova, V. N. Andreev, Composite Polyaniline/MF-4SK membranes: A chemical template synthesis and the sorption and conduction properties, *Russ. J. Electrochem.* 40 (2004) 286–293.
- [10] N. P. Berezina, N. A. Kononenko, A. A.-R. Sytcheva, N. V. Loza, S. A. Shkirskaya, N. Hegman, A. Pungor, Perfluorinated nanocomposite membranes modified by polyaniline: Electrotransport phenomena and morphology, *Electrochim. Acta* 54 (2009) 2342–2352.
- [11] N. P. Berezina, N. A. Kononenko, N. V. Loza, A. A.-R. Sycheva, Electrochemical behavior of MF-4SK/polyaniline composites as investigated by membrane voltammetry, *Russ. J. Electrochem.* 43 (2007) 1340–1349.
- [12] N. A. Kononenko, N. P. Berezina, S. V. Dolgoplov, T. P. Polovinko, I. V. Falina, RF Patent 2487145, 2011.
- [13] A. Nekrasov, V. Ivanov, A. Vannikov, A comparative voltabsorptometric study of polyaniline films prepared by different methods, *Electrochim. Acta* 46 (2001) 3301–3307.
- [14] Ya. O. Mezhuev, Extended Abstract of Cand. Sci. (Chem.) Dissertation, Moscow, 2011.

- [15] E. O. Fedorovskaya, Cand. Sci. (Chem.) Dissertation, Novosibirsk, 2014.
- [16] J. Wang, Anion exchange nature of emeraldine base (EB) polyaniline (PAn) and a revisit of the EB formula, *Synth. Met.* 132 (2002) 49–52.
- [17] E. N. Demidova, A. I. Drachev, G. A. Grigor'eva, Investigation of electrotransport properties of poly(ethylene terephthalate) track membranes modified by plasma of aniline, *Russ. J. Electrochem.* 45 (2009) 533–537.
- [18] N. A. Kononenko, S. V. Dolgoplov, N. V. Loza, N. V. Sheldeshov, Effects of pH variation in solutions under the polarization conditions of the MF-4SK membrane with surface modified by polyaniline, *Russ. J. Electrochem.* 51 (2015) 19–24.
- [19] G. Chamoulaud, D. Belanger, Modification of ion-exchange membrane used for separation of protons and metallic cations and characterization of the membrane by current–voltage curves, *J. Colloid Interface Sci.* 281 (2005) 179–187.
- [20] L. I. Kravets, A. B. Gil'man, M. Yu. Yablokov, Preparation of metal-polymer composite membranes with conductance asymmetry, *Petroleum Chem.*, 51 (2011) 634–643.
- [21] P. Yu. Apel, I. V. Blonskaya, N. V. Levkovich, O. L. Orelovich, Asymmetric track membranes: Relationship between nanopore geometry and ionic conductivity, *Petroleum Chem.* 51 (2011) 555–567.
- [22] N. P. Berezina, S. A. Shkirskaya, A. A.-R. Sycheva, M. V. Krishtopa, The electric transport of proton-bound water in MF-4SK/PAni nanocomposite membranes, *Colloid J.* 70 (2008) 397–406.
- [23] M. V. Kolechko, A. N. Filippov, S. A. Shkirskaya, S. V. Timofeev, N. P. Berezina, Synthesis and diffusion permeability of MF-4SK/polyaniline composite membranes with controlled thickness of the modified layer, *Colloid J.* 75 (2013) 289–296.
- [24] K. V. Protasov, S. A. Shkirskaya, N. P. Berezina, V. I. Zabolotskii, Composite sulfonated cation-exchange membranes modified with polyaniline and applied to salt solution concentration by electrodialysis, *Russ. J. Electrochem.* 46 (2010) 1131–1140.

Presentation of the article 2

In the previous article, the method for the preparation of an anisotropic composite membrane by formation of PANI layer within a cation-exchange membrane and investigation of the electrochemical behavior of the composite membrane have been described. The specificity of such type of membranes is in formation of an internal bipolar boundary between the cation- and anion-exchange layers. The anion-exchange layer formed by PANI presents a barrier for the transfer of multicharged cations, which is interesting for the use in metathesis electro dialysis. However, the bipolar boundary lead to catalytic water splitting that can stimulate the scale formation on the depleted surface of the modified membrane. On the other hand, modification of the membrane with PANI leads to a smoother surface, which should reduce the risk of nucleation of scale crystals on the membrane surface.

The main goal of the article presented in this section of the chapter is to study how PANI modification of heterogeneous membranes affects the scaling process. Scale formation on the surface of a heterogeneous cation-exchange MK-40 membrane and its modification MK-40/PANI is investigated by means of chronopotentiometry and voltammetry in a mixed solution with relatively high concentration of Ca^{2+} , Mg^{2+} and hydrocarbonates. The study is made in the range of current densities from $0.2 i_{\text{lim}}^{\text{exp}}$ to $1.5 i_{\text{lim}}^{\text{exp}}$, where $i_{\text{lim}}^{\text{exp}}$ is the experimentally determined (second) limiting current density.

This study allows us to conclude that the modification of the MK-40 membrane does not change its thickness: the thickness of MK-40/PANI membrane is equal to that of the pristine membrane. The conductivity of MK-40/PANI is about 16 % lower than that of MK-40 membrane. The contact angle of MK-40 and MK-40/PANI is nearly the same (and close to 55 °). The surface of modified membrane is smoother than that of the pristine one.

The bipolar junction formed by the PANI layer in the MK-40/PANI membrane causes an essential increase in water splitting rate and a reduction in electroconvection. As a result, a precipitate in the gel form is detected in the range $i \geq 0.8 i_{\text{lim}}^{\text{exp}}$ for the MK-40/PANI membrane.

However, at current densities $i < 0.8 i_{\text{lim}}^{\text{exp}}$ no scaling is observed. Thus, it is possible to recommend the MK-40/PANI composite membrane for monovalent-ion-selective electro dialysis at underlimiting current densities.

Effect of surface modification of MK-40 membrane with polyaniline on scale formation

In preparation

M.A. Andreeva^{a,b}, N.V. Loza^b, N.D. Pismenskaya^b, L. Dammak^a, N.A. Kononenko^b, C. Larchet^a, V.V. Nikonenko^b

^aInstitut de Chimie et des Matériaux Paris-Est (ICMPE) UMR 7182 CNRS – Université Paris-Est, 2 Rue Henri Dunant, 94320 Thiais, France.

^bKuban State University, 149 Stavropolskaya st., 350040 Krasnodar, Russia.

5.5 Experimental

5.5.1 Membranes

Two ion-exchange membranes (IEMs) are used in this study, an MK-40 (Fig. 5-9a) and its modification MK-40/PANI (Fig. 5-9b). The heterogeneous cation-exchange MK-40 membrane (Shchekinoazot, Russia) contains sulfonic acid fixed groups. The MK-40/PANI membrane is obtained by synthesizing polyaniline (PANI) within the MK-40 membrane near-surface layer in external electric field according to the method described in Ref. [1]. A four-chamber flow-through cell is used. A 0.01 M aniline solution in 0.05 M HCl and 0.002 M potassium dichromate solution in 0.05 M HCl are fed into the cell chambers next to the membrane on the anode and cathode sides, respectively. A 0.05 M HCl solution is circulated through the electrode chambers. The synthesis is carried out at $i=40\text{mA cm}^2$ for 90 min.

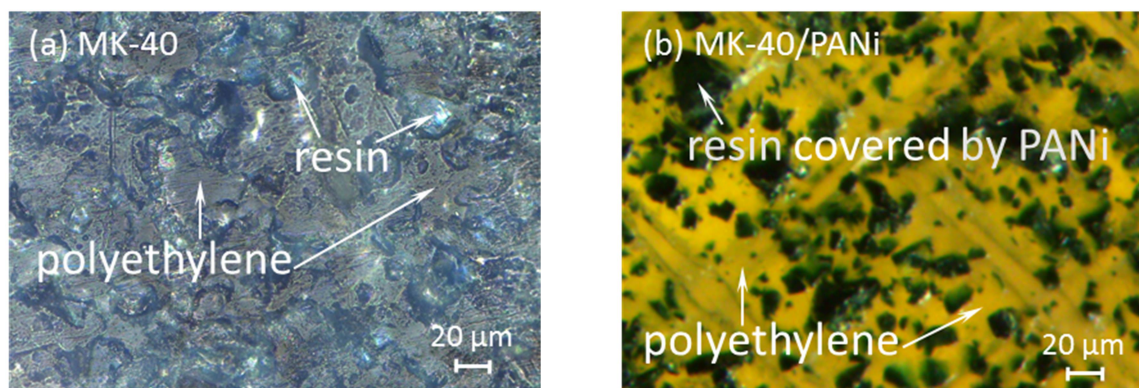


Fig. 5-9. Image of the surface of swollen (a) MK-40 and (b) MK-40/PANI membranes as obtained with a Zeiss AxioCam MRc5 light and Altami microscope, respectively.

5.5.2 Analyses

5.5.2.1 Membrane thickness

The membrane thickness, L , is measured with a Micrometer MK 0-25 (Model 102, Russia). The membrane thickness values are averaged from ten measurements at different locations on the effective surface of each membrane.

5.5.2.2. Membrane electrical conductivity

The membrane electrical conductance, G_m , is measured with a specially designed cell coupled to AKTAKOM multimeter (Model ABM-4084, Russia). 0.1 M NaCl reference solution is

used. According to the procedure developed by Lteif et al. [2], the transverse electric resistance of the membrane, R_m , is calculated according to:

$$R_m = \frac{1}{G_m} = \frac{1}{G_{m+s}} - \frac{1}{G_s} \quad (5.1)$$

Here G_{m+s} and G_s are the conductance of the solution with membrane and without membrane, respectively.

The membrane electrical conductivity, κ , can be calculated as [2]

$$\kappa = \frac{L}{R_m S} \quad (5.2)$$

Here S is the electrode area.

5.5.2.3. Contact angle measurements

Contact angles, θ , of the wet membranes are measured by the sessile drop method in the sodium form [3]. Data are treated using the software ImageJ.

5.5.3 Electrolysis cell and experimental setup

The investigations are carried out in the same flow-through four-chamber electrolysis cell, which was used earlier [4]. The cell comprises the tested MK-40 or MK-40/PANI membrane and two auxiliary heterogeneous membranes: an anion-exchange MA-41 membrane (Shchekinoazot, Russia) and a MK-40 membrane. The intermembrane distance in the cell compartments is 6.4 mm, the membrane area exposed to the current flow is 4 cm². The anode and the cathode are platinum polarizing electrodes. The experimental setup involves two closed loops containing a model salt solution and a 0.04 M NaCl electrolyte solution. The model solution circulates across the central desalination compartment; the 0.04 M NaCl solution, through an auxiliary and two electrode compartments in parallel; the solution flow rate through each compartment is 30 mL min⁻¹. The model salt solution is composed of Na₂CO₃ (1000 mg L⁻¹), KCl (800 mg L⁻¹), CaCl₂*2H₂O (4116 mg L⁻¹) and MgCl₂*6H₂O (2440 mg L⁻¹). In this solution, the Mg/Ca molar concentrations ratio is 2/5 and the total concentration of CaCl₂ and MgCl₂ is 0.04M. The pH of the solution is adjusted to 6.5 by adding HCl. The mineral composition of this solution corresponds approximately to that of trice concentrated milk. Each closed loop is connected to a separated external plastic reservoir, allowing continuous recirculation.

5.5.4 Protocol

The procedures for measuring I-V curve and chronopotentiograms (ChP) are described in [3]. A KEITHLEY 220 current source is used to supply the current between the polarizing electrodes. The potential drop (PD) across the membrane under study, $\Delta\varphi$, is measured using Ag/AgCl electrodes. These electrodes are placed in the Luggin capillaries. The Luggin tips are installed at both sides of the membrane under study in its geometric center at a distance of about 0.5 mm from the surface. PD is registered by a HEWLETT PACKARD 34401A multimeter. I-V curves are recorded when the current is swept from 0 to 10.5 mA/cm² at a scan rate of 0.8 μ A/s; the PD remains < 3 V. The chronopotentiometric measurements are made in the range of current densities from 0.2 i_{lim}^{exp} to 1.5 i_{lim}^{exp} , where i_{lim}^{exp} is the experimentally determined limiting current density. The experiment is carried out at 20⁰C.

5.6 Results and discussion

5.6.1. Physico-chemical characteristics of ion-exchange membranes

The thickness of MK-40/PANI membrane does not change in the process of its modification, i.e. the thickness of MK-40/PANI membrane is the same as that of MK-40 membrane (Table 5-3). The conductivity of MK-40/PANI is about 16% lower than that of MK-40 membrane. The contact angle of MK-40 and MK-40/PANI is nearly the same, close to 55 °.

The PANI layer within the MK-40 membrane has anion-exchange properties. Thus, its formation leads to a bi-layer membrane, whose the main layer is the non-modified part of the pristine cation-exchange membrane. The anion-exchange PANI layer presents a barrier for the transfer of multicharged cations. Besides, it can be expected that the bipolar boundary will stimulate the water splitting by the MK-40/PANI membrane.

membrane	L , mm	κ , S m ⁻¹	θ , °
MK-40	0.471	0.36	55
MK-40/PANI	0.479	0.30	53

Table 5-3. The main properties of the MK-40 and MK-40/PANI membranes.

5.6.2 Voltammetry

There are three regions on the I-V curve of IEMs, which are generally distinguished in the literature [5, 6]. An initial linear region is followed by a plateau of limiting current density,

and then by a region of a higher growth of current density. When approaching i_{lim} , the electrolyte interfacial concentration gets nearly zero that initiates coupled effects of membrane CP: current-induced convection (electroconvection and gravitational convection) and water splitting [5].

Fig. 5-10 shows the I-V curves obtained for MK-40 and MK-40/PANI membranes in the model salt solution. In the case of MK-40 membrane the shape of the curve is the typical one. In the case of MK-40/PANI membrane the I-V curve has two inflection points. The first inflection point is in the region of small displacements of the potential from equilibrium (about 300 mV); it is related to the depletion of the bipolar boundary within the membrane. Under the action of external electric field, the cations migrate from the bipolar junction into the bulk of the cation-exchange layer; the anions migrate from this junction into the bulk of the anion-exchange layer. Diffusion of anion through the thin PANI layer allows reduction of the deficit of ions at the bipolar boundary. However, this reduction is only partial, and at a certain current density the ion concentration at this boundary becomes sufficiently low to cause an essential increase in the membrane resistance. The latter is seen by appearing a plateau on the I-V curve in a range of current densities close to 4 mA cm^2 . This critical current density, which is caused by the depletion of the bipolar boundary, may be called the pseudo-limiting current density, $i_{pseudo-lim}^{exp}$.

When the concentration of salt ions at the depleted bipolar boundary becomes sufficiently low, water splitting there occurs similar to that, which takes place in the bipolar membranes [7, 8]. This process produces H^+ and OH^- ions, which are additional current carriers and whose emergence results in decreasing membrane resistance. Thus, an inflection point appears on the I-V curve, after which the rate of current density growth increases (Fig. 5-10). As the current continue to increase, the ion concentration at the external membrane surface decreases to a low value that causes a new increase in system resistance. This increase is manifested by appearance of a second inclined plateau on the I-V curve. This state relates to the “classical” limiting current density, i_{lim}^{exp} , observed in the case of conventional monopolar ion-exchange membranes [5].

The values of both limiting current density may be determined by the point of intersection of the tangents drawn to the linear parts of the I-V curve on the left and on the right of the region where a sharp change of the rate of current growth with potential drop occurs (Fig. 5-10). These values for both limiting current densities are present in Table 5-4.

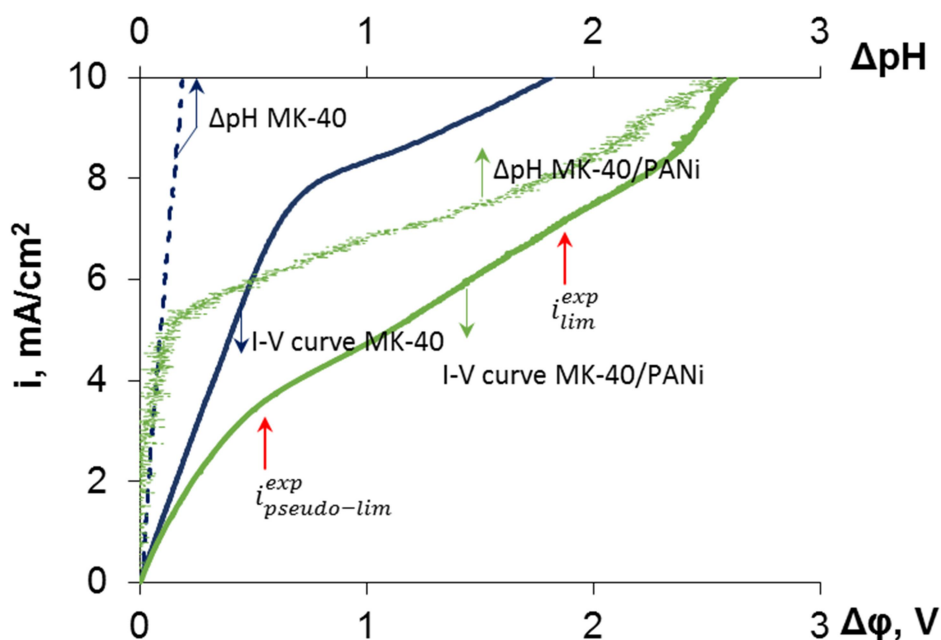


Fig. 5-10. I-V curves for MK-40 and MK-40/PANI membranes in the model solution and corresponding dependence of the pH of diluate solution.

membrane	$i_{pseudo-lim}^{exp}$, mA cm ⁻²	i_{lim}^{exp} , mA cm ⁻²
MK-40	-	7.7
MK-40/PANI	3.2	7.0

Table 5-4. The values of limiting current densities for MK-40 and MK-40/PANI membranes in the mixed model solution at 20 °C.

5.6.3 Chronopotentiometry

Fig. 5-11 shows the ChP of MK-40 membrane and its derivative obtained in the model solution at $i = 1.6 i_{lim}^{exp}$. The shape of the curve is typical for IEMs in a binary solution of monovalent ions at $i \geq i_{lim}$ [9, 10]. An immediate increase of PD is observed after switching-on the direct current. It is related to the ohmic potential drop, $\Delta\varphi_{Ohm}$, over the membrane and two adjacent solutions where the concentrations are not yet affected by CP. At $i < i_{lim}$ the value of PD does not increase significantly during one experimental run. At $i \geq i_{lim}$ the electrolyte concentration at the depleted membrane interface gradually decreased with time, the process is governed by electrodiffusion. As a result, the sharp increase in PD is observed on the ChPs. When the electrolyte concentration at the depleted membrane interface gets sufficiently low, along with electrodiffusion, current-induced convection arises. As a

consequence, the rate of PD growth slows down, and finally, PD tends to a quasi-steady state value, $\Delta\varphi_{St}$. The transition time, τ , related to the inflection point on the ChP corresponds to the appearance of an additional mechanism of ion transport, namely, the current-induced convection [9, 10]:

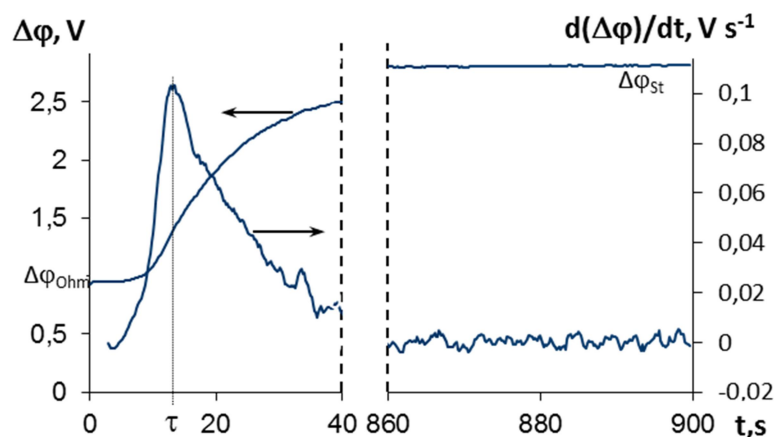


Fig. 5-11. Chronopotentiogram of the MK-40 membrane in the model solution, $\Delta\varphi$ vs. t , and its derivative, $d(\Delta\varphi)/dt$ vs. t , in the model solution at $i = 1.5 i_{lim}^{exp}$. $\Delta\varphi_{Ohm}$ is the ohmic potential drop just after the current is switched on; $\Delta\varphi_{St}$ is the potential drop at the steady-state; τ is the transition time.

Figs. 5-12 shows ChPs for the MK-40 and MK-40/PANI membranes measured in the model salt solution at different current densities. $\Delta\varphi' = \Delta\varphi_{St} - \Delta\varphi_{Ohm}$ is the reduced potential drop. It can be seen that an inflection point on the ChP of MK-40/PANI membrane appears at $i_{pseudo-lim}^{exp} < i < i_{lim}^{exp}$. This point corresponds to the appearance of an additional mechanism of ion transport: emergence of H^+ and OH^- ions due to water splitting at the internal bipolar boundary occurring when the ion concentration at this boundary becomes sufficiently low.

The scale formation begins at $i \geq 0.8 i_{lim}^{exp}$ for MK-40/PANI and at $i \geq 1.0 i_{lim}^{exp}$ for MK-40 membranes. This is evidenced by the growth of PD across the membrane at $i = 7.0 \text{ mA cm}^{-2}$ (for MK-40/PANI) and at $i = 8.8 \text{ mA cm}^{-2}$ (for MK-40) after reaching the quasi-steady state. In the case of MK-40/PANI membrane at higher currents, the PD reaches a maximum value and then slowly falls down during the experiment run.

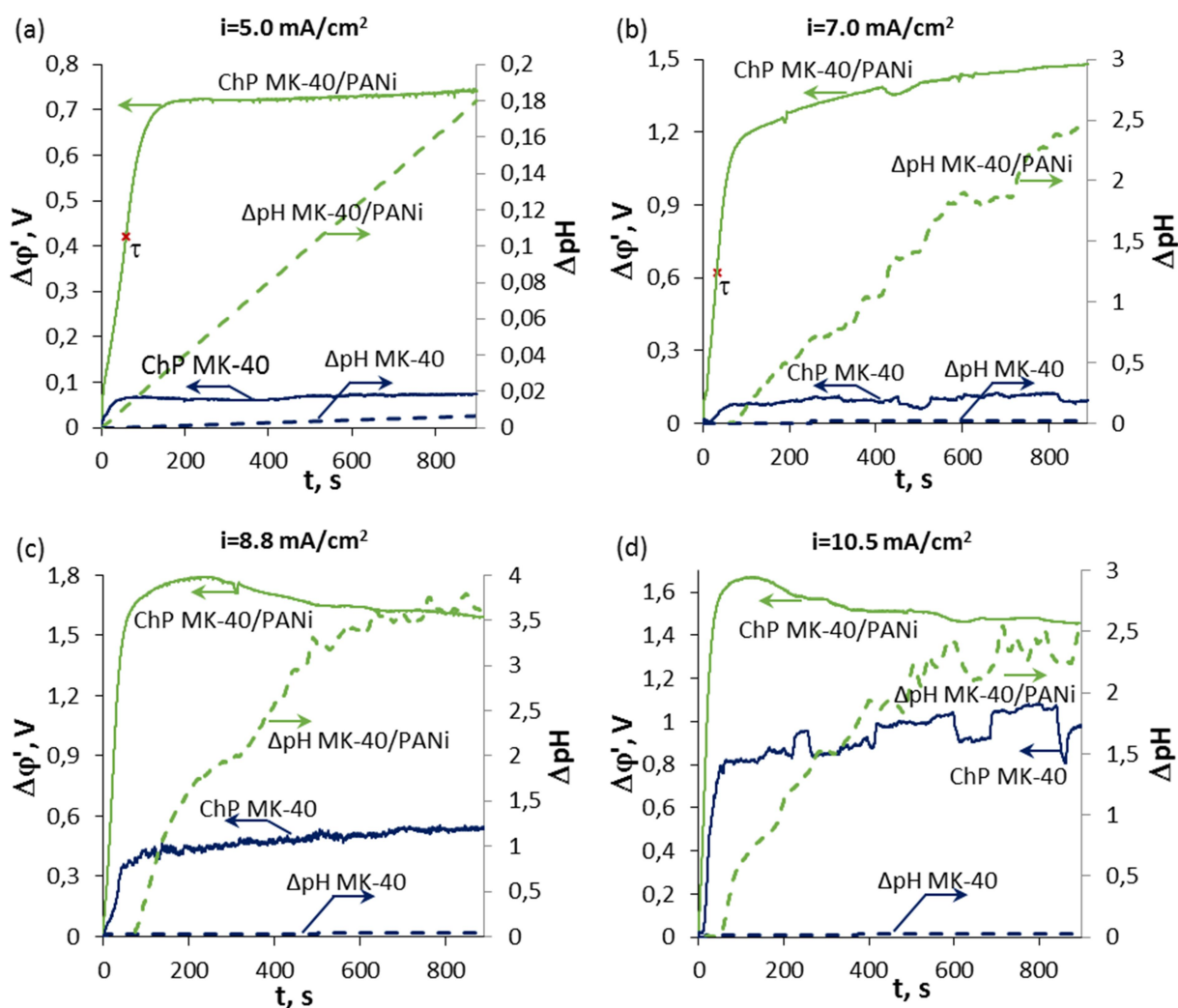


Fig. 5-12. Chronopotentiograms of MK-40 and MK-40/PANI membranes in the model solution and corresponding time dependence of the pH of diluate solution.

There is apparent contradiction between the behavior of the membrane presented by Fig. 5-12b and Fig. 5-12c. The increase in pH of diluate solution is higher at $i=8.8 \text{ mA cm}^{-2}$ (Fig. 5-12c) than at $i=7.0 \text{ mA cm}^{-2}$ (Fig. 5-12b). However, the growth of PD with time occurs only in the case of $i=7.0 \text{ mA cm}^{-2}$, in the case of $i=8.8 \text{ mA cm}^{-2}$ and $i=10.5 \text{ mA cm}^{-2}$ no PD growth is detected. On the contrary, there is even a slight decrease of PD with time in the $t > 200 \text{ s}$ range. The explanation is that at $i \geq 8.8 \text{ mA cm}^{-2}$ the precipitation on the MK-40/PANI membrane is in the form of gel (Fig. 5-13), while at lower current density the precipitation is in crystal form.

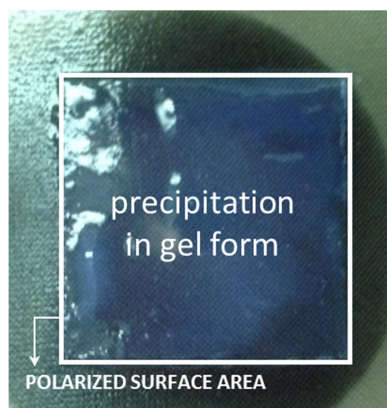


Fig. 5-13. The precipitate in the form of a gel on the MK-40/PANI membrane surface at $i=10.5 \text{ mA cm}^{-2}$.

Indeed, at $i \leq 7.0 \text{ mA cm}^{-2}$ in the case of MK-40/PANI membrane and at all current densities in the case of MK-40 membrane, the gel-form precipitation was not observed. Instead, a cake form of precipitation (the crystals) was observed on the MK-40 membrane at $i=10.5 \text{ mA cm}^{-2}$ (Fig. 5-14).

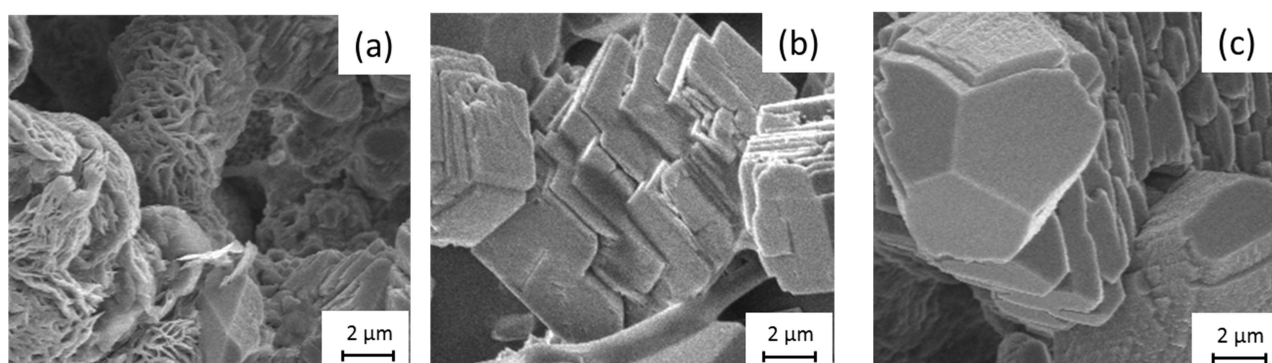


Fig. 5-14. SEM images of the surface of (a) $\text{Mg}(\text{OH})_2$, (b) CaCO_3 and $\text{Ca}(\text{OH})_2$ crystals on the MK-40 membrane surface facing the diluate after 5h of electro dialysis of model solution.

The possible foulants and fouling modes are presented in Table 5-5.

Foulants	Fouling modes
Large suspended particles	Can be presented in the original feed or created by scaling; can block membrane channels
Small colloidal particles	Can rise to become a fouling layer
Macromolecules	Can form a gel or a cake on membranes or within the structure of porous membranes
Small molecules	Can have strong interactions with plastic membranes; for example, antifoaming agents such as polypropylene glycols
Proteins	Can interact with surface or pores of membranes
Chemical reactions	Can lead to precipitation of salts and hydroxides with increase in concentration and/or pH
Bacteria	Can grow on membrane surfaces and excrete extracellular polymers

Table 5-5. The possible foulants and fouling modes.

In the case of MK-40 membrane at current density $1.0 i_{\text{lim}}^{\text{exp}} \leq i \leq 1.5 i_{\text{lim}}^{\text{exp}}$ the formation of scale occurs in the form of crystals of CaCO_3 , $\text{Mg}(\text{OH})_2$ и $\text{Ca}(\text{OH})_2$ (Fig. 5-14). In this case, a part of the surface is screened by these crystals, which form a type of the cake film. The area covered by this film increases with time. As a consequence, the PD across the membrane does not reach the steady-state value and growth with time.

The difference in conditions causing formation of crystals or gel may be explained as follows. Generally, the presence of positively and negatively charged ions results in formation of precipitate, if the product of their concentration is higher than the solubility product. When the concentrations of positively and negatively charged ions are in stoichiometric proportion, electrically neutral crystals are formed. However, when freshly prepared electrically neutral precipitate is treated with a solution, where one the ions constituted the crystal is in excess, charged colloidal particles can be formed. This process is called is called peptization [11, 12]. The cause is the selective adsorption of ions common to the colloidal particles. For example, if freshly prepared ferric hydroxide precipitate is treated with a small quantity of FeCl_3 (electrolyte) solution, positively charged colloidal particles of the type $\text{Fe}(\text{OH})_3\text{Fe}^{3+}$ are formed. Similarly, if instead of FeCl_3 , a NaOH solution for treating ferric hydroxide precipitate is used, negatively charged colloidal particles are formed.

Let us consider the $\text{Mg}(\text{OH})_2$ formation. In the case where the water splitting rate is relatively low (MK-40 at all current densities or MK-40/PANI at low current densities), the

concentrations of Mg^{2+} ions and OH^- ions are small, while Mg^{2+} may be slightly in excess. The scale crystals are formed by the Mg^{2+} and OH^- ions in stoichiometric proportion. Low concentration of Mg^{2+} ions does not allow peptization.

In the case of MK-40/PANI membrane at $i > i_{\text{lim}}^{\text{exp}}$, the water splitting rate is relatively high and there is an excess of OH^- ions in comparison with the Mg^{2+} ions. The excess of OH^- ions leads to the formation of negatively charged colloidal particles on the membrane surface. The micelle core consists of $\text{Mg}(\text{OH})_2$. In accordance with the Fajans–Paneth–Hahn law [13], there is a layer of preferentially adsorbed OH^- ions next to the core. The particle is now negatively charged and attracts positively charged ions from solution (Fig. 5-15). Since the surface layer formed by PANI contains positively charged fixed groups, the colloidal particles are attracted to the surface. That gives stability to the gel-type layer formed by colloidal particles. This layer contains mobile ions and conducts electric current, while the cake-type layer of crystals is non-conductive. The conductivity of the gel-type layer explains the fact that there is no PD growth with time across the MK-40/PANI membrane at $i > i_{\text{lim}}^{\text{exp}}$.

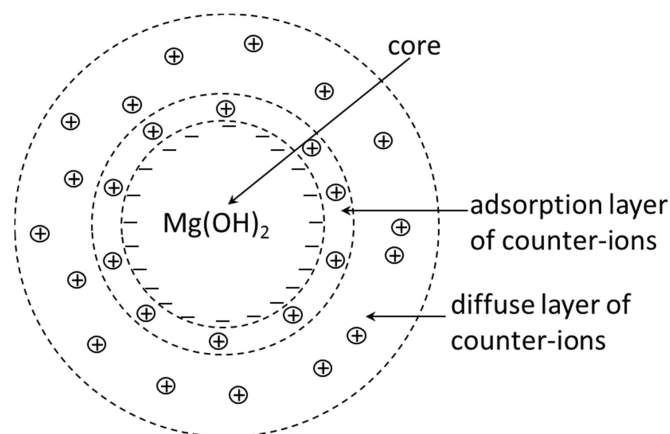


Fig. 5-15. The micelle structure.

5.7 Conclusions

The scale formation on the surface of two ion-exchange membranes, a heterogeneous MK-40 and its modification MK-40/PANI, during ED of a solution containing the scale-forming cations, Ca^{2+} and Mg^{2+} , is investigated. The membrane modification is carried out by synthesizing PANI within the MK-40 membrane near-surface layer in external electric field.

In the case of MK-40/PANI membrane in comparison with MK-40 membrane the I-V curve has two inflection points. The first pseudo-limiting current density, $i_{\text{pseudo-lim}}^{\text{exp}}$, is in the region of small displacements of the potential from equilibrium; it is related to the depletion of the

bipolar boundary within the membrane. As the current continue to increase, the ion concentration at the external membrane surface decreases to a low value that causes a new increase in system resistance and the “classical” limiting current density, i_{lim}^{exp} , is observed.

The precipitate is detected in the range $i \geq 0.8 i_{lim}^{exp}$ for MK-40/PANI and $1.0 i_{lim}^{exp} \leq i \leq 1.5 i_{lim}^{exp}$ for MK-40 membrane. In the case of MK-40 membrane at current density $1.0 i_{lim}^{exp} \leq i \leq 1.5 i_{lim}^{exp}$ the formation of scale occurs in the form of crystals of $CaCO_3$, $Mg(OH)_2$ и $Ca(OH)_2$. In this case, a part of the surface is screened by these crystals, which form a type of the cake film. As a consequence, the PD across the membrane does not reach the steady-state value and growth with time. The precipitation on the MK-40/PANI membrane is in crystal form at $i_{pseudo-lim}^{exp} < i < i_{lim}^{exp}$ and in the form of gel at $i > i_{lim}^{exp}$.

References

- [1] N. V. Loza, S. V. Dolgoplov, N. A. Kononenko, M. A. Andreeva, Yu. S. Korshikova, Effect of surface modification of perfluorinated membranes with polyaniline on their polarization behavior, *Russ. J. Electrochem.* 51 (2015) 538–545.
- [2] R. Lteif, L. Dammak, C. Larchet, B. Auclair Conductivité électrique membranaire: étude de l'effet de la concentration, de la nature de l'électrolyte et de la structure membranaire, *Eur. Polym. J.* 35 (1999) 1187–1195.
- [3] E. D. Belashova, N. A. Melnik, N. D. Pismenskaya, K. A. Shevtsova, A. V. Nebavsky, K. A. Lebedev, V. V. Nikonenko, Overlimiting mass transfer through cation-exchange membranes modified by Nafion film and carbon nanotubes, *Electrochim. Acta* 59 (2012) 412–423.
- [4] M. A. Andreeva, V. V. Gil, N. D. Pismenskaya, V. V. Nikonenko, L. Dammak, C. Larchet, D. Grande, N. A. Kononenko, Effect of homogenization and hydrophobization of a cation-exchange membrane surface on its scaling in the presence of calcium and magnesium chlorides during electrodialysis, *J. Membr. Sci.* 540 (2017) 183–191.
- [5] J. J. Krol, M. Wessling, H. Strathmann, Concentration polarization with monopolar ion exchange membranes: current-voltage curves and water dissociation, *J. Membr. Sci.* 162 (1999) 145–154.
- [6] J. Balster, M. H. Yildirim, D. F. Stamatialis, R. Ibanez, R. G. H. Lammertink, V. Jordan, M. Wessling, Morphology and microtopology of cation-exchange polymers and the origin of the overlimiting current, *J. Phys. Chem. B* 111 (2007) 2152–2165.
- [7] H. Strathmann, Chapter 3 – Preparation and Characterization of Ion-Exchange Membranes, *Ion-Exchange Membrane Separation Processes*, *Membr. Sci. Technol.* 9 (2004) 89–146.
- [8] Y. Tanaka, Chapter 7 Water dissociation, *Ion exchange membranes fundamentals and applications*, second edition, Elsevier Science, 2015.
- [9] J.J. Krol, M. Wessling, H. Strathmann, Chronopotentiometry and overlimiting ion transport through monopolar ion exchange membranes, *J. Membr. Sci.* 162 (1999) 155–164.
- [10] N. Pismenskaia, P. Sistat, P. Huguet, V. Nikonenko, G. Pourcelly, Chronopotentiometry applied to the study of ion transfer through anion exchange membranes, *J. Membr. Sci.* 228 (2004) 65–76.
- [11] C. Frank, *Analytical Chemistry*, 1st Edition, Academic Press, 1979.
- [12] A. K. Ghosh, *Physical Chemistry, Surface Chemistry and Colloids*, Patna–800 005.

[13] O. Hahn, Applied radiochemistry, Ithaca, N.Y., Cornell university press, London, H. Milford, Oxford university press, 1936.

General conclusions and perspectives

Les procédés utilisant des membranes échangeuses d'ions disposent maintenant d'un grand potentiel dans l'industrie moderne pour des applications de concentration, déminéralisation ou modification de divers produits et sous-produits. Au cours de ces dernières décennies, de nombreux chercheurs se sont intéressés au développement de nouvelles membranes échangeuses d'ions en raison de leurs valeurs académiques et industrielles. Cependant, ces procédés se heurtent à de nombreuses limitations telles que la polarisation de la concentration, le colmatage organique (fouling) et la formation de précipités minéraux (scaling), ce qui diminue considérablement l'efficacité du processus et augmente son coût. Afin d'atténuer, voir même d'éviter la formation de ces précipités, il est nécessaire de bien élucider les processus et mécanismes de précipitation. Pour ce faire, nous avons jugé nécessaire d'entreprendre une étude approfondie de la composition des dépôts, de la cinétique de leur formation et sa dépendance de certaines propriétés de la surface de la membrane, ainsi que de l'influence de ce processus sur les performances des membranes échangeuses d'ions.

Trois membranes échangeuses de cations ont été utilisées dans cette étude. La membrane hétérogène commerciale MK-40 et deux de ses modifications en laboratoire : MK-40/Nafion et MK-40/PANI. La membrane MK-40/Nafion est obtenue par revêtement mécanique de la surface de la membrane MK-40 avec un film homogène de résine perfluorée Nafion[®]. Les matériaux Nafion[®] et MK-40 ont les mêmes groupes sulfonés à charge négative. La préparation du MK-40/PANI s'effectue en synthétisant du polyaniline (PANI) dans la couche proche de la surface de la membrane MK-40 dans un champ électrique externe. Les chaînes de polymères PANI forment une couche à l'intérieur de la membrane MK-40 près de sa surface; cette couche contient des groupes fixes $= N^+H$ dont le signe de la charge est opposé à celui de la membrane MK-40. Une jonction bipolaire entre la couche PANI et le reste du matériau membranaire est donc formée à l'intérieur de la membrane MK-40/PANI.

L'épaisseur de la couche Nafion sur la membrane MK-40 à l'état sec est de 12 à 15 μm . L'épaisseur de la membrane MK-40/PANI ne change pas par rapport à la membrane vierge MK-40. Les conductivités des membranes MK-40 et MK-40/Nafion sont identiques, tandis que celle de MK-40/PANI est environ 16 % plus faible. L'angle de contact de MK-40 et MK-40/PANI est à peu près le même (près de 55 °), tandis que celui de la membrane MK-40/Nafion est plus élevé (63 °). La surface des deux membranes modifiées est plus lisse que celle de la membrane vierge.

Le comportement électrochimique des membranes est étudié au moyen de la chronopotentiométrie et de la voltamétrie dans des solutions de chlorure contenant des ions Na^+ , Ca^{2+} et Mg^{2+} .

Nous avons démontré que l'hydrophobicité relativement élevée de la surface de la membrane MK-40/Nafion et la structure spécifique de la couche proche de la surface (une couche homogène sur le substrat hétérogène, qui fournit une meilleure répartition des lignes de courant près de la surface) créent les conditions pour améliorer l'électroconvection. L'intensité de l'électroconvection dans le cas de MK-40/Nafion est significativement plus élevée, et dans le cas de MK-40/PANI est plus faible par rapport à celle de la membrane vierge. L'intensité de l'électroconvection dépend essentiellement du degré d'hydratation des contre-ions. Les ions de calcium et de magnésium hautement hydratés impliquent le mouvement d'un plus grand volume d'eau par rapport aux ions de sodium. Lorsqu'un courant surlimite constant est appliqué à la membrane, les vortex électroconvectifs dans des solutions 0,02 M de CaCl_2 et MgCl_2 sont générés dans les 3-8 secondes, ce qui est inférieur au temps de transition évalué à 7-16 secondes.

Une électroconvection plus intense dans le cas de la MK-40/Nafion améliore le transfert de masse et entraîne une réduction de la chute de potentiel et du taux de dissociation de l'eau. Ces facteurs ainsi que la surface plus lisse de la MK-40/Nafion entraînent une réduction significative du taux et de la vitesse de formation des précipités sur la surface membranaire, voir même de sa prévention totale dans les zones où le courant atteint sa valeur limite.

La couche PANI de la membrane MK-40/PANI constitue une barrière pour le transport de cations bivalents, tels que Ca^{2+} et Mg^{2+} . Cependant, la jonction bipolaire entre cette couche et le matériau de la MK-40/PANI provoque une augmentation du taux de dissociation de l'eau et une réduction de l'électroconvection. Par conséquent, le taux de précipitation des composés contenant du Ca^{2+} et du Mg^{2+} est plus élevé que dans le cas des membranes MK-40 et MK-40/Nafion. La formation de précipités se produit à des courants limites excessifs. Cependant, à des courants inférieurs au courant limite, aucune précipitation n'est observée. Ainsi, il est possible de recommander la membrane composite MK-40/PANI pour une électrodialyse sélective par ionisation monovalente à des densités de courant inférieures.

Deux facteurs influent sur la formation de précipités sur les surfaces de membranes : l'électroconvection et la valeur locale du pH. Le précipité est détecté dans l'intervalle $1.0i_{lim}^{exp} \leq i \leq 2.0i_{lim}^{exp}$ pour la MK-40, quand $i \geq 0.8i_{lim}^{exp}$ pour les membranes MK-40/PANI et dans l'intervalle $1.0i_{lim}^{exp} \leq i \leq 1.5i_{lim}^{exp}$ pour la MK-40/Nafion. Dans l'intervalle $1.0i_{lim}^{exp} > i > 2.0i_{lim}^{exp}$ pour la MK-40, quand $i < 0.8i_{lim}^{exp}$ pour les membranes MK-40/PANI et $1.0i_{lim}^{exp} > i > 1.5i_{lim}^{exp}$ pour la MK-40/Nafion, aucune précipitation n'est observée. Dans le cas de la membrane MK-40 et MK-40/Nafion, où une densité de courant suffisamment élevée est appliquée, la vitesse de dissociation de l'eau au niveau de la membrane MA-41 est

supérieure à celle de la membrane échangeuse de cations en cours d'étude. Ceci provoque une acidification de la solution dans tout le compartiment de dessalement et par conséquent la réduction ou l'élimination de la formation de précipités. L'analyse élémentaire du précipité sur la surface de la membrane réalisée par analyse des rayons X a montré la formation des cristaux de $Mg(OH)_2$, $Ca(OH)_2$, et de $CaCO_3$. Comparé au taux de précipitation des cristaux sur la surface de la MK-40, on établit expérimentalement que celui sur la surface de MK-40/Nafion est plus petit, mais celui sur la surface du MK-40/PANI est plus grand.

Un autre facteur important permettant l'atténuation de la formation de précipités est l'utilisation du mode de champ électrique pulsé. Pendant la pause, une relaxation du profil de concentration se produit en solution à la surface de la membrane. Les concentrations d'espèces retrouvent partiellement ou complètement leurs valeurs initiales en solution, et le produit des concentrations d'ions devient inférieur au produit de solubilité, ce qui provoque une dissolution partielle ou totale du précipité. Un tel mode permet, d'une part, de réduire de plus de deux fois le gap de potentiel, et d'autre part d'atteindre un état quasi stationnaire où se produit une dissolution périodique des précipités formés. Il est démontré que le taux de précipitation est significativement plus faible dans le mode du champ électrique pulsé. La tendance générale est que la vitesse de précipitation diminue en diminuant la valeur de T_{on} , tandis que T_{off} reste égal ou légèrement inférieur à T_{on} .

Perspectives

Ce travail de thèse nous a permis de mettre en évidence la faisabilité de l'utilisation du mode de champs électriques pulsés pour réduire le taux de formation de précipités sur la surface de membranes échangeuses d'ions. Cependant, la courte durée (environ 3 h) des essais expérimentaux où ces champs pulsés ont été appliqués lors de cette étude ne nous permet pas de dire avec certitude si la formation des cristaux serait stable et négligeable lors d'une longue opération d'électrodialyse, ou bien au contraire, elle augmenterait avec le temps. La question qui demeure posée est « comment le système se comportera-t-il sur des durées comparables au temps d'utilisation de la membrane à l'échelle industrielle ». Ainsi, il est intéressant de faire une étude expérimentale de l'électrodialyse dans les modes de champ électrique pulsé de longue durée (plusieurs dizaines d'heures) lors de l'utilisation d'une cellule similaire à celle utilisée dans les unités industrielles.

D'autres recherches devraient également être réalisées afin d'étudier l'effet du champ électrique pulsé à courte période (haute fréquence) dans des régimes galvanostatiques et potentiostatiques sur l'atténuation de la formation de précipités. Comme le montre Mishchuk et al., le régime du champ électrique pulsé devrait conduire à un effet plus significatif dans la réduction de la polarisation de la concentration, l'intensification de l'électrodialyse et,

éventuellement, l'atténuation de la formation des précipités. De plus, d'autres formes d'ondes de champ électrique pulsé peuvent être étudiées pour améliorer le mélange de solutions par les vortex électroconvectionnels. En effet, il est connu que dans la galvanoplastie des métaux, des alliages, des composites et des semi-conducteurs, cette approche est largement utilisée pour améliorer la nature et la qualité du dépôt. Les formes d'onde peuvent être assez compliquées impliquant par exemple une impulsion cathodique suivie d'une période sans courant (ou une impulsion anodique), un courant continu avec des modulations superposées, des impulsions duplex, une impulsion sur impulsion, un courant inverse d'impulsion, etc.

Les membranes modifiées par PANI ont une sélectivité vis-à-vis des ions monovalents. D'autres recherches devraient être entreprises pour vérifier l'intérêt de l'utilisation de ces membranes dans les procédés où une barrière pour le transport d'ions multivalent est nécessaire, comme par exemple la métathèse par électrodialyse et l'électrodialyse inverse.

Processes using ion-exchange membranes now have great potential in modern industry for concentration, demineralization or modification of various products and by-products. In recent decades, many researchers have been interested in developing new ion-exchange membranes because of their academic and industrial values. However, these processes are subject to numerous limitations such as concentration polarization, fouling and scaling, which considerably reduces the efficiency of the process and increases its cost. In order to mitigate, or even avoid the formation of these precipitates, it is necessary to elucidate the processes and mechanisms of minerals precipitation. To do so, it is necessary to undertake a thorough study of the composition of deposits, kinetics of scaling and its dependence of the membrane surface properties, as well as the influence of this process on the performances of ion-exchange membranes.

Three cation-exchange membranes were used in this study. The commercial heterogeneous MK-40 membrane and two of its lab-made modifications: MK-40/Nafion and MK-40/PANI. The MK-40/Nafion membrane is obtained by mechanical coating the MK-40 membrane surface with a homogeneous film of Nafion[®] perfluorinated resin. The Nafion[®] and the MK-40 materials have the same negative-charged sulfonate groups. The preparation of the MK-40/PANI is carried out by synthesizing PANI within the MK-40 membrane near-surface layer in external electric field. The PANI polymer chains form a layer within the MK-40 membrane near its surface; this layer contains fixed $=N^+H$ groups whose charge sign is opposite to that of the MK-40 membrane. A bipolar junction between the PANI layer and the bulk material is formed within the MK-40/PANI membrane.

The thickness of Nafion layer on the MK-40 membrane in the dry state is 12-15 μm . The thickness of MK-40/PANI membrane does not change in comparison with the pristine membrane. The conductivity of MK-40 and MK-40/Nafion membranes is identical, while that of MK-40/PANI is about 16 % lower. The contact angle of MK-40 and MK-40/PANI is nearly the same (close to 55 °), while that of MK-40/Nafion membrane is higher (63 °). The surface of both modified membranes is smoother than that of the pristine one.

The electrochemical behavior of the membrane samples is studied by means of chronopotentiometry and voltammetry in the chloride solutions containing Na^+ , Ca^{2+} and Mg^{2+} ions.

We have shown that the relatively high hydrophobicity of the MK-40/Nafion membrane surface, the specific structure of near-surface layer (a homogeneous layer on the heterogeneous substrate, which provides a “better” distribution of current lines near the surface) create conditions for enhancing electroconvection. The electroconvection intensity in the case of MK-40/Nafion is significantly higher, and in the case of MK-40/PANI is lower in

comparison with that of the pristine membrane. The electroconvection intensity substantially depends on the degree of counter-ion hydration. Highly hydrated calcium and magnesium ions involve in motion a larger volume of water as compared with sodium ions. When a constant overlimiting current is applied to the membrane, electroconvective vortices in 0.02 M CaCl₂ and MgCl₂ solutions are generated already within 3-8 s, which is lower than the transition time varying in the range of 7-16 s.

More intensive electroconvection in the case of MK-40/Nafion enhances the mass transfer, causes a reduction in the potential drop and in the water splitting rate. These factors together with the smoother surface of MK-40/Nafion lead to a significant reduction in the rate of scale formation, or to its total prevention in the overlimiting current ranges.

The PANI layer in the MK-40/PANI membrane forms a barrier for the transport of bivalent cations, such as Ca²⁺ and Mg²⁺. However, the bipolar junction between this layer and the bulk material of the MK-40/PANI causes an increase in water splitting rate and a reduction in electroconvection. As a result, the precipitation rate of Ca²⁺ and Mg²⁺ containing compounds is higher than that in the case of the MK-40 and MK-40/Nafion membranes. The scale formation occurs at overlimiting currents. However, at currents less than the limiting current no scaling is observed. Thus, it is possible to recommend the MK-40/PANI composite membrane for monovalent-ion-selective electrodialysis at underlimiting current densities.

Two factors affect the scaling: electroconvection and local *pH* value. The scale is detected in the range $1.0i_{lim}^{exp} \leq i \leq 2.0i_{lim}^{exp}$ for MK-40, $i \geq 0.8i_{lim}^{exp}$ for MK-40/PANI and $1.0i_{lim}^{exp} \leq i \leq 1.5i_{lim}^{exp}$ MK-40/Nafion membranes. In the range $1.0i_{lim}^{exp} > i > 2.0i_{lim}^{exp}$ for MK-40, $i < 0.8i_{lim}^{exp}$ for MK-40/PANI and $1.0i_{lim}^{exp} > i > 1.5i_{lim}^{exp}$ for MK-40/Nafion membranes, no scale is observed. In the case of MK-40 and MK-40/Nafion membranes, where a sufficiently high current density is applied, the water splitting rate at the MA-41 membrane is higher than that at the cation-exchange membrane under study. It provides an acidification of the solution throughout the desalination chamber and the reduction or the inhibition of the scale formation. The elemental analysis of the scale on the membrane surface made by X-ray analysis has shown the formation of Mg(OH)₂, Ca(OH)₂ and CaCO₃ scales. It is experimentally established that the scaling rate on the surface of MK-40/Nafion is smaller, and on the surface of the MK-40/PANI is larger in comparison with the MK-40 membrane.

Another important factor allowing mitigation of scaling is the use of pulsed electric field mode. During the pause lapse, a relaxation of the concentration profile occurs in solution at the membrane surface. The species concentrations return partially or completely to their values in the bulk solution, and the product of ion concentrations become lower than the solubility product, which causes partial or complete dissolving of the scale. Such mode allows

the reduction of the potential drop more than twice and achievement of a quasi steady-state where an unstable periodically crumbling scale occurs. We have shown that scaling rate is significantly lower in the pulsed electric field mode. The general tendency is that scaling rate decreases with decreasing the value of T_{on} , while T_{off} remains equal or somewhat less than T_{on} .

Perspectives

This thesis research work revealed the feasibility of the use of pulsed electric field modes to reduce the rate of scale formation. However, the duration of the experimental runs where pulsed electric fields were applied (about 3 h) in this study does not allow us to say with certainty if the scale would be stable and negligible during a long electro dialysis operation or it would increase with time. The question remains, how the system will behave during the time, which is comparable with the time of membrane use in industrial scale. Thus, it is of interest to make an experimental study of electro dialysis in pulsed electric field modes of long duration (several tens of hours) when using a cell similar to those used in industrial stacks.

Further investigations should be accomplished as well to study the effect of short period pulsed electric field (high frequency) in galvanostatic and potentiostatic regimes on the scale mitigation. As it was shown by Mishchuk et al., potentiostatic pulsed electric field regime should lead to a more significant effect in reduction of concentration polarization, intensification of electro dialysis and, eventually, mitigation of scaling. Moreover, other waveforms of pulsed electric field can be studied to enhance solution mixing by electroconvective vortices. It is known that in electroplating of metals, alloys, composites and semiconductors, this approach is widely used for improving the deposition. The waveforms can be quite complicated involving cathodic pulse followed by a period without current (or an anodic pulse), direct current with superimposed modulations, duplex pulses, pulse-on-pulse, pulse reverse current and others.

The membranes modified by PANI have selectivity to the monovalent ions. Further investigations should be undertaken to verify the reasonability of using these membranes in the processes where a barrier for multivalent ion transport is useful, such as electro dialysis metathesis and reverse electro dialysis.

Résumé

Le colmatage à la surface et dans la masse d'une membrane échangeuse d'ions est un obstacle majeur à son utilisation en électrodialyse. En bloquant les voies conductrices d'ions à travers la membrane, le dépôt réduit la surface active de la membrane et conduit à une résistance au transfert de matière supplémentaire.

Trois membranes échangeuses de cations ont été utilisées lors de ce travail: une membrane commerciale hétérogène MK-40 et deux de ses modifications (une membrane MK-40/Nafion obtenue par revêtement de la surface de MK-40 avec un film de Nafion[®] homogène conducteur d'ions, et une membrane MK-40/PANI obtenue par synthèse de polyaniline sur la surface de la MK-40). Les solutions utilisées sont des solutions de CaCl₂ et MgCl₂ aux concentrations 0,02 et 0,04 mol/L, ainsi qu'une solution modélisant la composition minérale du lait, concentrée 3 fois. La visualisation de la surface de la membrane est réalisée par microscopie optique et microscopie électronique à balayage. L'analyse élémentaire des dépôts sur la surface de la membrane est réalisée par l'analyse aux rayons X. Le caractère hydrophobe-hydrophile de la surface de la membrane est estimé par la mesure de l'angle de contact. La chronopotentiométrie et la voltamétrie ont été utilisées pour caractériser la vitesse de transport des cations à travers les membranes et la dissociation d'eau à la surface ; la mesure du pH de la solution dessalée a été effectuée en parallèle.

Il est démontré que l'hydrophobicité relativement élevée de la surface de la membrane, son hétérogénéité électrique et géométrique créent les conditions favorables au développement de l'électroconvection. L'intensité de l'électroconvection par rapport à la membrane non modifiée est significativement plus élevée dans le cas de la MK-40/Nafion mais plus faible dans le cas de la MK-40/PANI. L'électroconvection provoque le mélange de la solution à la surface de la membrane dans une couche d'environ 10 µm d'épaisseur. Cet effet augmente de manière significative le transfert de matière en mode de courant intensif, empêche ou réduit le colmatage et réduit aussi le taux de dissociation de l'eau sur la surface de la membrane. L'intensité de l'électroconvection dépend essentiellement du degré d'hydratation du contre-ion ; elle augmente avec son rayon de Stokes. Le taux de croissance des dépôts minéraux Mg(OH)₂, Ca(OH)₂ et CaCO₃ sur la surface de la membrane échangeuse d'ions est déterminé par la pente du chronopotentiogramme. On établit expérimentalement que, par rapport à la vitesse de colmatage sur la membrane MK-40 non modifiée, celle sur la surface de MK-40/Nafion devient plus petite mais celle sur la surface de la MK-40/PANI, devient plus grande.

Le taux du colmatage est considérablement réduit lorsqu'un mode de courant électrique pulsé est appliqué. Un tel mode permet de réduire de moitié la différence de potentiel et d'atteindre un état quasi-stable du fait que le précipité devient instable.

Mots clés : membrane échangeuse d'ions ; colmatage ; propriétés de surface ; électrodialyse ; électroconvection.

Abstract

Scaling on the surface and in the bulk of ion-exchange membranes is a considerable locker for electro dialysis. The scale reduces the effective surface area of the membrane and leads to additional resistance to the mass transfer and solution flow.

Three cation-exchange membranes are used in this study: a heterogeneous commercial MK-40 membrane and two of its modifications. The MK-40/Nafion membrane is obtained by mechanical coating the MK-40 membrane surface with a homogeneous ion-conductive Nafion[®] film. Modification of the MK-40/PANI membrane is carried out by polyaniline synthesis on the membrane surface. The solutions used in the study are 0.02 and 0.04 mol/L CaCl₂ and MgCl₂ solutions, as well as the solution, imitating the mineral composition of milk, concentrated 3 times. The visualization of the membrane surface is made using optical and scanning electron microscopy. The elemental analysis of the scale on the membrane surface is made by X-ray analysis. The hydrophobic-hydrophilic balance of the membrane surface is estimated by the contact angle measurements. To characterize the cation transport through and the water splitting rate, chronopotentiometry and voltammetry methods are used, pH measurement of the diluate solution is conducted at the same time.

It is shown that the relatively high hydrophobicity of the membrane surface, its electrical and geometric heterogeneity, create conditions for the development of electroconvection. The electroconvection intensity in the case of MK-40/Nafion is significantly higher, and in the case of MK-40/PANI is lower in comparison with that of the unmodified membrane. Electroconvection vortices cause the mixing of the solution at the membrane surface in a ≈10 µm thick layer. This effect significantly increases mass transfer in intensive current modes and prevents or reduces the scaling process, as well as reduces the water splitting rate at the membrane surface. The rate of electroconvection essentially depends on the counterion hydration degree, it increases with increasing the counterion Stokes radius. The rate of the scale formation on the membrane surface is determined by the slope of the chronopotentiogramme. The formation of Mg(OH)₂, Ca(OH)₂ and CaCO₃ scales is observed. It is experimentally established that the scaling rate on the surface of MK-40/Nafion is smaller, and on the surface of the MK-40/PANI is larger in comparison with the MK-40 membrane. The scaling rate is significantly reduced when the pulsed electric current mode is applied. Such mode allows the reduction of the potential drop more than twice and achievement of a quasi steady-state because an unstable periodically crumbling scale occurs.

Key words: ion-exchange membrane, scaling, surface properties, electro dialysis, electroconvection